# Microtubule-dependent mRNA transport is coupled to endosomes and important for unipolar growth in *Ustilago maydis*

(Der Endosomen-gekoppelte mRNA-Transport entlang von Mikrotubuli ist wichtig für unipolares Wachstum in *Ustilago maydis*)

## Dissertation


zur Erlangung des Doktorgrades
der Naturwissenschaften (Dr. rer. nat.)

dem Fachbereich Biologie
der Philipps-Universität Marburg
vorgelegt von

**Dipl. Biol. Sebastian Baumann**
aus Gelsenkirchen

Düsseldorf 2013

Vom Fachbereich Biologie
der Philipps-Universität Marburg (Hochschulkennziffer: 1180) als Dissertation
angenommen am: 29.04.2013

| | |
|---|---|
| Erstgutachter: | Herr Prof. Dr. Michael Feldbrügge |
| Zweitgutachter: | Herr Prof. Dr. Martin Thanbichler |
| Drittgutachter: | Herr Prof. Dr. Wolfgang Buckel |

Tag der mündlichen Prüfung am: 10.06.2013

Erklärung

Ich versichere, dass ich meine Dissertation mit dem Titel " **Microtubule-dependent mRNA transport is coupled to endosomes and important for unipolar growth in *Ustilago maydis*** " selbständig, ohne unerlaubte Hilfe angefertigt und mich dabei keiner anderen als der von mir ausdrücklich bezeichneten Quellen und Hilfen bedient habe.

Diese Dissertation wurde in ihrer jetzigen oder einer ähnlichen Form noch bei keiner anderen Hochschule eingereicht und hat noch keinen sonstigen Prüfungszwecken gedient.

_____ _____

(Ort/Datum) (Sebastian Baumann)

Die Untersuchungen zur vorliegenden Arbeit wurden von Oktober 2007 bis November 2009 in Marburg am Max-Planck-Institut für terrestrische Mikrobiologie in der Abteilung für Organismische Interaktionen durchgeführt und von Dezember 2009 bis Februar 2013 an der Heinrich-Heine Universität Düsseldorf am Institut für Mikrobiologie unter der Betreuung von Herrn Prof. Dr. Michael Feldbrügge fortgeführt.

Teile dieser Arbeit sind in folgenden Artikeln veröffentlicht oder

zur Veröffentlichung eingereicht:

König J*, **Baumann S***, Koepke J, Pohlmann T, Zarnack K, Feldbrügge M (2009) The fungal RNA-binding protein Rrm4 mediates long-distance transport of *ubi1* and *rho3* mRNAs. *EMBO J* **28:** 1855-1866
(***equal contribution**)

**Baumann S**, Pohlmann T, Jungbluth M, Brachmann A, Feldbrügge M (2012) Kinesin-3 and dynein mediate microtubule-dependent co-transport of mRNPs and endosomes. *J Cell Sci* **125:** 2740-2752

**Baumann S**, König J, Koepke J, Feldbrügge M (2013) Endosomal transport of septin mRNA and encoded protein mediates correct septin filamentation. *EMBO J* submitted

**Summary**

mRNA transport is an important mechanism to orchestrate polarised growth. Although basic principles of mRNA transport are well understood, key questions still remain open: Is mRNA transport connected to membrane trafficking and why do mRNAs move bidirectionally without accumulating subcellularly?

The phytopathogenic basidiomycete *Ustilago maydis* grows in a highly polar manner. On the surface of its host plant maize fungal hyphae migrate via extended tip growth, which is a prerequisite for infection. Recently, the RNA recognition motif-harbouring protein Rrm4 was shown to be important for this asymmetric growth, since deletion of the corresponding gene causes an increased number of hyphae to establish two growth cones. Previous *in vivo* studies furthermore showed that Rrm4 binds RNAs and shuttles rapidly along microtubules.

In this study RNA live imaging revealed that Rrm4 mediates cytoplasmic shuttling of a set of mRNAs encoding for example the ubiquitin fusion protein Ubi1, the small G-protein Rho3 and septin Cdc3. However, the investigated mRNAs do not accumulate subcellularly. It was demonstrated that mRNA binding is essential for Rrm4 function and polar growth. Furthermore, the molecular motors kinesin-3 and dynein carry out antero- and retrograde transport of mRNAs. Intriguingly, the same motors that are mandatory for mRNA transport also mediate endosome trafficking.

Investigating septin mRNA transport applying dynamic live cell imaging revealed Rrm4-mediated co-transport of septin mRNA and encoded protein. Septins are highly conserved GTPases that function either in limiting membrane diffusion or as scaffold. Septins polymerise into higher-order structures and are involved in symmetry breaking and polar growth. Since co-localisation of mRNA and protein is indicative for local protein synthesis it was tested whether septin mRNA is directly translated on endosomes. Consistently, the accumulation of septin protein on endosomes is tightly linked to the recruitment of septin mRNA. Furthermore, ribosomal proteins co-localise with shuttling endosomes, but only in the presence of mRNA. Importantly, endosomal trafficking is essential for an efficient delivery of septin protein to septin filaments at growth cones.

In sum, the novel mechanism of mRNA-hitchhiking on endosomes that are trafficking due to the action of kinesin-3 and dynein was uncovered. This constitutes a novel mechanism for loading endosomes with septin protein by local translation - a process that might be important for rapid and coordinated assembly of septin filaments at hyphal growth cones.

**Zusammenfassung**

mRNA-Transport ist ein wichtiger Mechanismus zur Steuerung polaren Wachstums. Die grundlegenden Prinzipien des mRNA-Transports sind intensiv erforscht, aber ob mRNA- und Membrantransport gekoppelt sind und warum mRNAs bidirektionale Bewegung zeigen, jedoch nicht subzellulär akkumulieren, ist bisher nicht bekannt.

Der phytopathogene Basidiomyzet *Ustilago maydis* bewegt sich auf der Pflanzenoberfläche durch striktes polares Spitzenwachstum fort. Dies ist eine Grundvoraussetzung für die Infektion seiner Wirtspflanze Mais. Kürzlich wurde das RNA-Erkennungsmotive enthaltenden Protein Rrm4 identifiziert. Das Protein ist wichtig für die Steuerung des Spitzenwachstums, da entsprechende Deletionsmutanten eine zweite, gegenüberliegende Wachstumszone etablieren. Vorhergehende *in vivo* Studien haben außerdem gezeigt, dass Rrm4 RNA bindet und sich schnell bidirektional entlang von Mikrotubuli bewegt.

In der vorliegenden Sudie wird mithilfe des „RNA live imaging“ visualisiert, dass Rrm4 eine Gruppe von mRNAs im Zytoplasma transportiert. Darunter befinden sich mRNAs, die für das Ubiquitin-Fusionsprotein Ubi1, für das kleine G-Protein Rho3, sowie für das Septin Cdc3 kodieren. Bemerkenswert ist jedoch, dass die mRNAs nicht subzellulär akkumulieren. Es konnte gezeigt werden, dass die Fähigkeit mRNA zu binden für die Rrm4 Funktionalität und für polares Wachstum essenziell ist. Des Weiteren wird der antero- und retrograde Transport durch Kinesin-3 und Dynein vermittelt. Interessant ist, dass diese für den mRNA-Transport notwendigen Motoren auch Endosomenbewegung ermöglichen.

Die eingehende Untersuchung von Septin mRNA-Transport mithilfe des dynamischen „live cell imagings“ hat den Kotransport von Septin mRNA und dem kodierten Protein aufgedeckt. Septine sind hochkonservierte GTPasen, die entweder Diffusion in Membranen beeinträchtigen oder als intrazelluläres Gerüst dienen. Septine polymerisieren zu komplexen Strukturen, sind wichtig für polares Wachstum und tragen dazu bei, die Symmetrie einer Zelle aufzuheben. Da die Kolokalisation von mRNA und Protein ein Indiz für die lokale Proteinsynthese ist, wurde getestet, ob Septin mRNA an Endosomen translatiert wird. In Übereinstimmung damit bedingt die Anwesenheit von mRNA die Akkumulation des entsprechenden Proteins an Endosomen. Ferner kolokalisieren ribosomale Proteine mRNA-abhängig mit beweglichen Endosomen. Bemerkenswerterweise ist für einen effizienten Einbau von Septinprotein in Septinfilamente an Wachstumskegeln der Endosomentransport essenziell.

Die Schlussfolgerung aus diesen Ergebnissen ist, dass mRNAs sich per „Anhalter“ auf Endosomen bidirektional durch die polarisierte Zelle bewegen. Dieser durch Kinesin-3 und Dynein vermittelte Transport stellt einen neuartigen Mechanismus dar, bei dem Endosomen durch lokale Translation mit Septinprotein beladen werden. Dies könnte dazu dienen, einen schnellen und koordinierten Zusammenbau von Septinfilamenten an Wachstumskegeln von Pilzhyphen zu gewährleisten.

# Index

# 1 General Introduction

## 1.1 mRNA transport and localised translation

Localising mRNAs is an important mechanism for spatial and temporal regulation of gene expression (Martin & Ephrussi, 2009). Local translation is crucial in determining the subcellular localisation of proteins and thus involved in a number of processes such as establishing and maintaining polarity. This is a widespread mechanism, e.g. in the early *Drosophila* embryo up to 70% of all mRNAs show a discrete localization pattern (Lécuyer et al, 2007). An important mechanism is the active transport of mRNAs along the actin or microtubule (MT) cytoskeleton. The mRNAs associate with accessory factors like RNA-binding proteins, molecular motors or the poly(A)-binding protein directly or indirectly to form large messenger ribonucleoprotein complexes termed mRNPs (Holt & Bullock, 2009; Martin & Ephrussi, 2009; St Johnston, 2005).

### 1.1.1 Actin-dependent mRNA transport

The best studied microbial example is *ASH1* mRNA transport in the yeast *Saccharomyces cerevisiae*. Here the mRNA is transported actin-dependent from the mother cell to the growing periphery of the budding daughter cell (Heym & Niessing, 2011). The mRNA contains *cis*-acting localisation elements, so called zipcodes (Jambhekar & Derisi, 2007), that are recognised and bound synergistically by the RNA-binding proteins She2p and She3p which are linked to Myo4p that drives motion along actin cables (Böhl et al, 2000; Long et al, 2000; Muller et al, 2011). During transport translation is repressed by interaction of Puf6p and Khd1p. Upon phosphorylation via CK2 and Yck1p, respectively, translation is released at the destination site (Deng et al, 2008; Heym & Niessing, 2011). If and how mRNAs are anchored before translation is still elusive (Jansen & Niessing, 2012). The encoded HO endonuclease that mediates mating type switching is only translated in the daughter cell and hence only acts in the daughter cell nucleus (Heym & Niessing, 2011). Interestingly, for a subset of transported mRNAs it was shown, that they are co-transported with cortical ER, while *ASH1* for example is not, suggesting two different transport pathways (Fundakowski et al, 2012; Schmid et al, 2006).

### 1.1.2 Microtubule-dependent mRNA transport

Microtubule-dependent mRNA transport is intensively studied during developmental processes in *Drosophila melanogaster* as well as in neuronal models where it contributes to neuronal outgrowth, synaptic function and plasticity (Doyle & Kiebler, 2011; St Johnston, 2005). During *Drosophila* oogenesis the localisation of *oskar* mRNA is driven by kinesin. A biased random walk along a weakly polarized cytoskeleton ensures posterior localization which defines formation of abdomen and germ cells (Bastock & St Johnston, 2008; Zimyanin et al, 2008). In concert with *bicoid* that localizes oppositely at the anterior, the anterior-posterior axis of the subsequent arising embryo is defined. The early steps in anterior localization of *bicoid* mRNA depends on members of the ESCRT II complex, in particular VPS36 which binds the zipcode of *bicoid* mRNA directly. Mutants in VPS22, VPS25 and VPS36 abolish the final step in *bicoid* localization through the non-specific double-stranded RNA-binding protein Staufen. This processs is thought to be independent of endosomal sorting, since the other ESCRT complexes (0, I and III) are not involved (Irion & St Johnston, 2007).

In the syncytial blastoderm embryo of *Drosophila* pair-rule transcripts such as *hairy* localize apically (Fig. 1-1; Bullock, 2007) Recent research led to a model in which Egalitarian (Egl), that has no apparent domain structure, is a selective RNA-binding protein that recognises mRNAs lacking any sequence or secondary structure similarity (Dienstbier et al, 2009; Nashchekin & St Johnston, 2009). Interestingly NMR spectroscopy studies on the tertiary structure on the *D. melanogaster fs(1)K10* signal revealed an unusual "A'-form" conformation of two canonical double stranded RNA helices within the *K10* signal (Bullock et al, 2010). A second player Bicaudal-D (Bic-D) is necessary to link mRNA and Egl to dynein. Surprisingly transport of non-localising mRNAs functions without zipcodes and without Egl and BicD (Dienstbier et al, 2009;

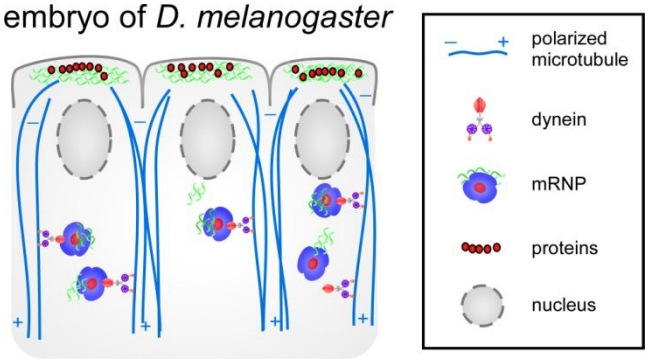


**Fig. 1-1** mRNP trafficking during embryogenesis in *Drosophila melanogaster*. Pair-rule transcripts whose encoded tran-scriptional regulators are involved in segmentation localise to the apical side of nuclei in the syncytial blastoderm embryo; e.g. *hairy* mRNA is recognized by Egl and connected to dynein via BicD. The mRNP travels along MTs facing the apical cortex with their minus end. Although movement is bidirectional, a slight bias exists, resulting in net movement towards minus ends. (from Vollmeister et al., 2012)

Nashchekin & St Johnston, 2009). But the frequency of minus end directed movement seems to be enhanced when all *cis*- and *trans*- acting factors are present (Amrute-Nayak & Bullock, 2012; Bullock et al, 2006; Bullock et al, 2003). One attractive model proposes that RNA-signals are necessary to recruit additional dynein molecules to augment minus end directed motility (Bullock, 2007).

In the nervous system mRNA transport and localized translation contribute to axon guidance, survival and regeneration as well as synaptic plasticity (Doyle & Kiebler, 2011; Jung et al, 2012). Neuronal axons transfer signals over long distances and in some cases, can elongate over several metres (Nelson, 2003). In immature neurites orientation of axonal growth cones takes place in response to environmental cues such as Ca2+ or the chemotropic protein Netrin-1 (Jung et al, 2012). Interestingly, Netrin-1 apperars to induce asymmetric local translation of *β-actin* mRNA thereby mediating growth cone turning of retinal neurites of Xenopus laevis (Leung et al, 2006). Thus, local translation contributes critically to the ability of axons to reach their destination e.g. in the brain (Doyle & Kiebler, 2011). In fully differentiated neurons of the hippocampus a set of different mRNAs has been identified to travel into dendrites. It has been posted that mRNAs are specifically translated postsynaptically after synaptic activation. This process is thought to regulate synaptic plasticity and memory consolidation (Doyle & Kiebler, 2011). So far no anchoring of mRNAs at dendrtitic spines has been observed either in cultured neurons that were injected with fluorescently labelled mRNAs (Gao et al, 2008; Mikl et al, 2011; Tubing et al, 2010), nor in neurons derived from a mouse model expressing components of the MS2 RNA-live imaging system (Beach et al, 1999; Bertrand et al, 1998), which allows the detection of endogenous mRNAs (Lionnet et al, 2011). In an attempt to explain this phenomenon the sushi-belt model was proposed. In this model mRNAs continuously shuttle bidirectionally within dendrites and synapses in demand for mRNAs are served transiently (Doyle & Kiebler, 2011).

Despite immense efforts some key questions are open, e.g. the interplay of plus- and minus-end directed molecular motors (Holt & Bullock, 2009) and a potential involvement of membrane trafficking (Cohen, 2005). Further important points are, why mRNPs shuttle bidirectionally without being anchored (Doyle & Kiebler, 2011) and how the translation is regulated during transport (Meignin & Davis, 2010).

## 1.2 Cell polarity

Generating cellular asymmetry is essential for most kinds of cells to carry out sophisticated functions. Mostly different shapes are coupled to specialised function (Nelson, 2003). For example in cells as small as the bacterium *Caulobacter crescentus* polar morphogenesis is essential to produce viable offspring (Thanbichler, 2009). In comparably huge cells like mammalian neurons, axons can elongate several meters in order to confer communication between different tissues (Nelson, 2003). Cell polarisation enables fibroblasts to migrate during wound healing (Neukirchen & Bradke, 2011) and polar tip growth allows fungi to move on plant surfaces or to explore a greater environment (Brand & Gow, 2009; Gladfelter, 2006; Vollmeister et al, 2012).

How is cellular asymmetry obtained? In order to achieve polarity or asymmetrical growth in eukaryotes, a complex interplay of cellular events has to occur e.g., signalling events, remodelling of the cytoskeleton, exo- and endocytosis and especially in fungi the cell wall needs to be remodelled and turgor pressure might enforce tip expansion (Fischer et al, 2008; Harris, 2006; Iden & Collard, 2008).

### 1.2.1 Cell polarisation in budding yeast

In order to establish polarity, symmetry needs to be broken. In general it means that proteins and lipids within a cell need to be asymmetrically distributed. In the yeast *S. cerevisiae* the small GTPase Cdc42 plays a central role in polarity establishment and maintenance during budding. Cdc42 polarises at the plasmamembrane and regulates the recruitment of, e.g. the polarisome protein Bni1 and septin proteins (Bi & Park, 2012). Septins form a ring and subsequently an hourglass structure at the incipent bud site and the later mother bud neck, respectively, to act as scaffold and membrane barrier (Oh & Bi, 2011). Septins anchor landmark proteins and are involved in chitin deposition as well as keeping the polarisome component Spa2 and the exocyst subunit Sec3 in place ((Oh & Bi, 2011) see section 1.2.3 for further details on septin proteins). Spa2 itself is a scaffold protein that binds the formin Bni1, which nucleates actin thereby triggering actin filament assembly. This enables the cell to move Golgi-derived vesicles along actin cables via the myosin motor protein Myo2 (Evangelista et al, 2003). The vesicles carry for example enzymes involved in cell wall synthesis. They are received by the exocyst which regulates polar exocytosis via tethering and fusion of vesicles with the plasmamembrane mediated by Rab GTPases (Bi & Park, 2012).

Since Cdc42 controls actin patch polarisation it is also implicated in endocytosis. Basically endocytosis is thought to support two processes. (i) Generation of polarity by internalising subapical plasmamembrane patches including slowly diffusing proteins and immediate redelivery to the growing tip as shown for Cdc42 itself (Wedlich-Söldner et al, 2003; Wedlich-Soldner & Li, 2003), suggesting a complex interplay between Cdc42 and actin polymerisation, endocytosis and exocytosis (Bi & Park, 2012). (ii) Regulating the level of lipids and proteins including membrane fusion-mediating proteins, cell wall synthetic enzymes and receptors (Bi & Park, 2012; Penalva, 2010). Receptor endocytosis has been shown to depend on cargo monoubiquitination which is recognised by Epsins and the ESCRT-0 protein Vps27/Hrs (Shih et al, 2002), mediating internalisation of receptors into vesicles and sorting to multivesicular bodies, respectively (Clague et al, 2012).

### 1.2.2 Polarised growth in filamentous fungi

Filamentous fungi are among the fastest unidirectional growing cells with up to 7.5 mm/h elongation rate (Harris et al, 2005). Hence, a tremendous amount of lipids and proteins needs to delivered to the growth cone. In agreement it was estimated that rapid growing *Neurospora crassa* hyphae require ~38,000 vesicles to fuse with the tip per minute (Collinge & Trinci, 1974). Unique to fungal hyphae is the so called Spitzenkörper (SKP) (Harris et al, 2005; Steinberg, 2007a) that determines the direction of hyphal growth (Fischer et al, 2008). According to current views, the SPK is thought to act as a vesicle supply center, receiving exocytic vesicles via MTs and distributing them further to the cell surface via actin cables (Harris et al, 2005). In agreement, the deletion of conventional kinesin in *Neurospora crassa* resulted in reduced growth, defects in SKP stability and protein secretion (Requena et al, 2001; Seiler et al, 1997). In *U. maydis* deletion of conventional kinesin (*kin-1*) causes bipolar growth and remarkably is disturbed in unconventional secretion (Koepke et al, 2011), which might be vesicle-mediated as well (Nickel, 2010).

Besides the SPK hyphae of filamentous fungi posses a polarisome that is comparable to *S. cerevisiae* (Steinberg, 2007a). In *C. albicans* it has been shown, that although some proteins overlap with both structures to a certain degree, SPK and polarisome seem to be distinct from each other, e.g. localisation of the SPK depends on MT integrity wich does not hold true for the polarisome. Notably, SPK formation depends on polarisome integrity (Crampin et al, 2005; Harris, 2006). Thus, the

polarisome might act as a scaffold for the vesicle supply center. The polarisome in filamentous fungi contains key components known from yeast as Cdc42, the Bni1 homologue SepA, Spa2 and Bud6 (Steinberg, 2007a). This suggests a similar role in organising exocyst and exocytosis as described for yeast (Bi & Park, 2012).

Evidence that endocytosis is important for hyphal tip expansion comes mainly from genetic analysis. Mutants in *arfB*, encoding a GTPase regulating endocytic internalisation, show polarity defects in *A. nidulans*. Type I myosins are essential in *A. nidulans* and *C. albicans* and show polarised localisation in hyphae (Penalva, 2010; Steinberg, 2007a). This is supported by the localisation of actin patches at hyphal tips of *N. crassa* and *A. nidulans* (Penalva, 2010) and the tip localisation of Epsin-like protein Ent1 in *U. maydis* (J. König and M. Feldbrügge, unpublished). Interestingly, in *A. nidulans* and *U. maydis* rapid movement of endosomal structures was observed. Since they are stainable with FM4-64 and are positive the GTPase Rab5a they are considered to be early endosomes (EE; Steinberg, 2007a; Penalva, 2010). Interference with the function of molecular motors that transport EEs leads to the aggregation of EEs and hyphae display polarity defects (Penalva, 2010). But if these defects are indeed only due to problems in endocytosis remains open.

At growth cones of different fungal species sterol rich domains (SRD) were identified (Fischer et al., 2008), where they might function in endocytosis (Munn et al, 1999) or they could act in conjunction with lipids and septins to form diffusion barriers and generate platforms for the accumulation of proteins at certain subcellular sites (Saarikangas & Barral, 2011). In *C. albicans* SRDs contribute to hyphal growth (Martin & Konopka, 2004) and notably, mutants in sphingolipid biosynthesis in *A. nidulans* and *U. maydis* causes depolarisation of filipin stained SRDs and results in mislocalised SepA, actin cables and the septin Cdc3 as well as polarity defects (Canovas & Perez-Martin, 2009; Fischer et al, 2008).

### 1.2.3 Septin structure and function

Recently it has become clear that besides the well known cytoskeletal components actin and microtubules, septins play a central role in symmetry breaking and establishment and maintenance of polarity (Lichius et al, 2011; McMurray & Thorner, 2009). Two functions have been described for septins. (i) They act as scaffold by direct binding to e.g. protein kinases. (ii) They form membrane diffusion barriers, e.g. at the base of

dendritic spines or the sperm annulus, thereby restricting localisation of certain integral membrane proteins to different compartments (Saarikangas & Barral, 2011).

Septins are ubiquitous guanine nucleotide-binding proteins that are highly conserved among eukaryotes except plants (Gladfelter, 2010). *In vitro* studies revealed an intrinsic capacity to form octameric rods under high salt conditions. Under low salt conditions they polymerise into filaments (Farkasovsky et al, 2005; Field et al, 1996; Frazier et al, 1998; Versele et al, 2004). The arrangement of septin octamers in *S. cerevisiae* is Cdc11:Cdc12:Cdc3:Cdc10:Cdc10:Cdc3:Cdc12:Cdc11. The interaction between monomers is mediated alternately through G and NC interfaces (Fig. 1-2). The G interface is located in the central GTP-binding domain. The NC interface is generated by a combination of N- and C-terminal positioned regions (Estey et al, 2011). These non-polar octameric rods assemble into filaments via end to end joining (Bertin et al, 2008). Additionally filaments pair into long parallel "railroad tracks" *in vitro* and *in vivo* (Bertin et al, 2008; DeMay et al, 2011). This lateral association appears to be mediated by heterotetrameric coiled-coils between the paired C-terminal extensions of Cdc3 and Cdc12 (Bertin et al, 2008). In *S. cerevisiae* filament formation is crucial for function (McMurray et al, 2011). The filaments can assemble into higher order structures, e.g. collars (hourglass), rings, bars and fibers at sites of cell division and morphogenesis where they act as scaffold or diffusion barrier (Bertin et al, 2008; DeMay et al, 2011; McMurray & Thorner, 2009; Sellin et al, 2011; Sirajuddin et al, 2007).

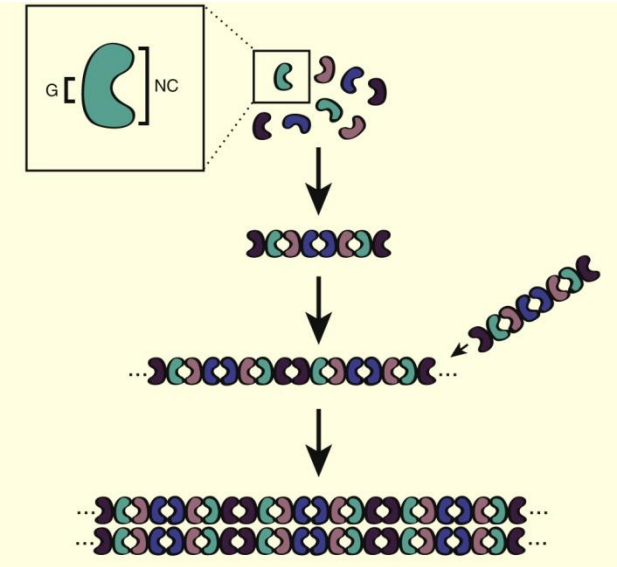


**Fig. 1-2** Jellybeanmodel of septin polymerisation. Four septin-monomers interact alternately via G and NC interfaces to generate octamers. Octamers polymerise into filaments that subsequently pair to form "railroadtracks". (from Estey et al., 2011)

In filamentous fungi septins are important for morphology, persistent hyphal growth and stable polarity axes (Gladfelter, 2006). Consistently, septins localise to hyphal tips and septa. Septin mutants are described to be impaired in chitin deposition (Gladfelter, 2006; Gladfelter, 2010). In *U. maydis* orthologues to the yeast septins Cdc3, Cdc10, Cdc11 and Cdc12 exist (Alvarez-Tabares & Perez-Martin, 2010). During

budding growth, septins localise to the future bud site and remain as collar structure at the bud neck which splits into two rings located at primary and secondary septum of mother and daughter cell, respectively (Alvarez-Tabares & Perez-Martin, 2010; Böhmer et al, 2009). Deletion of all four respective genes causes a temperature-sensitive phenotype. At 28° C budding sporidia show a lemon-shaped morphology and often a central septum is inserted (Alvarez-Tabares & Perez-Martin, 2010). For Cdc3 and Cdc10 localisation in cortical filamentous structures was observed that form parallel to the growth axis (Alvarez-Tabares & Perez-Martin, 2010; Böhmer et al, 2009). The localisation at septa and in filamentous structures could also determined in hyphae, the latter only for Cdc10. Interestingly hyphae grow bipolarly initially after switching to hyphal growth, but change to unipolar growth at later time points (Alvarez-Tabares & Perez-Martin, 2010). Thus septins contribute to polarized growth in *U. maydis* at least in the establishment phase. The information about septin localisation, architecture and posttranslational modification is comprehensive, but the knowledge on molecular trafficking, filament assembly and function during extended polar growth is only scarce.

### 1.3 *U. maydis* as a cell biological model organism

The pathogenic fungus *U. maydis* causes corn smut disease (Vollmeister et al, 2012). Infectious hyphae are formed upon recognition and subsequent mating of yeast like cells that proliferate asexually by budding. The underlying process is basically regulated on two levels. Firstly, two budding sporidia meet and recognise each other via a pheromone – pheromone receptor system, encoded at the biallelic *a* mating-type locus, which leads to the outgrowth of conjugation hyphae (Bölker et al, 1992). After physical contact these hyphae fuse to share a common cytoplasm with two distinct nuclei, each encoding different alleles of a heterodimeric transcription factor encoded at the *b* mating-type locus. An active bWest (bW) / bEast (bE) heterodimer consists of monomers derived from different alleles of compatible mating partners (Kämper et al, 1995). Once this key regulator is formed, it activates a cascade of genes resulting in filamentous growth. This heterokaryotic filamentous cell can be perfectly mimicked by haploid cells which express an active b-heterodimer under control of arabinose or nitrate- inducible promotors (Brachmann et al, 2001). By switching the carbon or nitrogen source hyphal growth can be elicited highly reproducible and synchronous (Brachmann et al, 2001). Hyphae expand at a defined growth cone at the apex and generate regularly spaced sections that include vacuoles by inserting septa thereby

generating characteristic empty sections (Vollmeister et al., 2012). In combination with its excellent genetic and biochemical tractability, *U. maydis* is perfectly suited to study cell biological processes either at the yeast or filamentous stage of growth.

With the release and manual annotation of the genomic sequence of *U. maydis* in the database MUMDB at MIPS ((Kämper et al, 2006); MIPS *U. maydis* database and the Munich information centre for protein sequences, respectively; http://mips.helmholtz-muenchen.de/genre/proj/ustilago/) new possibilities were opened up including efficient reverse genetics, DNA microarrays and proteome-wide approaches (Böhmer et al, 2007; Brachmann et al, 2004; Heimel et al, 2010; Kämper, 2004; Scherer et al, 2006; Zarnack et al, 2008). During the last decade *U. maydis* emerged as a model for studying cytoskeletal components, molecular motors and their cargos (Egan et al, 2012; Steinberg, 2007a; Steinberg, 2007b; Steinberg, 2007c). This became possible in particular through the establishment of various fluorescent proteins, e.g. eGfp and mRfp that give insights into the *in vivo* localization and co-localisation of proteins (Steinberg & Perez-Martin, 2008).

### 1.3.1 Microtubule-based transport

During budding growth microtubules (MT) and their cognate molecular motors, dynein and kinesins, regulate various processes in *U. maydis*. Cytoplasmic dynein, which consists of two subunits Dyn1 and Dyn2, is essential for cell survival. Conditional mutants revealed a role in cell morphogenesis, MT organization and nuclear migration (Fink & Steinberg, 2006; Straube et al, 2001). In addition clustering of nuclear pores in the nuclear membrane is prevented by the action of dynein and conventional kinesin (Kin1). Proper positioning of nuclear pores ensures chromosome organization and efficient import and export of proteins (Steinberg et al, 2012).

While dynein is essential during budding, kinesins are not needed for growth *per se*. In overexpression mutants of Kin1 a small percentage of cells show lateral budding indicating only minor problems in bud site selection (Straube et al, 2003). Deletions in *kin3*, encoding a kinesin-3 type motor, cause loss of the typical bipolar budding pattern of *wt* and additionally show a severe cell seperation defect, which is reflected in tree-like structures on cellular level and doughnut-shaped colonies (Göhre et al, 2012; Wedlich-Söldner et al, 2002). This defect was proposed to be based on failure in delivery of endosomal cargoes like lipids or proteins, since localization of the target-soluble N-ethylmaleimide-sensitive-factor attachment receptor (t-SNARE) Yup1, which marks

Rab5a-positive endosomes at sites of cell separation, was lost in *kin3Δ* (Fuchs et al, 2006; Wedlich-Söldner et al, 2000; Wedlich-Söldner et al, 2002). The *kin3Δ*- phenotype is reminiscent of *don1* and *don3* mutants, encoding a Cdc42 guanine nucleotide exchange factor and a dual-function germinal centre kinase, respectively, which are essential for formation of the secondary septum and subsequent cytokinesis (Böhmer et al, 2008; Weinzierl et al, 2002). Indeed, recently a connection between motor-based transport and targeting of Don1 to sites of cell division had been found (Schink & Bölker, 2009). Don1 carries a C-terminal FYVE domain which couples Don1 to endosomes via specific interaction with phosphatidylinositol-3-phosphate (Kutateladze, 2006; Kutateladze, 2007; Misra et al, 2001; Schink & Bölker, 2009; Simonsen et al, 2001). During early G1-phase, when septa are formed and cell division takes place, bidirectional endosome movement in *U. maydis* is driven by Kin3 and dynein (Steinberg, 2007c; Wedlich-Söldner et al, 2002). Disturbing endosomal targeting of Don1 via mutation of the FYVE domain interferes with Don1 function and leads to the deletion phenotype (Schink & Bölker, 2009). This study is the first example of a functionally important endosomal cargo delivered to sites of cytokinesis during budding growth.

During hyphal growth the function of MT-dependent endosome transport is far less clear. Extensive shuttling of endosomes is observed between the apex and basal pole. MT-dependent endosome transport supports polarized growth (Wedlich-Söldner et al, 2000) and is posited to act in communication of the growth cone with the nucleus whose position is maintained constantly about 40-50 µm behind the growth cone (Steinberg, 2007c). But so far no important cargo has been identified (Steinberg, 2007b). Interfering with motor function by deleting *kin1* or *kin3* leads to bipolar growing hyphae (Schuchardt et al, 2005). A combination of Kin1, Kin3 and dynein drives bidirectional movement of endosomes along the antiparallel MT-cytoskeleton that is only polarized at the apical and basal pole where plus ends are facing towards the poles (Schuster et al, 2011c). Kin1 is only indirectly involved by recycling dynein. Anterograde movement appears to be mediated solely by Kin3, whereas retrograde movement seems to be interplay of Kin3 and dynein (Schuster et al, 2011c). Dynein accumulates in comet-like structures at MT-plus ends which are most prominent at the poles where MTs are polarized (Lenz et al, 2006; Schuster et al, 2011a; Schuster et al, 2011c). Dynein is supposed to mediate retrograde movement in the polarized pole regions and when

entering antiparallel MTs Kin3 takes over to mediate long-range retrograde transport (Schuster et al, 2011c). Since MT-plus ends are also present in antiparallel regions it would not be surprising if retrograde movement by dynein is not restricted to parallel MTs. Interestingly, it has been observed that dynein can also associate with and change direction of endosomes before they arrive at plus ends (Schuster et al, 2011b).

### 1.3.2 RNA-transport

Recently the *U. maydis* RNA-binding protein Rrm4 was identified whose deletion phenotype strongly resembles those of the *kin1* and *kin3* deletion mutants during hyphal growth, namely increased bipolarity (Becht et al, 2006). Rrm4 consists of three RNA recognition motifs (RRM; (Maris et al, 2005)) placed in the N-terminal half and an MLLE domain (previously known as PABC) located at the C-terminus (Becht et al, 2005; Kozlov et al, 2010). A functional C-terminal Gfp-fusion revealed that the protein localises to distinct cytoplasmic particles which shuttle bidirectionally along MTs (Fig. 1-3; Becht et al, 2006). *In vivo* UV-cross-linking (CLIP) experiments demonstrated the RNA-binding capacity of Rrm4 in hyphae which exhibits a more than 6-fold increase in filaments compared to budding sporidia. Since there is no obvious phenoltype during budding growth Rrm4 is most likely only functional during hyphal growth. A mutation in the first RRM domain leads to loss of function which correlates with a reduced RNA-binding rate without interfering with the ability to shuttle along MTs (Becht et al, 2006). The MLLE domain is presumed to mediate protein-protein interactions and might couple Rrm4 to the transport units, since shuttling is completely abolished upon mutation of the MLLE domain (Becht et al, 2006). Deletion of *kin1* results in the accumulation of Rrm4 at the poles of bipolar growing hyphae where MT-plus ends are located. Therefore Kin1 appears to be only indirectly involved in Rrm4 shuttling (Becht et al, 2006).

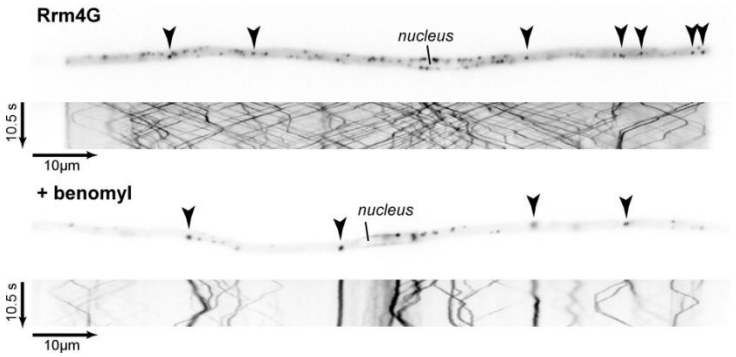


**Fig. 1-3** Filaments expressing Rrm4 fused to Gfp. (A) The fusion protein accumulates in defined cytoplasmic particles (arrow-heads in the inverted image detecting Gfp fluorescence) that shuttle bidirectionally along microtubules (kymograph in the lower part). In the kymograph, time is plotted vs. distance. Thus, motion of Rrm4 particles is visible as defined tracks (note the reversal of shuttling at the poles) (B) Filament as in A treated with MT inhibitor benomyl (from Vollmeister et al., 2012)

## 1.4 Aim of the work

Based on the results obtained by Becht et al., 2006 that the *U. maydis* RNA-binding protein Rrm4 shuttles extensively along microtubules and does indeed bind RNA , the hypothesis arose that Rrm4 is involved in MT-based mRNA transport. This work is intended to shed light on the mechanism of mRNA transport and on functional consequences of mRNA transport on polarised growth. In three interconnected sections different aspects of mRNA transport are addressed.

**Section 2.1** The fungal RNA-binding protein Rrm4 mediates long-distance transport of *ubi1* and *rho3* mRNAs. The aim of this work was to identify Rrm4 target mRNAs and to visualise their subcellular localisation via λN-based RNA live imaging and fluorescent *in situ* hybridisation (FISH). Secondly, we wanted to investigate the contribution of Rrm4 on a potential mRNA localisation.

**Section 2.2** Kinesin-3 and dynein mediate microtubule-dependent co-transport of mRNPs and endosomes. The aim of this section was to uncover the molecular motors that mediate mRNA trafficking and to find out how mRNPs are coupled to molecular motors. To this end the *U. maydis* poly-(A)-binding protein Pab1 was established as a molecular mRNA marker.

**Section 2.3** Endosomal transport of septin mRNA and encoded protein mediates correct septin filamentation. Based on preliminary results that Cdc3 protein localises asymmetrically and moved processively in particles (Dissertation J. König, 2009), we focussed on the transport of septin mRNA *cdc3*. The λN-based RNA live imaging system was improved to visualise endogenous expressed mRNAs. We aimed to uncover a direct link between mRNA transport of a polarity determinant and defects in polar growth. The main questions were (i) is *cdc3* mRNA transported Rrm4 dependently and (ii) does mRNA transport influence protein localisation and finally (iii) where does translation take place?

The results of all three sections contribute considerably to the understanding of microtubule-dependend mRNA transport in *U. maydis* so that a detailed picture of the underlying molecular processes emerges.

# 2 Results

## 2.1 The fungal RNA-binding protein Rrm4 mediates long-distance transport of *ubi1* and *rho3* mRNAs

Julian König*, Sebastian Baumann*, Janine Koepke, Thomas Pohlmann, Kathi Zarnack and Michael Feldbrügge

Max Planck Institute for Terrestrial Microbiology, Department for Organismic Interactions, Karl-von-Frisch-Straße, 35043 Marburg, Germany

* both authors contributed equally to the work

**Running title:** microtubule-dependent RNA transport in fungi

**Key words:** mRNP trafficking / microtubules / plant pathogen / polar growth / ubiquitin

**Characters:** 54753

**Subject category:** RNA / Microbiology & Pathogens

Corresponding author:
Dr. Michael Feldbrügge
Max Planck Institute for Terrestrial Microbiology
Department of Organismic Interactions
Karl-von-Frisch-Straße; 35043 Marburg, Germany
Telephone: +49-6421-178602
Fax: +49-6421-178609
E-mail: feldbrue@mpi-marburg.mpg.de

**Abstract**

Cytoskeletal transport promotes polar growth in filamentous fungi. In *Ustilago maydis*, the RNA-binding protein Rrm4 shuttles along microtubules and is crucial for polarity in infectious filaments. Mutations in the RNA-binding domain cause loss of function. However, it was unclear which RNAs are bound and transported. Here, we applied *in vivo* RNA binding studies and live imaging to determine the molecular function of Rrm4. This new combination revealed that Rrm4 mediates microtubule-dependent transport of distinct mRNAs encoding e.g. the ubiquitin fusion protein Ubi1 and the small G protein Rho3. These transcripts accumulate in ribonucleoprotein particles (mRNPs) that move bidirectionally along microtubules and co-localise with Rrm4. Importantly, the 3' UTR of *ubi1* containing a CA-rich binding site functions as zipcode during mRNA transport. Furthermore, motile mRNPs are not formed when the RNA-binding domain of Rrm4 is deleted, although the protein is still shuttling. Thus, Rrm4 constitutes an integral component of the transport machinery. We propose that microtubule-dependent mRNP trafficking is crucial for hyphal growth introducing *U. maydis* as attractive model for studying mRNA transport in higher eukaryotes.

### 2.1.1 Introduction

Establishment and maintenance of a defined axis of polarity determines growth and shape of filamentous fungi. Hyphae expand at the apical pole and are partitioned by septa that function as molecular barriers (Harris, 2006; Steinberg, 2007a). Apical surface expansion is supported by local exocytosis of transport vesicles containing building blocks and enzymes for the synthesis of membranes and cell walls. A key element involved is the so-called Spitzenkörper that is thought to function as vesicle supply centre containing exocytotic as well as endocytotic vesicles (Fischer, 2007; Harris, 2006). Recently, molecular components of the polarisome such as formins that nucleate actin cables as well as components of the exocyst have been proposed to communicate with the Spitzenkörper (Fischer, 2007; Harris, 2006). In addition, microtubules are associated with the Spitzenkörper suggesting that long-distance transport of molecular cargos is important for polar growth (Harris, 2006; Steinberg, 2007a).

The fungal pathogen *Ustilago maydis* causes corn smut disease (Feldbrügge et al, 2006). A prerequisite for infection is a switch from yeast-like to filamentous growth. This morphological transition is regulated at the transcriptional level by a homeodomain transcription factor encoded at the *b* mating-type locus. The dikaryotic filament grows

with a defined axis of polarity. It expands at the apical pole and inserts retraction septa at the distal pole that confine the cytoplasm to the tip compartment (Feldbrügge et al, 2006).

Recently, we discovered that the RNA-binding protein Rrm4 is needed for rapid polar growth. The protein contains three N-terminal RRMs (RNA recognition motifs) and a C-terminal PABC (poly[A]-binding protein C terminus) domain predicted to function in protein-protein interaction. *rrm4Δ* strains are impaired in filament formation and pathogenicity (Becht et al, 2005). The majority of *rrm4Δ* filaments grow bipolar and few retraction septa are formed indicating that Rrm4 is crucial for determining the axis of polarity (Becht et al, 2006). The protein shuttles in particles along defined cytoskeletal tracks. These were identified as microtubules, since treatment with the microtubule inhibitor benomyl interfered with particle movement and bidirectionally moving Rrm4 particles co-localised with microtubules *in vivo* (Becht et al, 2006). Deletion of the conventional kinesin Kin1 resulted in the formation of bipolar filaments with few retraction septa (Steinberg et al, 1998). In these strains, Rrm4-containing particles accumulate at the poles suggesting that shuttling is of functional importance (Becht et al, 2006). Point mutations in the N-terminal RRM1 domain resulted in loss of function suggesting that RNA binding is essential. *In vivo* UV crosslinking (CLIP; Ule et al., 2003) revealed that Rrm4 binds RNA and that this binding increases during filamentation (Becht *et al*, 2006). These data led to the hypothesis that Rrm4 is involved in microtubule-dependent transport of RNA (Feldbrügge et al, 2008). However, it was unclear which type of RNA is bound by Rrm4 and whether the bound RNA is part of transported particles.

Here, we combine CLIP and the λN-Gfp RNA reporter system (Daigle & Ellenberg, 2007; Ule et al, 2003) to demonstrate microtubule-dependent mRNA transport *in vivo*. We observe that Rrm4 binds a distinct set of mRNAs containing a potential CA-rich binding site. Target mRNAs accumulate in Rrm4-dependent mRNPs and these particles shuttle along microtubules. Importantly, the mRNA particles co-localise with Rrm4 *in vivo*, and removal of RRMs in Rrm4 causes loss of motile particles, while the protein is still shuttling. Thus, Rrm4 is not simply hitchhiking but functions as integral part of the mRNA transport machinery.

### 2.1.2 Results

*The poly(A)-binding protein co-localises with Rrm4 in moving particles*

According to our working model Rrm4 mediates transport of mRNA in filaments. Since it is generally accepted that the poly(A)-binding protein associates with most if not all poly(A) tails of eukaryotic mRNAs (Hogan et al, 2008), it can be used as molecular marker to investigate the subcellular localisation of mRNAs. Pab1 from *U. maydis* exhibits the characteristic domain structure of four RRMs in combination with a C-terminal PABC domain (um03494; 651 amino acids; MUMDB, http://mips.gsf.de/genre/proj/ustilago/; 47% SIMAP identity to ScPab1 from *Saccharomyces cerevisiae*, similarity matrix of proteins; (Rattei et al, 2006)). For verification of Pab1 function we expressed fluorescently tagged versions in a strain from *S. cerevisiae* carrying the mutated allele *pab1-53*$^{ts}$. This strain exhibited a temperature-sensitive growth phenotype. Expression of fluorescently tagged proteins was confirmed by fluorescence microscopy (Supplementary Fig. 1). The reduced growth rate at 28 °C was complemented by expression of the poly(A)-binding protein Pab1 from *S. cerevisiae* (ScPab1) as well as by fluorescently tagged Pab1G and Pab1R from *U. maydis* (Pab1 fused at the C terminus to eGfp, enhanced version of the green fluorescent protein, Clontech, and mRfp, monomeric form of the red fluorescent protein, respectively; (Campbell et al, 2002); Fig. 1A). Thus, Pab1 from *U. maydis* functions as poly(A)-binding protein in *S. cerevisiae* and a C-terminal fusion to fluorescent proteins does not interfere with its function.

Moreover, Rrm4G (Rrm4 fused at the C terminus to eGfp; Becht et al., 2006) was not able to complement temperature-sensitive growth, indicating that it cannot function as poly(A)-binding protein, although it contains a similar domain architecture (three N-terminal RRMs and a C-terminal PABC domain).

To analyse the subcellular localisation of Pab1 in *U. maydis* we generated a Pab1G-expressing strain by substituting the wildtype copy of strain AB33 by homologous recombination using an SfiI-mediated gene replacement system (Brachmann et al., 2004; see Materials and methods). AB33 is a derivative of wildtype strain FB2 that contains an active bW2/bE1 heterodimeric transcription factor under control of the nitrate-inducible promoter $P_{nar1}$. Thereby, b-dependent filamentation can be elicited by changing the nitrogen source in the medium (Becht et al., 2006; Brachmann et al., 2001).

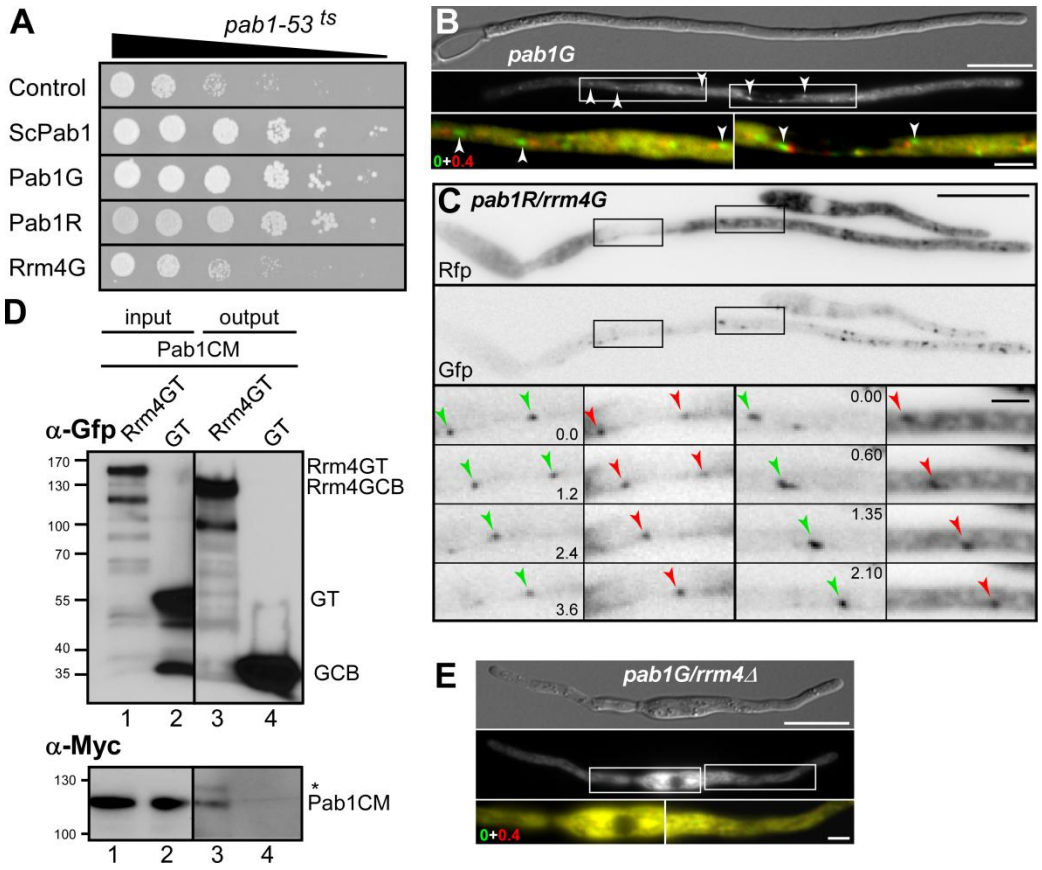


**Figure 1** Pab1 and Rrm4 co-localise in shuttling particles. (**A**) Growth of *S. cerevisiae* strain HKY171 carrying the mutation *pab1-53*$^{ts}$ conferring reduced growth at 28 °C. Proteins expressed are indicated on the left (black triangle, tenfold serial dilutions). (**B**) Filament of AB33pab1G. Rectangles indicate regions that are magnified below. Frames are taken from Supplementary Video 1 (upper part). To document motility of particles, overlays of two frames that are 0.4 s apart and coloured in red and green are shown. Arrowheads indicate moving particles (upper and lower size bar, 10 and 2 µm, respectively). (**C**) Filament of AB33pab1R/rrm4G. Inverted frames are taken from Supplementary Video 2 recorded with dual-colour detection. Simultaneous Gfp and Rfp images are shown juxtaposed. Red and green arrowheads mark Pab1R-and Rrm4G-containing particles, respectively. Elapsed time in seconds is indicated (size bar, 10 µm). (**D**) Western blots after tandem affinity purification of Rrm4GT or GT. Input fraction (after mechanical destruction of filaments) and output fraction (after TEV protease cleavage and second affinity purification step) are shown on the left and right, respectively. In the upper and lower part, proteins (given on the right) were detected using α-Gfp and α-Myc antibodies (size marker in kD on the left; *, note that α-Myc incubation detects residual amounts of Rrm4GT due to the protein A domain). (**E**) Filament of AB33pab1G/rrm4Δ (labelling as in B; size bar, 10 µm; frames of Supplementary Video 1, lower part).

In filaments grown for four hours under inducing conditions, Pab1G displayed a predominantly cytoplasmic localisation reflected by negative staining of the nucleus. In addition to the dispersed cytoplasmic distribution, the fusion protein accumulated in particles that moved bidirectionally along distinct tracks within filaments (Fig. 1B; Supplementary Video 1). Particle movement was inhibited in the presence of the microtubule inhibitor benomyl (50 µM for 20 min, data not shown) indicating that these particles travelled on microtubules in a similar way as Rrm4-containing particles (Becht et al., 2006). In order to test whether Pab1 and Rrm4 accumulated in the same particles,

we generated an AB33 derivative expressing Pab1R as well as Rrm4G by replacing the wildtype copy of each gene at the homologous loci. *In vivo* localisation was analysed simultaneously by recording time-lapse videos using dual-colour detection (see Materials and methods). This revealed that eGfp- and mRfp-containing particles followed the same trajectory indicative for co-localisation of Pab1R and Rrm4G in the same transport unit (97% of Rrm4G-containing particles co-localised with Pab1G-containing particles, 336 out of 347 particles, 10 videos; Fig. 1C; Supplementary Video 2).

For biochemical verification we generated an AB33 derivative expressing Rrm4GT and Pab1CM (Rrm4 fused at the C terminus to eGfp as well as Tap tag and Pab1 fused to the mRfp derivative mCherry as well as triple Myc epitope tag, respectively (Becht et al, 2006; Evan et al, 1985; Shaner et al, 2004). AB33GT/Pab1CM was used as control strain expressing eGfp-Tap tag under control of the *rrm4* promoter (translational fusion to 28 aa of Rrm4; see Materials and methods). After two rounds of affinity purification and TEV protease cleavage, Rrm4GCB and GCB (Gfp-calmodulin-binding domain) were detected using α-Gfp antibodies (Fig. 1D, upper panel, lane 3 and 4, respectively). Detection with α-Myc antibodies revealed that Pab1CM co-purified with Rrm4GCB but not with GCB (Fig. 1D, lower panel, lane 3 and 4, respectively).

By deleting *rrm4* in AB33pab1G, we addressed whether particle formation of Pab1G was dependent on Rrm4. Filaments grown for four hours under inducing conditions exhibited the characteristic loss-of-function phenotype of *rrm4Δ* strains, i.e. filaments failed to insert empty sections and a significant number of filaments grew bipolar (Fig. 1E). Recording time-lapse videos revealed that Pab1G-containing particles were undetectable (Fig. 1E; Supplementary Video 1). In addition, the cytoplasmic distribution of Pab1G was altered in *rrm4Δ* strains (Fig. 1A, E). While in AB33pab1G the fluorescence signal of Pab1G at the perinuclear region was only slightly higher compared to the growing pole, this ratio increased significantly in the absence of Rrm4 (the ratio of average fluorescent intensity in a defined perinuclear region and at the pole was 1.4 [+/- 0.01, s.e.m.] in AB33pab1G versus 2.8 [+/- 0.09, s.e.m.] in AB33pab1G/rrm4Δ; 45 filaments analysed, $n = 3$; $p < 0.005$ by paired two-tailed *t*-test). This indicated that Rrm4 is required for the distribution of mRNA-binding Pab1G. Thus, Rrm4-containing particles constitute the main unit for microtubule-dependent transport of mRNAs in filaments.

*Rrm4 binds distinct mRNAs in vivo during filamentous growth*

Previously, we applied CLIP (Ule et al., 2003) to demonstrate that Rrm4 binds RNA *in vivo* (Becht et al., 2006). Here, we followed an extended CLIP protocol to identify Rrm4 targets by purification of covalently bound RNA. AB33rrm4GT filaments grown for six hours under inducing conditions were treated with doses of UV-C irradiation that resulted in the formation of covalent bonds between RNA and protein (Becht et al., 2006; Ule et al., 2003). Rrm4GT was affinity purified and covalently bound RNA was radioactively labelled (see Materials and methods; Fig. 2A). In control experiments, we omitted UV-C irradiation or applied more stringent RNase T1 treatment (Fig. 2A). Bound RNA was reverse transcribed and the resulting cDNA CLIP tags were PCR amplified, cloned and sequenced (see Materials and methods). Sequence analyses of two independent experiments revealed 78 unique sequences. Their length ranged from 19 to 193 nucleotides (nt) with an average of 72 nt. Comparison with the genome sequence revealed that the CLIP tags corresponded to 61 genomic loci (Supplementary Table I; MUMDB; Kämper et al., 2006). In six cases, we identified overlapping sequences in two subsequent experiments indicating independent cloning events. All but six genomic loci comprised predicted transcribed regions of protein-coding genes strongly suggesting that the covalently bound RNAs corresponded to mRNA (Supplementary Table I). Two CLIP tags corresponded to the 5' untranslated region (UTR), 22 to the open reading frame, and 31 to the 3' UTR. In none of the cases, intron sequences were identified, while in three cases sequences spanned exon-exon borders.

Applying the pattern search algorithm MEME (Bailey et al, 2006) a CA-rich consensus sequence was identified as the only common motif within the dataset (Fig. 2B). This 21 nt motif was found in 36% of the sequences suggesting that Rrm4 recognises CA-rich sequences. Visual inspection of the remaining mRNAs revealed that many CLIP tags carry partially similar CA-rich sequences e.g. um04628, um11097, and um1162 (Supplementary Table I) indicating the presence of degenerated motifs. Gene ontology analysis revealed a significant enrichment of the identified genes within six functional categories (Fig. 2C; http://mips.gsf.de/projects/funcat; Ruepp et al, 2004).

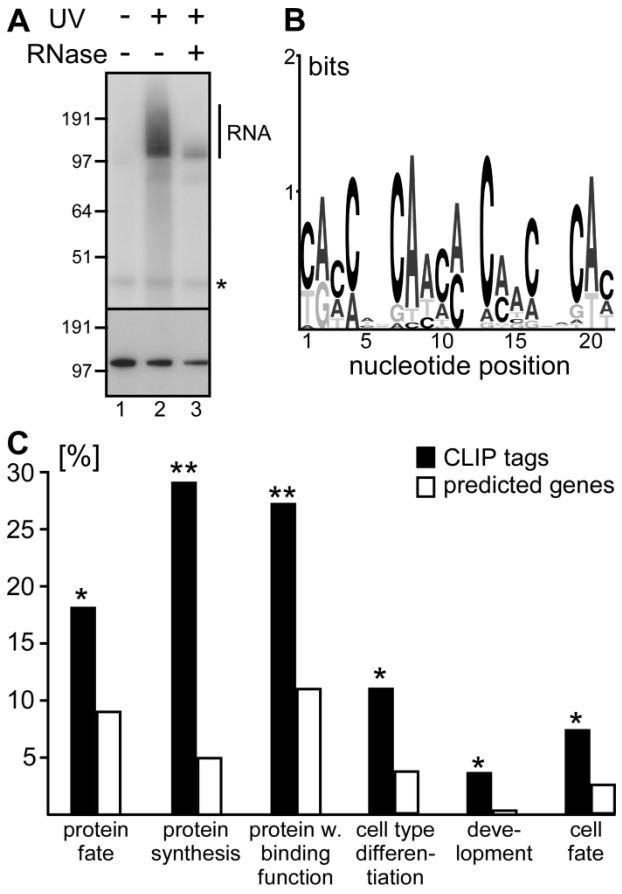


**Figure 2** Rrm4 binds distinct mRNAs containing a CA-rich motif. (**A**) CLIP analysis of AB33rrrm4GT filaments. Covalently bound RNA is detected as radioactively labelled protein-RNA complexes that are larger in size than Rrm4GT (117 kD after TEV cleavage; size markers on the left; asterisk, unspecific band). UV-C irradiation and RNase T treatment is indicated above the lanes. Equal loading was verified by Western blot using α-Gfp antibodies on the same membrane (bottom). (**B**) Graphic representation of the CA-rich consensus sequence. The height of each column represents the level of conservation, the relative height of each letter depicts its frequency at the respective position (Crooks et al, 2004). (**C**) Graph indicating significant enrichment of Rrm4 target genes (black bars) within the respective functional categories (Ruepp et al, 2004) relative to the frequency within the genome (white bars). One or two asterisks symbolise p value of enrichment <0.05 or <0.01, respectively (p values were determined using hypergeometric distribution, Ruepp et al, 2004).

In particular, the overlapping categories "cell type differentiation", "development" and "cell fate" were consistent with a potential role of Rrm4 target mRNAs during filament formation. 16 (29%) of the identified genes encoded novel proteins without functional annotation.

The most prominent target sequences were derived from the *ubi1* transcript encoding a fusion protein between ubiquitin and the ribosomal protein Rpl40. We found 13 overlapping CLIP tags. The predicted transcript carries 17 direct CA repeats in its 3' UTR. Other targets that might relate to polar growth encoded for the small G protein Rho3, the septin Cdc3 and the epsin Ent1 containing an ubiquitin interaction motif (Boyce et al, 2005; Weinzierl et al, 2002). We also noted the presence of four mRNAs encoding mitochondrial proteins. In summary, Rrm4GT binds a distinct set of mRNAs *in vivo* that carry CA-rich motifs as potential binding sites.

*rho3 mRNA accumulates in Rrm4-dependent particles*

In order to analyse the subcellular localisation of potential mRNA targets of Rrm4, we performed fluorescent *in situ* hybridisation (FISH) experiments using *rho3* as example. Filaments were grown for 4 hours under inducing conditions and fixed with

formaldehyde. For mRNA detection, fluorescently labelled DNA oligonucleotides were directed against *egfp* or *rho3* mRNA (see Materials and methods).

In AB33, hybridisation with *rho3* probes revealed a punctuated staining of *rho3* mRNA particles throughout the cytoplasm (Fig. 3A). Although the background signal was increased in the initial cell most likely due to the larger cell volume in this region, no subcellular accumulation or mRNA gradient e.g. at the poles of filaments were detected. To increase signal intensity, we generated strain AB33P$_{otef}$rho3G expressing Rho3 fused at the N terminus to eGfp under control of the strong constitutively active promoter P$_{otef}$ (Brachmann et al, 2004). Quantitative PCR confirmed that mRNA amounts of *rho3* were elevated ca. 28fold compared to AB33 (Fig. 3C). Hybridisation using either *rho3* probes or a mixture of *rho3* and *egfp* probes revealed the same qualitative staining pattern as seen in AB33 (data not shown or Fig. 3A, respectively). Since the number of mRNA particles detected strongly increased (Fig. 3A), we inferred that

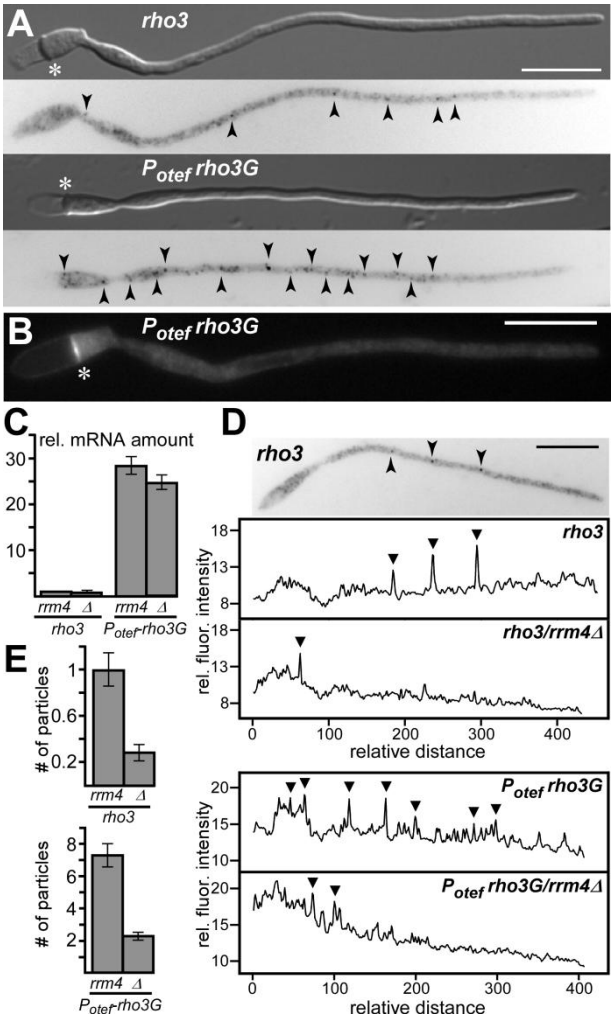


**Figure 3** FISH reveals accumulation of *rho3* mRNA in Rrm4-dependent particles. (**A**) Fixed filaments of AB33 and AB33P$_{otef}$rho3G (upper and lower part, respectively). Inverted pictures were obtained after FISH analysis with probes directed against *rho3* as well as *rho3* and *gfp* (upper and lower part, respectively). mRNA particles (filled arrowheads) and septa (asterisks) are highlighted (size bar, 10 µm). (**B**) Epiflourescence image of strain AB33P$_{otef}$rho3G (asterisk, septum; size bar, 10 µm). (**C**) Quantitative real-time PCR showing that the relative amount of *rho3* and *rho3G* mRNA is not altered in *rrm4Δ* strains (the relative amount in AB33 [*rrm4*/*rho3*] was set to 1; error bars, s.d.). (**D**) PIA analysis of FISH-treated filaments of AB33 and AB33P$_{otef}$rho3G as well as respective *rrm4Δ* strains. Image example of AB33 analysed with *rho3* probes (inverted image labelled as in A) followed by the corresponding fluorescence intensity graph. Exemplary graphs of filaments of strains AB33rrm4Δ as well as AB33P$_{otef}$rho3G and AB33P$_{otef}$rho3G/rrm4Δ are given below. Relative fluorescence signals were plotted against the longitudinal axis of filaments (relative distance, rear pole was set to 0). Detected peaks are indicated by filled arrowheads (see Materials and methods). (**E**) Bar diagram of mean particle numbers determined by PIA analysis. Particles were quantified in AB33 and AB33P$_{otef}$rho3G (upper and lower part, respectively) as well as respective *rrm4Δ* strains (as labelled below; error bars, s.e.m., n >= 3)

the probes are specific. Analysing the subcellular localisation of Rho3G protein revealed that the fusion protein accumulated at retraction septa. Thus, Rho3 might play a role in septum formation (Fig. 3B).

In order to investigate, whether the formation of *rho3* mRNA particles was dependent on Rrm4, we quantified the amount of *rho3* mRNA particles in AB33 and AB33$P_{otef}$rho3G as well as in respective *rrm4Δ* strains. For better comparison, FISH experiments were carried out investigating unipolarly growing filaments of comparable length. To enable objective detection and statistical evaluation we quantified peaks in two-dimensional line scans derived from microscopic images using a specifically designed peak-identifying algorithm (PIA, Fig. 3D; see Materials and methods, algorithm by K. Zarnack, J. König and M. Feldbrügge to be published elsewhere).

Analysing at least 130 filaments revealed that on average 1 and 7.3 *rho3* mRNA particles were detected in AB33 and AB33$P_{otef}$rho3G (n = 3 and n = 4, respectively). In both cases, deletion of *rrm4* did not influence the amount of *rho3* mRNA (Fig. 3C). Importantly, the loss of Rrm4 led to a significant reduction in particle formation (p value $< 0.05$ and $< 0.01$, respectively; according to paired, two-tailed *t*-test; Fig. 3E).

In summary, FISH experiments revealed that the potential Rrm4 target mRNA *rho3* accumulated in cytoplasmic mRNA particles. Formation of particles was significantly reduced in the absence of Rrm4.

*ubi1 and rho3 mRNAs move on microtubules within filaments*

In order to investigate the potential dynamic movement of Rrm4 target mRNAs, we applied RNA live imaging based on a modified version of the λN-Gfp RNA reporter system (Daigle & Ellenberg, 2007). We used a short peptide derived from the phage protein λN fused to triplicate eGfp repeats ($\lambda NG^3$) and its 15 nt minimal recognition hairpin, termed boxB. $\lambda NG^3$ was expressed under control of the arabinose-regulated promoter $P_{crg1}$ (Fig. 4A). The corresponding gene was integrated at the defined *ip* locus of strain AB33 by homologous recombination resulting in strain SB1 (Brachmann et al, 2001). As first mRNA we chose the most prominent target *ubi1* and inserted 16 boxB sequences downstream of the CA-rich region in the 3' UTR (*ubi1_B*; Fig. 4A).

The transgene was inserted at the homologous locus replacing the wildtype allele (see Materials and methods). Southern blot analysis of the resulting strain SB1ubi1_B revealed that all transformants carried multiple insertions of the construct. Apparently, transformants with single homologous insertion events exhibited a reduced fitness. A

possible explanation is that the boxB repeats in the 3' UTR interfered with the expression of the most likely essential gene *ubi1*. Thus, multiple copies of the boxB-containing transcript might compensate for reduced expression.

For the analysis of particle movement *in vivo*, we recorded time-lapse videos analysing strain SB1ubi1_B that was grown for seven hours under filament-inducing conditions (see Materials and methods). Three distinct classes of $\lambda NG^3$-labelled RNA particles were observed: i) particles that remained stationary (termed static particles), ii) those that moved significantly, but without directionality (< 0.75 µm in any single direction; termed stochastically moving particles), and iii) particles that moved in a distinct direction for more than 0.75 µm (termed directed particles; Fig. 4B, C; Supplementary Video 3). The average number of directed particles containing *ubi1_B* mRNA per filament was 7.1 that covered an average distance of 5.5 µm (Fig. 4D; 29 filaments analysed, n = 3). These particles moved with an average velocity of 1.65 µm/s, which was within the same range as transport of Rrm4-containing particles (Becht et al, 2006). In control strain SB1, hardly any directed particles were observed indicating that formation of particles was dependent on the presence of boxB binding sites (one particle in 30 filaments, n = 3).

Treatment with CCCP (carbonyl cyanide m-chlorophenyl-hydrazone; 100 µM; Becht et al, 2006), an uncoupler of the oxidative chain that depletes the cytosolic ATP pool, revealed a drastically reduced number of directed *ubi1_B* particles indicating that these depended on active transport. Remaining particles also covered shorter distances (Fig. 4D). A comparable reduction in particle number and covered distance was also observed during benomyl treatment (Fig. 4D) consistent with microtubule-dependent formation and transport of particles. In contrast, motion of stochastically moving particles was not affected indicating that their movement was not driven by ATP.

For verification and comparison to our FISH data, we chose *rho3* as a second target of Rrm4. Since pilot experiments revealed that *rho3_B* expression was not sufficient for detection, we generated an allele expressing *rho3_B* under control of the constitutively active promoter $P_{otef}$ (Brachmann et al, 2004). The corresponding construct was either used to replace the wildtype allele by homologous recombination or to insert the transgene ectopically (strains SB1rho3_B* or SB1rho3_B, respectively). The latter was important for selection of transformants that expressed *rho3_B* at comparable levels as control strains (see below). As control transcript, we inserted 16

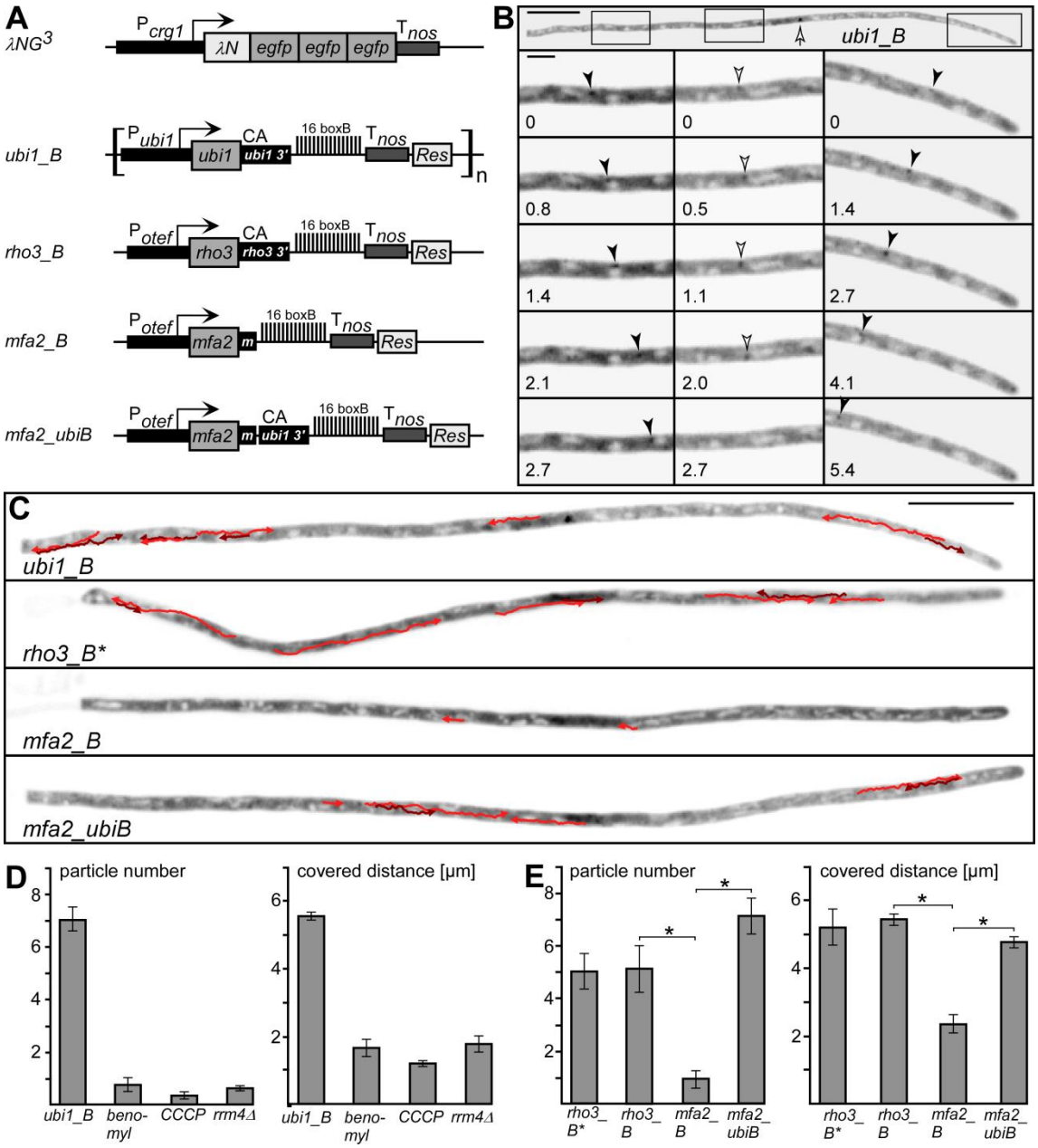


**Figure 4** λN-Gfp RNA reporter system reveals microtubule-dependent transport of *ubi1* and *rho3* mRNAs. (**A**) Schematic representation of the constructs used for the adapted version of the λN-Gfp RNA reporter system. Top: the arabinose-regulated promoter $P_{crg1}$ drives expression of a fusion protein consisting of the λN peptide (amino acid 2-22) fused to eGfp in triplicate (bent arrow = transcriptional start); $T_{nos}$ = heterologous transcriptional terminator of the nopaline synthase gene from *Agrobacterium tumefaciens* (Zarnack et al, 2006). Bottom: constructs carry 16 copies of the λN binding site boxB inserted in the 3' UTR (CA = CA-rich sequence; ubi1 3' = 311 nt fragment of the 3' UTR; rho3 3' = 159 nt fragment of the 3' UTR; m = 40 nt fragment of the *mfa2* 3' UTR; Res = resistance cassette; brackets = presence of multiple copies of the transgene in *ubi1_B*-containing strains). (**B**) Filament of SB1ubi1_B. Inverted frames are taken from Supplementary Video 3. Rectangles indicate regions that are magnified below. Arrow in upper panel indicates a static particle (top), open arrowheads show a stochastically moving particle, and filled arrowheads point towards directed particles (lower panels). Elapsed time is given in the left corner (upper and lower size bars, 10 and 2 µm, respectively). (**C**) Filaments of SB1 derivatives expressing different boxB-containing mRNAs. Inverted frames are taken from Supplementary Video 2 and 3 (*ubi1_B, rho3_B** and *mfa2_B, mfa2_ubiB*; respectively). Movement of directed particles is tracked by red arrows (dark and bright colours are used in regions of overlap). (**D**) Graphs representing the average particle number and the average distance covered by particles. Treatment with inhibitors benomyl and CCCP as well as deletion of *rrm4* was performed using strain SB1ubi1_B ( ≥29 filaments

analysed, n = 3; error bars, s.e.m.; p < 0.001, ANOVA test compared to ubi1_B). (**E**) Graphs with labelling as in D. For strains generated by ectopic insertion of the boxB-containing transgenes (*rho3_B*, *mfa2_B*, and *mfa2_ubiB*) the results of two independent transformants were combined (>60 filaments; n = 6; error bars, s.e.m.; asterisk, p < 0.005; by paired, two-tailed *t*-test).

boxB sequences in the 3' UTR of *mfa2* encoding mating pheromone a2 (*mfa2_B*). To address the question whether the CA-rich region might function as RNA zipcode, we inserted the CA-rich 3' UTR of *ubi1* in *mfa2_B* (Fig. 4A; *mfa2_ubiB*). Both alleles were placed under control of the constitutively active promoter $P_{otef}$ and the constructs were inserted ectopically (strains SB1mfa2_B and SB1mfa2_ubiB). To exclude an influence of expression strength on particle formation we selected a set of six transformants (two for each boxB-containing transcript; *rho3_B*, *mfa2_B*, and *mfa2_ubiB*) that expressed the transgenes at comparable levels according to Northern blot experiments (data not shown).

Recording time-lapse videos of strain SB1rho3_B* or SB1rho3_B after 15 hours under filament inducing conditions (see Materials and methods) revealed the same three classes of particles as observed for *ubi1_B*: static, stochastically moving and directed particles (Fig. 4C, E; Supplementary Video 3). However, in strains expressing the *mfa2_B* control transcript only few directed particles were observed and these covered only short distances (Fig. 4C, E; Supplementary Video 4). Importantly, *mfa2_ubiB* transcripts that carried the CA-rich 3' UTR of *ubi1* formed seven times more directed particles than control transcripts *mfa2_B*. These particles covered similar distances as *rho3_B*-containing particles (Fig. 4C, E; Supplementary Video 4). These data indicate that Rrm4 targets preferentially accumulate in microtubule-dependent particles and that the CA-rich 3' UTR of *ubi1* is sufficient to promote recruitment in directed particles.

*ubi1 mRNA and Rrm4 co-localise in directed particles in vivo*

In order to answer the question whether *ubi1* mRNA co-localised with Rrm4 in directed particles, we generated strain SB1ubi1_B/rrm4R expressing a functional fusion protein of Rrm4 and C-terminal mRfp at the homologous locus (Becht et al, 2006). Filament formation was induced for at least 12 hours and *in vivo* localisation was analysed simultaneously. We observed that $\lambda NG^3$-labelled *ubi1_B* mRNA and Rrm4R particles followed the same trajectory (Fig. 5) indicating that *ubi1* mRNA and Rrm4 co-localised in microtubule-dependent particles *in vivo*. The number of directed *ubi1_B* particles was smaller than the number of Rrm4R particles. Thus, *ubi1* mRNA might either not be

present in all Rrm4 particles or the amounts of *ubi1* mRNA in some particles are insufficient for detection. In summary, we demonstrated that the endogenous *ubi1* target mRNA and the RNA-binding protein Rrm4 are part of the same microtubule-dependent transport unit *in vivo*.

*Formation of directed particles containing ubi1 mRNA depends on Rrm4*

In order to investigate whether formation of the *ubi1_B* particles depended on Rrm4, we deleted *rrm4* in strain SB1ubi1_B. The resulting deletion strain exhibited the loss-of-function phenotype of *rrm4Δ* strains (Becht et al, 2006). Time-lapse videos of filaments grown for seven hours under inducing conditions revealed the formation of static and stochastically moving particles (Fig. 6A, Supplementary Video 5). However, the number of directed *ubi1_B* particles was drastically reduced and the remaining particles covered only short distances (Fig. 4D). Thus, consistent with our FISH results, Rrm4 was crucial for the formation of directed particles. We also noticed that the amount of stochastically moving particles was enriched in the region around the nucleus in comparison to the filament poles (Supplementary Video 5), indicating that the distribution of *ubi1_B* transcripts was disturbed in the absence of directed particles.

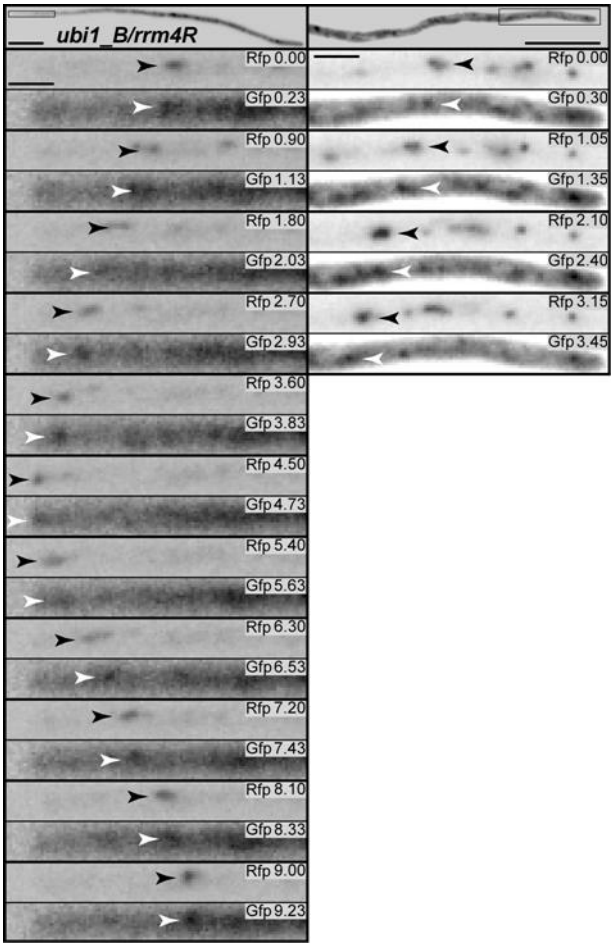


**Figure 5** Rrm4 and *ubi1* mRNA are part of directed mRNPs *in vivo*. Filaments of SB1ubi1_B/rrm4R 20 hours (left) and 12 hours (right) after induction. Inverted frames are taken from time-lapse video recorded with excitation filters on a spinning wheel. Black and white arrowheads indicate Rrm4R- and *ubi1_B* mRNA-containing ($\lambda NG^3$-labelled) particles, respectively. Elapsed time in seconds is given on the right. Exposure times were 225 ms (left) and 300 ms (right). Switching excitation filters from red to green fluorescence was faster than the reciprocal switch due to the experimental set-up (see Materials and methods; size bars, 10 µm).

*Rrm4 is an integral part of the ubi1 mRNA transport machinery*

For further investigation of the role of Rrm4 during mRNA transport, we genetically dissected its RNA binding function from the capacity of microtubule-dependent protein shuttling. To this end we generated strain SB1ubi1_B/rrm4$^{\Delta RRM}$R expressing an Rrm4 variant with a deletion from aa 18 to 499 resulting in the removal of all three RRMs. This truncated version still contained the C-terminal PABC domain that is necessary for microtubule-dependent shuttling of Rrm4 (Becht et al, 2006).

Microscopic analysis of filaments grown for seven hours under inducing conditions revealed that the strain displayed the loss-of-function phenotype, reflected by an increased amount of bipolar cells and hardly any retraction septa. Although the cytoplasmic staining was slightly increased, Rrm4$^{\Delta RRM}$R-containing particles still shuttled along microtubules comparable to the full length protein (Fig. 6B; Supplementary Video 6). Importantly, the number of directed *ubi1_B* particles was drastically reduced and the remaining particles covered only short distances (number of particles in SB1ubi1_B/rrm4$^{\Delta RRM}$R and SB1ubi_B/rrm4R = 0.2 +/- 0.03 s.e.m. and 4.2 +/- 0.3 s.e.m., respectively; covered distance 1.8 µm +/- 0.07 s.e.m. and 5.2 µm +/- 0.1 s.e.m.; p

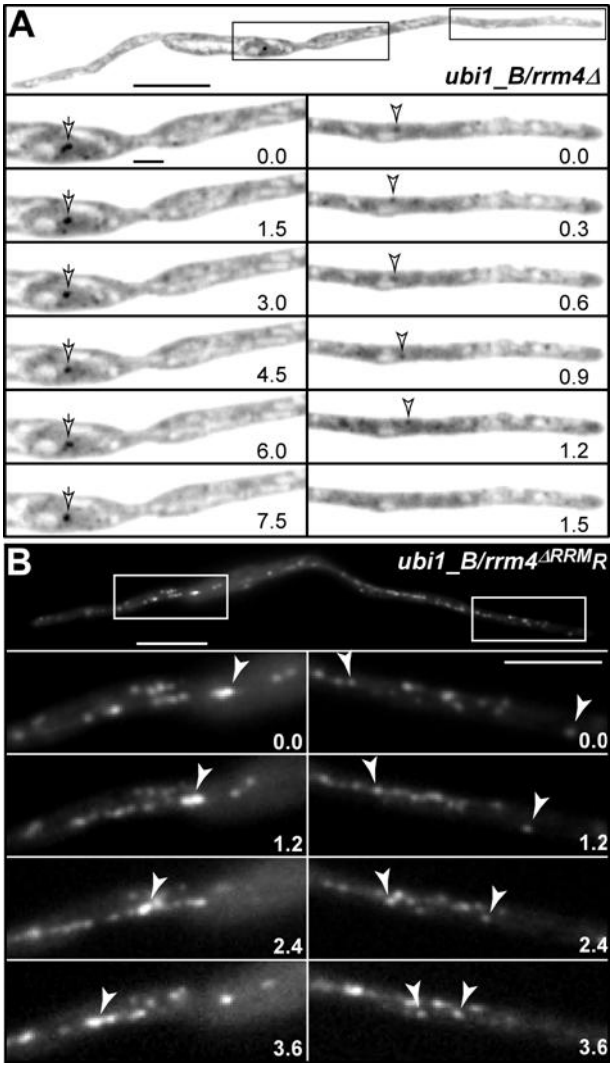


**Figure 6** Rrm4 is required for the formation of directed *ubi1_B* mRNA particles. (**A**) Filament of SB1ubi1_B/rrm4Δ. Inverted frames are taken from Supplementary Video 5. Rectangles indicate regions that are magnified below. Arrows show a static particle (left) and open arrowheads point towards a stochastically moving particle (right). No directed particles are detectable. Elapsed time is given on the right (upper and lower size bars, 10 and 2 µm, respectively). (**B**) Filament of SB1ubi1_B/rrm4$^{\Delta RRM}$R. Frames are taken from Supplementary Video 6 (upper part, labelling as in A). Rrm4$^{\Delta RRM}$R-containing particles that are moving bi-directionally along microtubules are indicted by white arrowheads (note that no directed *ubi_B* mRNA-containing particles are detectable, see Supplementary Video 6, lower part).

< 0.01 and 0.005, respectively, according to paired, two-tailed *t*-test, 30 filaments per strain, n = 3). Reminiscent with *rrm4Δ* strains, the formation of static and stochastically moving particles was still observed (Supplementary Video 6). Hence, mRNA transport was lost, although Rrm4 was still able to shuttle along microtubules. This indicated that Rrm4 is not simply hitchhiking as an mRNA-associated component but rather constitutes an integral part of the mRNA transport machinery.

### 2.1.3 Discussion

Combining CLIP, FISH and RNA live imaging revealed that Rrm4 is the key RNA-binding protein involved in microtubule-dependent transport of distinct mRNAs. Initially, we demonstrated that loss of Rrm4 resulted in drastically reduced formation of particles containing poly(A)-binding protein Pab1. Since this type of protein binds the poly(A) tails of most if not all mRNAs (Hogan et al, 2008), we conclude that Rrm4-containing mRNP particles are the main mRNA transport unit in filaments. The reduction of particles correlated with defects in filamentation. Elucidating the molecular connection between long-distance transport of mRNAs and determination of polarity will be one of the most important challenges for future experiments. At present, key RNA-binding proteins mediating mRNA transport are only known in few cases, e.g. She2p in *S. cerevisiae* and Staufen in *Drosophila melanogaster* (Martin & Ephrussi, 2009).

*Rrm4 recognises distinct mRNAs in vivo*

Previous attempts to discover Rrm4 targets applying SELEX and the yeast three-hybrid system failed to identify essential targets (König et al, 2007). Thus, we applied the CLIP technique that was established to investigate the RNA-binding capacity of mammalian splice regulator Nova (Ule et al, 2003). The strength of CLIP is the *in vivo* formation of irreversible covalent bonds between RNAs and the protein of interest, allowing rigorous purification schemes (Ule et al, 2005). The Tap tag enabled binding of the purified Rrm4 protein to solid beads for further enzymatic steps (Becht et al, 2006; Ule et al, 2005). Our CLIP analysis identified more than 50 candidate target mRNAs of Rrm4. The vast majority of mRNAs were only found once implying that future approaches such as high-throughput sequencing of CLIP-isolated RNAs will reveal additional target sequences (HITS-CLIP; (Licatalosi et al, 2008; Wang et al, 2009; Yeo et al, 2009)).

According to transcriptome-wide expression profiles of b-dependent filaments (J. Kämper, unpublished data), the target mRNAs comprised abundant but also scarce mRNAs e.g. *ubi1* and *rho3*, respectively. *ubi1* mRNA was identified 13 times suggesting that this highly expressed mRNA is heavily transported. Consistently, it contains an extended CA-rich region (see below).

The proteins encoded by putative Rrm4 target mRNAs were enriched in distinct functional categories implicated for example in development and cell fate. Bioinformatics revealed a CA-rich consensus sequence indicating a potential binding site of Rrm4. The assumption that CA-rich sequences are recognised by Rrm4 was strengthened by our observation that the CA-rich 3' UTR of *ubi1* functioned as zipcode during Rrm4-dependent mRNA transport. In comparable approaches analysing the mammalian splice regulators Nova and hnRNP A1, CLIP tags also contained the binding site of the respective protein (Guil & Cáceres, 2007; Ule et al, 2003). Interestingly, CA-containing motifs have previously been described to mediate mRNA localisation in neurons (Andken et al, 2007) and function as splice enhancer elements in animals that are specifically recognised by the RRM splice regulator hnRNP L (Hui et al, 2005).

*Target mRNAs accumulate in Rrm4-dependent particles*

In order to validate our CLIP analysis, we established FISH and RNA live imaging. FISH is a powerful *in situ* technique that was e.g. recently applied to demonstrate that ca. 70% of all analysed genes encode subcellularly localised mRNAs in *D. melanogaster* (Lécuyer et al, 2007). Our approach revealed that *rho3* mRNA accumulated in cytoplasmic particles. In the absence of Rrm4, particle numbers decreased significantly, consistent with the notion that *rho3* mRNA is a target of Rrm4. Overexpression of *rho3G* mRNA also demonstrated Rrm4-dependent particle formation. Moreover, the increased expression resulted in more mRNA molecules being incorporated into particles indicating that the amount of *rho3* mRNA in these particles is not saturated at wildtype expression levels.

Apparently, the absence of Rrm4 prevents formation of functional transport mRNPs. Since the amount of *rho3* mRNA did not differ in the absence of Rrm4, this effect is most likely not due to indirect processes such as altered mRNA stability, but a direct consequence of the loss of Rrm4. Consistently, RNA live imaging indicated that

this key RNA-binding protein functions as integral part of the transport machinery (see below).

*Target mRNAs of Rrm4 are transported on microtubules*

RNA live imaging was previously applied to investigate actin- or microtubule-dependent movement of specific mRNAs in a variety of systems, such as fungi, higher plants, flies and mammalian cells (Bertrand et al, 1998; Fusco et al, 2003; Hamada et al, 2003; Weil et al, 2006). Recent modifications include the inducible expression of a triplicate Gfp fusion protein (Haim et al, 2007) and use of a short peptide derived from λN as heterologous RNA-binding component (Daigle & Ellenberg, 2007). In our RNA live imaging system, we employed inducible expression of a fusion protein consisting of λN and triple eGfp in combination with genomic integration of boxB-containing targets to detect endogenous mRNAs.

Using this modified version revealed that mRNAs formed three distinct classes of particles: static, stochastically moving and directed particles. The motility of the latter was dependent on active transport along microtubules. Crucially, *ubi1* mRNA and Rrm4 co-localised in these directed particles. These results are consistent with our previous *in vivo* co-localisation and inhibitor studies demonstrating that Rrm4 moves bidirectionally along microtubules. So far, *in vivo* co-transport of an RNA-binding protein with its endogenous target mRNA was only shown for Staufen and *oscar* transcripts during oocyte development in *D. melanogaster* (Zimyanin et al, 2008).

Importantly, the CA-rich 3' UTR of *ubi1* was sufficient to confer an increase in frequency and length of mRNP movement. We infer that, although any mRNA seems to have the potential to be moved by this transport system, zipcode-containing Rrm4 targets are transported preferentially. Unspecific transport of bulk mRNA might function to distribute mRNA in filaments. This might also explain why distribution of the mRNA-binding protein Pab1 was disturbed in the absence of Rrm4 particles.

Genetic dissection of RNA binding and the capacity to shuttle in particles was achieved by introducing an Rrm4 variant without RNA-binding domain that still moved bidirectionally along microtubules. Crucially, the formation of directed mRNA particles was almost abolished in the respective strain. This important finding indicates that Rrm4 is not simple co-transported with mRNAs but rather constitutes an integral component of the mRNA transport machinery.

Using MS2-Gfp-based RNA live imaging, the same three classes of mRNA particles were detected in mammalian cells (Fusco et al, 2003). Directed particles also moved on microtubules and the presence of the *β-actin* mRNA zipcode augmented both the frequency and length of mRNP movement. mRNAs without zipcode were also transported indicating that unspecific transport might function to actively distribute mRNAs throughout the cytoplasm (Fusco et al, 2003). Consistently, in embryos of *D. melanogaster*, localising *hairy* as well as non-localising *krüppel* transcripts actively moved on microtubules. However, the presence of mRNA zipcodes increased frequency and duration of directed movement (Bullock et al, 2006).

*The role of microtubule-dependent mRNP transport in U. maydis*

One of the main functions of mRNA transport is the spatiotemporal regulation of gene expression (Martin & Ephrussi, 2009; St Johnston, 2005). Thus, microtubule-dependent transport of *rho3* mRNA might regulate local activity of Rho signalling. In accordance, we observed that Rho3 accumulates at retraction septa, where it might function in septum formation.

In *S. cerevisiae RHO3* mRNA is transported actin-dependently to the daughter cell pole prior to local protein accumulation (Aronov et al, 2007). Since Rho signalling regulates the action of polarisome and exocyst (Dong et al, 2003; Guo et al, 2001), local translation could lead to local activation of these important polarity determinants. A comparable concept of activation upon local translation has recently been shown for the mammalian counterpart RhoA during growth cone collapse in neurons (Wu et al, 2005).

For *ubi1* mRNA encoding a fusion protein of ubiquitin and the ribosomal protein Rpl40, the need for long-distance transport is less evident. At present, we can only speculate that e.g. distribution of *ubi1* mRNA is important to guarantee even proteasome-mediated degradation of cytoplasmic proteins. Rpl40 might exert extra-ribosomal functions as described for the human ribosomal protein L13a that is deposited with mRNAs to mediate transcript-specific translational regulation in the cytoplasm (Mazumder et al, 2003; Ray et al, 2007).

In principle, microtubule-dependent transport of mRNAs in *U. maydis* might support symmetric and/or asymmetric localisation of encoded proteins within filaments. This concept was initially proposed for actin-dependent mRNA transport during budding in *S. cerevisiae*. For example, mRNA transport promotes the symmetric distribution of the membrane protein Ist2p between mother and daughter cell as well as

the asymmetric accumulation of the transcription factor Ash1p in the daughter cell nucleus (Jansen, 2001).

In conclusion, using a combination of CLIP, FISH, and λN-Gfp RNA reporter system we present the first *in vivo* evidence for microtubule-dependent mRNA transport in fungi. The exquisite compatibility of the two *in vivo* approaches is exemplified by the fact that the CLIP-derived CA-rich 3' UTR of *ubi1* functioned as zipcode during λN-Gfp-visualised mRNA transport. At present, microtubule-dependent transport is only known from higher eukaryotes and intensively studied during development, cell migration and neuronal processes (Lécuyer et al, 2007; Rodriguez et al, 2008; St Johnston, 2005). Since the basic concepts appear to be conserved in fungi, flies and humans, *U. maydis* will serve as a simple model system to uncover fundamental principles of long-distance mRNA transport.

### 2.1.4 Materials and Methods

*Strains and growth conditions*

*E. coli* K-12 derivatives DH5α (Bethesda Research Laboratories) and Top10 (Invitrogen) were used for cloning purposes. For complementation studies in *S. cerevisiae*, the temperature-sensitive strain HKY171 was used (*pab1::HIS3* [*pab1-53$^{ts}$ TRP1 CEN*], *ura3*, *leu2*, *trp1*, *his3*, *ade2*, *MATα*; (Morrissey et al, 1999)). Transformation and cultivation were performed using standard techniques. Growth conditions for *U. maydis* strains and source of antibiotics were described previously (Brachmann et al, 2004). Strains were constructed by transformation of progenitor strains with linearised plasmids (Supplementary Table II). All homologous integration events were verified by Southern blot analysis (Brachmann et al, 2004). Filamentous growth of AB33 variants was induced by shifting 20, 50, or 150 ml of exponentially growing cells ($OD_{600}$ = 0.4 - 0.5) from complete medium (CM) to nitrate minimal medium (NM) each supplemented with 1% glucose (glc) unless otherwise noted. Cells were incubated at 28°C shaking at 200 rpm. AB33pab1G, AB33pab1R/rrm4G and AB33pab1G/rrm4Δ were induced for 4 h. For FISH analysis, strains AB33, AB33rrm4Δ, AB33$P_{otef}$rho3G and AB33$P_{otef}$rho3G/rrm4Δ were grown in CM (1% glc) to an $OD_{600}$=0.35 at 28°C and 200 rpm. Filaments were induced by shifting the medium

to NM (1% glc) and additional growth for 4 h. For live imaging of RNA, the duration of filament induction was adjusted to compensate for varying expression levels of boxB-containing target mRNAs. Strains SB1, SB1ubi1_B and SB1ubi1_B/rrm4Δ were grown in CM medium containing 1% arabinose (ara) to elicit $P_{crg1}$-mediated expression of $\lambda NG^3$ and shifted to NM medium with 1% ara to induce filament formation. Filaments were induced for 7 h prior to microscopic analysis. Strains SB1rho3_B*, SB1rho3_B, SB1mfa2_B, and SB1mfa2_ubiB were grown in CM (1% glc) and shifted to NM (1% ara) for 15 h prior to microscopic analysis. Strain SB1ubi1_B/rrm4R was shifted comparably and analysed after 12 and 24 h.

*Plasmids and plasmid constructions*

Standard molecular techniques were followed. Plasmids pCR2.1-Topo (Invitrogen) and pBluescriptSKII (Stratagene) were used as cloning vehicles. Genomic DNA of wildtype strain UM521 (*a1b1*) was used as template for PCR amplifications unless otherwise noted. All constructions were confirmed by sequencing. Plasmid sequences are available upon request.

For C-terminal fusion of Pab1 with eGfp, we followed a SfiI-dependent gene replacement strategy (Brachmann et al, 2004) resulting in pPab1G-NatR (pUMa805). This plasmid consisted of 3 kb upstream flanking region including the 1.9 kb *pab1* ORF (*um03494*), a 2.4 kb SfiI/SfiI insert containing *egfp* ORF, the heterologous terminator $T_{nos}$, and a nourseothricin (Nat) resistance cassette, followed by a 1 kb downstream flanking region. Upstream and downstream flanking regions were amplified by PCR using oMF911/oSL12 and oMF912/oMF914, respectively (see Supplementary Table III).

pPab1R-HygR (pUMa895) was comparable to pPab1G-NatR (pUMa805), containing a 3.7 kb SfiI/SfiI insert with *mrfp* ORF, $T_{nos}$ terminator, and hygromycin (Hyg) resistance cassette.

pPab1CM-HygR (pUMa1208) was comparable to pPab1R-HygR (pUMa895), carrying a 3,9 kb SfiI/SfiI insert of the plasmid pCM_HygR (pUMa1093) containing the ORF encoding mCherry ((Shaner et al, 2004)) with a C-terminal triple repeat of the c-Myc epitope EQKLISEEDL (Evan et al, 1985). The ORF was followed by the heterologous terminator $T_{nos}$ and a Hyg resistance cassette.

pRrm4R-HygR (pUMa992) was comparable to pRrm4G-NatR (pUMa496; Becht et al, 2006), carrying a Hyg resistance cassette and the *mRfp* ORF (3.7 kb SfiI/SfiI fragment; pUMa890).

pGT-NatR (pUMa894) was derived from pRrm4GT-NatR (pUMa603, Becht et al, 2006) by removing a 2325 bp fragment of the *rrm4* ORF. Thus, 28 aa of Rrm4 (17 and 11 of the N and C terminus, respectively) are still present in the fusion protein. Its expression is under control of the native *rrm4* promoter.

The plasmid p$P_{otef}$rho3G-NatR (pUMa1173) consisted of a 1.6 kb upstream flanking region, a 3 kb SfiI/SfiI insert containing a Nat resistance cassette and a fusion of the constitutively active promoter $P_{otef}$ and the *egfp* ORF, followed by a 1.7 kb downstream flanking region including the *rho3* ORF (*um04070*). Upstream and downstream flanking regions were amplified by PCR using oSL140/oSL141 and oSL138/oSL139, respectively (see Supplementary Table III).

pBoxB16-NatR (pUMa927) contained a 2.2 kb SfiI/SfiI insert including 16 copies of the λN recognition site boxB (Daigle & Ellenberg, 2007) followed by the terminator $T_{nos}$ and a Nat resistance cassette.

pUbi1_B-NatR (pUMa929) contained a 2.6 kb upstream flanking region including the 1 kb *ubi1* ORF with 278 bp 3' UTR (*um02440*, containing a 631 bp intron)and the 2.2 kb SfiI/SfiI insert from pBoxB16-NatR (pUMa927), followed by a 1 kb downstream flanking region. Upstream and downstream flanking regions were amplified by PCR using oSL128/oSL152 and oSL127/oSL151, respectively (see Supplementary Table III).

pRho3_B-NatR (pUMa989) contained a 1.6 kb upstream flanking region (PCR amplified using oSL196/oSL515 [see Supplementary Table III] introducing a KpnI recognition site at the downstream end) followed by the promoter $P_{otef}$ (896 bp KpnI/NcoI fragment) and the *rho3* ORF (*um04070*; 696 bp containing a 99 bp intron) with 159 bp of the 3' UTR (PCR amplified using oSL194/oSL516 [see Supplementary Table III] introducing NcoI and SfiI recognition sites at 5' and 3' ends, respectively). The 3' UTR was followed by the 2.2 kb SfiI/SfiI insert from pBoxB16-NatR (pUMa927). The consecutive 1.5 kb downstream flanking region was PCR amplified using oligonucleotides oSL195/oSL197.

pMfa2_B-HygR (pUMa1024) contained $P_{otef}$ (896 bp KpnI/NdeI fragment) followed by the *mfa2* ORF (U37796; 117bp) with 141 bp of the 3' UTR containing a 101 nt long intron (PCR amplified using oSL551/oSL552 [see Supplementary Table III]

from genomic DNA of strain AB33 introducing NdeI, ClaI, and XhoI recognition sites). This was followed by 16 copies of boxB and $T_{nos}$ (826 bp XhoI/NotI fragment). For ectopic integration the plasmid contained a Hyg resistance cassette.

Plasmid pMfa2_ubiB-HygR (pUMa1025) was comparable to pMfa2_B-HygR (pUMa1024) but contained the 3' UTR of *ubi1* (316 bp ClaI/XhoI fragment PCR amplified using oSL553 and oSL554 [see Supplementary Table III]) inserted downstream of the *mfa2* 3' UTR and upstream of 16 copies of boxB.

Plasmid pRrm4$^{\Delta RRM}$R-HygR (pUMa1064) was a derivative of pRrm4G-NatR (pUMa496; Becht et al, 2006), lacking a 1.5 kb XhoI/HindIII fragment comprising the three RRM domains. The gap was closed by a short linker with the respective cohesive ends. In addition it carried a Hyg resistance cassette and the *mRfp* ORF (3.7 kb SfiI/SfiI fragment, pUMa890).

pλNG3-CbxR (pUMa975) contained the promoter $P_{crg1}$ (2115 bp HindIII/NcoI fragment) followed by a fragment encoding amino acids 2-22 of the λN peptide (87 bp NcoI/SacII fragment; Daigle & Ellenberg, 2007) fused to a triplicate version of eGfp (2164 bp SacII/AscI fragment). Downstream of the fused ORF the plasmid carried $T_{nos}$ (300 bp AscI/NotI fragment). For homologous integration at the *ip* locus the plasmid contained a carboxin resistance cassette (*ip*$^R$).

For complementation in *S. cerevisiae*, the vector pACTIIAde was used (pUMa399), carrying *LEU2* and *ADE2* auxotrophy markers. This plasmid was initially used in the three-hybrid assay to express the Gal4 activation domain under control of a constitutively active *ADH1* promoter (König et al, 2007). Plasmid pRrm4G-LEU2 (pUMa1222) was generated by replacing the Gal4 encoding fragment with a respective fragment derived from pRrm4$^{AD-G}$-pACTIIA (pUMa427; König et al, 2007) encoding Rrm4 fused to eGfp. Plasmid pPab1G-LEU2 (pUMa1224) was constructed by insertion of a fragment downstream of the *ADH1* promoter that was derived from pPab1G-NatR (pUMa805) and encoded Pab1 fused to eGfp. Plasmid pPab1R-LEU2 (pUMa1225) contained a fragment downstream of the *ADH1* promoter that was derived from pPab1R-HygR (pUMa895) and encoded Pab1 fused to mRfp. In case of plasmid pScPab1-LEU2 (pUMa1227) the ORF encoding Pab1 from *S. cerevisiae* and ca. 760 nt the *PAB1* 3' UTR derived from plasmid pBMK75 (provided by Dr. M. Ashe) were inserted downstream of the *ADH1* promoter.

*CLIP experiments*

CLIP experiments were performed as described previously (Becht et al, 2006) including the following steps. After resuspension in 80 µl CB-PNK buffer the first linker was ligated over night at 16°C with shaking intervals as described. The reaction contained 60 U T4 RNA ligase 1 (NEB), 40 U RNasin, 10 µl 10 mM ATP and 5 µl kinase-treated RNA oligonucleotide oR043802 (20 pM/µl; 5´GAUCUGAGCCUGGGAGCU3´; modified at the 3' end with fluorescein). Beads were washed three times with 1 ml CB-PNK buffer and resuspended in 80 µl CB-PNK buffer.

After membrane transfer the RNA was prepared as follows. 1-2 mm membrane slices containing Rrm4 crosslinked to RNA were excised. 200 µl PK1 (100 mM Tris-HCl, pH 7.5; 50 mM NaCl; 10 mM EDTA; 10 U/ml proteinase K, Roche; pre-incubated for 20 min at 37°C) were added before incubating for 20 min at 37°C shaking at 1000 rpm. 200 µl PK2 (100 mM Tris-HCl, pH 7.5; 50 mM NaCl; 10 mM EDTA; 7 M urea) were added followed by 20 min incubation as before. Addition of 530 µl AE-phenol/chloroform (pH 5.3) was followed by 20 min incubation as before. RNA was precipitated by adding 50 µl 3 M sodium acetate (pH 5.3), 0.5 µl glycogen (5 mg/ml, Ambion), 500 µl ethanol and 500 µl isopropanol followed by incubation at -20°C over night. RNA was pelleted by centrifugation for 10 min at 45000 g and washed with 1 ml 70% ethanol. Pellet was resuspended in 20 µl $H_2O$. For second linker ligation, 3 µl 10 mM ATP, 3 µl 10x T4 RNA ligase 1 buffer (NEB), 2 µl RNA oligonucleotide oR043801 (40 pM/µl; 5´GCAGUUGAUGUUUUUCUGAUGC3´), 1.5 µl T4 RNA ligase 1 (NEB) and 0.5 µl RNAsin were added followed by over night incubation at 16°C. DNA was removed by adding 53 µl $H_2O$, 10 µl 10x DNAse I buffer (Roche), 2 µl RNAsin and 5 µl 10 U/µl DNAse I (Roche) before incubating 20 min at 37°C. 300 µl $H_2O$ and 400 µl AE-phenol/chloroform (pH 5.3) were added followed by 30 s of shaking at 1400 rpm and centrifugation for 5 min at 16000 g. RNA was precipitated by adding 50 µl 3M sodium acetate (pH 5.3), 1 µl glycogen, 500 µl ethanol and 500 µl isopropanol followed by incubation at -20°C over night. RNA was pelleted by centrifugation for 10 min at 50000 g and washed with 1 ml 70% ethanol. Pellet was resuspended in 10 µl $H_2O$. For reverse transcription, 2 µl 10x buffer RT (Qiagen), 2 µl dNTP mix (Qiagen), 2 µl 10 µM oMF970 (see Supplementary Table III), 1 µl RNasin (1:4 dilution), 1 µl Sensiscript S RT (Qiagen) and 2 µl $H_2O$ were added followed by incubation at 37°C for 60 min. Resulting cDNA was amplified by standard polymerase

chain reaction (PCR) using oligonucleotides oMF970 and oMF973 (see Supplementary Table III). PCR products ranging from 100 to 400 bp were purified using agarose gel electrophoresis. The DNA was subjected to a second round of PCR using oMF969 as well as a mixture of oMF974, oMF975 and oMF976 (see Supplementary Table III) reducing primer dimer amplification. Resulting products were purified using agarose gel electrophoresis, cloned and sequenced.

*Tandem affinity purification and and Western Blot experiments*

The initial protocol followed the CLIP protocol described previously (Becht et al, 2006) using the following modifications. Six hours old filaments were harvested by centrifugation and resuspended in 5 ml UmTT buffer containing 1 mM DTT. Cells were frozen in liquid nitrogen and ground 15 min in a pebble mill. After incubation for 60 min at 4°C on a turning wheel the beads were washed three times with 1 ml IPP150 buffer without DTT and three times with TEV buffer. Beads were resuspended in 150 µl TEV buffer, 50 U TEV protease (Invitrogen) and 40 U RNasin, and incubated over night at 4°C. After centrifugation (6000 g for 10 sec), 250 µl supernatant (including a washing step with 150 µl TEV buffer) were combined with 900 µl CB buffer (10 mM Tris/HCl, pH 8; 150 mM NaCl; 0.1% NP40; 1 mM MgAcetate; 1 mM imidazol, 2 mM $CaCl_2$; 10 mM β-mercaptoethanol, and 40 U RNasin [1 µl 1 M $CaCl_2$ was freshly added per sample]). After the second purification step with 70 µl calmodulin affinity resin (Stratagene) and two washing steps with CB buffer the beads were incubated in SDS-PAGE loading buffer at 95°C for 10 min. The protein concentration of the input fraction was determined by Bradford assay (Bio-Rad), resolved by 8% SDS-PAGE and transferred to a PVDF membrane (GE Health Care) by semi-dry blotting (note that 5 µg input sample as well as 10 µl eluate fraction and 2.5 µg input sample as well as 30 µl eluate were loaded for Western blot analysis with α-Gfp [Roche] and α-Myc [Sigma] antibodies, respectively). An anti-mouse IgG HRP conjugate (H+L; Promega) was used as secondary antibody. Activity was detected using the ECL plus western blotting detection system (GE Health Care).

*Quantitative real-time PCR*

*U. maydis* cells were grown in CM (1% glc) to an $OD_{600}$=0.5 at 28°C and 220 rpm. Filaments were induced by shifting the medium to NM (1% glc) and additional

growth for 4 h. 25 ml of culture were harvested at 8500 g for 5 min. Total RNA was extracted with Trizol Reagent (Invitrogen) according to the manufacturer's protocol. Total RNA was treated with RNase-free DNaseI (Roche) and purified using the RNeasy clean-up kit (Qiagen). cDNA was synthesised from 2 µg of total RNA using First Strand cDNA Synthesis Kit (Fermentas) with oligo-dT primers. Next, 12.5 µl SYBR Green PCR Master Mix (Applied Biosystems) was added to 1µl 1:5 diluted cDNA and 100 nM (f.c.) of each primer. For amplification of a *rho3* cDNA fragment primers oSL758 and oSL759 were used (see Supplementary Table III). To normalise expression of *rho3* a fragment of the *cpr1* cDNA (*um03726.2*, encoding peptidylprolyl isomerase) was amplified using primers oSL768 and oSL769 (see Supplementary Table III). The qRT-PCR was performed on a 7300 Real Time PCR System (Applied Biosystems) using standard conditions. The cDNA was prepared from RNA isolated from three independent biological replicates and tested in two technical replicates.

*Fluorescence in situ hybridisation*

For FISH analysis an *S. cerevisiae* protocol was adapted from (Long et al, 1995) and http://www.singerlab.org/protocols. Multi-well object slides were washed in $H_2O$. After drying 5 µl of 0.025% poly-L-lysine (Sigma) was added to each well and incubated for 3 min. 3 µl were removed and the slides were dried. After washing with $H_2O$ (three times for 10 min), the slides were stored at 4°C. Cells were grown to $OD_{600}$=0.35, filaments were induced for 4 h (see above) and subsequently fixed for 1 h at room temperature by adding 15 ml of 16% formaldehyde (Polysciences) to 15 ml culture. The fixative was removed by three rounds of centrifugation (5 min, 10000 g, 4°C), and resuspension in 10 ml of ice-cold buffer B (1.2 M sorbitol, 0.1 M potassium phosphate, pH 7.4). Cells were further resuspended in 250 µl of buffer B, and 7.5 µl/well was added to each well of poly-lysine-coated slides. Cells were left to adhere to the slides for 30 min at 4°C. Residual culture was removed and the slides were washed two times in buffer B, which was subsequently replaced by 70% ethanol. The slides were incubated at least overnight at -20°C. Cells were rehydrated for 5 min in 2x SSC (300 mM NaCl, 30 mM sodium citrate, pH 7.0) and washed for 5 min in 2x SSC with 40% formamide. For each slide a 6 µl oligonucleotide mixture was prepared composed of four or eight Cy3-labelled probes (oSL748-751 for *rho3*, 4 pmol each, and oSL748-751 as well as oSL387-390 for *rho3*/*gfp*, 2 pmol each, respectively; see Supplementary Table III), 20 µg hering sperm DNA and 20 µg yeast tRNA. The mixture was added to

24 µl of solution H1 (12.5 mM sodium phosphate buffer, pH 7.0; 98.5% formamide). The mixture is incubated for 3min at 80°C, cooled on ice and supplemented with 30 µl solution H2 (34 µg BSA, 4x SSC, 15U RNasin [Promega]). This hybridisation mix was centrifuged for 10 min at 16000 g and 4°C before 5 µl were added to each well of the prepared object slides. The wells were protected with a coverslip and incubated in a hybridisation chamber at 37°C for 16-24 h. After hybridisation the slides were washed two times in 2x SSC with 40% formamide and once in 1x PBS pH 7.2 (11.3 mM disodium phosphate, 1.8 mM potassium phosphate dihydrate, 2.7 mM potassium chloride, 137 mM sodium chloride) at 37°C and 150 rpm. PBS was removed and 5µl DAPI-Mix (Vectas H1200) was added to each well. The slides were covered with a coverslip and stored in hybridisation chambers at 4°C prior to microscopic analysis.

To enable objective quantification of signal accumulation in microscopic images, line scans of filaments were performed to extract fluorescence intensity values (line width was broadened to cover the whole filament width and maximum intensity values at each position were recorded). Peaks in the resulting fluorescence intensity graphs were identified using PIA (peak identifying algorithm by K. Zarnack, J. König and M. Feldbrügge to be published elsewhere). This algorithm detects all positions within the graph that surmount their local environment (to a maximum distance *w* to either side) by at least height *h*. Peak identification was performed using the parameters 230 for *h* and 4 for *w* during the analysis of images of strains AB33 and AB33rrm4Δ. In case of AB33$P_{otef}$rho3G and AB33$P_{otef}$rho3G/rrm4Δ the parameters were 200 and 5 for *h* and *w*, respectively (values were optimised for varying imaging techniques and signal intensities).

*Microscopy, image processing and quantitative analysis*

Cell suspensions were dropped on glass slides covered by a thin layer of agarose (2% w/v) and analysed using a Zeiss Axioplan II microscope equipped with objective lenses Plan Neofluar and Plan Apochromat (both 100x ; NA 1.3 and 1.4, respectively). Epifluorescence was observed using Gfp (ET470/40BP, ET495LP, BP525/50) and TexasRed (HC562/40BP, HC593LP, HC624/40BP) filter sets. To detect Cy3 either TexasRed or TRITC (HC543/22BP, HC562LP, HC593/40BP) filter sets were used. Filters were obtained from AHF Analysentechnik. Frames were taken with a cooled CCD camera (CoolSNAP HQ, Photometrics). Microscope and camera were controlled

by MetaMorph 7.5 (Molecular Devices). The same software was used for measurements and image processing including adjustment of brightness, contrast and gamma values as well as correction of background unevenness. Particle intensity was enhanced by applying camera binning of 2x2. For co-localisation studies of *ubi1* mRNA and Rrm4 time-lapse videos were recorded using a filter wheel (Visitron Systems) equipped with excitation filters for Gfp (S480/25) and Rfp (S565/25). Filter switch and detection of fluorescence were controlled using the multidimensional acquisition mode. The settings were optimised to avoid bleed-through of the fluorescence signal resulting in intervals of 225 (or 300) ms and 670 (or 705) ms for the switch from Rfp to Gfp and Gfp to Rfp, respectively. This was controlled recording time-lapse videos with mixtures of strains that expressed either eGfp or mRfp fusion proteins. Exposure time was 225 (or 300) ms. Emission was detected using a dual-band filter (Gfp: FT 480, BP503-545; Rfp: FT565, BP591-647).

For simultaneous dual-colour detection the dual-view device (MAG Biosystems) was used. A dichroic beamsplitter and a filter designed for Gfp and Rfp (eGfp/mRfp; Chroma) were used to simultaneously excite the respective fluorophores. A second dichroic beamsplitter (dcxr565) within the dual-view device splitted the fluorescent signals into the respective colours, which were separately filtered with emission filters (Gfp HQ510/30; Rfp HQ650/75), before the different channels were simultaneously imaged on different regions of the CCD chip.

For quantification of mRNA particles, time-lapse videos (80 frames, 150 ms exposure time) were recorded for at least 29 filaments per strain in three independent experiments. Particles were tracked manually. Those that travelled more than 0.75 µm in a single direction were classified as directed particles. For strains carrying ectopic insertion of a boxB-containing transgene, data obtained from two independent transformants were combined. To quantify Pab1G signals in filaments, the average fluorescence intensity at the hyphal tip and at the perinuclear region was determined using a mask of 1.67 $\mu m^2$. 45 filaments were analysed for each strain in three independent experiments.

*Inhibitor studies*

20 ml of cell suspension were incubated in the presence of either 100 µM CCCP (Sigma-Aldrich) or 50 µM benomyl (Sigma-Aldrich). Samples were incubated for 15 to 30 min at 28°C with agitation followed by microscopic analysis (Becht et al, 2006).

## 2.1.5 Supplementary information

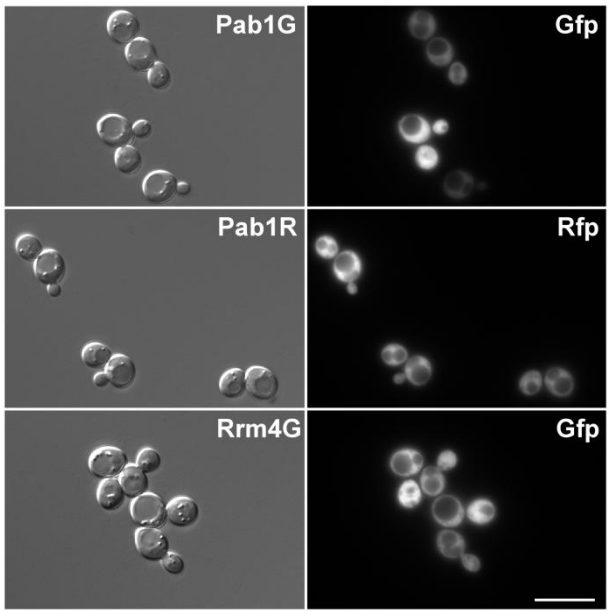


**Supplementary Figure 1** Pab1 and Rrm4 fused to fluorescent proteins are expressed in *S. cerevisiae*. Epifluorescence images of strains HKY171 expressing either Gfp or Rfp fusion proteins (indicated on the right) under control of the constitutively active *ADH1* promoter (size bar, 10 µm).

Supplementary Table I **CLIP tags**

| um nr.[a] | MUMDB annotation[b] | len.[c] | nucleotide sequence[d] |
|---|---|---|---|
| 00160 | Sec17 - probable SEC17 - transport vesicle fusion protein | 193 | GAACAGGTGGCGAGCATGTCGTTGGAAAGCAATCTGACCAAGTACAGCGT CAAAGACTATTACCTGAACGCTGGCATGTGCTACCTTGCTATTCCCGACT ACGTGGCTGCAGTTCGAGCGATGCAGTTCTACGCCGAACAAGACACCAGC TTCCCCACCACCATGGAAGGCCGCTTCCTCCACTCGCTCGTAC |
| 00379 | related to eukaryotic initiation factor 3e subunit | 76 | GGTCATCCAGGACCCCAGCGTCGCCTCTGCGCTAAAGCAGGACAAGGCAC AGAACTTGCAATGGCTCGAGGAAAAG |
| 00714 | Npl4 - probable NPL4 - nuclear protein localisation factor and ER translocation component | 83 | GATCAGGTACGCGACAAGCTTGTTGGTGTGCTCAGTGACTGGCATCTGCT CGCCTTCCTCGACACGAGCGGCTTCCTTGACCA |
| 00786 | conserved hypothetical protein | 111 | ACCCAGCGAGCATCACAAACACAATGCCGGCGGCTCTGGCAAGTGGAGTC AGTGGTTCGGCTTCTCCTGAAGCCGGCAGTGGCCAACTCGTCCGCACCAT GTAATCCCATC |
| 00851 | related to BFR1 - Nuclear segregation protein | 70 | GCGCTGCCAACGACACGTTTTATGCCAAGCTCAACCAGGAGCGCGAACGT CGACTTGCTAAACAGCGTGA |
| 00897 | conserved hypothetical protein | 45 | ACCGCTGCCCTCACCCACAACTTCTAGCCGTAAATCCCCGTCACA |
| 00961 | conserved hypothetical protein | 65 | CATCGCCCTTGTTGCCGGTGTTCTCGGCGTCACTGCCGCCTACGACCCCG CTCACATGCCCGCCA |
| 00986 | Ras1 - small G-protein Ras1 | 57 | GCCGGCAAACCGCTACATCGTTCGAAACGCAACTCGCGCCTCGCAGGTTG TTCAAAA |
| 01146 | conserved hypothetical protein | 78 | CAGCGCCTCGGTGCTCAAGGATGAGCAAGACAAGTGGTGCACATTCTTCG TCTTCCAAGATATTTCGGTCCGCACCGA |
| 01167 | hypothetical protein | 69 | GACACCCCGCGTCAAAAACCGCATCCCTCCGCCCCCACGTCACGATGCTG GTGTTGACAATCCCAGCCA |
| 01189 | Efb1 - probable EFB1 - translation elongation factor eEF1beta | 26 | GTTGACGAAACCCAACTATTTCCAAG |
| 01434 | Fer3 - siderophore peptide synthetase involved in ferrichromeA biosynthesis | 58 | GCTTATCTCCTCTCTTGCCGTCTTCGCGGGACATCTCGATCGGATGCGAT GCGGACGA |
| 02440 | Ubi1 - probable RPL40A - Ubiquitin | 86 | CACACACACACACACACACACACACACACACACACACACGCACATCTACATATA TGCAACACATCGCACACCACACATGGCACAGTACAA |
| 03033 | conserved hypothetical protein | 60 | CAACAACAACAACAACAACAACAACAACAACAACAACAACAACAACAACA AAATACCCAG |

| | | | |
|---|---|---|---|
| 03306 | Prs4 - probable PRS4 - ribose-phosphate pyrophosphokinase 3 | 81 | ACGTCATCACGATGGACCTCCACGCCAGTCAGATTCAGGGCTTCTTCGAC ATCCCCGTCGATAACCTCACCAGTGAGCCCA |
| 03598 | Ent1 - related to ENT2 - clathrin binding protein, required for endocytosis | 51 | GCAGCAGGAGCTCATGCAGCAGCAGTACATGCAACAGCAACAAGTCGAGT A |
| 03854 | Pda1 - probable PDA1 - pyruvate dehydrogenase (lipoamide) alpha chain precursor | 72 | GTGGCAGGGACCGCACCGAGATCCACCGATACCGCTTAATCCCTCCTTGT AACACATCGCCTACCTCCACTC |
| 03959 | probable t-complex-type molecular chaperone, epsilon subunit | 61 | ACAGCACAACATCGAATAATTACGCCATTCCCCCTTGTACGATACTTTGA TCTCCTTCGAA |
| 03965.2 | conserved hypothetical protein | 69 | GCCTACACCATAGACGTATCCCCTCTCACACTGTGGGGAATCGTGAATGC AAAATCATCACCATTGCTT |
| 04070 | Rho3 - GTP binding protein | 84 | CAACCCACCCGCGTTCAACGCCAACCAACACGCCTCCGCGCAGCAAACTG TATTCTACACCCCTGATACCCGCTCCAGCAGATN |
| 04136 | related to serine/threonine protein kinase | 67 | GTCCGTGCCCATATGCGAAGAGGGAAAGCAGAACGATCATATCCCATCTC GAGCGCGCCCAGNTAGG |
| 04270 | Dps1 - probable DPS1 - aspartyl-tRNA synthetase, cytosolic | 52 | GCGAGCAACGTCAGCACACCCCTATGCAAACATACAGTTTATCTTCCATT CA |
| 04628 | conserved hypothetical protein | 53 | CCACACCACACGNTCGACATCCATGCACTCACATTACACGCACATCCCTT CAC |
| 04632 | probable ribosomal protein P2 | 116 | CACATCGCCGCCTACCTTTTGCTCACCCTCGGTGGTAAGGAGTCGCCGTC GGCTGCCGACATCAAGGCTCTGCTCGAGACGGTTGGTATCGAGGCCGAGT CGGAGCGTCTCGACAA |
| 04855 | probable 60S ribosomal protein L26A | 25 | CCACCCAAAATATCAAACACACCAG |
| 05031 | probable ribosomal protein L10a.e, cytosolic | 150 | ACGCCATCGATGGTGTGATTCTGCCTCTTGTTTCGCCCCGNTTTCTCCTT TGGGTTCGATGAATCCCTTGGTCACATGCATCCTACAAAGCATTACGCAC GCTTACACCCAGTTCCATTCAACCGTCGTAGCACGTTTGACTTGGGATGA |
| 05104 | putative protein | 137 | GCCGGCTGCTACTGCACATGTACCTCGGGCTGGAACCCAGCCAACGGTCC TTGGGGCGGCAACGGTGCTGGATGGGGCTCTGGCTCTGGCTCTGGCTCTG GCTCTGGTAGCGGTTCCGGTTCCGGTTCCGGCACCAA |
| 05644 | related to alcohol dehydrogenase | 36 | CACCACTTCGCCAGCTTCATCCAGCACACCAGACCG |
| continues next page | | | |
| 05818 | probable chimeric spermidine synthase/saccharopine reductase | 75 | GATTCACCTCAACCTAATCGGCGAGCTTCGACGATCCACTAAGGAGCTCT TCCCTGTCGCCGACTACGCTTTCAC |
| 06078 | conserved hypothetical protein | 111 | GCGCGTTACAACTGTTAATCATGACGATCTCAATCCCGCTTATCCGCAAC AACCGCGGTATCATGAAACGCAGCAGTACGCACAGCACTATCAGCACCAA GCCTATCCTCA |
| 06139 | related to zinc transporter | 145 | AGCCCCACGGACTGCACGCAGCAACACCGCATCCGCCACACTGGTCTCCC ATAACTGCACATCGTCCTTCGCACCACCATCACCACCATCACTAGTCATG CTGGACTGTGTATGATCATTCCAATTACTAAGTTCATTTCACTCA |
| 06323 | probable translation initiation factor eIF3 | 71 | GACCGTCAGGTACTTTCGGGACCACCGGAGAACACGCGTGACCACATCAT GCAGGCATGCAAGGCGCTCCA |
| 06509 | related to Phenylalanine ammonia-lyase | 60 | CAACCTCGAGGCACAGCAGCAAAGCGTCGCACATGACCCTGAACCATCCC CATCTGCCCA |
| 10095 | probable RNA helicase dbp2 (DEAD box protein) | 46 | ACGACTGAATGGCACGCTCACGTTTCGATCTGTTTATCATTGTCAA |
| 10339 | related to fatty acid synthase, beta and alpha chains | 117 | GCTCTCCAGGCAGGCTACACCGGTACTCTTGGAAAGACCACTTCCAACTG GTGACTCGAACTGTCGCCGGAAAGCTGCCTGGTGGCTTCAATCTCTCCCC GTCAATTCACACTTCCA |
| 10360 | probable 40S Ribosomal protein S14 | 71 | GCACACGGCTCGCAATCCAGCGACTCGGAGTCCTTGTGGCTCAAAGCATC TCTTGCCGTCCTTCTTGGGAA |
| 10433 | Rpo26 - probable Rpo26 - 18kD subunit of DNA-directed RNA polymerases I, II, III | 71 | GACGCTGGAGTTAGCCTCCATTTCGGACCCNATCTATACCTGCAAACTCA ACTCGTTCTGGCTCAAAAAAA |
| 10503 | probable cell division control protein CDC3 | 58 | AACCGCAACAAGCTACAGGACAACCGTGTTCATGCCTGCATCTACTTTGT GCAGCCCA |
| 10625 | probable ribosomal protein L24.e.A, cytosolic | 54 | TCCATGGATCTTGCATCCTATGCACTTAGGCGCTCATCTCCAGCGTTCAC ATAA |
| 10733 | putative protein | 36 | CAACAACAACAACAACAACACCTCAACCCTAACCAG |
| 10926 | Tfp1 - probable TFP1p - H+-ATPase V1 domain 69 KD catalytic subunit, vacuolar | 37 | GTCGCCGAGAAGCTCACTGCTAACAACCCGCTGCTTA |
| 11047 | conserved hypothetical protein | 45 | GAACTGCAAGGTTAGTACGAACCGGCCAAGCTCCCATATGCAATG |
| 11097 | related to QCR10 - ubiquinol-cytochrome-c reductase 8.5 kDa subunit | 50 | CACACACGCAGAGCATCAAACGAACAACATAACTTAGCAGCAAGGCGGCT |

| | | | |
|---|---|---|---|
| 11103 | Rpl3 - probable RPL3 - 60s ribosomal protein l3 | 57 | AACACCTGCATCTGTCATGACTGCAACCCCCAAAAAATCTAAGCGATTACCTGGCAA |
| 11168 | Tim8 - probable TIM8 - Translocase of the mitochondrial inner Membrane | 118 | ATTGCAAGAGCAACGAGGTCAGATGTCCTAACTACCGTACCAGCTGATTCGGCATCATGTAACAACATTACCTAAAAAGCATCGCCGGCCGACTAGAGCAATCAACATCCACTACTCA |
| 11238 | conserved hypothetical protein | 19 | CACTAAAAACCCCATCACG |
| 11261 | Rps17b - probable RPS17B - ribosomal protein S17.e.B | 48 | ACACATATCACACACATGCACCGTCTCTGACGGTGCTTTGACCTCGAT |
| 11326 | conserved hypothetical protein | 42 | GCACACGATGGTTCTCGCAACTCCAAGCCCAACGGCTCGCAA |
| 11499 | Rps29b - probable RPS29B - ribosomal protein S29.e.B | 48 | TGGCACCGGACGCTCTACGCCAAGCAAAACTACTACACATCTCATACA |
| 11536 | Rpl5 - probable RPL5 - 60S large subunit ribosomal protein L5.e | 34 | ACGATCGTCAGCTCTCTATGCATTCGCAATACCA |
| 11731 | Nuo1 - related to nadh-ubiquinone oxidoreductase 9.5 kDa subunit | 36 | CAACACATACCGATACCTTCAATATGCAGCACACGA |
| 11948 | related to ubiquitin-like protein Hub1 | 84 | GTCCACAAAGACCACATCACCTTGGCCGACTACGAGATCGCCGATGGCTTCTCGTTCGAGATGCACTAGTTTCCTCGCTTTCCC |
| 12159 | conserved hypothetical protein | 67 | GACGAGCCGTGGCAACTACCTGAGCGACCTGTCGTGTCGGTGCGAAGACATTGATTTTACCTGGCAA |
| 12241 | related to COX19 - Cytochrome c oxidase assembly protein | 53 | CACAAAGCGGAACTGCAAGGTTAGTATGAACCGGCCAAGCTCCCATATGCAAT |
| 15090 | conserved hypothetical protein | 160 | GCAACAACAGCAACAGCAACAGCAGCAACAGCAACAGCAACAGCAACAGCAACAGCAACAGCAACAGCAACAGCACCAGCACCAGCAGCAACAGCAACAGCAACAGCCAACTTCTCATCACGAGATGCAGCCGCTGCCGAACCTAACACTCATCCAA |
| - | - | 87 | CGATACAGAGAAGATCAGCGATGCCCCGGCAGACGGACGGCAAGATTTGAACAGAAGAGCTGCTTTCTACGGAAAGCAAATATGTT |
| - | - | 88 | GGGCGGCGACTGAATTCGGGCGCAGGTTTACTTGTTTGCATCAATAACGACAAAGTGTTCCGTCAAGGTACAGGCAGAAAGGTTTCTC |

[a] *U. maydis* gene number; MIPS *U. maydis* database (MUMDB; http://mips.gsf.de/genre/proj/ustilago/)
[b] MUMDB annotation
[c] length of CLIP tag in nucleotides
[d] sequence of the longest corresponding CLIP tag, CA-rich motifs identified by MEME are underlined.

## **Supplementary Table II** *U. maydis* strains used in this study

| **Strains** | **Relevant genotype** | **UMa** | **Reference** | **Plasmid transformed** | **Locus** | **Progenitor** |
|---|---|---|---|---|---|---|
| *AB33* | *a2 $P_{nar}$bW2bE1* | *133* | *(Brachmann et al, 2001)* | | *b* | *FB2* |
| AB33pab1G | *pab1G* | 389 | this study | pPab1G-NatR (pUMa805) | *pab1* | AB33 |
| AB33pab1R/rrm4G | *rrm4G pab1R* | 428 | this study | pPab1R-HygR (pUMa895) | *rrm4 pab1* | AB33rrm4G |
| AB33pab1G/rrm4Δ | *pab1G rrm4Δ* | 472 | this study | pRrm4Δ-HygR (pUMa495; Becht *et al*, 2006) | *rrm4 pab1* | UMa389 |
| AB33rrm4GT | *rrm4GT* | 303 | (Becht *et al*, 2006) | | *rrm4* | |
| AB33rrm4GT/pab1CM | *rrm4GT pab1CM* | 554 | this study | pPab1CM_HygR (pUMa1208) | *pab1* | AB33rrm4GT |
| AB33GT | *Gfp-Tap Tag* | 397 | this study | pGT-NatR (pUMa894) | *rrm4* | AB33 |
| AB33GT/pab1CM | *Gfp-Tap tag pab1CM* | 556 | this study | pPab1CM_HygR (pUMa1208) | *pab1* | UMa397 |
| AB33rrm4Δ | *rrm4Δ* | 273 | (Becht *et al*, 2006) | | *rrm4* | |
| AB33$P_{otef}$rho3G | *rho3* | 508 | this study | p$P_{otef}$Rho3G-NatR (pUMa1173) | *rho3* | AB33 |

| | | | | | | |
|---|---|---|---|---|---|---|
| AB33P$_{otef}$rho3G/rrm4Δ | *rho3 / rrm4Δ* | 581 | this study | pRrm4D-HygR (pUMa495; Becht *et al*, 2006) | *rrm4* | AB33P$_{otef}$rho3G |
| SB1 | *λNG*[3] | 409 | this study | pλNG3-CbxR (pUMa975) | *ip* | AB33 |
| AB33ubi1_B | *ubi1_B* | 403 | this study | pUbi1_B-NatR (pUMa929) | *ubi1* | AB33 |
| SB1ubi1_B | *ubi1_B* | 415 | this study | pλNG3-CbxR (pUMa975) | *ip* | AB33ubi1_B |
| SB1rho3_B[*] | *rho3_B* | 430 | this study | pRho3_B-NatR (pUMa989) | *rho3* | SB1 |
| SB1rho3_B | *rho3_B* | 430#1,2 | this study | pRho3_B-NatR (pUMa989) | ectopic | SB1 |
| SB1mfa2_B | *mfa2_B* | 456#1,2 | this study | pMfa2_B-HygR (pUMa1024) | ectopic | SB1 |
| SB1mfa2_ubiB | *mfa2_ubiB* | 457#1,2 | this study | pMfa2_ubiB-HygR (pUMa1025) | ectopic | SB1 |
| SB1ubi1_B/rrm4R | *ubi1_B rrm4R* | 431 | this study | pRrm4R-HygR (pUMa992) | *rrm4* | SB1ubi1_B |
| SB1ubi1_B/rrm4Δ | *ubi1_B rrm4Δ* | 432 | this study | pRrm4Δ-HygR (pUMa495; Becht *et al*, 2006) | *rrm4* | SB1ubi1_B |
| SB1ubi1_B/rrm4$^{\Delta RRM}$R | *ubi1_B rrm4$^{DRRM}$R* | 465 | this study | pRrm4$^{\Delta RRM}$R-HygR (pUMa1064) | *rrm4* | SB1ubi1_B |

## **Supplementary Table III** DNA oligonucleotides used in this study

| ***Designation*** | **Nucleotide sequence** [(a)] |
|---|---|
| oMF911 | GGTGGCCGCGTTGGCCTTAGCCTCAGTCTTGGGAGC |
| oMF912 | ATAGGCCTGAGTGGCCTGAGCGGTTTCAGATCATC |
| oMF914 | TGCTCTCGGATTCGAGGC |
| oMF969 | AGTTGATGTTTTTCTGATGC |
| oMF970 | AGCTCCCAGGCTCAGATC |
| oMF973 | GCAGTTGATGTTTTTCTGAT |
| oMF974 | AGCTCCCAGGCTCAGATCA |
| oMF975 | AGCTCCCAGGCTCAGATCT |
| oMF976 | AGCTCCCAGGCTCAGATCC |
| oSL12 | TTGCTGACTTGTCGTGCG |
| oSL127 | TTCACGCTTCCGCTTCGG |
| oSL128 | GACGATGTCGGCAAGTCC |
| oSL151 | ATAGGCCTGAGTGGCCCGTTCTATTCGTCTAGCGG |
| oSL152 | TGCGGCCATCTAGGCCCGGCACAACCAAGAATAAC |
| oSL194 | TACGGCCATCTAGGCCTCGGCATTTGAGCGAATCC |
| oSL195 | ACTGGCCTGAGTGGCCCATCGTGCATATGTTAGTTG |
| oSL196 | AGCCTCGAGTCGGACATC |
| oSL197 | ATTACGGCGGCGTGTACC |
| oSL387 | (T)TGTAGTTGCCG(T)CGTCCTTGAAGAAGA(T)GGTGCGCTCC(T) |
| oSL388 | (T)AGACGTTGTGGC(T)GTTGTAGTTGTAC(T)CCAGCTTGTGC(C) |
| oSL389 | (G)TGGCGGATCT(T)GAAGTTCACCTTGA(T)GCCGTTCTTCTG(C) |
| oSL390 | (T)CACGAACTC(C)AGCAGGACCATG(T)GATCGCGCTTCTCGT(T) |

| | |
|---|---|
| oSL515 | ATAGGTACCCGTGCTCCAGATCCTGTG |
| oSL516 | ATACCATGGGCACGCTGTGCGGACTTGTG |
| oSL551 | GTACATATGCTCTCTATTTTCGAAAC |
| oSL552 | TAGCTCGAGATCGATTGTTCACATATCTAGCGGC |
| oSL553 | GCTATCGATACTAGTCAAGAAGAAGTTGAAGTAAG |
| oSL554 | GTACTCGAGTCTAGACGGCACAACCAAGAATAAC |
| oSL748 | (T)ACCGTCGGCTCG(T)ATGTCTGTGGAAAC(T)CGTGTCTGAC(G) |
| oSL749 | (T)GTATCCCACAGTG(T)CAGTTCCACCG(C)GAGTCCTGTATG(C) |
| oSL750 | (A)CGAGCATGATCT(T)GACGGCTGGACAG(T)GGTGGCGGATT(T) |
| oSL751 | (A)GTTCGGTGAAGCAC(T)CGGTGACGCC(T)CTGTTGGATTTG(G) |
| oSL758 | GTGTTGGTTGGCGTTGAAC |
| oSL759 | GTCACCGAGTGCTTCACC |
| oSL768 | TCGACATCGTCAAGGCTATC |
| oSL769 | CGATGGTGATCTTGGACTTG |

[(a)] Cy3-labelled nucleotides in brackets

## Legends to Supplementary Video 1-6

### Supplementary Video 1

Upper part: Pab1G-containing particles move bidirectionally along cytoskeletal tracks in filaments of AB33pab1G expressing Pab1 fused to eGfp. Lower part: Pab1G-containing particles are no longer detectable in the absence of Rrm4. Filament of AB33pab1G/rrm4Δ is shown. Time-lapse videos correspond to Fig. 1A and 1E (200 ms exposure time, 60 frames, five frames/second display rate; QuickTime format, 5175 kB).

### Supplementary Video 2

Pab1R- and Rrm4G-containing particles (upper and lower part, respectively) co-localise in filaments of AB33pab1R/rrm4G. Simultaneous time-lapse videos using dual-colour detection correspond to Fig. 1C (150 ms exposure time, 58 frames, 6 frames/second display rate; QuickTime format, 6775 kB).

### Supplementary Video 3

$\lambda NG^3$-containing particles move bidirectionally along cytoskeletal tracks in filaments expressing boxB-containing transcripts *ubi1_B* and *rho3*_B* (upper as well as left and lower as well as right part, respectively). Directed particles are marked with arrowheads. Time-lapse videos correspond to Fig. 4C (150 ms exposure time, 80 frames, six frames/second display rate; QuickTime format, 5219 kB).

**Supplementary Video 4**

λNG$^3$-containing particles move bidirectionally along cytoskeletal tracks in filaments expressing boxB-containing transcripts *mfa2_B* and *mfa2_ubiB* (upper as well as left and lower as well as right part, respectively). Directed particles are marked with filled arrowheads. Time-lapse videos correspond to Fig. 4C (150 ms exposure time, 80 frames, six frames/second display rate; QuickTime format, 4849 kB).

**Supplementary Video 5**

Directed particles containing λNG$^3$ that move bidirectionally along cytoskeletal tracks are drastically reduced in the absence of Rrm4. Filament of SB1ubi1_B/rrm4Δ is shown. Time-lapse video correspond to Fig. 6A (150 ms exposure time, 80 frames, six frames/second display rate; QuickTime format, 2332 kB).

**Supplementary Video 6**

Removal of RRMs in Rrm4R cause a drastic reduction in directed particles containing λNG$^3$ (upper part), while Rrm4$^{\Delta RRM}$R still shuttles in particles along cytoskeletal tracks (lower part). Filament of SB1ubi1_B/rrm4$^{\Delta RRM}$R is shown. Lower part of the time-lapse video correspond to Fig. 6B (150 ms exposure time, 60 frames, 6 frames/second display rate; QuickTime format, 7508 kB).

*Acknowledgements*

We acknowledge Dr. A. Brachmann and lab members for valuable discussion and critically reading the manuscript as well as Drs. J. Ule and J. Ellenberg for helpful advice on CLIP and λN-Gfp RNA reporter system, respectively. We thank Drs. H. Krebber and M. Ashe for *S. cerevisiae* strain HKY171 and plasmid pBMK75, respectively. We are grateful to P. Happel for excellent technical assistance, to E. Vollmeister for initial work on Pab1G, and to Dr. S. Feldbrügge-Wegener for advice in real-time PCR. Grants from the DFG to MF (FE 448/3) supported this work.

## 2.2 Kinesin-3 and dynein mediate microtubule-dependent co-transport of mRNPs and endosomes

Sebastian Baumann[*,†], Thomas Pohlmann[*,†], Marc Jungbluth[†,‡], Andreas Brachmann[†,§] and Michael Feldbrügge[*,†]

[*] Heinrich-Heine University Düsseldorf, Institute for Microbiology, 40204 Düsseldorf, Germany

[†] Max-Planck Institute for Terrestrial Microbiology, Department for Organismic Interactions, Karl-von-Frisch-Str. 10, 35043 Marburg, Germany

**Present addresses:**

[‡] Philipps-University Marburg, Department of Genetics, Karl-von-Frisch-Str. 8, 35043 Marburg, Germany

[§] Biocenter of the Ludwig-Maximilians University Munich, Genetics Section, Grosshaderner Str. 2-4, 82152 Planegg-Martinsried, Germany

**Running Title:** mRNP and endosome co-transport

**Key words:** RNA recognition motif, long distance transport, vesicle trafficking, *Ustilago maydis*

Corresponding author:
Dr. Michael Feldbrügge
Institute for Microbiology
Heinrich-Heine University Düsseldorf
40204 Düsseldorf, Germany
Phone: +49 (211) 81-15475
Fax: +49 (211) 81-15370
feldbrue@hhu.de

**Summary**

Long-distance transport of mRNAs is important in determining polarity in eukaryotes. Molecular motors shuttle large ribonucleoprotein complexes (mRNPs) containing RNA-binding proteins and associated factors along microtubules. However, precise mechanisms including the interplay of molecular motors and a potential connection to membrane trafficking remain elusive. Here, we solve the motor composition of transported mRNPs containing the RNA-binding protein Rrm4 of the pathogen *Ustilago maydis*. The underlying transport process determines the axis of polarity in infectious filaments. Plus end-directed Kin3, a Kinesin-3 type motor, mediates anterograde transport of mRNPs and is also present in transport units moving retrogradely. Split-dynein Dyn1/2 functions in retrograde movement of mRNPs. Plus end-directed conventional kinesin Kin1 is indirectly involved by transporting minus end-directed Dyn1/2 back to plus ends. Importantly, we additionally demonstrate that Rrm4-containing mRNPs co-localise with the t-SNARE Yup1 on shuttling endosomes and that functional endosomes are essential for mRNP movement. Either loss of Kin3 or removal of its lipid-binding pleckstrin homology domain abolish Rrm4-dependent movement without preventing co-localisation of Rrm4 and Yup1-positive endosomes. In summary, we uncovered the combination of motors required for mRNP shuttling along microtubules. Furthermore, intimately linked co-transport of endosomes and mRNPs suggests vesicle hitchhiking as novel mode of mRNP transport.

### 2.2.1 Introduction

Localised translation in eukaryotes is crucial in determining the subcellular localisation of proteins and thus involved in a number of cellular processes such as establishing and maintaining polarity. An important mechanism is the active transport of mRNAs along the cytoskeleton of actin cables and microtubules for short and long-distance transport, respectively. Cargo mRNAs are recognised by RNA-binding proteins that associate with accessory factors to form large ribonucleoprotein complexes designated mRNPs (Holt & Bullock, 2009; Martin & Ephrussi, 2009; St Johnston, 2005).

Microtubule-dependent mRNP transport is important for oogenesis, embryogenesis and neuronal processes in higher eukaryotes as well as for polar growth in fungi (Doyle & Kiebler, 2011; King et al, 2005; Palacios, 2007; Zarnack & Feldbrügge, 2007). Active transport is mediated by unidirectionally moving molecular motors. In

most cases, kinesins move cargo towards the plus end of microtubules whereas their counterpart dynein transports cargo towards the minus end (Gennerich & Vale, 2009; Li & Gundersen, 2008).

During oogenesis of *Drosophila melanogaster* transport and localisation of mRNAs encoding morphogens are essential in determining both main body axes. A well-studied example is the role of Staufen during mRNP trafficking (St Johnston, 2005; Martin & Ephrussi, 2009). This RNA-binding protein is required for *oskar* mRNA localisation and most likely binds stem-loop zip codes in the 3' UTR (Jenny et al, 2006). Staufen *and oskar*-containing mRNPs that shuttle along microtubules are transported by conventional kinesin predominantly towards the plus ends of microtubules. A biased random walk along a weakly polarised cytoskeleton might result in accumulating *oskar* mRNA at the posterior pole of the oocyte (Zimyanin et al, 2008). During embryogenesis pair-rule transcripts localise to the apical cytoplasm. Here, mRNA zip codes are recognised by the RNA-binding protein Egalitarian (Egl) that binds dynein in concert with Bicaudal-D (Bic-D; Dienstbier et al, 2009). It was hypothesized that shuttling mRNPs reach their final destination, because the zip code-mediated coupling of mRNPs to dynein promotes the processivity of the motor complex and thus drives its movement towards microtubule minus ends that are facing to the apical site (Bullock et al, 2006). In addition, dynein plays a part in anchoring mRNPs at the site of their localisation (Delanoue & Davis, 2005; Delanoue et al, 2007).

In *Ustilago maydis*, microtubule-dependent mRNA trafficking is important for pathogenic development (Feldbrügge et al, 2008; Vollmeister & Feldbrügge, 2010). In this pathogen a morphological switch from yeast-like sporidia to infectious filaments is essential to cause corn smut disease (Brefort et al, 2009). The filamentous program is triggered by a homeodomain transcription factor whose activity is regulated at the level of heterodimerisation (*i.e.* the formation of a bW/bE heterodimer; Kämper et al, 1995; Vollmeister et al, 2012). Infectious filaments grow with a defined axis of polarity. They expand at the hyphal tip and insert retraction septa at regular intervals at the basal pole leading to the formation of characteristic empty sections. Nuclei are positioned in the central regions of filaments (Steinberg et al, 1998). Studies using the microtubule inhibitor benomyl revealed that microtubules are essential for efficient filamentous growth (Fuchs et al, 2005). In the absence of microtubules filaments are shorter and the formation of retraction septa is impaired. Moreover, the axis of polarity is disturbed as cells initiate bipolar growth (Fuchs et al, 2005). Analysis of microtubule orientation in

*U. maydis* filaments revealed that about 90% of microtubules face towards the poles with their plus ends (Lenz et al, 2006; Schuchardt et al, 2005; Schuster et al, 2011c). They serve as tracks for molecular transport units such as endosomes. This was discovered studying the t-SNARE-like protein Yup1 that is involved in the endocytotic uptake of the lipophilic styryl dye FM4-64. Loss-of-function mutants showed a disturbed morphology, most likely due to alterations in cell wall composition (Wedlich-Söldner et al, 2000). Yup1 and the small GTPase Rab5a co-localise on shuttling endosomes (Fuchs et al, 2006; Schuster et al, 2011b; Schuster et al, 2011c). Their plus end-directed transport is mediated through Kin3, an UNC-104/KIF1A-like Kinesin-3 and the minus end-directed transport through split dynein Dyn1/2 whose subunits are encoded by separate genes, *dyn1* and *dyn2* (Straube et al, 2001; Wedlich-Söldner et al, 2002; Schuster et al, 2011a; Schuster et al, 2011b; Schuster et al, 2011c). This process might mediate the transport of cargo to the basal vacuole for degradation or could promote membrane recycling for a continuous supply of membranes at the apical growth cone (Steinberg, 2007a; Steinberg, 2007b). During sporidial proliferation, shuttling endosomes function in subcellular targeting of small GTPase regulators to septation sites in order to coordinate cytokinesis and cell separation (Schink and Bölker, 2009).

A second important long-distance transport process is the microtubule-dependent trafficking of mRNAs, which was discovered studying the function of Rrm4 (Vollmeister and Feldbrügge, 2010). Rrm4 is an ELAV-type RNA-binding protein (embryonic lethal abnormal vision, the closest human homologue belongs to the ELAV/HuD family; Becht et al, 2005). It contains three N-terminal RNA recognition motifs (RRMs) and a C-terminal MLLE domain (MademoiseLLE, protein/protein interaction domain found at the C terminus of poly[A]-binding protein PABPC, (Kozlov et al, 2010; Kozlov et al, 2001)). Loss of Rrm4 causes aberrant filament formation and reduced pathogenicity (Becht et al, 2005). The protein moves bidirectionally along microtubules in wild-type filaments. Deletion of *kin1* encoding conventional kinesin (Lehmler et al, 1997) results in an accumulation of Rrm4 at the poles (Becht et al, 2006). This accumulation at the microtubule plus ends is most likely an indirect effect, since Kin1 recycles dynein to maintain a constant reservoir of accessible dynein at the plus ends (Lenz et al, 2006). Combining in vivo UV crosslinking and RNA live imaging demonstrated that Rrm4 recognises and transports a distinct set of mRNAs encoding, for example, translation and polarity factors (König et al, 2009). Consistently, the poly(A)-binding protein Pab1, which associates with the poly(A) tail of most eukaryotic mRNAs

(Hogan et al, 2008), co-localises with Rrm4 in shuttling particles. In the absence of Rrm4, Pab1 is no longer transported indicating that Rrm4 is part of the primary transport unit and functions as the key RNA-binding protein during mRNA transport (König et al, 2009). Its target mRNAs contain potentially CA-rich binding sites that function as RNA zip codes to promote frequency and processivity of microtubule-dependent transport (König et al, 2009). Removal of the three RRMs of Rrm4 results in a non-functional protein that still shuttles along microtubules. However, microtubule-dependent transport of target mRNA is hampered. Consequently, filaments grow like the *rrm4Δ* strain exhibiting impaired formation of retraction septa and altered polarity. Thus, the RNA-binding domain is functionally important, and Rrm4 does not hitchhike on transported mRNAs but is an integral part of the transport unit (König et al, 2009). According to current views, microtubule-dependent transport of mRNPs is important in determining the subcellular localisation of targets such as the small G protein Rho3 at retraction septa as well as crucial for efficient secretion of the endochitinase Cts1 (Koepke et al, 2011; König et al, 2009; Zarnack & Feldbrügge, 2010)

### 2.2.2 Results

*Loss of Kin1 causes accumulation of mRNPs at both poles of mutant filaments*

To investigate the involvement of Kin1 in mRNP transport we analysed the subcellular localisation of Rrm4 and Pab1 in filaments in the absence of Kin1. Studies were performed using strain AB33 expressing an active bW2/bE1 heterodimeric transcription factor controlled by the nitrate-inducible *nar1* promoter (Table 1). Thus, changing the nitrogen source of the medium activates bW2/bE1 expression and subsequent formation of an active heterodimer. This is sufficient to trigger filamentous growth synchronously and highly reproducible (Brachmann et al, 2001).

As previously shown (König et al, 2009), Rrm4G and Pab1R (functional C-terminal fusion proteins of Rrm4 and Pab1 with the enhanced version of the green fluorescence protein eGfp and the monomeric red fluorescence protein mRfp, respectively) co-localised in mRNPs that were transported along microtubules (Supplemental Fig. S1A; Supplemental Movie S1). Rrm4G$^{RRM\Delta}$ lacking all three RRMs

**Table 1** *U. maydis* strains used in this study

| Strain | Locus | Progenitor | Specific comment |
|---|---|---|---|
| FB1 | | | wild-type, mating type *a1b1*[1] |
| FB2 | | | wild-type, mating type *a2b2*[1] |
| UM521 | | | wild-type, mating type *a1b1*, genome sequenced[2] |
| AB33 | *b* | FB2 | $P_{nar}$*:bW2bE1*, expression of active b heterodimer under control of the *nar1* promoter, strain grows filamentously upon changing th nitrogen source[3] |
| AB5 | *b* | FB1 | $P_{nar}$*:bW2bE1*, comparable to AB33 but in the genetic background of FB1 |
| AB5dyn2$^{ts}$ | *dyn2* | AB5 | carrying a temperature sensitive allele of *dyn2*[4] |
| AB5dyn2$^{ts}$/rrm4G | *dyn2*<br>*rrm4* | AB5dyn2$^{ts}$ | expressing Rrm4 fused to enhanced version of eGfp[5] |
| AB5dyn2$^{ts}$/rrm4G/pab1R | *dyn2*<br>*rrm4*<br>*pab1* | AB5dyn2$^{ts}$/rrm4G | expressing Pab1 fused to monomeric version of Rfp |
| AB33rrm4G | *rrm4* | AB33 | expressing Rrm4 fused to eGfp[5] |
| AB33rrm4G/pab1R | *rrm4*<br>*pab1* | AB33rrm4G | expressing Pab1 fused to mRfp[6] |
| AB33rrm4G$^{RRM\Delta}$/pab1R | *rrm4*<br>*pab1* | AB33pab1R/rrm4G | expressing Rrm4 without RRMs fused to eGfp |
| AB33rrm4G/kin1Δ | *rrm4*<br>*kin1* | AB33rrm4G | carrying a deletion in *kin1* |
| AB33rrm4G/pab1R/kin1Δ | *rrm4*<br>*pab1*<br>*kin1* | AB33pab1R/rrm4G | carrying a deletion in *kin1* |
| AB33rrm4G$^{RRM\Delta}$/pab1R/kin1Δ | *rrm4*<br>*pab1*<br>*kin1* | AB33rrm4G$^{RRM\Delta}$<br>/pab1R | expressing Rrm4 version without RRMs fused to eGfp and carrying a deletion in *kin1* |
| AB33rrm4R/dyn2G[3] | *rrm4*<br>*dyn2* | AB33rrm4R | expressing Dyn2 fused at the C-terminus to triple eGfp |
| AB33rrm4G/kin3Δ | *rrm4*<br>*kin3* | AB33rrm4G | carrying a deletion in *kin3* |
| AB33rrm4G/pab1R/kin3Δ | *rrm4*<br>*pab1*<br>*kin3* | AB33pab1R/rrm4G | carrying a deletion in *kin3* |
| AB33kin3G[3] | *kin3* | AB33 | expressing Kin3 fused at the C-terminus to triple eGfp |
| AB33rrm4R/kin3G[3] | *rrm4*<br>*kin3* | AB33rrm4R | expressing Kin3 fused at the C-terminus to triple eGfp |
| AB33rrm4G/P$_{otef}$yup1C | *rrm4*<br>*ip$^s$* | AB33rrm4G | expressing Yup1 fused to monomeric Cherry under control of the constitutively active promoter P$_{otef}$; defined ectopic integration at the *ip$^s$* locus[7], encoding a carboxin sensitive iron sulfur protein [7] |
| AB33rrm4Δ/P$_{otef}$yup1C | *rrm4*<br>*ip$^s$* | AB33rrm4G | carrying a deletion in *rrm4* |
| AB33rrm4R/kin3Δ | *rrm4*<br>*kin3* | AB33rrm4R | carrying a deletion in *kin3* |
| AB33rrm4R/kin3$^{PH\Delta}$G[3] | *rrm4*<br>*kin3* | AB33rrm4R/kin3Δ | expressing Kin3 version without pleckstrin homology domain and fused at the C-terminus to triple eGfp |
| AB33rrm4GT/P$_{otef}$yup1CM | *rrm4*<br>*ip$^s$* | AB33rrm4GT | expressing Rrm4 with tandem affinity protein tag fused to eGfp an Yup1 fused to monomeric Cherry containing a triple Myc epitope t |
| AB33rrm4GT/P$_{otef}$yup1CM/ kin3$^{PH\Delta}$–HA[3] | *rrm4*<br>*ip$^s$*<br>*kin3* | AB33rrm4GT/<br>P$_{otef}$yup1CM | expressing Kin3 version without pleckstrin homology domain and fused at the C-terminus to triple HA epitope |
| AB33rrm4GT/P$_{otef}$yup1CM/ kin3Δ | *rrm4*<br>*ip$^s$*<br>*kin3* | AB33rrm4GT/<br>P$_{otef}$yup1CM | carrying a deletion in *kin3* |
| AB33yup1$^{ts}$ | *yup1* | AB33 | carrying a temperature sensitive allele of *yup1*[8] |

| | | | |
|---|---|---|---|
| AB33yup1$^{ts}$/rrm4G | *yup1* *rrm4* | AB33yup1$^{ts}$ | expressing Rrm4 fused to eGfp |
| AB33yup1$^{ts}$/rrm4G/P$_{otef}$yup1C | *yup1* *rrm4* *ip$^{s}$* | AB33yup1$^{ts}$/rrm4G | expressing Yup1-mCherry under control of the constitutively activ promoter P$_{otef}$ in order to complement the mutant; defined ectopic integration at the *ip$^{s}$* locus[7] |
| AB33P$_{otef}$rab5aG | *rab5a* | AB33 | expressing eGfp-Rab5a ectopically under control of the constitutiv active promoter P$_{otef}$ at the *ip$^{s}$* locus[7] |
| AB33yup1$^{ts}$/P$_{otef}$rab5aG | *yup1* *ip$^{s}$* | AB33yup1$^{ts}$ | expressing eGfp-Rab5a ectopically under control of the promoter P at the *ip$^{s}$* locus[7]; temperature sensitive allele of *yup1*[8] |

[1] Banuett and Herskowitz, 1989; [2] Kämper et al., 2006; [3] Brachmann et al., 2001; [4] Wedlich-Söldner et al., 2002; [5] Becht et al., 2006; [6] König et al., 2009; [7] Loubradou et al., 2001; [8] Wedlich-Söldner et al., 2000 (kindly provided by G. Steinberg)

also shuttled along microtubules even though mRNA transport was lost. Consequently, the respective strains showed the loss-of-function phenotype (Supplemental Fig. S1B; König et al, 2009). Here, we show that Pab1R was no longer part of the transport units in this strain (Supplemental Fig. S1B; Supplemental Movie S2). This is consistent with earlier results investigating the transport of *ubi1* mRNA by RNA live imaging (König et al, 2009), We observe a high concentration of Pab1R in the initial cell with decreasing intensity towards both poles (Supplemental Fig. S1B). This is reminiscent of the Pab1 gradient observed in *rrm4Δ* filaments, suggesting a disturbed mRNA distribution (König et al, 2009). Thus, Rrm4 can be considered as an integral part of the transport unit while Pab1 serves as a molecular marker for the presence of transported mRNAs. The presence of both proteins is an indicator for intact mRNPs (König et al, 2009; Zarnack and Feldbrügge, 2010).

The mRNP markers were used to investigate the role of conventional kinesin Kin1 by deleting *kin1* in AB33rrm4G/pab1R. As shown before (Becht et al, 2006), loss of Kin1 led to defects in filamentous growth that resembled those of *rrm4Δ* strains (Supplemental Fig. S1C). In accordance with the observation that Kin1 transports split dynein Dyn1/2 to the plus ends of microtubules at hyphal tips (Lenz et al, 2006) movement of Rrm4G was drastically reduced, and the protein accumulated at both poles of the aberrantly growing filaments (Supplemental Fig. S1C; Becht et al, 2006). Here, we demonstrate that distribution of Pab1R was also disturbed in that a gradient of Pab1R emanated from the filament centre. In addition, Pab1R co-localised with Rrm4G at the hyphal poles, indicating an accumulation of mRNPs at these sites (48 of 49 polar Rrm4G accumulations in 26 filaments also showed Pab1R accumulation; Supplemental Fig. S1C). Residual moving units contained both Rrm4G and Pab1R (Supplemental Movie S3). In strains expressing Rrm4G$^{RRM\Delta}$, Pab1 no longer accumulated at the poles (none of 40 polar Rrm4 accumulations in 24 filaments co-localised with Pab1R;

Supplemental Fig. S1D), demonstrating that Rrm4G$^{RRM\Delta}$ particles were devoid of mRNA. These observations validated that Rrm4G movement is independent of the presence of mRNA in the particles while Pab1R hitchhikes on transported mRNAs and can thus serve as an in vivo marker for mRNP transport. Taking advantage of these markers, we showed that conventional kinesin is involved in the transport of mRNPs containing Rrm4 and Pab1. As previously suggested this influence is indirect, since Kin1 is essential for the accumulation of Dyn1/2 at the plus ends of microtubules, forming a potential dynein loading zone (Lenz et al, 2006; Schuster et al, 2011a).

*Dyn2 is necessaryfor mRNP shuttling an co-localises with Rrm4 in vivo*

The observed role of Kin1 during mRNA transport suggested that split dynein Dyn1/2 mediates retrograde transport of mRNPs (Lenz et al, 2006). To test this hypothesis we made use of a temperature-sensitive allele of *dyn2* that causes inactivation of dynein at restrictive temperatures (Wedlich-Söldner et al, 2002a; Table 1). The allele was originally identified in the genetic background of strain FB1 (mating type *a1b1*). So far, it was impossible to generate viable transformants carrying the *dyn2*$^{ts}$ allele at the homologous locus of FB2 (mating type *a2b2*) or its derivative AB33, suggesting that its temperature sensitivity is closely linked to the genetic background of FB1 (Table 1). Therefore, we used strain AB5 carrying an active bW2/bE1 heterodimeric transcription factor under control of the *nar1* promoter in the genetic background of FB1, which tolerated integration of the temperature-sensitive allele (see Materials and Methods; Table 1). Comparable to AB33 filamentous growth can be elicited in AB5 by changing the nitrogen source of the medium (see above). To examine mRNP movement in the absence of functional Dyn2 we generated the marker strain AB5dyn2$^{ts}$/rrm4G/pab1R. Growth assays with yeast-like cells verified that *dyn2*$^{ts}$-carrying strains were viable at permissive temperatures but failed to grow under restrictive conditions (Fig. 1A). Under filament-inducing conditions at permissive temperatures the vast majority of filaments grew unipolar, and shuttling of Rrm4G/Pab1R-containing mRNPs was comparable to wild-type (Supplemental Movie S4; Fig. 1B,D). Occasionally, mRNPs accumulated within the cytoplasm indicating that the temperature-sensitive motor exhibited minor transport defects (Fig. 1B, lower panel). At restrictive temperatures, however, 89% of filaments grew bipolar and 11% even tripolar, indicating that minus end-directed transport is essential in determining the axis

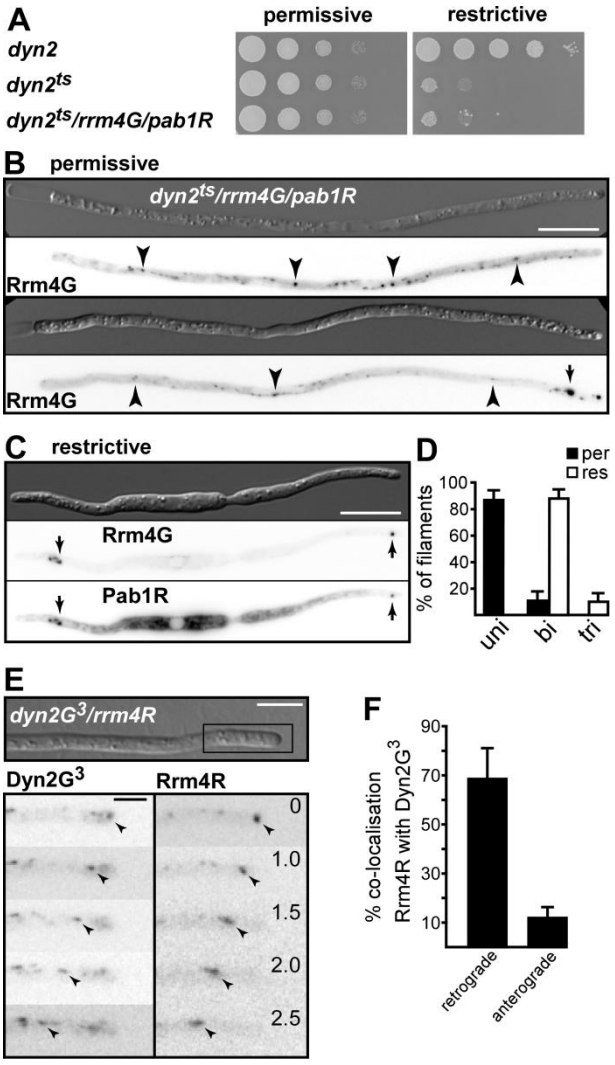


**Fig. 1. Dyn2 is essential for Rrm4 transport and co-localises with Rrm4-containing units.** (A) Growth of AB5 and derivatives carrying a temperature-sensitive mutation in *dyn2*. Plates were incubated at permissive or restrictive temperatures. (B-C) Filaments of AB5dyn2$^{ts}$/rrm4G/pab1R at permissive (B, two Rrm4G examples) and restrictive (C) temperatures. Filamentous growth was elicited by changing the nitrogen source of the medium resulting in transcriptional activation of the bW2/bE1 heterodimer (see text for details). Arrowheads and arrows indicate moving particles and large immobile accumulations, respectively (size bars, 10 µm; see Supplemental Movies S4 and S5). (D) Bar diagram showing percentage of filaments that grow unipolarly (uni), bipolarly (bi) and tripolarly (tri) at permissive (per) and restrictive (res) temperatures (error bars, sem). (E) Filaments of AB33dyn2G$^{3}$/rrm4R. Rectangle indicates region magnified below. Inverted frames are taken from Supplemental Movies S6 recorded with dual-colour detection. Rfp and Gfp images recorded simultaneously are shown juxtaposed (size bars: top 5 µm and bottom 2.5 µm). The elapsed time is given in seconds. (F) Bar diagram showing the percentage of mobile Rrm4R signals that co-localise with Dyn2G$^{3}$ in the retrograde and anterograde direction (error bars, sem).

of polarity in b-dependent infectious filaments (Fig. 1C,D). Importantly, mRNPs containing Rrm4G and Pab1R accumulated at the plus ends of microtubules at both poles (Fig. 1C; 24 filaments with 42 Rrm4G accumulations, 100% co-localisation with Pab1R accumulations; Supplemental Movie S5). In addition, a Pab1R gradient was observed emanating from the filament centre indicating disturbed mRNA distribution. No residual movement of mRNPs could be detected. Consequently, the split dynein subunit Dyn2 is essential for the transport of Rrm4-containing mRNPs.

To verify whether Rrm4-containing mRNPs are still transported towards the poles in the absence of functional Dyn2, we analysed strain AB5dyn2$^{ts}$/rrm4G at permissive temperature and shortly after shifting to restrictive temperature (Supplemental Fig. S2). The number of shuttling Rrm4G-containing units was drastically reduced at restrictive temperature. However, most of the remaining Rrm4G signals moved processively towards the poles suggesting that Rrm4 reaches the poles at least in part by plus end-directed movement along microtubules. Interestingly, during this process Rrm4 pauses

shortly and instead of reversing it continues movement towards the plus ends (Supplemental Fig. S2). Apparently, in the absence of the minus end-directed motor turning to retrograde movement is impossible.

To analyse co-localisation in vivo we generated strain AB33dyn2G$^3$/rrm4R expressing functional fusion proteins of Dyn2 and Rrm4 fused C-terminally to triple Gfp and mRfp, respectively (Becht et al, 2006; Lenz et al, 2006). Upon filament induction Dyn2G$^3$ and Rrm4R co-localised in shuttling units suggesting that dynein is involved in transporting Rrm4-containing mRNPs (Fig. 1E; Supplemental Movie S6 and S7). Since polarisation of the microtubule cytoskeleton is highest at the poles, where about 90% of plus ends face towards filament tips (Schuchardt et al, 2005; Lenz et al, 2006), we quantified the co-localisation of Rrm4-containing mRNPs with Dyn2G$^3$ in the hyphal apex (three independent experiments, ten filaments per experiment, zone of measurement 10 µm from the tip, 62 and 80 Rrm4R signals moving anterogradely and retrogradely, respectively). 12% of anterogradely and 69% of retrogradely moving Rrm4R signals co-localised with Dyn2G$^3$ (Fig. 1F), indicating that Dyn2G$^3$ is mainly associated with minus end-directed Rrm4R particles. Since Dyn2G$^3$ signals were close to the detection limit, a higher degree of co-localisation cannot be expected with our experimental setup (Supplemental Movie S6 and S7). Thus, the involvement of additional motors for retrograde movement appears unlikely. Taken together, our experiments demonstrate that split dynein mediates retrograde transport of Rrm4-containing mRNPs.

*Kin3 is necessary for mRNP shuttling and co-localises with Rrm4 in vivo*

Kin1 plays only an indirect role in Rrm4 transport. Hence, the motor mediating plus end-directed movement of mRNPs is still unknown. At present, only Kin1 and Kin3 have been described to exhibit defects in filamentous growth (Schuchardt et al, 2005). Therefore, we deleted *kin3* in the marker strain AB33rrm4G/pab1R (Table 1). The vast majority of respective filaments grew with a disturbed axis of polarity, and the insertion of retraction septa was impaired (Fig. 2A,B; Schuchardt et al, 2005). Rrm4G and Pab1R mainly co-localised in large immobile accumulations in the initial cell (Fig. 2A; Supplemental Movie S8). These accumulations resembled the localisation of cytoplasmic and perinuclear microtubule-organising centres, indicating that in the absence of Kin3 mRNPs are trapped at the minus ends of microtubules (Straube et al,

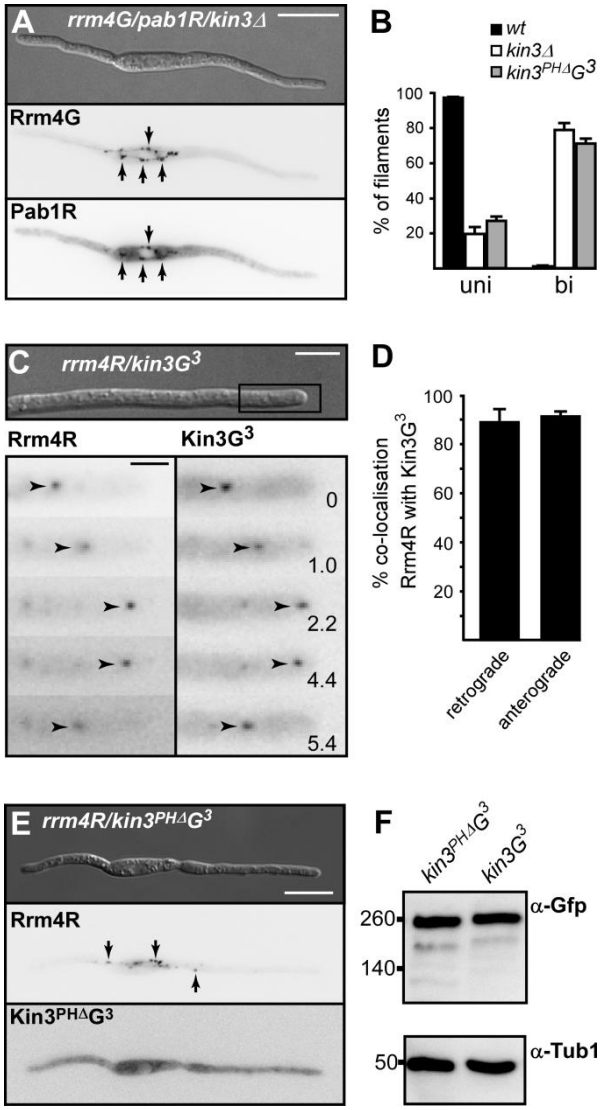


**Fig. 2. Kin3 is essential for mRNP transport and co-localises with Rrm4 in shuttling mRNPs.** (A) Rfp and Gfp images of AB33rrm4G/pab1R/kin3Δ filament recorded simultaneously are shown juxtaposed (size bar, 10 µm; see Supplemental Movie S8). Filamentous growth was elicited by changing the nitrogen source of the medium resulting in transcriptional activation of the bW2/bE1 heterodimer (see text for details). Arrows indicate larger immobile accumulations. (B) Bar diagram showing percentage of filaments that grow unipolarly (uni) and bipolarly (bi; error bars, sem; wt, *kin3Δ* and *kin3$^{PH\Delta}$G$^{3}$* correspond to strains AB33rrm4G/pab1R, AB33rrm4G/pab1R/kin3Δ and AB33rrm4R/kin3$^{PH\Delta}$G$^{3}$, respectively). (C) Filament of AB33rrm4R/kin3G$^{3}$. Rectangle indicates region that is magnified below. Arrowheads indicate moving particles. Inverted frames are taken from Supplemental Movie S9 recorded with dual-colour detection. Rfp and Gfp images recorded simultaneously are shown juxtaposed (size bars, 5 µm top and 2 µm bottom). Elapsed time is given in seconds. (D) Bar diagram showing the percentage of mobile Rrm4R signals that co-localise with Kin3G$^{3}$ in the anterograde and retrograde direction (error bars, sem). (E) Filament of AB33rrm4R/kin3$^{PH\Delta}$G$^{3}$. Inverted frames are taken from Supplemental Movie S11 recorded with dual-colour detection. Rfp and Gfp images recorded simultaneously are shown juxtaposed (size bar, 10 µm). Arrows indicate larger immobile accumulations. (F) Western blot detecting Kin3 variants fused to triple Gfp (indicated above the lanes). Antibodies used are given on the right (marker in kDa). Detection of Tub1 served as loading control.

2003; Lenz et al, 2006). The amount of Rrm4-containing units was reduced about threefold compared to the control strain with functional Kin3 (three independent experiments, ten filaments per experiment, average Rrm4G signals 55 +/- 1.7 and 20 +/- 1.1 in AB33rrm4G/pab1R and AB33rrm4G/pab1R/kin3Δ, respectively), which is most likely due to an accumulation of Rrm4G particles so that fewer signals can be resolved. Importantly, there was hardly any residual movement detectable, suggesting that Kin3 is exclusively responsible for anterograde transport.

To test co-localisation of Rrm4 and the anterograde motor we generated strain AB33rrm4R/kin3G$^{3}$. Rrm4R and Kin3G$^{3}$ co-localised in shuttling particles throughout the filament (Fig. 2C; Supplemental Movie S9-10). Particles were moving with comparable frequency in both directions suggesting that the plus end-directed Kin3 does

not dissociate from the transport complex during retrograde motion (Fig. 2D; 92% in anterograde and 90% in retrograde direction; three independent experiments, eight to ten filaments per experiment, zone of measurement 10 µm from the tip, 49 and 53 Rrm4R signals moving anterogradely and retrogradely, respectively).

Kin3 contains a conserved pleckstrin homology (PH) domain at its C terminus (position 1570 -1670 of 1676 amino acids; SMART accession SM00233, E-value $1.69e^{-11}$; (Letunic et al, 2009)). For UNC-104 it was shown that this evolutionarily conserved domain interacts specifically with phosphatidylinositol-4,5-bisphosphate and is necessary for vesicle transport in nematodes (Klopfenstein et al, 2002; Klopfenstein & Vale, 2004). In order to address whether this domain of Kin3 is important for mRNP transport in *U. maydis* we generated the strain AB33rrm4R/kin3$^{PH\Delta}$G$^{3}$ expressing a Kin3G$^{3}$ variant lacking the PH domain. The respective strain exhibited a growth phenotype comparable to *kin3Δ* mutants with the vast majority of filaments growing bipolar (Fig. 2B, E). This suggests that Kin3$^{PH\Delta}$G$^{3}$ is non-functional. Consistently, fluorescence microscopy revealed that Rrm4R accumulated in large immobile units in the central region of mutant filaments (Fig. 2E, Supplemental Movie S11), reminiscent of the results obtained for *kin3Δ* strains (Fig. 2A). Analysing the subcellular localisation of Kin3$^{PH\Delta}$G$^{3}$ revealed no accumulations but rather a dispersed distribution throughout the cytoplasm indicating that the specific localisation to shuttling units was lost (Fig. 2E, Supplemental Movie S11). This was not due to altered expression or protein stability, since Western blot experiments verified that the mutation does not cause drastic changes in protein amounts (Fig. 2F). To sum up, Kin3 mediates anterograde transport of Rrm4-containing mRNPs and the vesicle-binding domain of Kin3 is essential for this transport process.

*Rrm4 co-localises with FM4-64-positive endosomes*

The lipid-binding PH domain of Kinesin-3 type motors is crucial for endosomal transport (Klopfenstein and Vale, 2004), and the same set of motors is used for the transport of endosomes and mRNPs in filaments of *U. maydis* (this study; Wedlich-Söldner et al, 2002; Schuster et al., 2011b). This suggests that endosomes and mRNPs share their transport system. To validate this assumption we stained filaments with the styryl dye FM4-64. This dye labels membranes and enters eukaryotic cells by endocytosis. Thus, it initially stains the plasma membrane, then the vesicles classified as

early endosomes and finally the vacuole (Vida & Emr, 1995; Wedlich-Söldner et al, 2000). Staining of AB33kin3G$^3$ revealed that Kin3G$^3$ co-localised with FM4-64-labelled vesicles that shuttle throughout the filament (Fig. 3A) consistent with previous results demonstrating that Kin3 is the plus end-directed motor for endosome transport (Wedlich-Söldner et al., 2002; Schuster et al., 2011b; Schuster et al., 2011c).

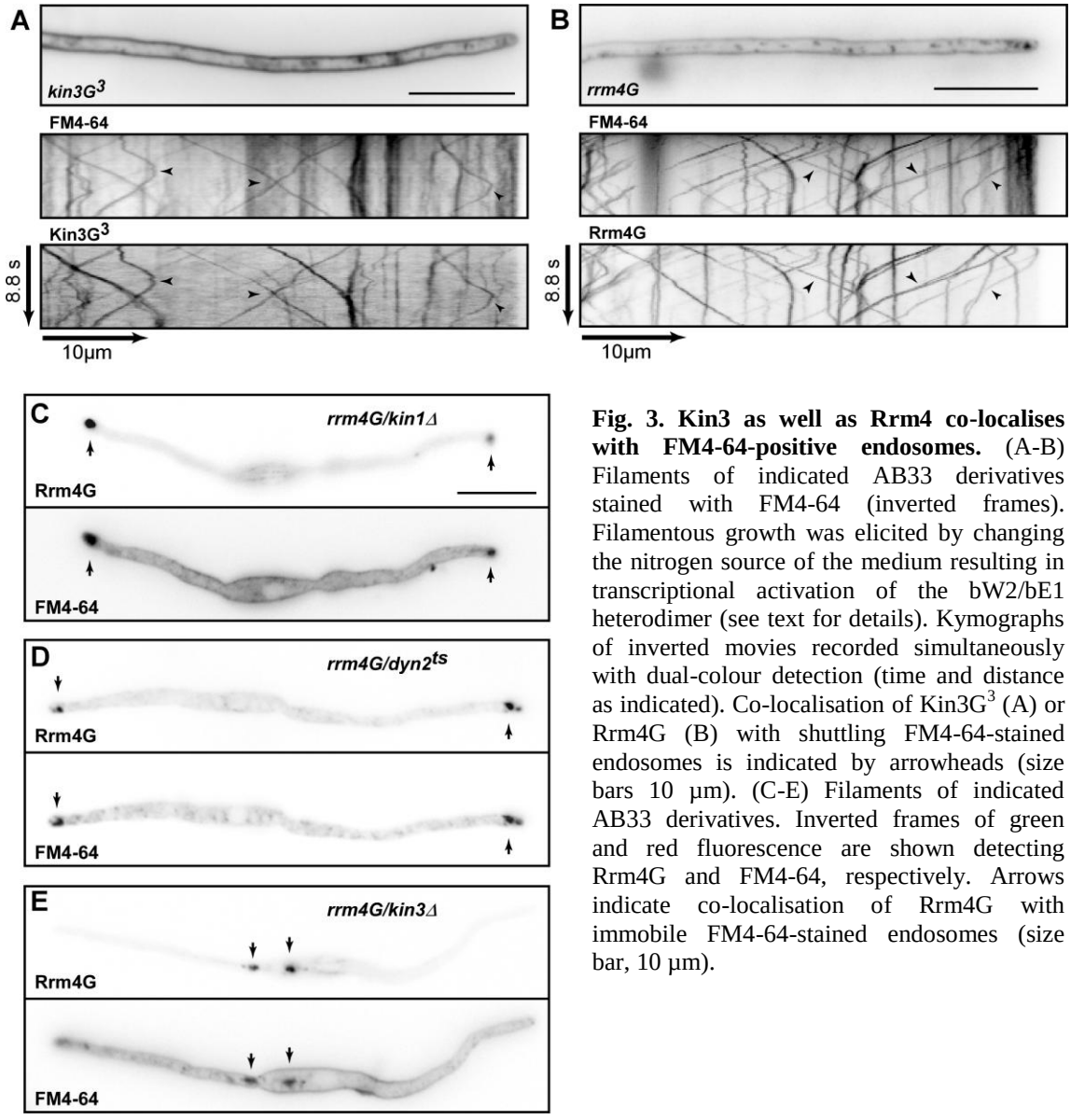


**Fig. 3. Kin3 as well as Rrm4 co-localises with FM4-64-positive endosomes.** (A-B) Filaments of indicated AB33 derivatives stained with FM4-64 (inverted frames). Filamentous growth was elicited by changing the nitrogen source of the medium resulting in transcriptional activation of the bW2/bE1 heterodimer (see text for details). Kymographs of inverted movies recorded simultaneously with dual-colour detection (time and distance as indicated). Co-localisation of Kin3G$^3$ (A) or Rrm4G (B) with shuttling FM4-64-stained endosomes is indicated by arrowheads (size bars 10 µm). (C-E) Filaments of indicated AB33 derivatives. Inverted frames of green and red fluorescence are shown detecting Rrm4G and FM4-64, respectively. Arrows indicate co-localisation of Rrm4G with immobile FM4-64-stained endosomes (size bar, 10 µm).

Importantly, staining of AB33rrm4G with FM4-64 revealed that also Rrm4G co-localises with these shuttling endosomes (Fig. 3B). To further substantiate our finding that Rrm4G co-localises with FM4-64-positive endosomes, we subjected strains with impaired functions in microtubule-dependent motors to FM4-64 staining. In filaments of AB33rrm4G/kin1Δ or AB5rrm4G/dyn2$^{ts}$ the staining at restrictive temperature revealed co-localisation of Rrm4G and FM4-64 at the growing poles suggesting that neither Kin1

nor active split Dyn1/2 are essential for co-localisation (Fig. 3C,D). Filaments of stained AB33rrm4G/kin3Δ showed that Rrm4G and FM4-64 co-localise in the centre of the initial cell suggesting that the presence of Kin3 is also not crucial for co-localisation (Fig. 3E). In essence, Rrm4G co-localises with FM4-64-positive endosomes in vivo and Kin1, active split Dyn1/2 or Kin3 are dispensable for this co-localisation.

*Shuttling Rrm4 particles are present almost exclusively on Yup1-positive endosomes*

The t-SNARE Yup1 is a characteristic marker for FM4-64-positives endosomes that shuttle bidirectionally along microtubules and are transported by Kin3 and Dyn1/2 (Wedlich-Söldner et al., 2000; Wedlich-Söldner et al., 2002; Schuster et al., 2011b). For verification and quantification of the important finding that Rrm4 and endosomes co-localise and are co-transported along microtubules we generated strain AB33rrm4G/$P_{otef}$yup1C expressing a C-terminal fusion of Yup1 with mCherry (derivative of mRFP; Shaner et al, 2004) under control of the constitutively active promoter $P_{otef}$ (Brachmann et al, 2004). The corresponding construct was targeted to the $ip^S$ locus resulting in the high expression of Yup1C in addition to the wild-type protein version (see Materials and Methods, Table 1). This results in strong signals without interfering with cell morphology (Wedlich-Söldner et al, 2000).

The vast majority of shuttling Rrm4G co-localised with Yup1C on endosomes throughout the filament (Fig. 4A, Supplemental Movie S12-13). Quantification of the co-localisation in the hyphal tip region revealed that 89% and 88% of anterogradely and retrogradely moving Rrm4G signals, respectively, coincided with moving Yup1C (3 independent experiments, 5 filaments per experiment, zone of measurement 10 µm from the tip, 67 and 71 Rrm4 signals moving anterogradely and retrogradely, respectively, Fig. 4B).

Since Kin3 co-localised with Rrm4 in the same unit shuttling in both directions (Fig. 2C,D), we verified if co-localisation of Rrm4 and Yup1-positive endosomes was dependent on Kin3. To this end we generated the strains AB33rrm4GT/yup1CM/kin3Δ and AB33rrm4GT/yup1CM/kin3$^{PH\Delta}$HA both expressing two functional fusion proteins: Rrm4 fused to eGfp and a tandem affinity tag as well as Yup1 fused to mCherry and a triple c-Myc epitope tag (König et al, 2009). The first strain carried a deletion in *kin3* and the second expressed Kin3 lacking its PH domain fused to a triple HA epitope tag (influenza hemagglutinin peptide, (Niman et al, 1983); Table 1). Investigating the

corresponding filaments revealed that, in both cases Rrm4GT and Yup1CM co-localised in accumulations at the centre of the initial cell indicating that Kin3 as well as its lipid-binding domain were dispensable for the co-localisation of Rrm4 and Yup1-positive endosomes. In summary, Rrm4-containing mRNPs are almost always travelling in concert with Yup1-positive endosomes and their co-localisation is independent of Kin3.

*Functional Yup1- and Rab5a-positive endosomes are essential for Rrm4 movement*

To investigate whether Rrm4 influences endosome movement we generated strain AB33P$_{otef}$yup1C/rrm4Δ. Analysing this strain in comparison to the control strain expressing Rrm4G and Yup1C revealed that shuttling of Yup1C-containing endosomes was not changed in the absence of Rrm4. This indicates that lack of mRNPs does not impair long-distance movement of endosomes (Fig. 5A). To study their reciprocal relationship, *i.e.* whether functional Yup1-positive vesicles are needed for Rrm4 transport we used a temperature sensitive mutant

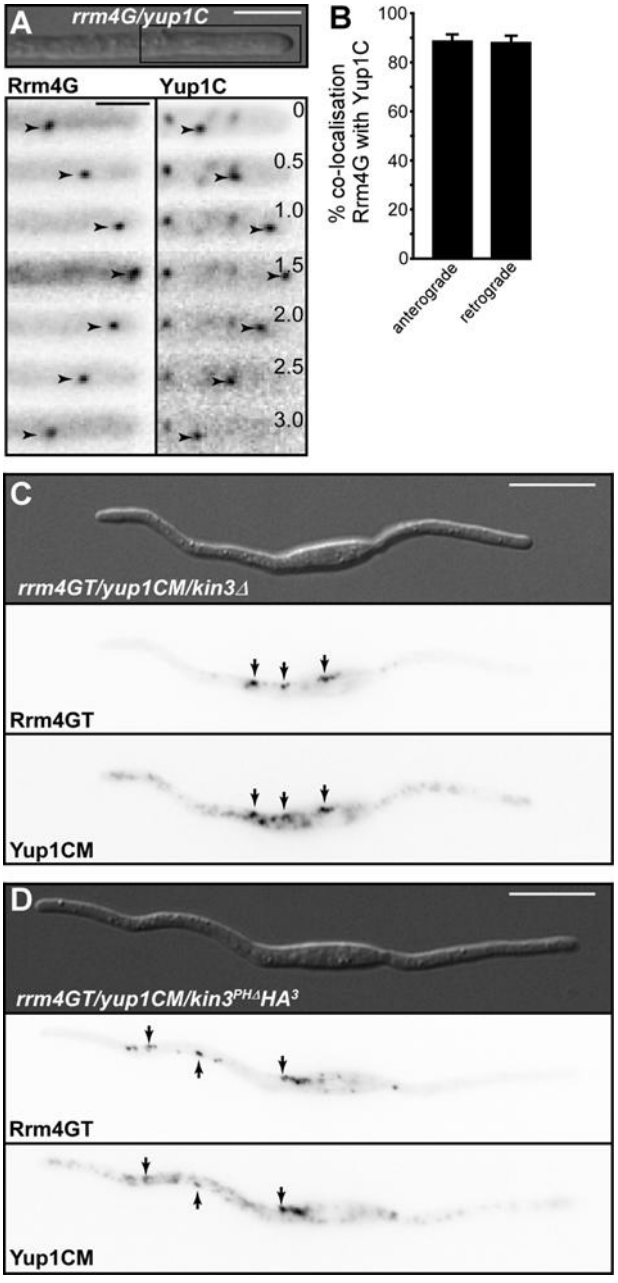


**Fig. 4. Rrm4 associates with Yup1-positive endosomes independent of Kin3.** (A) Filament tip of AB33rrm4G/yup1C. Filamentous growth was elicited by changing the nitrogen source of the medium resulting in transcriptional activation of the bW2/bE1 heterodimer (see text for details). Rectangle indicates region magnified below. Inverted frames are recorded with dual-colour detection and taken from Supplemental Movie S12. Images of green and red fluorescence recorded simultaneously and are shown juxtaposed (size bars, top 5 µm and bottom 2.5 µm). Arrowheads indicate moving units. Elapsed time is given in seconds. (B) Bar diagram showing the percentage of mobile Rrm4G signals that co-localise with Yup1C in the retrograde and anterograde direction (error bars, sem). (C-D) Filaments of AB33 derivatives as indicated. Inverted frames of green and red fluorescence (dual-colour mode) are shown detecting Rrm4GT and Yup1CM, respectively. Arrows indicate co-localisation of Rrm4GT with immobile Yup1-positive endosomes (size bar, 10 µm).

of *yup1*. We introduced *rrm4G* in the genetic background of AB33yup1$^{ts}$ (G. Steinberg, unpublished strain) carrying the temperature sensitive allele of *yup1$^{ts}$* (Wedlich-Söldner et al, 2000) at the homologous locus. Growth assays verified that *yup1$^{ts}$*-carrying strains grew filamentously at permissive temperature but failed to form filaments under restrictive conditions (Supplemental Fig. S3). Mutant growth under restrictive conditions could be complemented by expressing Yup1C under control of the constitutively active $P_{otef}$ promoter at the *ip$^{S}$* locus (Supplemental Fig. S3; Table 1). Fluorescence microscopy of AB33yup1$^{ts}$/rrm4G filaments under permissive temperature revealed that Rrm4G moved bidirectionally along microtubules comparable to Rrm4G of the control strain AB33rrm4G/pab1R (Fig. 5B, restrictive temperature at time point $t_0$). However, after prolonged growth under restrictive temperature Rrm4G movement was affected and after 60 minutes processive movement of Rrm4G could hardly be observed (Fig. 5B, kymograph lower right panel at $t_3$). In order to address whether this altered movement of Rrm4 is due to the detachment of mRNPs and endosomes, we investigated the loss of Yup1 during filamentous growth in closer detail. To check whether endosome disintegrate at restrictive temperature we aimed to stain endosomes with FM4-64. However, loss of Yup1 at restrictive temperature prevented uptake of the fluorescent dye to shuttling endosomes (Supplemental Fig. S4) showing that FM4-64 staining is not applicable to answer the question. Therefore, we used the small G protein Rab5a that has been intensively studied as endosomal marker in *U. maydis* to label endosomes (Schuster et al., 2011a, Schuster et al., 2011b, Schuster et al., 2011c). Ectopic expression of an N-terminal fusion of eGfp to Rab5a in the genetic background of AB33 under control of the constitutively active $P_{otef}$ promoter (Table 1) enabled detection of shuttling endosomes during filamentous growth (Supplemental Fig. S5). Investigating the same allele in the genetic background of AB33yup1$^{ts}$ revealed that prolonged growth at restrictive temperature causes defects in endosomal movement as indicated by the fact that the amount and the processivity of shuttling Rab5a-positive endosomes decreases (Supplemental Fig. S5). Thus, loss of Yup1 function does not simply cause the detachment of Rrm4-containing mRNPs but has a profound influence on membrane trafficking at the level of endocytosis and endosome shuttling. Therefore, we conclude that microtubule-dependent shuttling of functional Yup1- and Rab5a-positive endosomes is essential for Rrm4 transport through the filament.

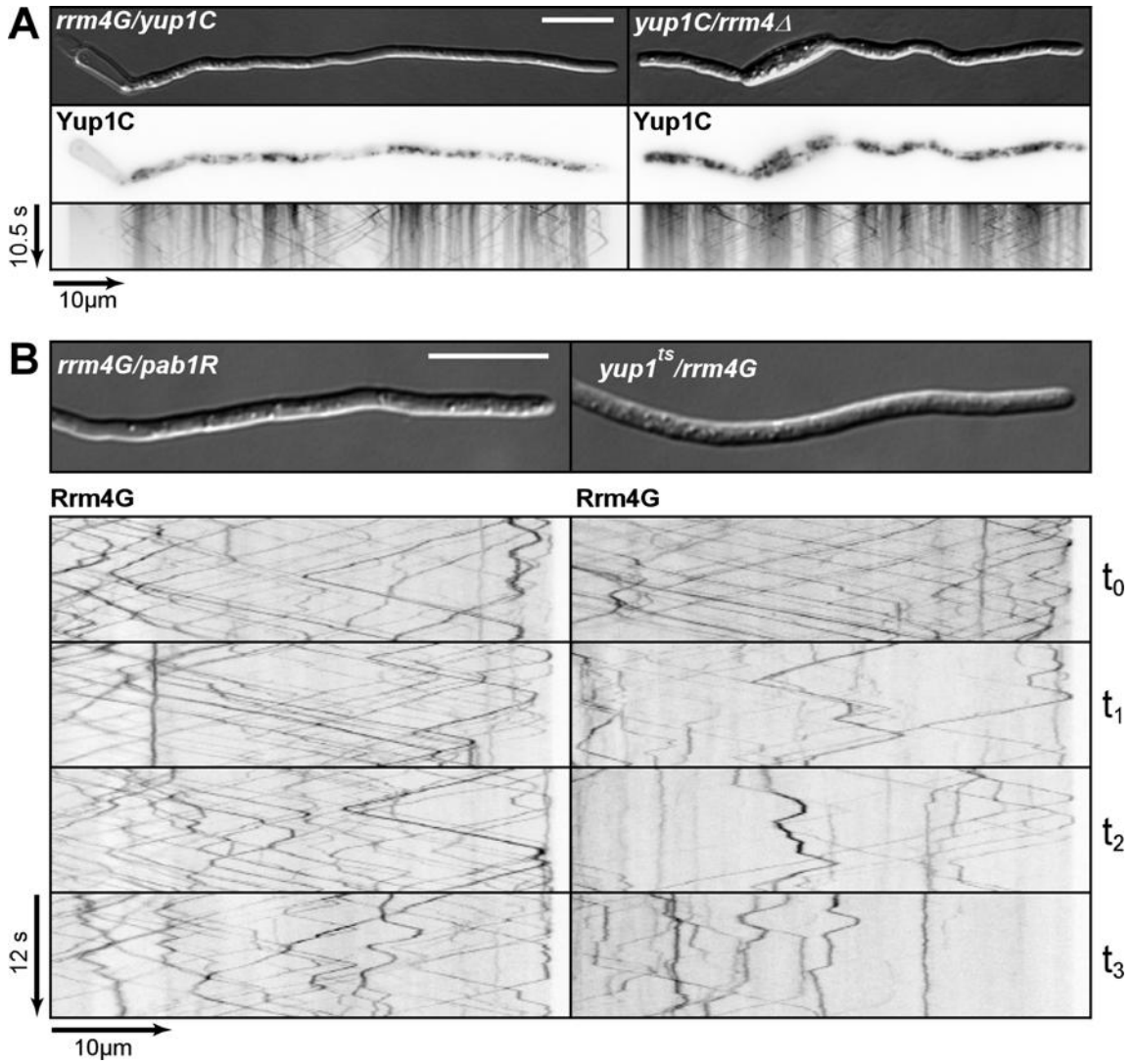


**Fig. 5. Functional Yup1-positive vesicles are essential for mRNP transport.** (A) Filaments of AB33rrm4G/yup1C and AB33rrm4Δ/yup1C on the left and right, respectively (size bar, 10 µm). Filamentous growth was elicited by changing the nitrogen source of the medium resulting in transcriptional activation of the bW2/bE1 heterodimer (see text for details). Inverted frames detecting Yup1C fluorescence and corresponding kymographs are shown (time and distance is given on the left). (B) Filaments of AB33rrm4G/pab1R and AB33rrm4G/yup1$^{ts}$ on the left and right, respectively (size bar, 10 µm). Kymographs (time and distance is given on the left) of inverted movies detecting Rrm4G fluorescence at different time intervals at restrictive temperature are shown ($t_0$ to $t_3$ = 0, 30, 53 and 60 minutes, respectively). Note that the frames of the respective kymographs were recorded from the same filament and that both filaments were analysed in the same field of view to guarantee equal temperature conditions. Strains could be differentiated by the red fluorescence signal of Pab1R in AB33rrm4G/pab1R.

### 2.2.3 Discussion

Despite considerable efforts and substantial progress the precise mechanisms of microtubule-dependent mRNP transport in eukaryotes are still elusive (Holt & Bullock, 2009; Meignin & Davis, 2010). In particular, the exact motor composition as well as the involvement of membrane trafficking are not clear. In this study, we identify the motor combination that mediates microtubule-dependent mRNP shuttling and provide in vivo

evidence for the co-transport of mRNPs and endosomes along microtubules. An important strength of our experimental system is the ability to generate strains by homologous recombination. Therefore, the dynamics and subcellular localization of mRNP components as well as molecular motors can be recorded at native expression levels.

*Kinesin-3 and split dynein mediate shuttling of mRNPs in* U. maydis

In many eukaryotic model systems, molecular motors mediate active shuttling of mRNPs along microtubules. This can be achieved by a single unidirectional motor along antipolar microtubules or by two motors with opposite directionality along polarised microtubule arrays. The motor repertoire of mRNP transport was studied to varying extends in different systems. In mammalian neurons, biochemical purification of Staufen-containing mRNPs revealed the presence of conventional kinesin (Mallardo et al, 2003). In oocytes of *Xenopus laevis* Kinesin-1-type and Kinesin-3-type motors coordinate mRNP transport to the vegetal cortex on subpopulations of microtubules (Messitt et al, 2008). In oocytes of *D. melanogaster oskar* mRNPs move bidirectionally along a weakly polarised microtubule cytoskeleton, and conventional kinesin is responsible for most of the transport (Zimyanin et al, 2008). Furthermore, in syncytial blastoderm embryos of *D. melanogaster* the RNA-binding protein Egalitarian interacts with the dynein light chain together with Bicaudal-D and forms a functional transport complex in concert with dynactin and the dynein heavy chain (Dienstbier et al, 2009). However, in none of these systems the whole motor composition has been identified to completely explain the shuttling mechanism of mRNPs during microtubule-dependent transport.

In this study, we addressed the motor composition of Rrm4-containing mRNPs in *U. maydis* filaments and uncovered the concerted action of the kinesin Kin3 and the split dynein Dyn1/2 mediating mRNP shuttling along microtubules. These findings were based on previous work studying the role of molecular motors in microtubule-dependent transport of endosomes in *U. maydis* (Steinberg, 2007b). Microtubules form 2 to 4 bundles that span the entire length of the filament. Within these bundles individual microtubules are arranged in an antipolar array. At the poles the microtubules no longer overlap and thus form a short unipolar region with plus ends facing towards the poles. Consequently, the region close to the poles is devoid of minus ends (Schuster et al, 2005a). Studying endosomal transport revealed that 2 to 5 Kin3 motors mediate plus

end-directed and highly processive movement throughout the whole filament (Schuster et al, 2011a, Schuster et al, 2011c). Split dynein Dyn1/2 is responsible for minus end-directed movement. Since microtubule-bundles are unipolar at the poles Dyn1/2 is particularly important for the transport from the poles towards the zone of antipolar microtubules. In this region, endosomes can either be transported by split dynein or Kin3 (Schuster et al, 2005a, Schuster et al, 2011c). Earlier work demonstrated that conventional kinesin Kin1 is, e.g., in fruit flies and filamentous fungi, important to transport dynein back to the plus ends of microtubules (Januschke et al, 2002; Lenz et al, 2006; Zhang et al, 2003). This explains the observation that Rrm4-containing mRNPs accumulate at the poles in the absence of Kin1 (Becht et al, 2006; this study).

Using a previously characterized temperature-sensitive allele of *dyn2* (Wedlich-Söldner et al, 2002) we were able to demonstrate that the minus end-directed transport of mRNPs in infectious filaments is mediated by dynein. Consistently, Dyn2 co-localised mainly with minus end-directed Rrm4-containing mRNPs at the poles. Since microtubules are clearly unipolarly organized at the growing poles, our study focused on this region of the filament (Schuster et al, 2005a). Analysis of Kin3 revealed that this motor is essential for transport of mRNPs towards the plus ends of microtubules. Kin3 and Rrm4 also co-localise on retrograde moving units indicating that the motor is recycled and that no independent backward transport of Kin3 towards minus ends of microtubules by an additional molecular motor is needed. Again, this becomes particularly evident in the unipolarly arranged region at the hyphal poles. The idea of Kin3 recycling is also supported by our observation that the protein variant lacking its PH domain is as stable as full length Kin3. In contrast, UNC-104 from *C. elegans* is degraded in the absence of vesicle cargo suggesting that in this model system the motor is not reused after cargo deposition (Kumar et al, 2010). In sum, plus end-directed transport along microtubules in *U. maydis* is mediated by Kin3 that does not dissociate from the transport unit, whereas split Dyn1/2 mediates minus end-directed movement and is then independently returned to the microtubule plus ends by the action of Kin1. Thus, the combination of these three motors mediates bidirectional long-distance transport of mRNPs along microtubules.

*Active co-transport of mRNPs and endosomes along microtubules*

The contribution of membrane trafficking to mRNP transport is presently not clear. Even in the best studied actin-dependent system, *ASH1* mRNA transport in *S.*

*cerevisiae*, controversial models are reported for the transport mechanisms. The traditional model describes the formation of a "locasome" consisting of cargo mRNAs containing mRNA zipcodes that are recognised by the concerted action of two unconventional RNA-binding proteins, She2p and She3p (Böhl et al, 2000; Muller et al, 2011). The resulting mRNP complex is transported by the molecular motor Myo4p along actin cables to the daughter cell (Müller et al, 2007; Paquin & Chartrand, 2008). This model was recently challenged by demonstrating a coordination of endoplasmic reticulum (ER) transport with cargo mRNA movement, suggesting a close link between mRNP and membrane trafficking (Gerst, 2008; Schmid et al, 2006).

Microtubule-dependent shuttling of mRNPs is crucial for a variety of different cellular events such as developmental and neuronal processes (Martin & Ephrussi, 2009; Meignin & Davis, 2010; Doyle & Kiebler, 2011). Among the best-studied examples is transport of pair-rule transcripts during embryogenesis. Egl recognizes mRNA zip codes and associates with Bic-D, which interacts with dynein and apparently increases motor processivity (Dienstbier et al, 2009). Intriguingly, Bic-D is also important for vesicle transport in neurons. However, this is an Egl independent process. Thus, at least in neurons mRNA transport and vesicle transport seem to be independent (Li et al, 2010).

In oocytes, it was shown that shuttling occurs along a weakly polarised cytoskeleton involving the RNA-binding protein Staufen and Kinesin 1 (Zimyanin et al, 2008). However, the orientation of the microtubule arrays and the potential role of dynein are not solved. Interestingly, a potential connection to membrane trafficking has also been described in this system. The endosomal marker Rab11, for example, is important for *oskar* mRNA localisation and this small G protein accumulates like the mRNA target at the posterior poles of oocyetes (Cohen, 2005; Dollar et al, 2002). Additional hints for a connection to membrane trafficking are the observation that mutants in components of ESCRT-II (endosomal sorting complex required for transport) abolish a Staufen-dependent step in the localisation of *bicoid* mRNA (Irion & St Johnston, 2007), and that genomic RNAs of mammalian retroviruses are transported on recycling endosomes in mammals (Basyuk et al, 2003; Molle et al, 2009).

In this study, we provide the first direct in vivo evidence for the co-transport of mRNPs and endosomes. As mentioned above, Rrm4-containing mRNPs rely on the same motor repertoire as shuttling endosomes suggesting their co-transport (Lenz et al, 2006; Steinberg, 2007a; Schuster et al, 2011a; Schuster et al, 2011b). This was verified by in vivo studies demonstrating that functional Kin3 or its lipid-binding PH domain are

crucial for mRNP transport and that Rrm4 co-localises with the lipophilic dye FM4-64 as well as the endosomal marker Yup1.

In theory, the endosome/mRNP co-transport could be mediated by at least two different mechanisms that may both include the action of adapter proteins: (i) molecular motors contain two distinct interaction domains, one for Rrm4 binding and one for the interaction with endosomes such as the lipid-binding PH domain or (ii) Rrm4 binds to endosomes and transport is mediated e.g. via the PH domain of Kin3. An example for such an adaptor is Bic-D from *D. melanogaster* that interacts with dynein and plays a role in both vesicle and mRNP transport (Dienstbier & Li, 2009; Li et al, 2010). In *U. maydis*, direct binding to dynein as the sole mode of mRNP shuttling can be excluded, because dynein is absent from most of the anterograde moving Rrm4 units. Direct binding to kinesin Kin3 could be possible, since it has been reported that conventional kinesin appears to interact directly with the RNA-binding protein FMRP during dendritic mRNA transport (Dictenberg et al, 2008). However, we favor the hypothesis that Rrm4 binds to endosomes independent of Kin3. This is based on our findings that Rrm4 co-localises with Yup1 in the absence of Kin3 or in strains expressing Kin3 without lipid-binding PH domain. It remains to be seen whether Rrm4 needs an adapter or can directly bind for example to specific endosomal lipids. Our analysis of the functional relationship of Rrm4 and endosome transport revealed that whereas endosome transport does not need mRNPs, mRNP transport depends on functional Rab5a-positive endosomes. Thus, we demonstrate that long-distance transport of Rrm4-containing mRNPs is functionally linked to endosome transport.

Microtubule-dependent transport is crucial in determining the axis of polarity in infectious filaments of *U. maydis*. Inhibiting polymerisation of microtubules with benomyl results in the formation of filaments that are shorter, grow bipolarly and are impaired in the insertion of retraction septa (Fuchs et al, 2005). The same is true in the absence of the plus end-directed molecular motors Kin1 and Kin3 (Becht et al, 2005; Schuchardt et al, 2005; this study) and when interfering with the split dynein function (this study). Importantly, the axis of polarity and the formation of retraction septa are also disturbed in Rrm4 mutants that are affected in RNA binding, resulting in transport of endosomes without Pab1-associated mRNAs (König et al, 2009, this study). Since loss of Rrm4 does not interfere with endosome movement, these effects are likely to reflect the functional importance of mRNP transport during polar growth.

In conclusion, we present strong evidence for a novel and unexpected link between endosome and mRNP transport. This adds yet another function to trafficking endosomes and is consistent with current views that these vesicular carriers function as multi-purpose platforms (Gould & Lippincott-Schwartz, 2009). Elucidating further mechanistic details will be critical to advance our understanding of mRNA transport and its function in spatio-temporal gene expression.

### 2.2.4 Materials and Methods

*Strains and growth conditions*

*E. coli* K-12 derivatives DH5α and Top10 (Invitrogen, Darmstadt, Germany) were used for cloning purposes. Transformation and cultivation were performed using standard techniques. Growth conditions for *U. maydis* strains and source of antibiotics were previously described (Brachmann et al, 2004). Strains were constructed by the transformation of progenitor strains with linearised plasmids (Table 1 and Supplemental Table S1). All homologous integration events were verified by Southern blot analysis (Brachmann et al., 2004). In case of strain AB33$P_{otef}$Yup1C, AB33$P_{otef}$Yup1CM, or AB33$P_{otef}$Rab5aG vector p$P_{otef}$Yup1C,p$P_{otef}$Yup1CM, or p$P_{otef}$Rab5aG, respectively, was linearised with Ssp1 and targeted to the $ip^S$ locus of AB33 (Loubradou et al, 2001). In case of strain AB5, vector pAB33 (Brachmann et al, 2001) linearised with SspI was transformed into FB1. Homologous integration and the functionality of both *nar1* promoters driving *bW2* and *bE1* expression was verified by Southern and Northern analysis, respectively.

Filamentous growth of AB33 and AB5 variants was induced by shifting 20 or 50 ml of exponentially growing cells ($OD_{600}$ = 0.4 - 0.5) from complete medium (CM) to nitrate minimal medium (NM) each supplemented with 1% glucose (glc). Cells were incubated at 28°C shaking at 200 rpm for 4 to 8 h prior to microscopy. The temperature sensitive strain AB5dyn2$^{ts}$/rrm4G/pab1R was induced for 15 h at permissive (18°C) and restrictive (28°C) temperatures. For verification of temperature sensitivity on plate, cells were grown to an $OD_{600}$ of 1. Tenfold dilutions were spotted on CM-agar and incubated at either 18 or 30°C. Analysis of temperature sensitive growth was performed as indicated in the legend of Supplemental Fig. S2.

*Plasmids and plasmid constructions*

Standard molecular techniques and strain generation for *U. maydis* were followed. Plasmids pCRII-Topo (Invitrogen) and pBluescriptSKII (Stratagene, California, USA) were used as cloning vehicles. Genomic DNA of wild-type strain UM521 (*a1b1*) was used as a template for PCR amplifications unless otherwise noted. All constructs were confirmed by sequencing. Detailed information is given in Supplemental Table S3 and plasmid sequences are available upon request.

*Chemicals and media*

Chemicals and media used in this study were purchased from Difco (Augsburg, Germany), Sigma-Aldrich (Steinheim, Germany), Merck (Darmstadt, Germnany), Baker (Griesheim, Germany), VWR (Darmstadt, Germany) and Roth (Karlsruhe, Germany). Restriction enzymes were obtained from NEB (Frankfurt, Germany), Phusion-Polymerase from Finnzymes (Schwerte, Germany) and T4-Ligase from Roche (Mannheim, Germany).

*Microscopy, image processing, quantitative analysis and FM4-64 staining*

Microscopy was performed on the following wide-field microscopes from Visitron Systems (Munich, Germany): i) Zeiss (Oberkochen Germany) Axiovert 200M equipped with a charge-coupled device camera (CCD; Photometrics CoolSNAP HQ, Tucson, AZ, USA) and objective lenses Plan Neofluar (40x, numerical aperture [NA] 0.75) and Plan Apochromat (63x and 100x; NA 1.4). ii) Zeiss Axio Observer.Z1 equipped with a CCD camera (Photometrics CoolSNAP HQ2) and objective lenses Plan Neofluar (40x, NA 1.3), Plan Apochromat (63x and 100x, NA 1.4) and α-Plan Apochromat (100x, NA 1.46). iii) Zeiss Axio Imager.M1 equipped with a Spot Pursuit CCD camera (Diagnostic Instruments, Sterling Heights, MI, USA) and objective lenses Plan Neofluar (40x and 100x, NA 1.3; 63x, NA 1.25).

Excitation of fluorescently-labelled proteins was carried out using an HBO 103 mercury lamp or HXP metal halide lamps (LEj, Jena, Germany) in combination with filter sets for Gfp (ET470/40BP, ET495LP, ET525/50BP) and Rfp/mCherry (ET560/40BP, ET585LP, ET630/75BP; Chroma, Bellow Falls, VT, USA). For detection of weak signals we used laser-based epifluorescence-microscopy. A VS-LMS4 Laser-

Merge-System (Visitron System) combines solid state lasers for the excitation of Gfp (488 nm/50 mW) and Rfp/mCherry (561 nm/50 mW).

Co-localisation studies of dynamic processes were carried out with a two-channel imager (DV2, Photometrics) that permits the simultaneous detection of Gfp and Rfp/mCherry. A dichroic beamsplitter and an excitation filter designed for Gfp and mCherry (GFP/mCherry; Chroma) were used to simultaneously excite the respective fluorophores. A second dichroic beamsplitter (dcxr565) within the dual-view device split the fluorescent signals into the respective colours that were separately filtered with emission filters (Gfp ET520/40; Rfp/mCherry ET632/60) prior to simultaneous imaging on different regions of the CCD chip.

To observe RrmG in strain AB5dyn2$^{ts}$/rrm4G a 472nm LED (CoolLED, precisExcite, Andover, UK) was used to reduce photobleaching to a minimum. All parts of the microscope systems were controlled by the software package MetaMorph (Molecular Devices, version 6 and 7, Sunnyvale, CA, USA), which was also used for image processing including the adjustment of brightness and contrast as well as the generation of kymographs.

For the quantification of co-localising proteins on moving vesicles, a segment of 10 µm from the apical pole in each filament was defined. Rrm4 containing units were counted and tested for the presence of Dyn2, Kin3, or Yup1. In each case three independent experiments were carried out with 10 (Dyn2), 8 to 10 (Kin3) and 5 (Yup1) filaments per experiment. The average amount of co-localising proteins as well as the standard error was determined.

For FM4-64 staining 1 ml of filament suspension was labelled in 0.8 µM FM4-64 (Invitrogen; in case of AB5dyn2$^{ts}$/rrm4G 4 µM FM4-64 was used). After 30-60 seconds of incubation at room temperature samples were subjected to microscopic analysis. In case of AB33yup1$^{ts}$/rrm4G, filaments were also incubated at restrictive temperature (Supplemental Fig. S4).

*Microscopic analysis of temperature sensitive mutants*

For the analysis of AB33yup1$^{ts}$/rrm4G the temperature in the sample was adjusted by pumping water from a waterbath (Huber, Offenburg, Germany) controlled by Metamorph software through a flexible tube connected to a metal ring plugged onto the objective. Thereby, heat is transferred via the immersion oil to the sample. Since the exact temperature in the sample cannot be determined the temperature sensitive strain

AB33yup1$^{ts}$/rrm4G and control strain AB33rrm4G/pab1R were mixed in equal amounts. In initial experiments a temperature of 48.5°C in the waterbath was determined to have an impact on Rrm4G movement in AB33yup1$^{ts}$/rrm4G but not in AB33rrm4G/pab1R. Immediately after identifying regions containing both strains in the field of vision, the observation of Rrm4G movement was started. Four subsequent movies were recorded at time points 0, 30 minutes, 53 minutes and 60 minutes. Each movie is 12 seconds long (80 frames, 150ms). The resulting movies were converted to kymographs.

For experiments with AB33yup1$^{ts}$/rab5aG (Supplemental Fig. S5) a waterbath temperature of 45°C was determined to confer restrictive conditions at the microscopic sample. This temperature had an effect on Rab5aG-positive endosomes in *yup1$^{ts}$* mutants after prolonged exposure but had no effect on control strain AB33rab5aG expressing endogenous Yup1. Four subsequent movies were recorded at time points 0, 12 minutes, 46 minutes and 92 minutes. Each movie is 15 seconds in length (100 frames, 150 ms). The resulting movies were converted to kymographs. The lower temperature (45°C versus 48.5°C, see above) probably reflects a minor defect caused by expression of Rab5aG.

The same experimental setup was used to analyse AB5dyn2$^{ts}$/rrm4G. Filaments were observed microscopically either at permissive temperature (21°C) or at restrictive temperature (waterbath set to 45°C). Single movies with 500 frames of 300 ms were recorded and converted to kymographs.

*Protein preparation and Western blot analysis*

Filaments were harvested by centrifugation (10.000 g, 5 minutes) and resuspended in 2 ml UmVIB buffer (20 mM HEPES-NaOH pH7.4, 400 mM Sorbitol, 150 mM NaCl, 5 mM $MgCl_2$, 1 mM EDTA, 1 mM DTT). Cells were frozen in liquid nitrogen and ground for 15 minutes in a pebble mill. The protein concentration was determined by Bradford assay (Bio-Rad, Munich, Germany). Protein samples were resolved by 8% SDS-PAGE and transferred to a PVDF membrane (GE Health Care, Munich, Germany) by semi-dry blotting (5 µg of protein were loaded for Western blot analysis with α-Gfp [Roche, Freiburg, Germany] and α-Tub [Sigma, Steinheim, Germany] antibodies). An α-mouse IgG HRP conjugate (H+L; Promega, Madison, WI, USA) was used as a secondary antibody. Activity was detected using the ECL plus Western blotting detection system (GE Health Care).

## 2.2.5 Supplementary information

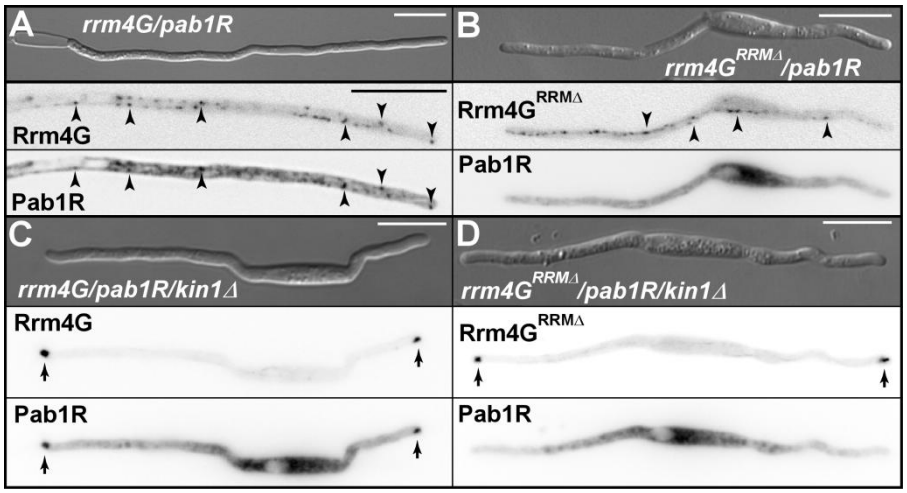


**Supplemental Fig. S1.** Loss of Kin1 results in the accumulation of Rrm4-containing mRNPs at the poles. (A-D) Filamentous growth was elicited by changing the nitrogen source of the medium resulting in transcriptional activation of the bW2/bE1 heterodimer. Filaments of the respective AB33 derivatives are shown. Inverted frames of A and B are taken from Supplemental Movies S1 and S2 recorded with dual-colour detection. Simultaneous Gfp and Rfp images are shown juxtaposed. Arrowheads and arrows indicate moving particles and large immobile accumulations, respectively (size bars, 10 µm).

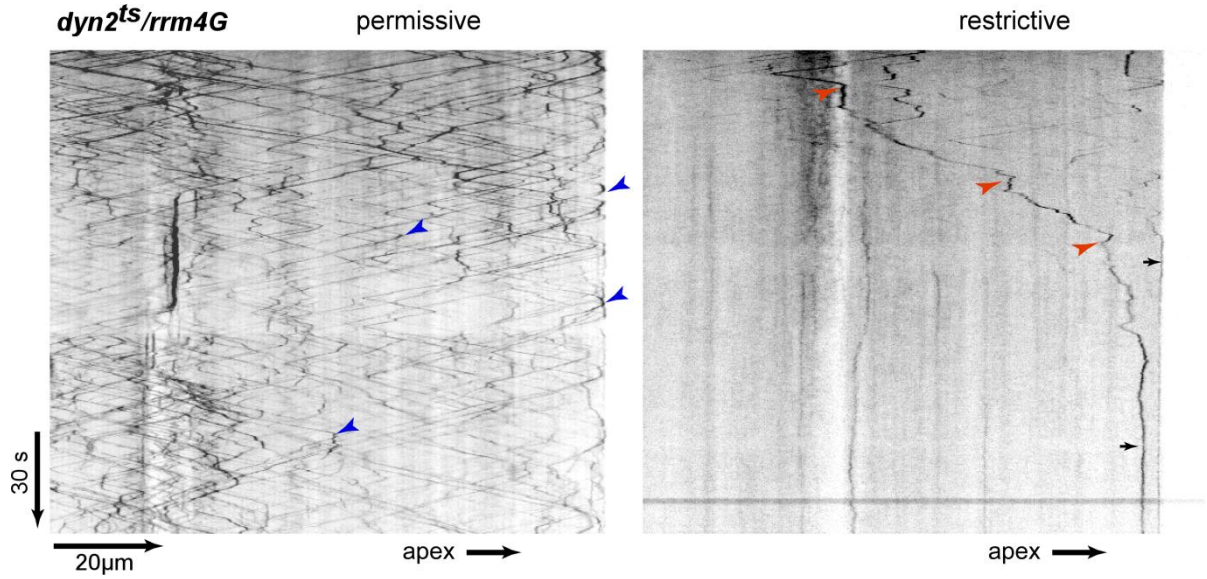


**Supplemental Fig. S2.** Rrm4G reaches the pole by processive movement, even in the absence of active Dyn2. Filaments of AB5dyn2$^{ts}$/rrm4G were analysed under permissive and restrictive temperature. Kymographs (time and distance is given on the left) of inverted movies detecting Rrm4G fluorescence are shown. Blue arrowheads point to particles that turn from anterograde to retrograde movement (left). Red arrowheads indicate anterograde movement with unsuccessful attempts of turning in the absence of a retrograde motor (right). Arrows point towards immobile accumulations at the pole.

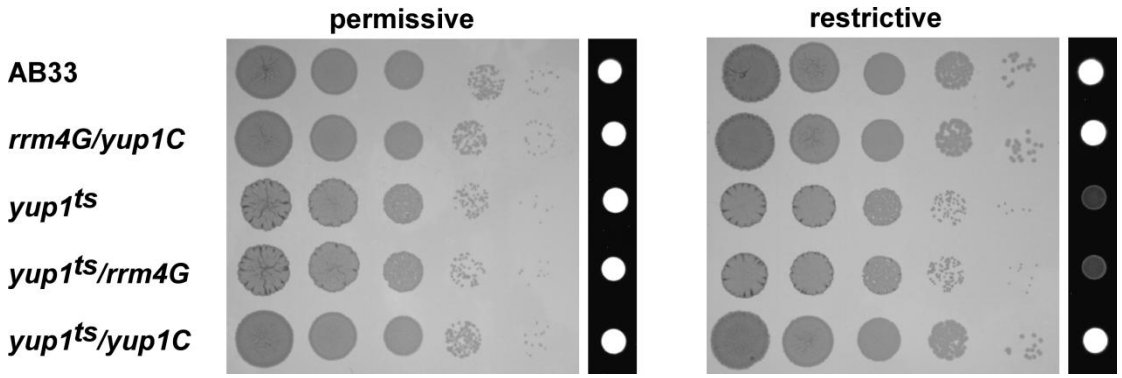


**Supplemental Fig. S3.** Defects in filamentous growth of *yup1ts* strains under restrictive conditions can be complemented by expression of Yup1C. The effect of temperature sensitivity on filamentous growth was tested on NM-agar supplemented with charcoal and glc. To this end cells were grown to OD600 of 1 and spotted on NM-charcoal-agar. Control strains as well as strain AB33yup1ts/rrm4G/Potefyup1C that was used to rescue the *yup1*$^{ts}$ phenotype were treated equally. Filamentous growth can be scored by the formation of white aerial mycelium resulting in white colonies. Strains with defects in filament formation appear grey (right side). Sporidial growth was tested on CM-agar in tenfold dilutions with initial OD600 of 1. Plates were incubated at permissive (23.5°C) and restrictive (26.5°C) temperatures, respectively.

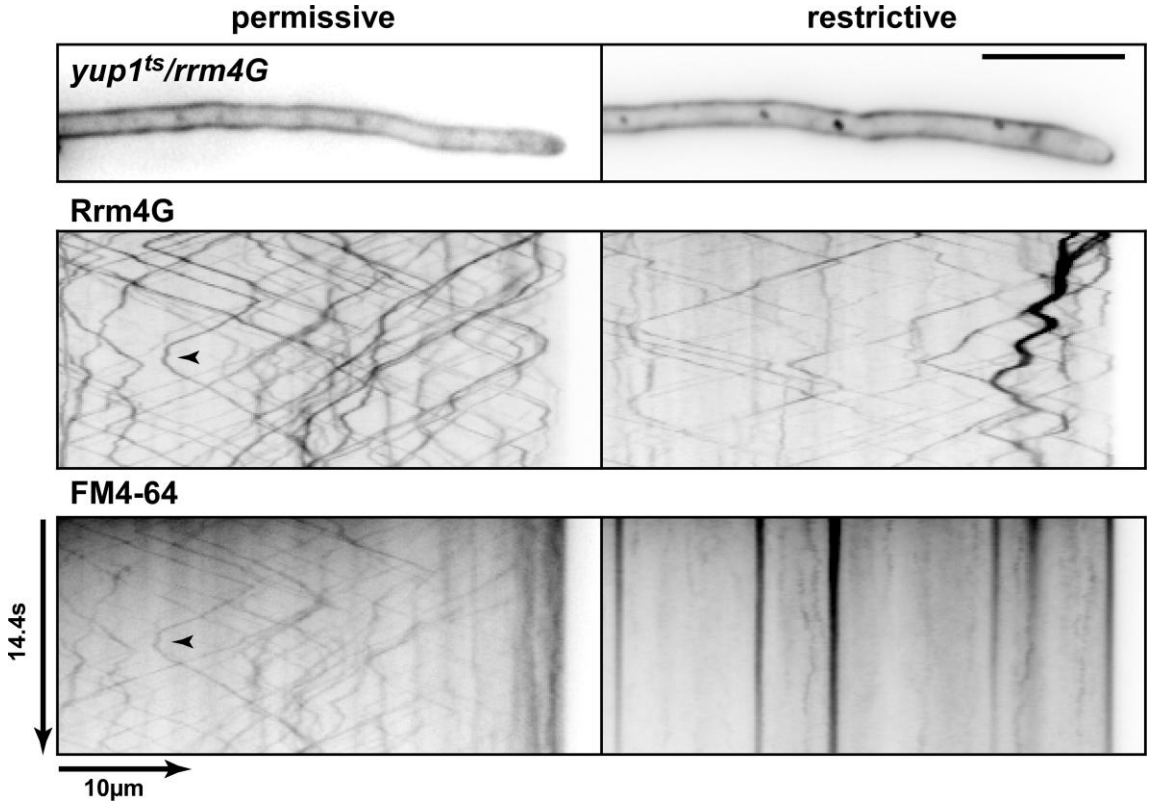


**Supplemental Fig. S4.** Loss of Yup1 results in the impaired uptake of the dye FM4-64. Filamentous growth was elicited by changing the nitrogen source of the medium resulting in transcriptional activation of the bW2/bE1 heterodimer. Filaments of AB33yup1ts/rrm4G are shown (size bar, 10 µm). Kymographs (time and distance is given on the left) of inverted movies detecting Rrm4G or FM4-64 fluorescence (middle and bottom panels, respectively) at permissive (left) and restrictive temperature (right; 25 minutes at 34°C) are given. Frames of the respective kymographs were recorded simultaneously from the same filament. Note that at restrictive temperature FM4-64 does no longer stain shuttling Rrm4-containing endosomes most likely due to the impaired Yup1 function.

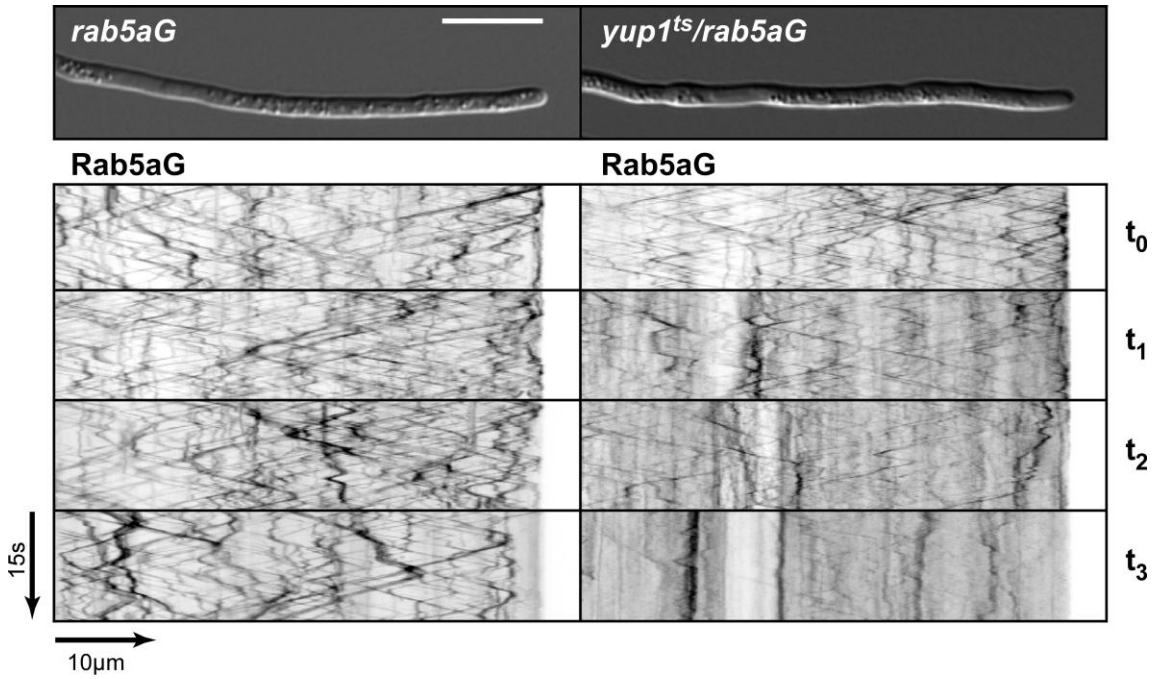


**Supplemental Fig. S5.** Loss of Yup1 results in the impaired movement of the endosomal marker Rab5a. Filamentous growth was elicited by changing the nitrogen source of the medium resulting in transcriptional activation of the bW2/bE1 heterodimer. Filaments of AB33Potefrab5aG and AB33yup1ts/Potefrab5aG on the left and right, respectively (size bar, 10 µm). Kymographs (time and distance is given on the left) of inverted movies detecting Rab5aG fluorescence in defined time intervals at restrictive temperature are shown (t0 to t3 = 0, 12, 46 and 92 minutes, respectively). Frames of the respective kymographs were recorded from the same filament. Note that movies were recorded with LED illumination resulting in lower photobleaching. Thus, the intensitiy and number of shuttling units cannot be directly compared to those shown in Fig. 5B.

**Supplemental Table S1** *U. maydis* strains used in this study

| Strains | Relevant genotype | Uma | Reference | Transformed plasmid | Locus | Progenitor |
|---|---|---|---|---|---|---|
| AB33pab1R/rrm4G | *rrm4G pab1R* | 428 | König et al., | pPab1R-HygR (pUMa895) | *rrm4 pab1* | AB33rrm4G |
| AB33rrm4G$^{RRM\Delta}$/pab1R | *rrm4$^{RRM\Delta}$G pab1R* | 575 | this study | pRrm4G$^{RRM\Delta}$-CbxR (pUMa1220) | *rrm4 pab1* | AB33pab1R/rrm4G |
| AB33rrm4G/pab1R/kin1Δ | *rrm4G pab1R kin1*Δ | 594 | this study | pKin1Δ–CbxR (pUMa1230) | *rrm4 pab1R kin1* Δ | AB33pab1R/rrm4G |
| AB33rrm4G$^{RRM\Delta}$/pab1R/kin1Δ | *rrm4$^{RRM\Delta}$G pab1R kin1*Δ | 611 | this study | pKin1Δ–GenR (pUMa1274) | *rrm4 pab1R kin1* Δ | AB33rrm4G$^{RRM\Delta}$ |
| AB5 | *Pnar:bW2bE1* | 256 | this study | pAB33 | *b* | FB1 |
| AB5dyn2$^{ts}$ | *dyn2$^{ts}$* | 346 | this study | pDyn2$^{ts}$-HygR (pUMa631) | *dyn2* | AB5 |
| AB5dyn2$^{ts}$/rrm4G | *dyn2$^{ts}$ rrm4G* | 400 | this study | pRrm4G-NatR (pUMa496) | *dyn2 rrm4* | |
| AB5dyn2$^{ts}$/rrm4G/pab1R | *dyn2$^{ts}$ rrm4G pab1R* | 600 | this study | pPab1R-CbxR (pUMa1233) | *dyn2 rrm4 pab1R* | AB5dyn2$^{ts}$/rrm4G |
| AB33rrm4R/dyn2G$^{3}$ | *dyn2G$^{3}$ rrm4R* | 420 | this study | pDyn2G$^{3}$-HygR (pUMa965) | *dyn2 rrm4* | AB33rrm4R |
| AB33rrm4G/pab1R/kin3Δ | *rrm4G pab1R kin3*Δ | 595 | this study | pKin3Δ–CbxR (pUMa1231) | *rrm4 pab1R kin3* Δ | AB33pab1R/rrm4G |
| AB33rrm4R/kin3G$^{3}$ | *rrm4R kin3G$^{3}$* | 622 | this study | pKin3G$^{3}$–HygR (pUMa1295) | *rrm4 kin3* Δ | AB33rrm4R |
| AB33rrm4G | *rrm4G* | 274 | Becht et al., 2006 this study | pRrm4G-NatR (pUMa496) | *rrm4* | AB33 |
| AB33rrm4G/P$_{otef}$yup1C | *rrm4G P$_{otef}$yup1C* | 564 | this study | pP$_{otef}$Yup1C-CbxR (pUMa1216) | *rrm4 ip$^{S}$* | AB33rrm4G |
| AB33P$_{otef}$yup1C/rrm4Δ | *P$_{otef}$yup1C rrm4*Δ | 624 | | pRrm4Δ–HygR (pUMa495) | *ip$^{S}$ rrm4* | AB33rrm4G |
| AB33rrm4R/kin3Δ | *rrm4R kin3*Δ | 664 | this study | pKin3Δ–CbxR (pUMa1231) | *rrm4 kin3* | AB33rrm4R |
| AB33rrm4R/kin3$^{PH\Delta}$G$^{3}$ | *rrm4R kin3$^{PH\Delta}$G$^{3}$* | 684 | this study | pKin3$^{PH\Delta}$G$^{3}$-HygR (pUMa1373) | *rrm4 kin3* | AB33rrm4R/kin3Δ |
| AB33rrm4GT/P$_{otef}$yup1CM | *rrm4GT yup1CM* | 686 | this study | pP$_{otef}$Yup1CM-bxR (pUMa1376) | *rrm4 ip$^{S}$* | AB33rrm4GT |
| AB33rrm4GT/P$_{otef}$yup1CM/ kin3$^{PH\Delta}$–HA$^{3}$ | *rrm4GT yup1CM kin3$^{PH\Delta}$HA$^{3}$* | 727 | this study | pKin3$^{PH\Delta}$HA$^{3}$-(pUMa1420) | *rrm4 ip$^{S}$ kin3* | AB33rrm4GT/ P$_{otef}$yup1CM |
| AB33rrm4GT/P$_{otef}$yup1CM/ kin3Δ | *rrm4GT yup1CM kin3*Δ | 755 | this study | pKin3Δ-CbxR (pUMa1288) | *rrm4 ip$^{S}$ kin3* | AB33rrm4GT/ P$_{otef}$yup1CM |
| AB33yup1$^{ts}$/rrm4G | *yup1$^{ts}$ rrm4G* | 723 | this study | pRrm4G-NatR (pUMa496) | *yup1 rrm4* | AB33yup1$^{ts}$ |
| AB33yup1$^{ts}$/rrm4G/ P$_{otef}$yup1C | *yup1$^{ts}$ rrm4G P$_{otef}$yup1C* | 746 | this study | pP$_{otef}$Yup1C-CbxR (pUMa1216) | *yup1 rrm4 ip$^{s}$* | AB33yup1$^{ts}$/rrm4G |
| AB33P$_{otef}$rab5aG | *rab5aG* | 826 | this study | pP$_{otef}$rab5aG-CbxR (pUMa1481) | *rab5a* | AB33 |
| AB33yup1$^{ts}$/ P$_{otef}$rab5aG | *rab5Ga yup1$^{ts}$* | 825 | this study | pP$_{otef}$rab5aG-CbxR (pUMa1481) | *yup1 ip$^{s}$* | AB33yup1$^{ts}$ |

**Supplemental Table S2** DNA oligonucleotides used in this study

| Designation | Nucleotide sequence |
|---|---|
| oMF838 | TGAGGCCTGAGTGGCCGACCTCGCCTTCGATTCC |
| oMF839 | AATCGCTCGGGCTCAACC |
| oSL314 | TAGTTCGAAATCGTCCCCTTTTCCTTTGTCG |
| oSL315 | TGGCGGCCGCACTCCTACAGCTTGCAAATTAAAGC |
| oSL802 | GCATGCAATATTCACGAGAGAGGAGACCC |
| oSL803 | ACCTGGTGGCCGCGTTGGCCGCGCAAAACACATGGCCCGC |
| oSL804 | TGAGGCCTGAGTGGCCCTAGAAGGCGTCATGGCC |
| oSL805 | ACCGTAATATTGGGCTGTAAGCCACTCCG |
| oSL900 | AATTTCGGCGGCCAACG |
| oSL901 | TGGCCGCCGA |

**Supplemental Table S3** Plasmids used in this study

| Plasmid | pUMa | Resistance cassette[1] | Short description |
|---|---|---|---|
| pRrm4G-NatR | 496 | SfiI insert of pMF5-1n[2] | published[2] |
| pRrm4G$^{RRM\Delta}$-CbxR | 1220 | SfiI insert of pMF5-1c | derivative of pRrm4$^{RRM\Delta}$R-HygR[3] |
| pKin1Δ-CbxR | 1230 | SfiI insert of pMF1c[1] | derivative of pKin1Δ-HygR[2] |
| pKin1Δ-GenR | 1274 | SfiI insert of pMF1g | derivative of pKin1Δ-HygR[2] |
| pDyn2$^{ts}$-HygR | 631 | SfiI insert of pMF1h[1] | upstream region comprises 1.3 kb promotor region, 4.8 kb ORF and 237 base pairs 3′ UTR. Mutations conferring temperature sensitivity of *dyn2* were derived from plasmid pDyn2ts-Nat-pNEBUN (pUMa510, carrying point mutations encoding Q1373R, L1392P, D1395G, I1343N, E1452G and E1497G amino acid exchanges as published[4]; kindly provided by Dr. G. Steinberg). 2 kb downstream flanking region was amplified by PCR using primers oMF838 and oMF839 |
| pPab1R-CbxR | 1233 | SfiI insert of pMF5-2c | derivative of pPab1R-HygR[3] |
| pKin3Δ-CbxR | 1231 | SfiI insert of pMF1c[1] | derivative of pKin3-kohyg-RWS74 (pUMa509; kindly provided by Dr. G. Steinberg); resistance cassette is flanked by 0.9 kb upstream and 2.5 kb downstream regions of *kin3*; upstream region comprises 884 bp promotor region and 36 bp ORF; downstream region comprises base pairs 2653 to 5031 of *kin3* |
| pKin3Δ-GenR | 1288 | SfiI insert of pMF1g | derivate of pKin3Δ-CbxR |
| pKin3G[3]-HygR | 1295 | SfiI insert of pMF5-4h | 5.5 kb upstream flanking region (PCR using oSL802/oSL803) including the *kin3* ORF is fused to the cassette containing triple *egfp* and resistance gene; this is followed by a 1.4 kb downstream flanking region (PCR using oSL804/oSL805). |
| pKin3$^{PH\Delta}$G[3]-HygR | 1373 | SfiI insert of pMF5-4h | derivative of pKin3G[3]-HygR; upstream flanking region of *kin3* lacks the last 348 bp of the *wt* ORF encoding the PH domain of Kin3 (aa position 1561 to 1676) |
| pKin3$^{PH\Delta}$HA[3]-HygR | 1420 | SfiI insert of pMF5-9h | derivative of pKin3$^{PH\Delta}$G[3]-HygR; SfiI cassette was introduced containing triple repeats of the HA tag followed by the heterologous terminator $T_{nos}$ in combination with a hygromycin resistance cassette |
| p$P_{otef}$Yup1C- | 1216 | CbxR for | kindly provided by Drs. K. Schink and M. Bölker (unpublished data); derived from |

| | | | |
|---|---|---|---|
| CbxR | | integration at *ip*$^S$ locus | p123-mCherry[5]; contains the 900 bp *yup1* ORF fused to mCherry flanked by constitutively active promoter $P_{otef}$ and transcriptional terminator $T_{nos}$ upstream and downstream, respectively |
| $pP_{otef}$Yup1CM-CbxR | 1376 | CbxR for integration at *ip*$^S$ locus | derivative of $pP_{otef}$Yup1C-CbxR; a 465 bp BsrGI/NotI fragment from pMF5-5h[3] was introduced encoding a triple c-Myc epitope tag and $T_{nos}$ |
| $pP_{otef}$Rab5aG-CbxR | 1481 | CbxR for integration at *ip*$^S$ locus | contains ORF of Rab5a (um10615), N-terminally fused to eGfp under control of $P_{otef}$; Rab5a ORF was inserted as an 928 bp NdeI/AscI fragment (PCR using oRL114/oRL115) in p123-Gfp_NdeI (pUMa1479) containing a carboxin resistance cassette |
| pMF1g | 1057 | Part of the SfiI gene replacement system[1] | encodes an aminoglycoside 3'-phosphotransferase (APH) conferring geneticin resistance under control of the constitutively active promoter $P_{otef}$ [1] followed by the heterologous terminator $T_{cyc1}$ from the *iso-1-cytochrome c* gene of *S. cerevisiae* $P_{otef}$ derives from plasmid pUCLII Otef-Neo (pUMa971; kindly provided by William K. Holloman) and $T_{cyc1}$ was amplified using primers oSL314 and oSL315 for PCR on linearised pMF1n[1] as DNA template |
| pMF5-1c | 1132 | Part of the SfiI gene replacement system[1] | encodes a SfiI cassette for C terminal fusion containing *egfp*, followed by heterologous terminator $T_{nos}$ of nopaline synthase gene from *Agrobacterium tumefaciens* in combination with a carboxin resistance cassette |
| pMF5-2c | 1232 | Part of the SfiI gene replacement system[1] | encodes a SfiI cassette for C terminal fusion containing *mrfp*, followed by $T_{nos}$ in combination with a carboxin resistance cassette |
| pMF5-4h | 647 | Part of the SfiI gene replacement system[1] | encodes a SfiI cassette for C terminal fusion containing triple *egfp*, followed by heterologous terminator $T_{nos}$ in combination with a hygromycin resistance cassette |
| pMF5-9h | 792 | Part of the SfiI gene replacement system[1] | encodes a SfiI cassette for C terminal fusion containing triple copies of the HA epitope (YPYDVPDY), followed by heterologous terminator $T_{nos}$ in combination with a hygromycin resistance cassette |
| pDyn2G[3]-HygR | 965 | hygromycin | published[6] |

[1] Brachmann et al., 2004; [2] Becht et al., 2006; [3] König et al., 2009; [4] Wedlich-Söldner et al., 2002; [5] Schink and Bölker, 2009; [6] Lenz et al., 2006

## Legends to Supplemental Movies

### Supplemental Movie S1

Rrm4G and Pab1R (upper and lower part, respectively) co-localise in shuttling units in filaments of AB33pab1R/rrm4G. Real-time movies were recorded simultaneously using dual-colour detection and correspond to Fig. 1A (150 ms exposure time, 80 frames, 6 frames/second display rate; QuickTime format, 280 kB).

### Supplemental Movie S2

Removal of RRMs in Rrm4G causes a complete loss of Pab1R transport (lower part), while Rrm4G $^{RRM\Delta}$ still shuttles in units along cytoskeletal tracks (upper part). Filament of AB33 Rrm4G$^{RRM\Delta}$/Pab1R is shown. Movies were recorded simultaneously using dual-colour detection and correspond to Fig. 1B (80 ms exposure time, 65 frames, 10 frames/second display rate; QuickTime format, 402 kB).

### Supplemental Movie S3

Rrm4G and Pab1R co-localise at the poles in bipolar filaments (upper and lower part, respectively) of AB33rrm4G/pab1R/kin1Δ. Residual moving particles contain both, Rrm4G and Pab1R. Note, that due to weak signals the movies were not recorded simultaneously (120 ms exposure time, 40 frames, 7.5 frames/second display rate; QuickTime format, 446 kB).

### Supplemental Movie S4

Rrm4G and Pab1R (upper and lower part, respectively) co-localise in shuttling units in filaments of AB5dyn$^{ts}$/rrm4G/pab1R at permissive temperature. Movies were recorded simultaneously using dual-colour detection (207 ms exposure time, 50 frames, 5 frames/second display rate; QuickTime format, 605 kB).

### Supplemental Movie S5

Rrm4G and Pab1R accumulate at the poles of bipolar filaments (upper and lower part, respectively) of AB5dyn$^{ts}$/rrm4G/pab1R. Movies were recorded simultaneously using dual-colour detection (170 ms exposure time, 50 frames, 6 frames/second display rate; QuickTime format, 265 kB).

**Supplemental Movie S6**

Rrm4R co-localises with Dyn2G$^3$ at the apex of AB33rrm4R/dyn2G$^3$ filaments. The Rrm4R and Dyn2G$^3$ containing transport unit moves retrogradely, originating from the filament tip. Movies were recorded simultaneously using dual-colour detection and correspond to Fig. 2E (100 ms exposure time, 23 frames, 10 frames/second display rate; QuickTime format, 222 kB).

**Supplemental Movie S7**

Rrm4R co-localises with Dyn2G$^3$ in the center of AB33rrm4R/dyn2G$^3$ filaments. Movies were recorded simultaneously using dual-colour detection. Note that the precise orientation of microtubules is not known in the central regions of filaments. The hyphal apex is located at the right (207 ms exposure time, 23 frames, 3 frames/second display rate; QuickTime format, 43 kB).

**Supplemental Movie S8**

Rrm4G and Pab1R co-localise in distinct accumulations mainly in the central region of the initial cell (upper and lower part, respectively) of AB33rrm4G/pab1R/kin3Δ. Movies were recorded simultaneously using dual-colour detection (150 ms exposure time, 30 frames, 6 frames/second display rate; QuickTime format, 283 kB).

**Supplemental Movie S9**

Rrm4R and Kin3G$^3$ co-localise in shuttling units at the hyphal apex of filament AB33rrm4R/kin3G$^3$ in anterograde and retrograde direction. Movies were recorded simultaneously using dual-colour detection and correspond to Fig. 3C (200 ms exposure time, 23 frames, 5 frames/second display rate; QuickTime format, 176 kB).

**Supplemental Movie S10**

Rrm4R and Kin3G$^3$ co-localise in shuttling units throughout the filament of AB33rrm4R/kin3G$^3$. Movies were recorded simultaneously using dual-colour detection (200 ms exposure time, 60 frames, 5 frames/second display rate; QuickTime format, 824 kB).

**Supplemental Movie S11**

Rrm4R localises in distinct accumulations mainly in the central region of the initial cell, while Kin3$^{PH\Delta}$G$^{3}$ is dispersed in the cytoplasm. Filament of AB33rrm4R/kin3$^{PH\Delta}$G$^{3}$ is shown. Movies were recorded simultaneously using dual-colour detection and correspond to Fig. 3E (150 ms exposure time, 50 frames, 6 frames/second display rate; QuickTime format, 510 kB).

**Supplemental Movie S12**

Rrm4G co-localises with Yup1C-positive endosomes during anterograde and retrograde shuttling. The filament apex of AB33rrm4G/yup1C is shown. Movies were recorded simultaneously using dual-colour detection and correspond to Fig. 5A (125 ms exposure time, 32 frames, 7.5 frames/second display rate; QuickTime format, 194 kB).

**Supplemental Movie S13**

Rrm4G co-localises with Yup1C-positive endosomes during anterograde and retrograde shuttling. Filament of AB33rrm4G/yup1C is shown. Movies were recorded simultaneously using dual-colour detection (150 ms exposure time, 60 frames, 6 frames/second display rate; QuickTime format, 382 kB).

*Acknowledgements*

We acknowledge Dr. K. Zarnack as well as lab members for valuable discussion and critical reading of the manuscript. We are grateful to Dr. G. Steinberg for insights on microtubule-dependent transport and for constructs pDyn2G$^{3}$-HygR, pKin3-kohyg-RWS74 and the *dyn2$^{ts}$* allele as well as strain AB33yup1$^{ts}$. Drs. K. Schink and M. Bölker provided construct pP$_{otef}$Yup1C-CbxR and Dr. W.K. Holloman plasmid pUCLII Otef-Neo carrying the geneticin resistance gene. Drs. K. Zarnack, P. Müller and E. Islamovic constructed plasmids pMF5-4h, pMF5-9h, and pMF5-1c, respectively. Special thanks to P. Happel and U. Gengenbacher for excellent technical assistance and Dr. R. Kahmann from the Max-Planck Institute for Terrestrial Microbiology for support on microscopy infrastructure and laboratory equipment. The work was supported by grants from the Deutsche Forschungsgemeinschaft to MF (FE 448/5-1) as part of the German/Mexican research group FOR1334.

## 2.3 Endosomal transport of septin mRNA and encoded protein mediates correct septin filamentation

**Sebastian Baumann[1,2], Julian König[2,3], Janine Koepke[2,4] and Michael Feldbrügge[1,2,*]**

[1] Heinrich Heine University Düsseldorf, Institute for Microbiology, Cluster of Excellence on Plant Sciences, 40204 Düsseldorf, Germany
[2] Max Planck Institute for Terrestrial Microbiology, Department of Organismic Interactions, Karl-von-Frisch-Str. 10, 35043 Marburg, Germany
[3] present address: Medical Research Council, Laboratory of Molecular Biology, Hills Road, Cambridge, CB2 0QH, UK
[4] present address: Philipps University Marburg, Biomedical Research Centre, Pneumology, Hans-Meerwein-Str. 2, 35043 Marburg, Germany

**Running title:** Endosomal transport of septin mRNA and protein

**Word count:** 41.000 characters including space

**Key words:** endosome / membrane trafficking / RNA transport / RNA live imaging / septin

**[*] Corresponding author:**

Dr. Michael Feldbrügge
Institute for Microbiology, Cluster of Excellence on Plant Sciences
Heinrich Heine University Düsseldorf
40204 Düsseldorf, Germany,
Phone: +49 (211) 81-15475,
Fax: +49 (211) 81-15370
feldbrue@hhu.de

**Abstract**

Long-distance transport of lipids and proteins is mediated by endosomes that receive their cargo mainly from other membrane compartments. Particularly in highly polarized cells like neurons and fungal hyphae, endosomes shuttle extensively along microtubules during trafficking. Endosomes also carry mRNAs as unconventional cargo, but the precise molecular function of this trafficking process is unknown. Applying dynamic live cell imaging in polarized fungal cells we discovered microtubule-dependent transport of septin mRNA and encoded septin protein on shuttling endosomes. Since co-localisation of mRNA and protein is indicative for local protein synthesis, we tested whether septin mRNA is directly translated on endosomes. Consistently, the accumulation of septin protein on endosomes is tightly linked to the recruitment of septin mRNA. Furthermore, ribosomal proteins co-localize with shuttling endosomes, but only in the presence of mRNA. Importantly, endosomal trafficking is essential for an efficient delivery of septin protein to filaments at growth cones, a process apparently necessary to establish unipolar growth. Thus, we hypothesize that local mRNA translation loads endosomes with septin protein for correct endosomal delivery to septin filaments.

### 2.3.1 Introduction

Cellular logistics depend on intracellular long-distance trafficking. A wide-spread mechanism is the microtubule-dependent transport of endosomes that function as carrier platforms for membrane lipids and proteins (Rusten et al, 2012). Particularly in highly polarized cells, endosomes shuttle extensively along microtubules in order to coordinate antero- and retrograde trafficking (Steinberg, 2007b; Yap & Winckler, 2012). In addition to the typical cargos, it was discovered that endosomes are important for the transport and subcellular localisation of mRNAs (Baumann et al, 2012; Cohen, 2005; Irion & St Johnston, 2007; Rusten et al, 2012).

Cytoskeletal transport of mRNAs is commonly assumed to position mRNAs within the cell for their local translation, an important mechanism to mediate spatial gene expression (Doyle & Kiebler, 2011; St Johnston, 2005). Key components of the transport machinery are sequence-specific RNA-binding proteins that act in concert with other RNA-binding proteins, such as the poly(A)-binding protein, to form large complexes called messenger ribonucleoproteins (mRNPs). These mRNPs are connected

to molecular motors via adaptor proteins for transport along the cytoskeleton. mRNA translation commonly occurs upon their deposition at the final destination (Czaplinski & Singer, 2006). In *Drosophila melanogaster*, for example, the RNA-binding protein Egalitarian recognizes the A´-form RNA helix of zipcodes in target mRNAs such as *hairy* and *K10* (Bullock et al, 2010; Dienstbier et al, 2009). The resulting mRNPs are connected with Bicaudal-D to the molecular motor dynein for transport along microtubules (Bullock, 2011). It is a widespread phenomenon that mRNPs shuttle extensively back and forth during transport but the precise molecular reason for this bidirectional movement remains elusive (Doyle & Kiebler, 2011).

In *Ustilago maydis* a morphological switch form yeast cells to unipolarly growing hyphae is prerequisite for pathogenicity. The formation of these highly polarized filaments depends on microtubule-dependent mRNA transport. In the absence of functional microtubules or molecular motors such as kinesins and dynein, hyphae grow bipolar and the insertion of retraction septa is disturbed (Vollmeister et al, 2012). A crucial component in this process is the RNA-binding protein Rrm4, which is responsible for the transport of specific mRNAs such as *ubi1* and *rho3* encoding a natural ubiquitin fusion protein and a small G protein, respectively (Supplementary Figure S1, Supplementary Movie S1, (Becht et al, 2006; Koepke et al, 2011; König et al, 2009)). However, transported mRNAs do not accumulate at distinct subcellular sites. Thus, the precise role of mRNA transport is still unclear in this fungus (König et al, 2009). Recently, we discovered the mechanistic details of this mRNA transport process: mRNAs are co-transported with Rab5a-positive endosomes that shuttle along microtubules (Baumann et al, 2012). Importantly, loss of Rrm4 does not interfere with endosomal movement, but endosomes lacking mRNAs appear to be disturbed in promoting polar growth (Baumann et al, 2012). In this study we focused on the septin Cdc3 (Alvarez-Tabares & Perez-Martin, 2010; Böhmer et al, 2009), because its mRNA was identified as an *in vivo* target of Rrm4 in previous CLIP experiments (König et al, 2009).

Septins are ubiquitous guanosine triphosphatases (GTPases) that assemble into higher-order structures such as filaments, gauzes and rings (Barral, 2010; Barral & Kinoshita, 2008; McMurray & Thorner, 2009). These structures associate with membranes and cytoskeletal components functioning as membrane barriers and cytoskeletal scaffolds (Saarikangas & Barral, 2011; Spiliotis & Gladfelter, 2012; Weirich et al, 2008). Septin filaments have been described to modify microtubular functions during the regulation of

cell polarity (Gladfelter, 2010; Spiliotis & Gladfelter, 2012). Thus, the *U. maydis* septin Cdc3 was a prime candidate to link Rrm4 function to defects in the morphology of corresponding mutants.

### 2.3.2 Results

**Cdc3 is important during establishment of unipolar growth**

To investigate the role of Cdc3 in cell polarity we analysed deletion strains in the genetic background of strain AB33 (Table I) in which unipolar hyphal growth can be elicited by switching the nitrogen source. Hyphae grow with a defined axis of polarity. They expand at the apical growth cone and insert retraction septa at the basal pole (Supplementary Figure S1A; (Vollmeister & Feldbrügge, 2010)). Four hours post induction (h.p.i), a significant number of *cdc3Δ* hyphae grew bipolar, lacking retraction septa reminiscent of defects observed in *rrm4Δ* strains (Figure 1A-B; (Alvarez-Tabares & Perez-Martin, 2010)). However, the majority of *cdc3Δ* cells switched to correct unipolar growth and also formed septa after prolonged induction (6 and 9 h.p.i.; Figure 1A-B). To further investigate these temporal morphology differences, hyphae were treated with calcofluor-white that stains chitin at growth cones and retraction septa (Figure 1C). Remarkably, even in bipolar *rrm4Δ* hyphae only one growth cone was stained predominantly (Figure 1C), indicating that these aberrant hyphae initially elongate at one pole and subsequently switch growth direction to form an alternative second growth cone (Figure 1C). Consistently, the number of bipolar *rrm4Δ* hyphae is increasing over time (Figure 1B). In contrast, bipolar *cdc3Δ* hyphae are able to switch to correct unipolar growth at later time points (Figure 1C).

In comparison to each single deletion mutant the *rrm4Δ*/*cdc3Δ* double mutant was more severely affected in unipolar growth and septum formation (Figure 1A-B), indicating that both Rrm4-mediated mRNA transport and correct septin function are crucial for efficient unipolar growth.

**Rrm4 mediates microtubule-dependent transport of septin *cdc3* mRNA**

To confirm that transport of *cdc3* mRNA is Rrm4-dependent we applied RNA live imaging (König et al, 2009). For mRNA visualisation, a modified $\lambda N^{*}$ peptide (Austin et al, 2002) fused to triple Gfp ($\lambda N^{*}G^{3}$) was expressed under control of an arabinose-

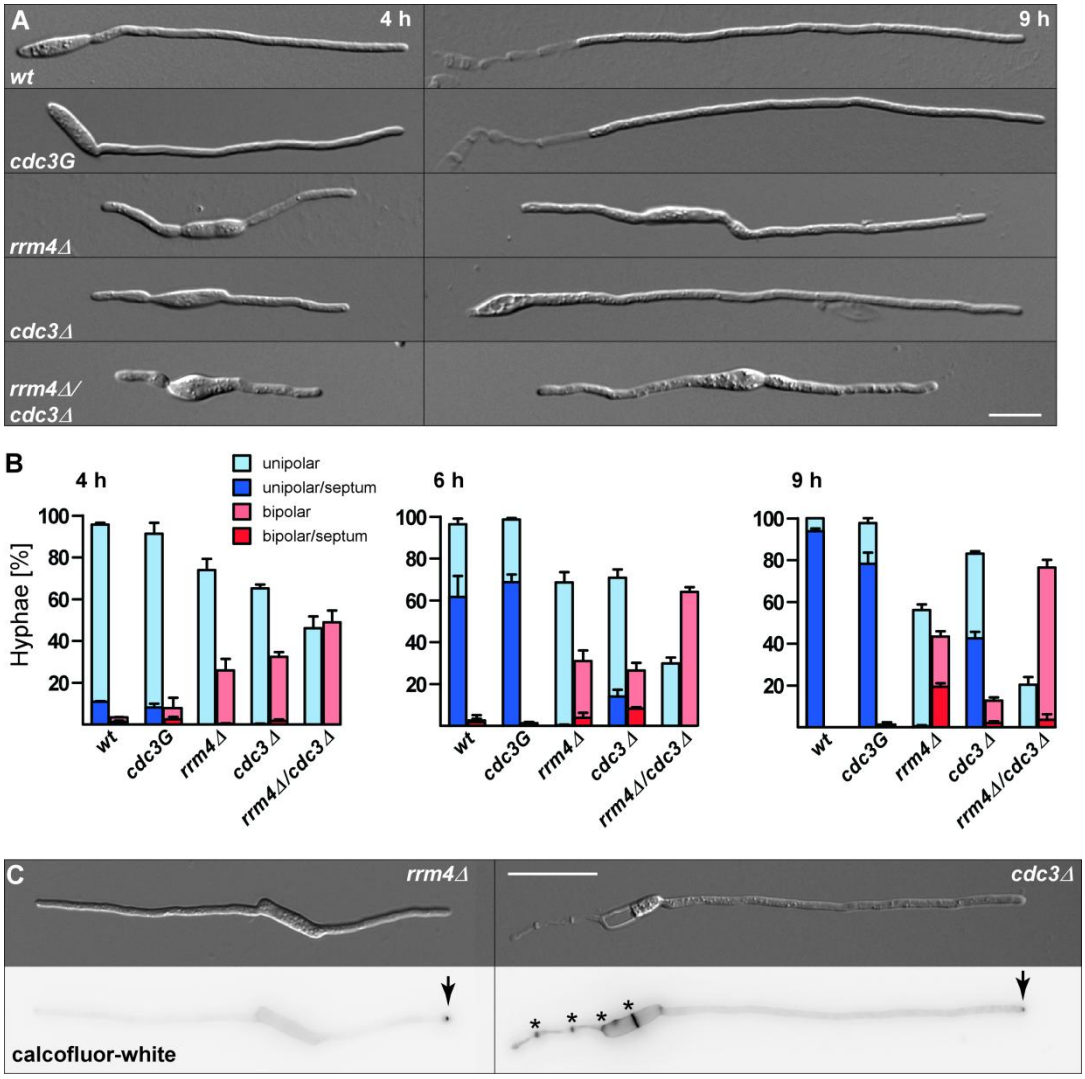


**Figure 1** Loss of *cdc3* causes defects in establishing polar growth. (**A**) Hyphae of AB33 derivatives 4 h (left) and 9 h (right) after induction of polar growth (DIC images; size bar, 10 µm). (**B**) Percentages of hyphae after 4, 6 and 9 h.p.i.. Unipolarity, bipolarity, and septum formation was quantified (error bars, s.e.m.; n = 3 independent experiments, 5848 filaments were counted in total; note that septum formation is given relative to the values of unipolar or bipolar hyphae set to 100%). (**C**) Comparison of *rrm4Δ* and *cdc3Δ* filaments (7 h.p.i.). Growth cones and retraction septa (depicted by arrows and asterisks, respectively) are stained with calcofluor-white (size bar, 10 µm). Staining chitin marked predominantly one single growth cone even in bipolarly growing *rrm4Δ* hyphae (16 filaments: 75 % single signal, 6% two signals, 19% no staining). This suggests that *rrm4Δ* hyphae initially elongate at one pole and subsequently completely switch their growth direction to form a second growth cone resulting in bidirectional growth.

inducible promoter and 16 copies of the corresponding *boxB* binding sites were inserted in the 3´ UTR of *cdc3* (*cdc3B*$^{16}$). This set-up for the first time allowed the detection of $\lambda N^{*}G^{3}$-labelled *cdc3B*$^{16}$ mRNAs in processively moving units at endogenous expression levels (Figure 2A-B; Supplementary Movie S2). As expected, the velocity and the bidirectional shuttling were reminiscent of microtubule-dependent transport of endosomes (Supplementary Movie S2, (Baumann et al, 2012; König et al, 2009)). About one $\lambda N^{*}G^{3}$-labeled *cdc3B*$^{16}$ mRNA particle moved processively per filament (Figure

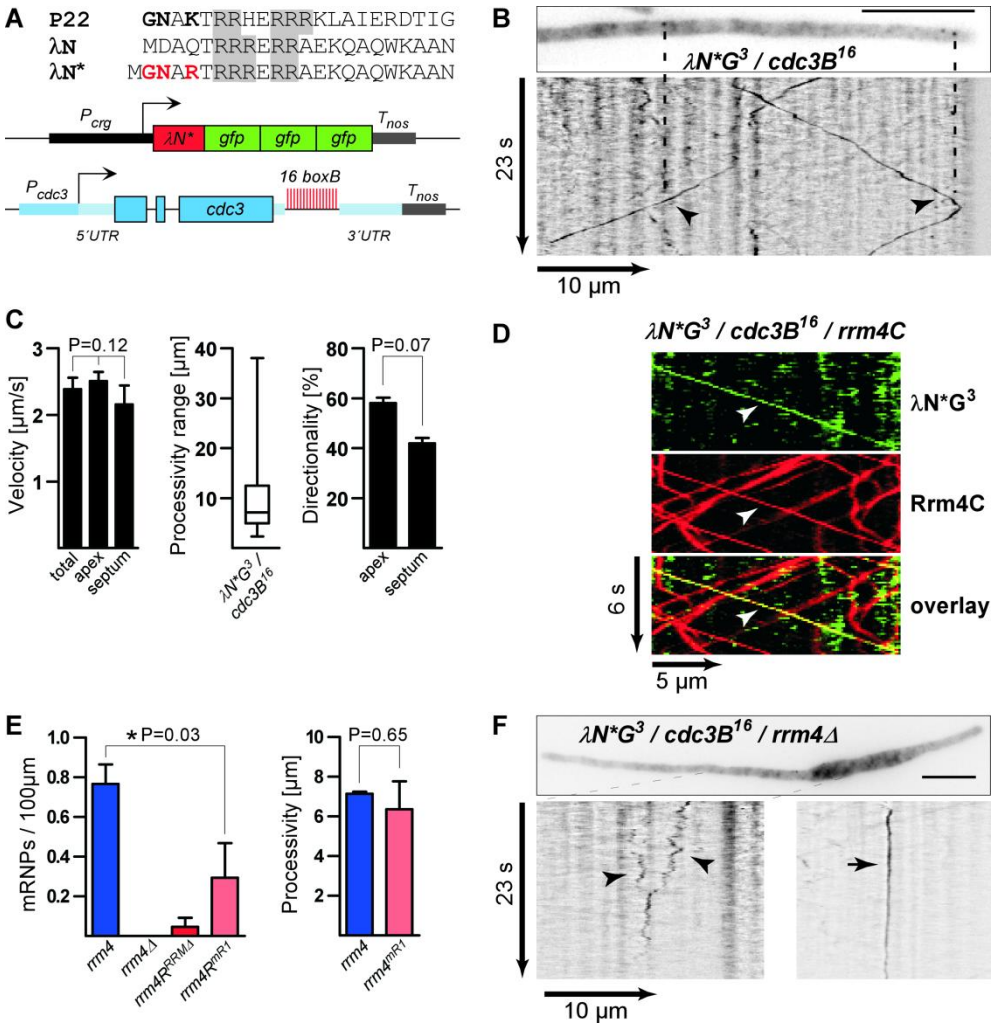


2E). No significant difference in velocity was observed comparing mRNAs moving towards the apex or the septum of hyphae (Figure 2C) and no accumulation of *cdc3B*$^{16}$ mRNA at growth cones was detectable (Figure 2B). For co-localisation Rrm4C (fusion to mCherry) was expressed in hyphae and visualized by recording real time movies via millisecond alternating laser excitation microscopy (msALEX). λN$^{*}$G$^{3}$-labeled *cdc3B*$^{16}$ mRNAs co-localized *in vivo* with Rrm4C at shuttling endosomes (Figure 2D).

Although no drastic changes in the amount of *cdc3* mRNA or protein were observed (Supplementary Figure S2A-B), deletion of *rrm4* in an identical genetic background resulted in the loss of processive units leaving only immobile or stochastically moving *cdc3B*$^{16}$ signals (Figure 2E-F; Supplementary Movie S3). In summary, the results of CLIP (König et al, 2009) and RNA live imaging consistently indicate that *cdc3* mRNA is a target of the Rrm4-dependent mRNA transport machinery. However, we did not detect any deposition of *cdc3* mRNAs at distinct subcellular sites, contradicting the commonly held view of local translation upon mRNA delivery to the target site.

**Figure 2** Rrm4 transports *cdc3* mRNA along microtubules. (**A**) Modified $\lambda N^*$ RNA reporter system. Top: sequence comparison of arginine-rich peptides ($\lambda N^*$ exhibits increased binding affinity, exchanged amino acids in red, (Austin et al, 2002)). Bottom: components of the $\lambda N^*$ RNA reporter system ($P_{crg1}$, arabinose-regulated promoter; $T_{nos}$, heterologous transcriptional terminator; $cdc3B^{16}$ carries 16 copies of *boxB* hairpin in its 3´ UTR). (**B**) Hyphal tip of a strain expressing the $\lambda N^*G^3$ protein and $cdc3B^{16}$ mRNA. Micrograph (size bar, 10 µm) and the corresponding kymograph show processive particles (arrowheads; Supplementary Movie S2). (**C**) Velocity (total processive particles and those moving towards apex or septum; one way ANOVA, P>0.05), processivity range (whisker diagram showing median, min/max values and 25 / 75% percentiles) and directionality of processive particles (n = 3, 69 particles in 97 hypha; error bars represent s.e.m.; paired two-tailed t-test, P>0.05). (**D**) Kymographs of $\lambda N^*G^3$-labeled $cdc3B^{16}$ mRNA (green) and Rrm4C (red). Co-localisation (yellow) is indicated by arrowheads. (**E**) Left: number of processive mRNPs in 100 µm of hyphae (note, length of hyphae varies in tested strains; paired two-tailed t-test, * P < 0.05 significant). Right: processivity of particles (n = 3, paired two-tailed t-test, P = 0.65, error bars, s.e.m.). (**F**) Micrograph (size bar, 10 µm) and kymographs (bottom) showing stochastically moving and static particles (arrowheads and arrow, respectively; Supplementary Movie S3).

## Rrm4-dependent localisation of Cdc3 on shuttling endosomes and in a gradient emanating from the tip of septin filaments

To address the question whether transport of *cdc3* mRNA supports the correct subcellular localisation of the corresponding Cdc3 protein, we analysed a functional N-terminal Gfp fusion (Cdc3G; Figure 1A-B). We confirmed septin accumulations at distinct subcellular sites such as septa and filaments that have previously been described (Supplementary Figure S3, Supplementary Movie S4, (Alvarez-Tabares & Perez-Martin, 2010; Böhmer et al, 2009)). We further found that the Cdc3G signal was stronger in filaments at growth cones than through the rest of the hyphae (Figure 3A). Notably, this unequal distribution was abolished by treatment with the microtubule inhibitor benomyl and not detectable in *rrm4Δ* mutants (Figure 3A-C). Instead, in both cases, Cdc3G formed small circles (< 1 µm in diameter; Figure 3A-B), which have been described for the septin Cdc10 in cells grown under suboptimal conditions (Böhmer et al, 2009). This suggests that Rrm4-dependent microtubule transport is essential for correct septin filamentation, particularly at hyphal tips (see below).

Intriguingly, Cdc3G exhibited an additional, previously undescribed localisation on shuttling units that resembled Rab5a-positive endosomes (Figure 3D, Supplementary Movie S5). Bidirectional movement of Cdc3G was inhibited by benomyl (Figure 3D) and was no longer detectable in *rrm4Δ* mutants (Figure 3E, Supplementary Movie S6). In contrast, in budding cells Cdc3G was rarely observed at shuttling units (Five events in 80 cells; Supplementary Figure S3C). For co-localisation studies the signal of Cdc3G was increased by using a strong, constitutively active promoter ($P_{otef}$; Table I). This did not alter hyphal morphology but resulted in the expected enhanced endosomal Cdc3G signals. Co-staining with the red-fluorescent dye FM4-64, which marks endosomes

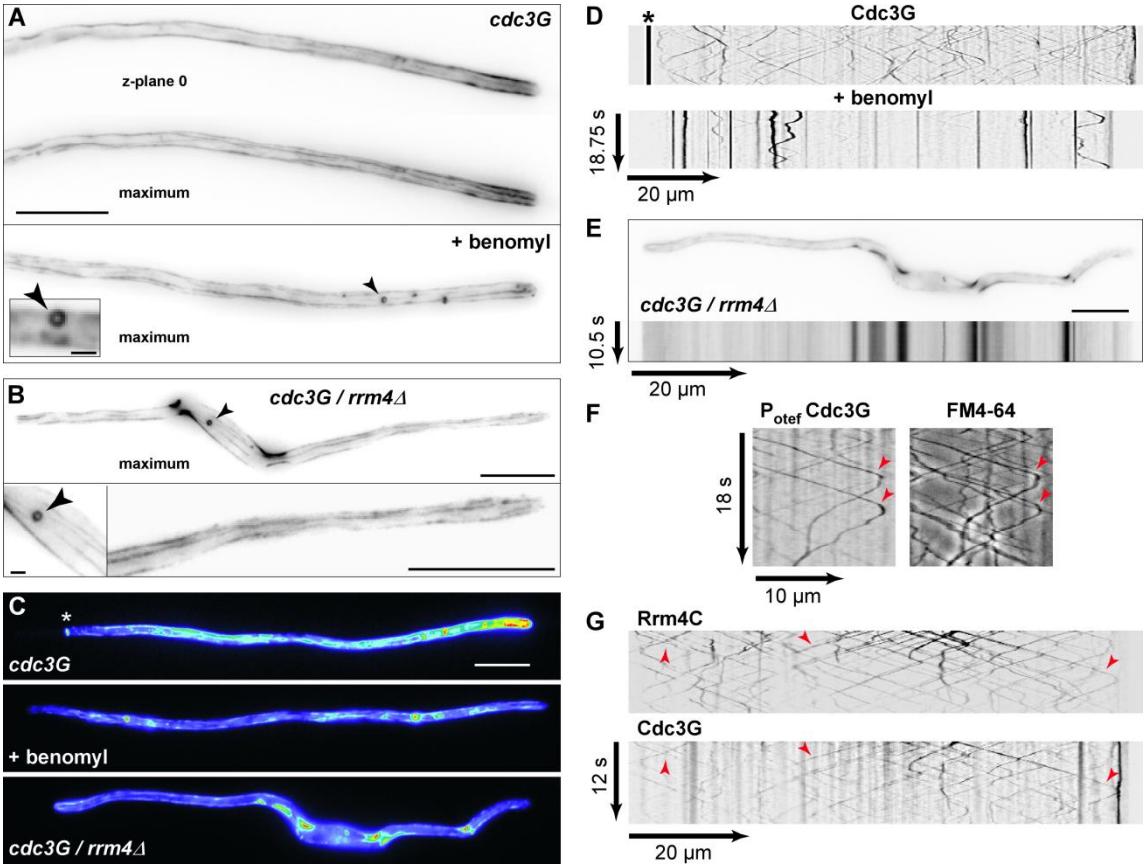


**Figure 3** Rrm4-dependent accumulation of Cdc3G in septin filaments and on shuttling endosomes.
(**A**) Micrographs of Cdc3G expressing hypha (z-plane 0 or maximum projection of z-stacks with 0.25 µm steps; size bar, 10 µm). Hypha at the bottom was treated with benomyl for 1 hour (arrowheads mark small circle; see inlay, size bar, 1 µm). (**B**) Bipolarly growing *cdc3G/rrm4Δ* hypha (size bars 10, 1 and 5 µm for top, bottom left, and bottom right, respectively). (**C**) False color images of Cdc3G (asterisk marks septum), benomyl treated and *rrm4Δ* mutant. (**D**) Kymographs of Cdc3G expressing hypha (asterisk marks septum; top untreated and bottom treated with benomyl). (**E**) Micrograph (top) and corresponding kymograph (bottom) of *cdc3G/rrm4Δ* hypha (size bar, 10 µm; Supplementary Movie S6). (**F**) Kymograph showing co-localisation of Cdc3G and FM4-64-stained endosomes (red arrowheads). FM4-64 labels endosomes positive for the small G-protein Rab5a and Rrm4 ((Baumann et al, 2012; Schuster et al, 2011c)). The Cdc3G signal was enhanced by overexpression without affecting hyphal growth. (**G**) Kymographs showing co-localisation of Cdc3G and Rrm4C (red arrowheads), both expressed at endogenous levels (Supplementary Movie S7).

positive for SNARE Yup1, the small G-protein Rab5a and Rrm4 (Baumann et al, 2012; Schuster et al, 2011c), revealed that Cdc3G is associated with Rrm4-positive endosomes (Figure 3F). For verification, co-localisation of Cdc3G and Rrm4C (Rrm4 fused to mCherry) was studied. Consistently, Cdc3G co-localized almost exclusively with Rrm4-positive endosomes (Figure 3G; Supplementary Movie S7). As co-localisation of mRNA and the encoded protein is indicative for the site of translation (St Johnston, 2005), the simultaneous presence of *cdc3* mRNA and Cdc3 protein at shuttling endosomes strongly points towards its local translation on endosomes.

**Table I** Description of *U. maydis* strains used in this study

| Strain | Locus | Progenitor strain | Specific comment |
|---|---|---|---|
| FB1 | | | wild-type, mating type *a1b1 (*(Banuett & Herskowitz, 1989)) |
| FB2 | | | wild-type, mating type *a2b2 (*(Banuett & Herskowitz, 1989)) |
| UM521 | | | wild-type, mating type *a1b1,* genome sequenced ((Kämper et al, 2006)) |
| AB33 | *B* | FB2 | *Pnar:bW2bE1*, expression of active b heterodimer under control of the *nar1* promoter, strain grows filamentously upon changing the nitrogen source ((Brachmann et al, 2001)) |
| AB33rrm4C | *rrm4* | AB33 | expressing Rrm4 fused to mCherry |
| AB33rrm4G | *rrm4* | AB33 | expressing Rrm4 fused to eGfp ((Becht et al, 2006)) |
| AB33pab1G/rrm4C | *pab1* *rrm4* | AB33pab1G | co-expressing Pab1 and Rrm4 fused to eGfp and mCherry, respectively |
| AB33λN*G$^3$/cdc3B$^{16}$ | *ip$^s$* *cdc3* | AB33λN*G$^3$ | expressing λN*-peptide fused to triple eGfp and *cdc3* mRNA tagged with 16 copies of boxB binding site |
| AB33λN*G$^3$/cdc3B$^{16}$/rrm4C | *ip$^s$* *cdc3* *rrm4* | AB33λN*G$^3$/ cdc3B$^{16}$ | expressing Rrm4 fused to mCherry and λN*-peptide fused to triple eGfp and *cdc3* mRNA tagged with 16 copies of boxB binding site |
| AB33cdc3Δ | *cdc3* | AB33 | carrying a deletion in *cdc3* |
| AB33cdc3Δ/rrm4Δ | *cdc3* *rrm4* | AB33cdc3Δ | carrying a deletion in *cdc3* and *rrm4* |
| AB33cdc3G | *cdc3* | AB33 | expressing Cdc3 fused N-terminally to eGfp |
| AB33cdc3Gc | *cdc3* | AB33 | expressing Cdc3 fused C-terminally to eGfp |
| AB33cdc3G/rrm4Δ | *cdc3* *rrm4* | AB33cdc3G | expressing Cdc3 fused N-terminally to eGfp and carrying a deletion in *rrm4* |
| AB33P$_{otef}$cdc3G | *ip$^s$* | AB33 | expressing Cdc3 fused to eGfp under control of the constitutively active promoter P$_{otef}$; defined ectopic integration at the *ip$^s$* locus, encoding a carboxin sensitive iron-sulfur protein(Loubr |
| AB33 cdc3G/rrm4C | *cdc3* *rrm4* | AB33cdc3G | co-expressing Cdc3 and Rrm4 fused to eGfp and mCherry, respectively |
| AB33pab1R/rrm4G$^{RRMΔ}$ | *pab1* *rrm4* | AB33pab1R | expressing Rrm4 without RRMs fused to eGfp and Pab1 fused to Rfp ((Baumann et al, 2012)) |
| AB33pab1G/ rrm4R$^{mR1}$ | *pab1* *rrm4* | AB33pab1G | expressing Rrm4 with mutated first RRM domain fused to Rfp and Pab1 fused to eGfp |
| AB33cdc3G/rrm4R$^{RRMΔ}$ | *cdc3* *rrm4* | AB33cdc3G | expressing Cdc3 fused N-terminally to eGfp and Rrm4 without RRMs fused to Rfp |
| AB33cdc3G/rrm4R$^{mR1}$ | *cdc3* *rrm4* | AB33cdc3G | expressing Cdc3 fused N-terminally to eGfp and Rrm4 with mutated first RRM domain fused to Rfp |
| AB33λN*G$^3$/cdc3B$^{16}$/rrm4R$^{mR1}$ | *ip$^s$* *cdc3* *rrm4* | AB33λN*G$^3$/ cdc3B$^{16}$ | expressing Rrm4 with mutated first RRM domain fused to Rfp and λN*-peptide fused to triple eGfp and *cdc3* mRNA tagged with 16 copies of boxB binding site |
| AB33λN*G$^3$/cdc3B$^{16}$/rrm4R$^{RRMΔ}$ | *ip$^s$* *cdc3* *rrm4* | AB33λN*G$^3$/ cdc3B$^{16}$ | expressing Rrm4 without RRMs fused to Rfp and λN*-peptide fused to triple eGfp and *cdc3* mRNA tagged with 16 copies of boxB binding site |
| AB33rrm4R | *rrm4* | AB33 | expressing Rrm4 fused to Rfp |
| AB33rrm4Gp$^3$ | *rrm4* | AB33 | expressing Rrm4 fused to photoactivatable triple eGfp |
| AB33rrm4R/rps19G | *rrm4* *ectopic* | AB33rrm4R | expressing Rrm4 fused to Rfp and Rps19 fused to eGfp, ectopic integration at unknown locus |
| AB33rrm4C/rps2G | *rrm4* *ip$^s$* | AB33rrm4C | expressing Rrm4 fused to mCherry and Rps2 fused to eGfp defined ectopic integration at *ip$^S$* locus |
| AB33rrm4C/rpl25G | *rrm4* *ip$^s$* | AB33rrm4C | expressing Rrm4 fused to mCherry and Rpl25 fused to eGfp, defined ectopic integration at *ip$^S$* locus |
| AB33rps2G/rrm4Δ | *ip$^s$* *rrm4* | AB33rrm4C/rps2G | carrying a deletion in *rrm4* and expressing Rps2 fused to eGfp |

**mRNA transport is crucial for endosomal localisation of Cdc3**

To test whether Rrm4-dependent localisation of *cdc3* mRNA is prerequisite for the presence of Cdc3G protein on endosomes, we made use of the loss of function mutants Rrm4$^{mR1}$ carrying a four amino acid block mutation in RNP1 of RRM1 and Rrm4$^{RRM\Delta}$ lacking all three RRMs (Baumann et al, 2012). Both mutant Rrm4 versions still shuttled on endosomes (Supplementary Figure S4B-C). In contrast, movement of Pab1-labeled mRNA was strongly reduced in strains expressing Rrm4$^{mR1}$ or not detectable in strains expressing Rrm4$^{RRM\Delta}$, verifying that these Rrm4 variants are strongly affected in RNA binding (Supplementary Figure S4B-C). Analysing the same mutants by RNA live imaging revealed that endosomal co-transport of $\lambda N^{*}G^{3}$-labelled *cdc3B*$^{16}$ mRNA was drastically reduced (Figure 2E, 4A) or completely abolished (Figure 2E, 4B). Importantly, both variants resulted in the loss of Cdc3G protein on shuttling endosomes (compare Figure 3D with Figs. 4C and 4D) confirming that the presence of *cdc3* mRNA is crucial for endosomal localisation of the encoded protein.

**Ribosomal proteins co-localise with shuttling Rrm4-positive endosomes**

As a second line of evidence for endosome-coupled translation we studied ectopically expressed C-terminal Gfp fusions of ribosomal proteins originating from both subunits. Based on structural predictions and previous work performed in *Saccharomyces cerevisiae* the ribosomal proteins Rps2, Rps19, and Rpl25 (*um05139*, *um11551*, and *um05998*, respectively) were selected (Table I). All three proteins predominantly localised in the cytoplasm with a faint accumulation in the nucleus or nucleolus (Figure 4E). Moreover, shuttling of all three ribosomal proteins with Rrm4-positive endosomes was detectable after local photobleaching (Figure 4E-F; Supplementary Movie S8). Closer inspection of Rps2G revealed that shuttling was lost in the absence of Rrm4 (Figure 4G). Thus, Rrm4 is not only required for the recruitment of the poly(A)-binding protein Pab1 to endosomes (Supplementary Figure S4, Supplementary Movie S1, (König et al, 2009) but also essential for endosomal localisation of ribosomal proteins, *cdc3* mRNA and Cdc3 protein. This is consistent with our hypothesis that Rrm4 recruits mRNAs to endosomes for subsequent local translation.

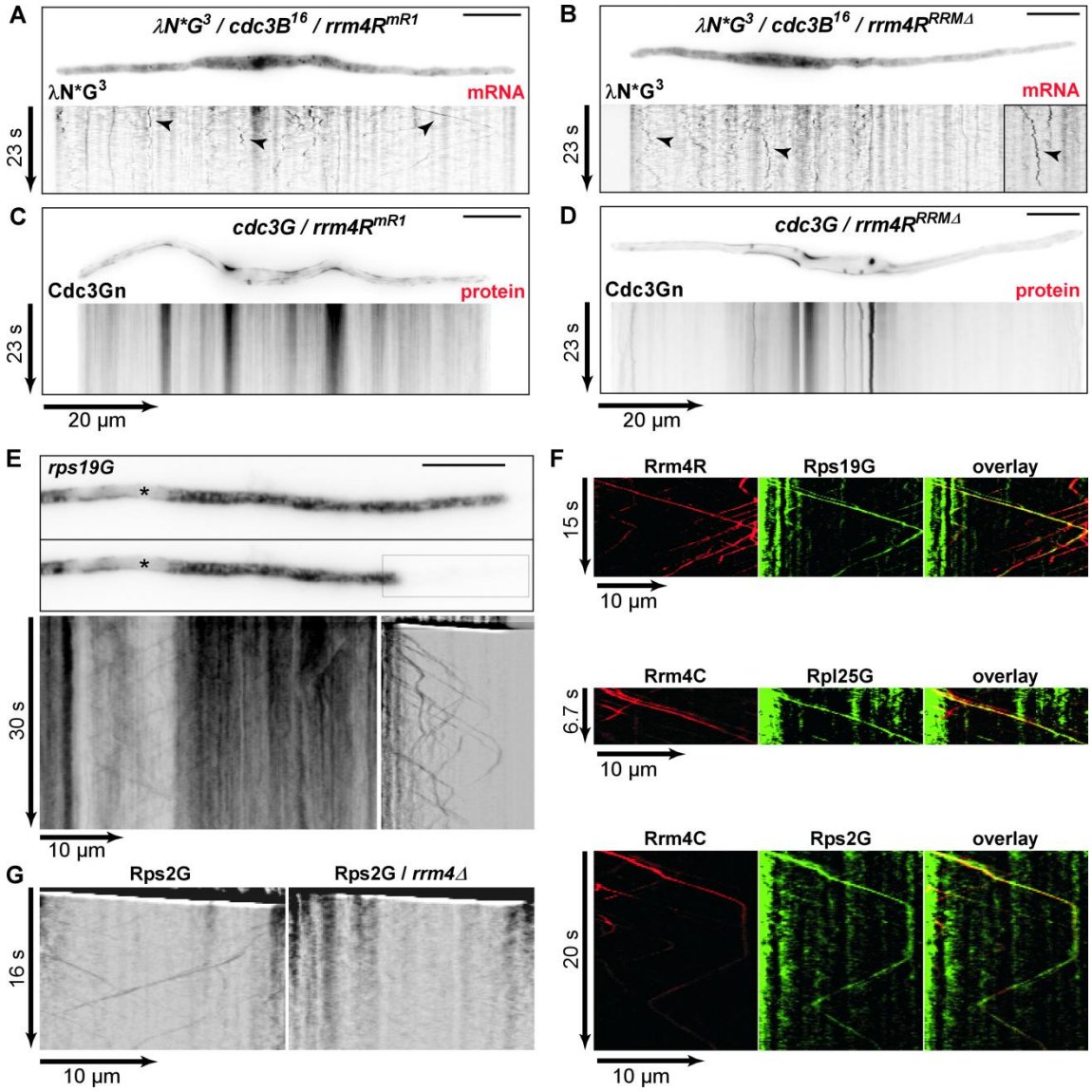


**Figure 4** Endosome-coupled translation of *cdc3* mRNA. (**A-D**) Micrographs and corresponding kymographs depicting $\lambda N^{*}G^{3}$-labeled *cdc3B*$^{16}$ mRNA (A and B) or Cdc3G protein (C and D). Strains carry either allele *rrm4R*$^{mR1}$ (A and C) or *rrm4R*$^{RRM\Delta}$ (B and D). (**E**) Top: micrograph before and after (upper and lower micrograph) photobleaching of Gfp fluorescence (size bar, 10 µm; asterisk indicates nucleus). Bottom: kymograph of Supplementary Movie S8 (after photobleaching). (**F**) Co-localisation (yellow) of Rrm4 (red) and ribosomal proteins (green) on shuttling endosomes. (**G**) Shuttling of Rps2G is Rrm4 dependent. Kymographs (in F and G) of movies recorded after photobleaching.

## Rrm4 function is essential for correct formation of Cdc3 filaments

In order to elucidate the functional consequences of endosome-coupled translation, we studied the Rrm4-dependent localisation of Cdc3G (Figure 3C, E). We observed that the disruption of the endosomal Cdc3G localisation correlates with its disturbed filamentous accumulation at hyphal growth cones (Figure 3C). Hence, endosomes may transport Cdc3 along microtubules and deposit it for assembly at hyphal tips. To test this assumption, we analysed the dynamics of Cdc3G accumulation at hyphal tips

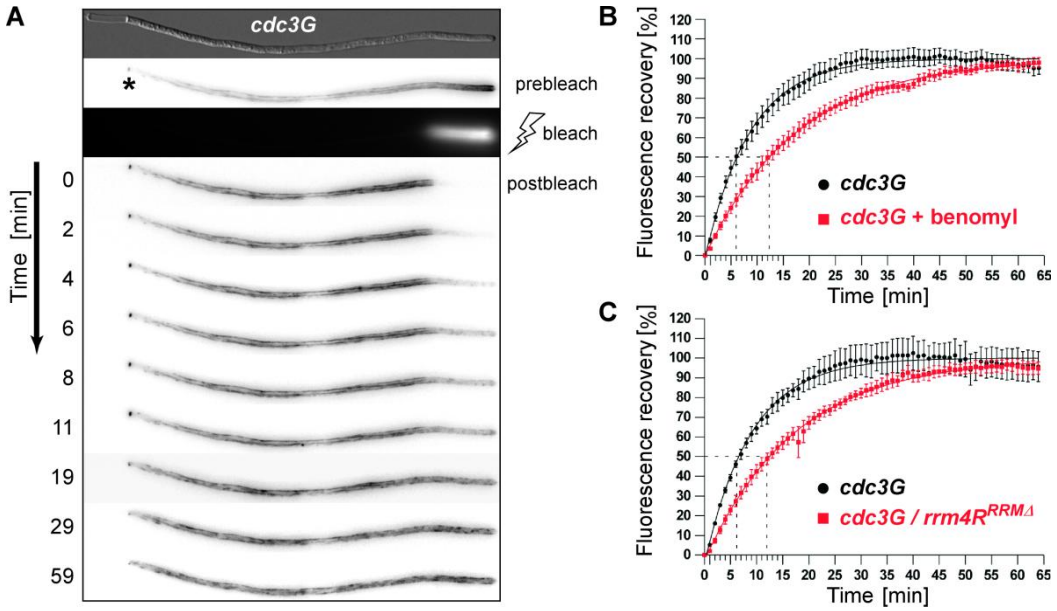


**Figure 5** Endosomal septin transport is important for its accumulation in filaments. (**A**) Representative FRAP experiment analyzing hypha expressing Cdc3G (Supplementary Movie S9; asterisk marks septum). (**B-C**) FRAP analysis of Cdc3G at hyphal tips of indicated strains (data were fitted to uniphasic exponential equation, dotted lines indicated half time of recovery; further details in Supplementary Figure S5 and SI Methods; n = 6 and n = 3 in b and c, respectively; error bars represent s.e.m.).

performing FRAP experiments (Figure 5A, Supplementary Figure S5, Supplementary Movie S9). Hyphae expressing Cdc3G were bleached in a defined 15 µm area at the growth cone and fluorescence recovery was determined over time. The half time of recovery ($t_{1/2}$) was 6 min (Figure 5B-C) which is comparable to previous studies on septin rings in *S. cerevisiae* (Dobbelaere et al, 2003) and consistent with a dynamic assembly process (Figure 5B-C, Supplementary Figure S5, (Sprague & McNally, 2005), suggesting that Cdc3G is indeed incorporated into septin filaments at the hyphal growth cone.

In hyphae treated with benomyl, $t_{1/2}$ was substantially increased to 12 min (Figure 5B), indicating that microtubule-dependent transport is crucial for the accumulation of Cdc3G at growth cones. This is in accord with the altered steady-state distribution of Cdc3G in benomyl-treated hyphae (Figure 2C). Consistently, FRAP analysis of hyphae expressing Rrm4R$^{RRM\Delta}$ also revealed an elevated $t_{1/2}$ of recovery of 12 min (Figure 5C, Supplementary Figure S5). In conclusion, endosomal mRNA translation supported by Rrm4 appears to be the key mechanism for the microtubule-dependent delivery and accumulation of Cdc3G in septin filaments at hyphal growth cones.

**Extensive fission of Rrm4-positive endosomes**

During our study of endosome-coupled translation of septin Cdc3 we observed an apparent contradiction: Cdc3G protein is present at almost all endosomes (Figure 3G), whereas *cdc3B*[16] mRNA is detectable at only a few of them (Figure 2E). To investigate this finding in more detail we performed laser activation experiments with Rrm4 fused to photo-activatable Gfp (triple version; Rrm4Gp$^3$) which visualized highly dynamic and extensive fission of Rrm4Gp$^3$-positive endosomes (Figure 6, at least four fission events in 24 s), suggesting that an intensive exchange of membrane-associated cargo does occur. Thus, the necessary distribution of translated Cdc3 throughout the entire endosome population can be achieved by frequent fusion and fission events of endosomes.

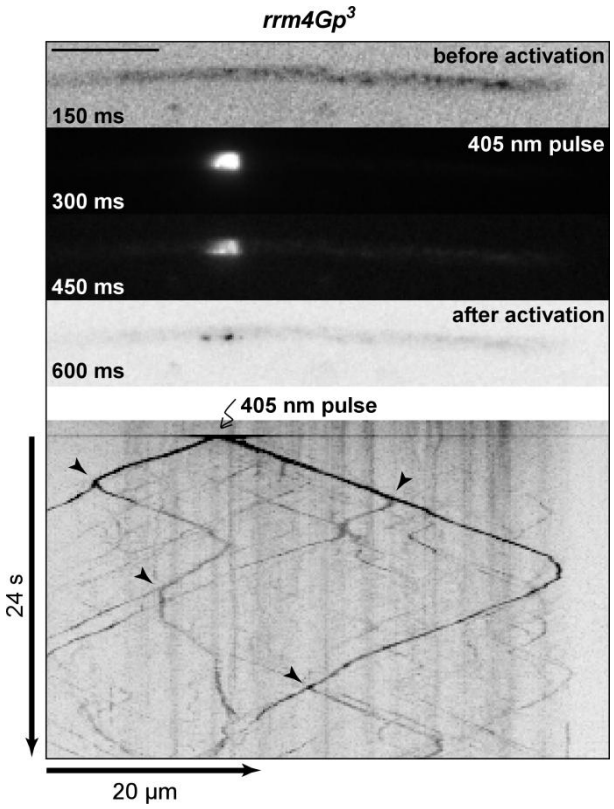


**Figure 5** Endosomal septin transport is important for its accumulation in filaments. (**A**) Representative FRAP experiment analyzing hypha expressing Cdc3G (Supplementary Movie S9; asterisk marks septum). (**B**-**C**) FRAP analysis of Cdc3G at hyphal tips of indicated strains (data were fitted to uniphasic exponential equation, dotted lines indicated half time of recovery; further details in Supplementary Figure S5 and SI Methods; n = 6 and n = 3 in b and c, respectively; error bars represent s.e.m.).

### 2.3.3 Discussion

Septins constitute important cellular proteins involved in cytokinesis and membrane dynamics (Barral, 2010; Spiliotis & Gladfelter, 2012). Their assembly into higher-order structures such as rings and filaments is essential for septin function. The building blocks of these superstructures are short nonpolar rods consisting of defined palindromic hetero-octamers (McMurray et al, 2011; Weirich et al, 2008). In filamentous fungi, septins form diffuse “clouds” at the growth cones that coalesce into ring-like structures during septum formation (Gladfelter, 2010). The occurrence of septin filaments is known, for example, from *Aspergillus nidulans* (Hernandez-Rodriguez et al, 2012) and *U. maydis* (Alvarez-Tabares & Perez-Martin, 2010; Böhmer et al, 2008). However,

despite the detailed knowledge on their structure and their precise subcellular localisation, information on subcellular trafficking of septins is scarce.

In this study we investigated the subcellular localisation and microtubule-dependent transport of *cdc3* mRNA and the encoded protein. Besides the known subcellular structures (Alvarez-Tabares & Perez-Martin, 2010; Böhmer et al, 2009), we discovered two additional septin localisations that were dependent on Rrm4 and functional microtubules: Cdc3 resides on Rrm4-positive endosomes and forms a gradient in filaments emanating from growth cones. Based on our results we hypothesize that Cdc3 is loaded onto endosomes and delivered by endosomal transport to septin filaments at growth cones. The directionality of septin transport was addressed by FRAP experiments. The determined half time of recovery was in the order of minutes, which is indicative for a diffusion-uncoupled recovery (recovery solely based on diffusion is in the order of seconds (Sprague & McNally, 2005). This suggests the involvement of protein interaction partner(s) and/or the existence of an assembly process (Sprague & McNally, 2005). In accordance, comparable recovery rates have been observed for septin assembly in *S. cerevisiae* and *C. albicans* (Caviston et al, 2003; Dobbelaere et al, 2003; Li et al, 2012). Importantly, the recovery rate is dependent on Rrm4-mediated mRNA transport along microtubules strongly supporting the notion that Cdc3 locates first on shuttling Rrm4-positive endosomes and subsequently assembles in filaments at the growth cones.

Studying mRNA transport revealed that *cdc3* mRNA is an *in vivo* target of the Rrm4-dependent transport machinery that was recently shown to function via co-transport of Rab5a-positive endosomes (Baumann et al, 2012). Inspired by this finding we developed the hypothesis that loading of endosomes with septin protein is mediated by endosome-coupled translation of *cdc3* mRNA. This hypothesis is supported by several *in vivo* observations: (i) *cdc3* mRNA and protein co-localize at shuttling endosomes. It is widely accepted that such a co-localisation is indicative for the site of translation (Bullock, 2011; St Johnston, 2005). (ii) Ribosomal proteins of both subunits also co-localize with shuttling endosomes, and this is dependent on the presence of mRNA. Consistently, also the localisation of Pab1 on endosomes is dependent on mRNA (Baumann et al, 2012). (iii) The accumulation of Cdc3 protein on endosomes is dependent on the presence of *cdc3* mRNA on endosomes. (iv) Cdc3 protein is hardly found at shuttling endosomes in the yeast form. This correlates with our previous finding that Rrm4 binding is drastically reduced in yeast cells (Becht et al, 2006).

Active bi-directional transport of mRNAs without an obvious destination has been widely observed and seems like a waste of energy. Thus, its cellular role has been a long-lasting mystery (Bullock, 2011; Zimyanin et al, 2008). RNA live imaging in oocytes of *D. melanogaster* revealed microtubule-dependent transport of mRNAs in all directions with a slight bias towards the destination at the posterior pole. Thus, a biased random walk along a weakly polarized cytoskeleton was proposed to finally deliver mRNAs for subcellular accumulation (Zimyanin et al, 2008). An alternative mechanism is reported during embryonic development: RNA zipcodes can influence the directionality of shuttling mRNAs directly by recruitment of additional dynein motors to enhance minus-end directed transport (Amrute-Nayak & Bullock, 2012). However, in mammalian neurons intensive shuttling of mRNAs is observed without strong accumulation at specific subcellular sites. This was compared to a sushi belt continuously serving demanding synapses with mRNAs (Doyle & Kiebler, 2011). Similarly, we observed that mRNAs shuttle extensively in *U. maydis* without subcellular accumulation. We discovered that the underlying mechanism is microtubule-dependent co-transport with Rab5a-positive endosomes (Baumann et al, 2012). Our latest findings provide a more comprehensive understanding of this trafficking phenomenon: mRNAs shuttle because of their local translation on moving endosomes.

The concept of co-transport of mRNAs and membranous compartments such as ER or vesicles is prevalent (Kraut-Cohen & Gerst, 2010; Trautwein et al, 2004), and it is known that endosomal components such as Rab11 and the ESCRT-II complex are needed for mRNA transport during development (Cohen, 2005; Irion & St Johnston, 2007). However, we now describe an unanticipated direct link between mobile mRNA translation and septin protein trafficking on membranous carrier platforms. Interestingly, septins were previously purified from presynaptic vesicles and they exhibit vesicle-like staining patterns in neurons (Beites et al, 1999; Spiliotis & Gladfelter, 2012; Xie et al, 2007). Thus, endosomal trafficking might be a common mechanism for septin transport and conserved from fungi to humans.

Here, we demonstrate that septin is a novel cargo of fungal endosomes and that this transport mode is important for the dynamic assembly of septin filaments at the growth cones of unipolar hyphae. Thus, long-distance transport of septins constitutes an additional function of these so-called early endosomes, which, up to date, were believed to mainly function in endocytosis during fungal growth (Penalva, 2010; Steinberg,

2007b). This process is functionally important for polarity, because loss of Cdc3 causes defects in establishing unipolar growth.

In general, endosomes receive their cargo mainly from other membranous compartments by fusion with transport vesicles (Huotari & Helenius, 2011). We uncover that septin cargo can also be loaded onto moving endosomes by local translation comparable to the aerial refueling of planes. This new mechanism targets the cargo to the correct endosomal compartment opening up additional unanticipated potential for protein trafficking via these multipurpose platforms (Gould & Lippincott-Schwartz, 2009).

### 2.3.4 Materials and Methods

*Standard techniques, plasmid construction, strain generation and growth conditions*

Standard molecular biology techniques were applied (Baumann et al, 2012; Brachmann et al, 2004). Strain generation (Table S1-3, MUMDB; http://mips.helmholtz-muenchen.de/genre/proj/ustilago/) (Kämper et al, 2006) was performed with an SfiI-based cloning strategy (Baumann et al, 2012; Brachmann et al, 2004). Most constructs were stably integrated in single copy using homologous recombination (Brachmann et al, 2004). For defined ectopic integration, constructs were targeted to the $ip^S$ locus (Loubradou et al, 2001) (Table S1-2). Proteins were tagged with eGfp, enhanced version of green fluorescent protein (Clontech), mCherry, a derivative of mRfp (monomeric red fluorescent protein) (Campbell et al, 2002; Shaner et al, 2004), and photo-activatable Gfp (triple version) (Patterson & Lippincott-Schwartz, 2002).

For tagging RNA, boxB hairpins were inserted in *cdc3* (*um10503*) mRNA 100 nt downstream of the stop codon. The $\lambda N^*$ peptide carrying three point mutations derived from a related arginine-rich RNA-binding peptide of phage P22 was inserted at the $ip^S$ locus (Fig. 1C). This version was reported (Austin et al, 2002) to exhibit an about 60-fold higher *in vitro* binding affinity for the λN binding sites boxB (a direct comparison of λN and $\lambda N^*$ for RNA *in vivo* approaches will be published elsewhere).

*rpl25G* and *rps2G* (*um11551* and *um05139*) were inserted as single and tandem copies at the $ip^S$ locus, respectively. Expression was controlled by the constitutively active $P_{otef}$ promoter (Table S1-2). *rps19G* (*um05998*) was inserted ectopically and expression was controlled by its endogenous promoter. Ribosomal proteins for expression of fusion proteins were chosen according to published work (Klinge et al, 2012; Milkereit et al, 2003).

Growth conditions were described previously (Baumann et al, 2012). Microscopy was performed 4-16 h.p.i. of hyphal growth. The phenotypic analysis of *cdc3* strains was performed after incubating budding cells at 21°C in complete medium (CM) supplemented with 1% glucose (glc), and subsequent shifting at $OD_{600}$ = 0.5 to nitrate minimal medium (NM + glc) followed by incubation at 30°C.

*Microscopy and image processing*

The Zeiss Axio Observer.Z1-based microscopy set-up was described elsewhere (Baumann et al, 2012). For RNA live imaging and co-localization studies we used laser-based epifluorescence microscopy. A VS-LMS4 Laser-Merge-System (Visitron Sys-ems, Munich, Germany) combines solid state lasers for excitation of Gfp (488 nm/50 mW) and Rfp/mCherry (561 nm/50 mW). Co-localization studies of dynamic processes were either carried out with a two-channel imager (DV2, Photometrics) (Baumann et al, 2012) or by applying millisecond alternating laser excitation (msALEX) (Lange et al, 2008; Lee et al, 2005). Switching of 488 nm (Gfp) and 561 nm (Rfp/mCherry) laser lines was achieved with an acousto-optic tuneable filter. The different fluorophores of Gfp and mRfp/mCherry were excited alternately for 60 or 70 ms with 488 nm and 561 nm laser lines, respectively. Fluorescence signals were collected using α-Plan-Apochromat (100x, NA 1.46) and EC Plan-Neofluar (100x, NA 1.3) objectives. A CoolSNAP HQ2 CCD camera (Photometrics) was driven in the 20 MHz mode to achieve overlapping exposure and read-out. Binning of 2 was applied to raise the signal intensity. The settings allowed for frames of 60-70 ms enabling detection of alternating green and red fluorescent signals that overlapped between successive frames. All parts of the microscope systems were controlled by the software package MetaMorph (Molecular Devices, version 7), which was also used for image processing including the adjustment of brightness and contrast as well as measurements, quantifications, kymographs and maximum projections of z-stacks. Fluorescence micrographs are displayed inverted unless otherwise stated.

*RNA live imaging*

20 ml cultures of cells were grown to an $OD_{600}$ of 0.5 in CM medium supplemented with 1% arabinose (ara) and shifted to NM (1% ara) medium to induce filamentous growth for 12-16 h. The ara-inducible $P_{crg}$ promoter controlled the

expression of the $\lambda N^{*}G^{3}$ peptide. For excitation of Gfp the 488 nm laser line was set to 50%. Hyphae were observed with a 63x Plan-Apochromat (NA 1.4, Zeiss) in combination with a CoolSNAP HQ2 camera (Photometrics). Each movie was recorded with 150 ms / frame and contained 150 frames.

For quantification of processive movement, kymographs were generated to study the number, velocity, processivity, and direction of particles (only distances > 2 µm were scored). For analysis of directionality, particles that reversed direction were counted twice. To determine the average number of particles per 100 µm hypha, the total length of hyphae was measured and divided by the number of particles.

For AB33$\lambda N^{*}G^{3}$/cdc3B$^{16}$ we counted 69 particles in 9,249 µm corresponding to 96 hyphae with an average length of 96.3 µm (n=3 independent experiments). In AB33$\lambda N^{*}G^{3}$/ cdc3B$^{16}$/rrm4Δ no particles were detected in 2,755 µm (n=3; 36.5 hyphae with an average length of 75.5 µm). In AB33$\lambda N^{*}G^{3}$/cdc3B$^{16}$/rrm4R$^{RRM\Delta}$ a single particle was observed in 2,762 µm (n=3; 36 hyphae with an average length of 76 µm). In AB33$\lambda N^{*}G^{3}$/cdc3B$^{16}$/*rrm4R$^{mR1}$* 18 particles were scored in 5157 µm (79 hyphae with an average length of 65 µm).

Each bar chart in Fig. 1 represents mean values and s.e.m. of three independent experiments. The following statistical tests were applied (Prism5, Graphpad): one way ANOVA for velocity of mRNAs and for number of processive mRNPs / 100 µm (Fig. 1G, all columns P=0.003). Paired two-tailed t-test for directionality of mRNAs, mean processivity of mRNPs and direct comparison of number of processive mRNPs / 100 µm (rrm4 vs. *rrm4R$^{mR1}$* and rrm4 vs. *rrm4R$^{RRM\Delta}$*, P=0.03 each). P-values below 0.05 were considered as statistically significant.

*Fluorescence recovery after photobleaching (FRAP)*

For FRAP experiments we chose the 40x EC Plan-Neofluar objective (NA 1.3; Zeiss) to obtain a wide field of view with sufficient resolution. To excite Gfp we used a 472 nm LED (CoolLED, precisExcite, Andover, UK) to reduce photobleaching. The HQ2 camera was operated in a low read-out noise mode (10 MHz); gain was set to 3. Photobleaching was achieved with a VisiFRAP 2D-System (Visitron Systems, Munich, Germany) including a 405 nm/80 mW diode laser that was regulated by a UGA-40 controller (Rapp OptoElectronic GmbH, Hamburg, Germany) and a VisiFRAP 2D control software for Meta Series 7.6 (Visitron Systems, Munich, Germany). An area of

15 µm from hyphal tips was bleached with 10% laser power. The beam diameter was 10 pixels and the bleach time was six ms per pixel. Bleaching was carried out in 10 z-planes through fungal hyphae with a z-distance of 0.5 µm. z-stacks were obtained using a PIFOC P-737 (Physik Instrumente GmbH & Co. KG, Karlsruhe, Germany) high-speed Piezo z-stage. Fluorescence recovery was acquired with an exposure time of 500 ms in a z-stack of 10 planes with a z-distance of 0.5 µm (open camera shutter). Every minute a z-stack was collected for a period of 65 minutes. Before acquiring Gfp fluorescence, the software driven autofocus was used in the DIC channel to assure that acquisition started in the correct focal plane. All settings were carried out by the "multidimensional acquisition" tool of MetaMorph.

In order to analyze collected data the acquired z-stacks were merged to a maximum projection, the average background was subtracted and the images were corrected for the drift of the observed hypha during the time of data acquisition (65 min). Fluorescence recovery was determined in the bleached hyphal growth cones over time. Fluorescence intensity in the first frame after bleaching (t0) was set to 0. The obtained data were corrected for acquisition bleaching at each time point. Acquisition bleaching was determined by loss of fluorescence in complete frames during the postbleach acquisition period. Mean values of three and six independent experiments (with 6 and 5-8 filaments per strain and experiment, respectively) were plotted against time. The resulting plateau levels were set to 100%. The obtained data followed an uniphasic exponential curve that could be fitted to the exponential equation $f(t) = A(1-e^{-kt})$. This allowed the extraction of half time recovery $t_{1/2}$ where A is the mobile fraction of fluorescent molecules and k ($min^{-1}$) the rate constant. Curve fitting was done with Prism5 (Graphpad). In order to determine total fluorescence recovery obtained values at each time point were normalized to prebleach intensities.

*Photobleaching and photoactivation*

To visualize moving ribosomal proteins we photobleached 20 µm of the respective hyphae prior to detecting Gfp fluorescence. The 405 nm laser was set to 20% output power with a beam diameter of 20 pixels and 100 ms bleach time per pixel. The 488 nm laser was set to 50% output. The HQ2 camera detected signals with exposure time of 150 ms and a binning of 2. When analyzing potential co-localization of ribosomal proteins and Rrm4 we performed msALEX and exposure times for Gfp and Rfp/mCherry were reduced to 70 ms, while the laser output power was set to 60% and

40% for 488 nm and 561 nm, respectively. For photoactivation of Rrm4Gp3 the 405 nm laser was operated with 2% power and a circle of 12 pixels was activated for 200 ms activation time. The HQ2 camera was driven with 150 ms exposure time and binning as well as gain of 3.

*Benomyl treatment and FM4-64 staining*

50 µM benomyl was added to 20 ml of liquid culture that was grown for at least one additional hour at 28°C and 200 rpm before microscopical analysis. For FM4-64 staining an aliquot of the filament suspension was labeled with 0.8 µM FM4-64 (Molecular Probes). After 30-60 seconds of incubation at room temperature samples were subjected to microscopic analysis (Fuchs et al, 2005).

### 2.3.5 Supplementary Information

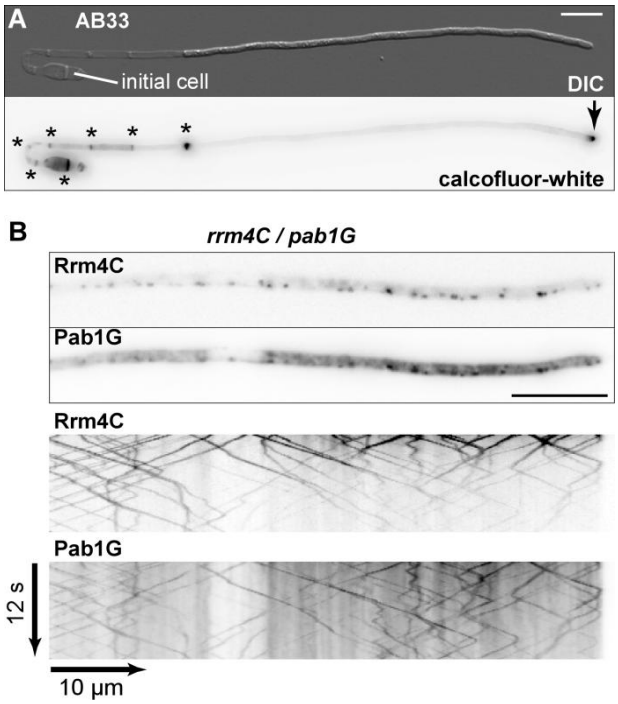


Supplementary Figure S1. **Rrm4-containing mRNPs shuttle along microtubules.** (**A**) Hypha of strain AB33 after induction (DIC image in upper and calcofluor-white staining in lower panel). Changing the nitrogen source triggers expression of the bW2/bE1 transcription factor eliciting a morphological switch: cells that proliferate by budding switch to hyphal growth synchronously and highly reproducibly (Baumann et al, 2012; Brachmann et al, 2001). Calcofluor-white stains chitin at retraction septae (asterisks) and the growth cone (arrow; size bar, 10 µm). (**B**) Hypha of strain AB33rrm4C/pab1G. Micrographs and kymographs (upper two and lower two panels, respectively) were taken from Supplementary Movie S1 recorded simultaneously with dual-colour detection (time and distance as indicated; size bar, 10 µm).

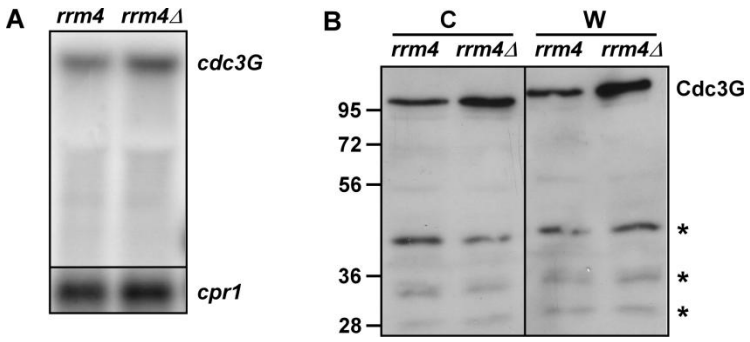


Supplementary Figure S2. ***cdc3* mRNA and corresponding protein levels are not drastically altered in *rrm4Δ*.** (A) Northern blot analysis showing total RNA of AB33cdc3G and AB33cdc3G/rrm4Δ hybridized with radioactively-labelled *gfp* probe. As loading control constitutively expressed *cpr1* mRNA (MUMDB *um03726.2* encoding a peptidylprolyl isomerase) was detected. (B) Western blots analysing cytosolic fractions (C) and whole cell lysate (W) of AB33cdc3G and AB33cdc3G/rrm4Δ. α-Gfp antiserum was used for detection (equal amounts of protein were loaded; marker sizes in kDa; asterisks mark degradation bands).

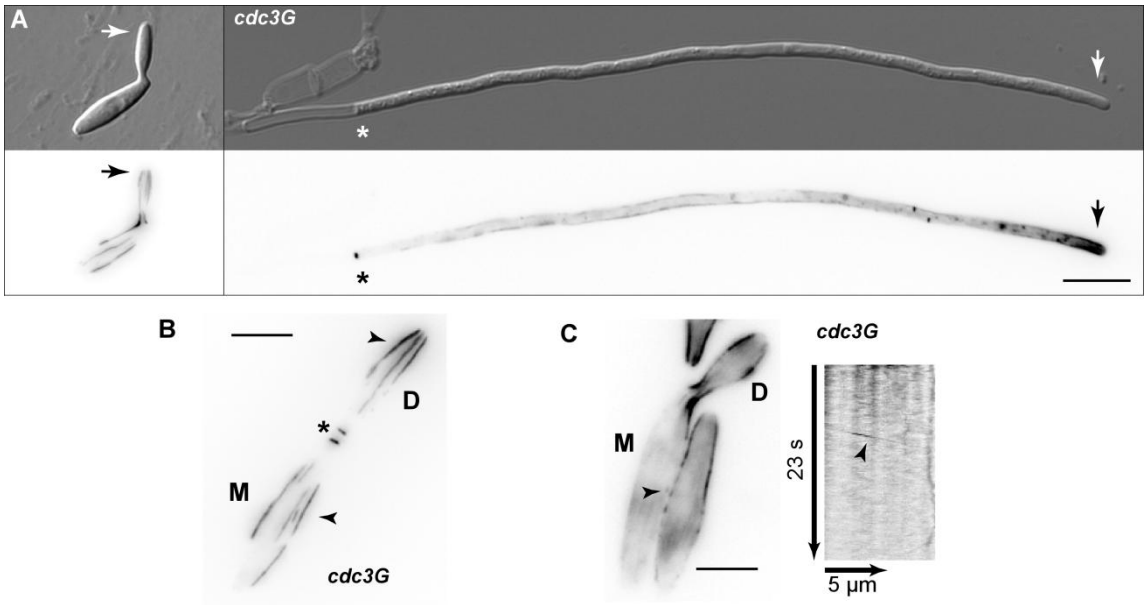


Supplementary Figure S3. **Subcellular localisation of functional Cdc3G.**(**A**) Budding cell and hypha expressing Cdc3G. Growth cones and retraction septa are indicated by arrows and asterisks, respectively (DIC image and inverted fluorescence micrographs are shown at the top and bottom, respectively; size bar, 10 µm). (**B**) Budding cell expressing Cdc3G (M, mother and D, daughter; maximum projection of z-stacks; size bar, 5 µm). Cdc3G localizes to filaments (arrowheads, as described for Cdc10) as well as to primary and secondary septa (asterisk; see Supplementary Movie S4 for Cdc3G at retraction septa, (Alvarez-Tabares & Perez-Martin, 2010; Böhmer et al, 2009)). (**C**) Micrograph and kymograph of AB33cdc3G budding cells (size bar, 5 µm). Cdc3G rarely localizes to shuttling units (one example depicted by arrowhead; five events in 80 cells). This correlates with the finding that RNA binding of Rrm4 is strongly reduced in budding cells (Becht et al, 2006).

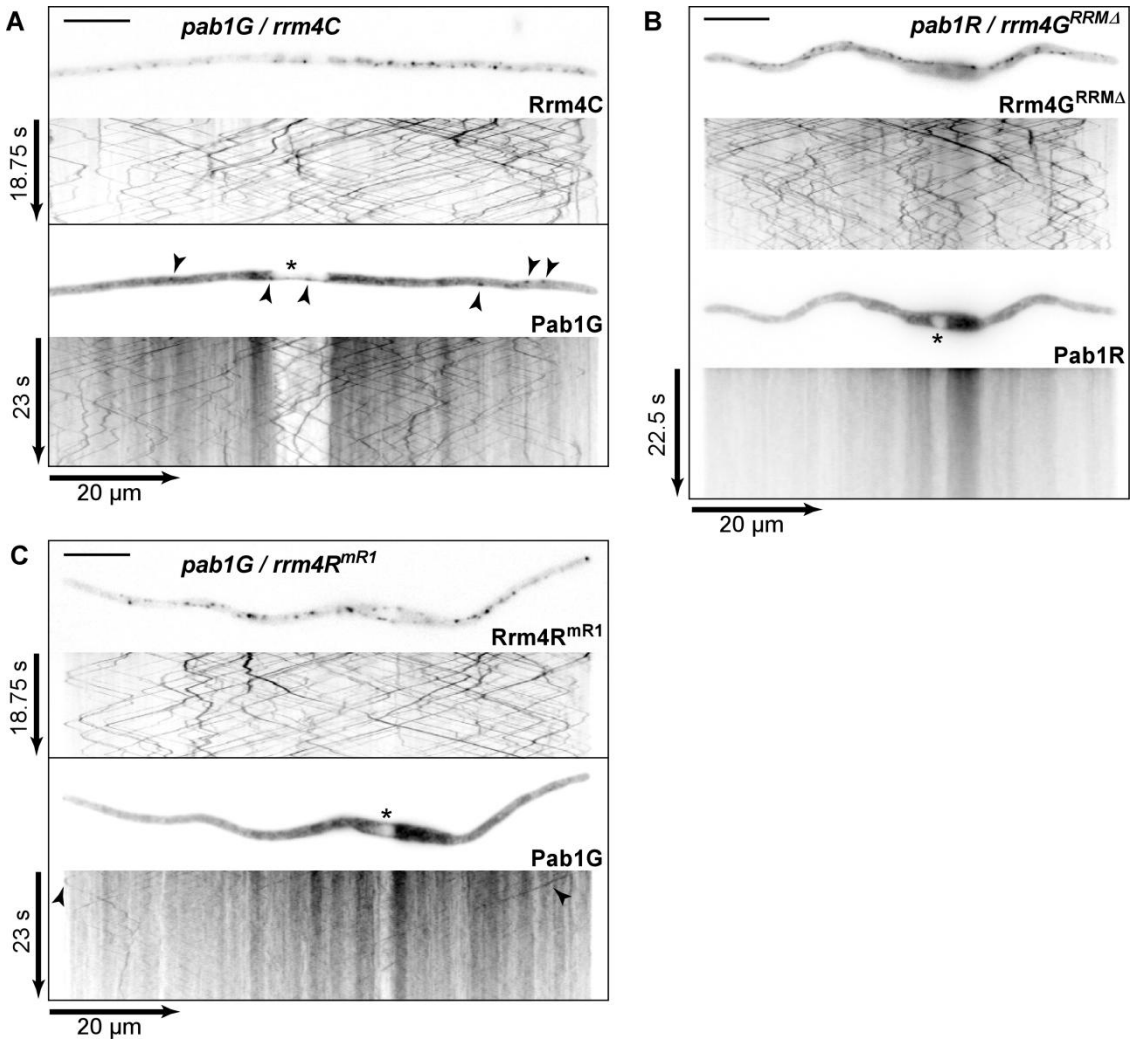


Supplementary Figure S4. **Shuttling of Pab1G-labeled mRNA is severely affected in Rrm4 mutants.** (**A**) Hyphal tip of an AB33 derivative expressing Rrm4 fused to mCherry (upper part) and Pab1 fused to Gfp (lower part). Micrographs (arrowheads indicate shuttling Pab1G-labeled mRNP) and kymographs are shown (time and distance as indicated). Arrowheads mark Pab1G on processive units. (**B**) Strain expressing an allele of Rrm4 lacking the RNA binding domains RRM1-3 fused to Gfp (upper part) and Pab1 fused to mRfp (lower part). Micrographs and kymographs as in a. (**C**) Strain expressing the mutant version Rrm4R$^{mR1}$ fused to mRfp (upper part) and Pab1 fused to Gfp. The four amino acid block mutation in the first RRM domain reduces mRNA binding and polar growth is disturbed (Baumann et al, 2012; Becht et al, 2006). Micrographs and kymographs as in a (kymographs were obtained from movies recorded sequentially to ensure highest sensitivity; size bars = 10 µm).

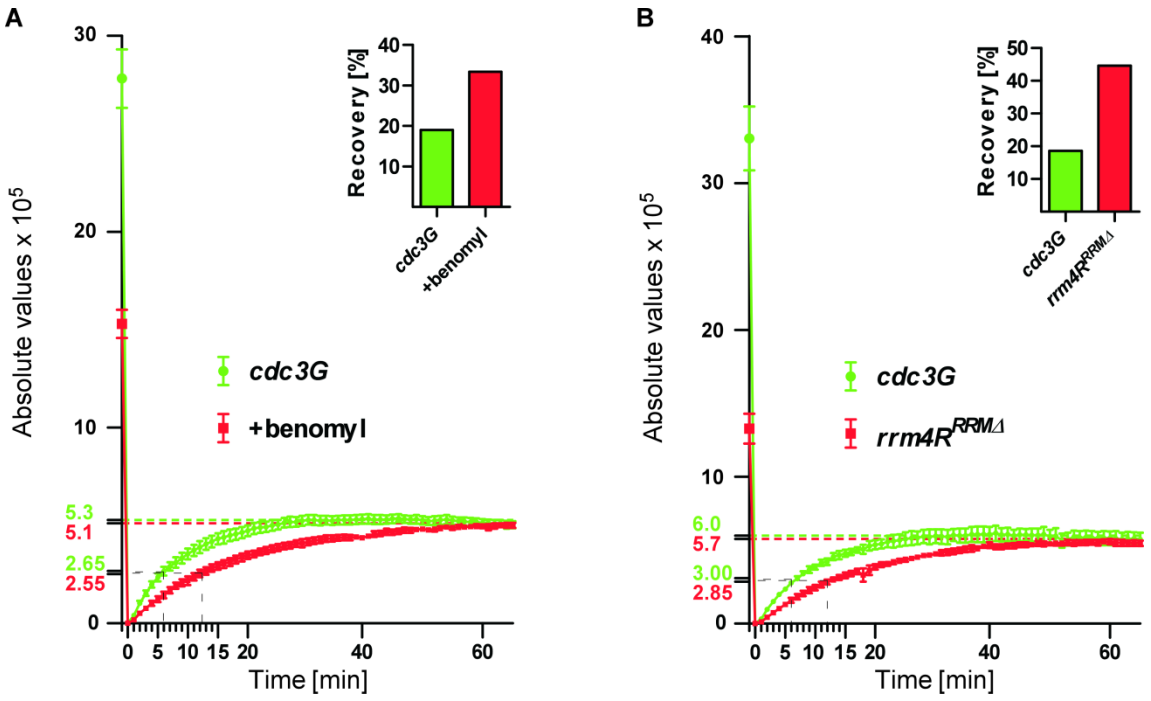


Supplementary Figure S5. **FRAP recovery rate of Cdc3G at growth cones depends on functional Rrm4.** (**A-B**) Determination of FRAP recovery rates of Cdc3G at growth cones of hyphae. A 15 µm stretch at the tips of hyphae was bleached. The strong accumulation of Cdc3G at the tip did not recover (compare Figure 2C). This signal also declined during extended time of microscopic analysis (in the range of 5 – 10 minutes). Non normalized data of fluorescence recovery (%) are plotted against time (min). 0 on the time axis indicates the fluorescence intensity before bleaching. The plateau reached after recovery is in the same range in untreated or benomyl-treated hyphae. The higher prebleach intensity in *cdc3G* is due to the strong accumulation of Cdc3G at hyphal tips. This might reflect a mobile protein fraction (White & Stelzer, 1999) that is unable to recover under prolonged time of microscopic analysis (see above). Data followed a uniphasic exponential curve. In hyphae treated with benomyl or in hyphae expressing $Rrm4R^{RRM\Delta}$ half time of recovery $t_{1/2}$ was substantially increased (6 and 3 independent experiments with 5-8 hyphae per strain and experiment; $t_{1/2}$ is not influenced by normalisation of the data, compare Figure 4). Bar diagrams indicated relative recovery in % (s.e.m. error bars not visible). In order to determine fluorescence recovery obtained values at each time point were normalized to prebleach intensities.

**Supplementary Table SI** Details on the generation of *U. maydis* strains used in this study

| Strains | Relevant genotype | UMa | Reference | Transformed plasmid | Locus | Progenitor strain |
|---|---|---|---|---|---|---|
| AB33 | *Pnar:bW2bE1* | 133 | Brach-mann et al., 2001 | pAB33 | *B* | FB2 |
| AB33rrm4C | *rrm4C* | 830 | this study | pRrm4C-HygR (pUMa1468) | *rrm4* | AB33 |
| AB33pab1G/rrm4C | *pab1G rrm4C* | 769 | this study | pRrm4C-HygR (pUMa1468) | *pab1 rrm4* | AB33pab1G |
| AB33λN*G$^3$ | *λN*G$^3$* | 760 | this study | pλN*G$^3$-CbxR (pUMa1044) | *ip$^s$* | AB33 |
| AB33λN*G$^3$/cdc3B$^{16}$ | *λN*G$^3$ cdc3B$^{16}$* | 848 | this study | pP$_{otef}$Cdc3B$^{16}$–NatR (pUMa1448) | *ip$^s$ cdc3* | AB33λN*G$^3$ |
| AB33λN*G$^3$/cdc3B$^{16}$/rrm4C | *λN*G$^3$ cdc3B$^{16}$ rrm4C* | 879 | this study | pRrm4C-HygR (pUMa1468) | *ip$^s$ cdc3 rrm4* | AB33λN*G$^3$/cdc3B$^{16}$ |
| AB33rrm4G | *rrm4G* | 274 | Becht et al., 2006 | pRrm4G-NatR (pUMa496) | *rrm4* | AB33 |
| AB33cdc3Δ | *cdc3Δ* | 442 | this study | pCdc3Δ–HygR (pUMa1004) | *cdc3* | AB33 |
| AB33cdc3Δ | *cdc3Δ* | 724 | this study | pCdc3Δ–HygR (pUMa1004) | *cdc3* | AB33cdc3G |
| AB33cdc3Δ/rrm4Δ | *cdc3Δ rrm4Δ* | 716 | this study | pRrm4Δ–NatR (pUMa865) | *cdc3 rrm4* | AB33cdc3Δ |
| AB33cdc3G | *cdc3* | 449 | this study | pCdc3G-NatR (pUMa1028) | *cdc3* | AB33cdc3Δ |
| AB33cdc3Gc | *cdc3* | 441 | this study | pCdc3Gc-NatR (pUMa990) | *cdc3* | AB33 |
| AB33cdc3G/rrm4Δ | *cdc3G rrm4Δ* | 462 | this study | pRrm4Δ–HygR (pUMa495) | *cdc3 rrm4* | AB33cdc3G |
| AB33P$_{otef}$cdc3G | *P$_{otef}$cdc3G* | 421 | this study | pP$_{otef}$cdc3G -CbxR (pUMa987) | *ip$^s$* | AB33 |
| AB33 cdc3G/rrm4C | *cdc3G rrm4C* | 722 | this study | pRrm4C-HygR (pUMa1468) | *cdc3 rrm4* | AB33cdc3G |
| AB33pab1R/rrm4G$^{RRMΔ}$ | *pab1 rrm4* | 575 | Baumann et al., 2012 | pRrm4G$^{RRMΔ}$-CbxR (pUMa1220) | *pab1 rrm4* | AB33pab1R |
| AB33pab1G/rrm4R$^{mR1}$ | *pab1 rrm4 $^{mR1}$* | 758 | this study | pRrm4R$^{mR1}$-HygR (pUMa1006) | *pab1 rrm4* | AB33pab1G |
| AB33cdc3G/rrm4R$^{RRMΔ}$ | *cdc3G rrm4R$^{RRMΔ}$* | 713 | this study | pRrm4R$^{RRMΔ}$-HygR (pUMa1064) | *cdc3 rrm4* | AB33cdc3G |
| AB33cdc3G/ rrm4R$^{mR1}$ | *cdc3G rrm4 $^{mR1}$* | 836 | this study | pRrm4R$^{mR1}$-HygR (pUMa1006) | *cdc3 rrm4* | AB33cdc3G |
| AB33λN*G$^3$/cdc3B$^{16}$/rrm4R$^{mR1}$ | *λN*G$^3$ cdc3B$^{16}$ rrm4R$^{mR1}$* | 877 | this study | pRrm4R$^{mR1}$-HygR (pUMa1006) | *ip$^s$ cdc3 rrm4* | AB33λN*G$^3$/cdc3B$^{16}$ |
| AB33λN*G$^3$/cdc3B$^{16}$/rrm4R$^{RRMΔ}$ | *λN*G$^3$ cdc3B$^{16}$ rrm4R$^{RRMΔ}$* | 878 | this study | pRrm4R$^{RRMΔ}$-HygR (pUMa1064) | *ip$^s$ cdc3 rrm4* | AB33λN*G$^3$/cdc3B$^{16}$ |
| AB33rrm4R | *rrm4R* | 458 | this study | pRrm4R–HygR (pUMa992) | *rrm4* | AB33 |
| AB33rrm4paG$^3$ | *rrm4paG$^3$* | 739 | this study | pRrm4paG$^3$-NatR (pUMa1363) | *rrm4* | AB33rrm4Δ |
| AB33rrm4R/rps19G | *rrm4R rps19G* | 603 | this study | pRps19G-NatR (pUMa829) | *rrm4 ectopic* | AB33rrm4R |
| AB33rrm4C/rps2G | *rrm4C rps2G* | 1003 | this study | pRps2G-CbxR (pUMa1725) | *rrm4 ip$^S$* | AB33rrm4C |
| AB33rrm4C/rpl25G | *rrm4C rpl25G* | 993 | this study | pRpl25G-CbxR (pUMa1726) | *rrm4 ip$^S$* | AB33rrm4C |
| AB33rps2G/rrm4Δ | *rps2G rrm4Δ* | 1008 | this study | pRrm4Δ-NatR (pUMa865) | *ip$^S$ rrm4* | AB33rrm4C/rps2G |

**Supplementary Table SII** DNA oligonucleotides used in this study

| Designation | Nucleotide sequence (5´- 3´orientation) |
|---|---|
| oMF502 | ACGACGTTGTAAAACGACGGCCAG |
| oSL613 | ATATGGCCTGAGTGGCCATGGGCAACGCTCGCACGCGTCGTCGCGAGCG |
| oSL463 | ATACCATGGCCGCGGTGAGCAAGGGCGAGGA |
| oRL703 | ATAGGATCCATGGCTGACGCTGCTCCC |
| oRL704 | ATACCCGGGGTAGAGCGACTTCTTCTGGGTG |
| oRL705 | ATAGGATCCATGCCCGCTGCCAACAAG |
| oRL706 | ATACCATGGGCCTTAGGATGAAGCCGATACGGTTCGAG |
| oSL86 | ACGGCACTTTGATGCGCC |
| oSL88 | CCATGGTGGCCGCGTTGGCCGCCTCGTCATCCTCCTCCTCGTCATCCTCCTCCTCAGAC TCG |
| oSL89 | ATAGGCCTGAGTGGCCTCTTGTCGTTACGCCGCC |
| oSL90 | ACAAGTTGGTACGAAGCGTCCATC |
| oSL499 | AGCTGTACACCATGGACGGAGGTTCTCACGACG |
| oSL500 | ATCCTGCAGTGCTCTCGGCGATTGCTG |
| oSL157 | CACGTCTCGTCAACCAGC |
| oSL158 | GGTGGCCGCGTTGGCCGCGTTTCGCAGTGAGAAACCT |
| oSL159 | ATAGGCCTGAGTGGCCAAGAGCTCAACTCTTTCTTGG |
| oSL160 | CAAACCATGCGCTCGCTC |
| oSL503 | ATAGGCGCGCCAAGAAAGGTTTCTCACTGCG |
| oSL504 | ATAGGCGCGCCTGCTCTCGGCGATTGCTG |
| oSL525 | GACATTTAAATCAGATGTTGTCAGTGA |
| oSL526 | CGAGGCCATCTAGGCCTTGTCTAGATTTGGATGTAG |
| oSL527 | TGAGGCCTGAGTGGCCAGGGACTCCATCGTCGAG |
| oSL528 | AGCATTTAAATGCGCGAACTGCCAATG |
| oSL533 | CGTCCATGGTGTCTAGATTTGGATGTAGAG |
| oSL534 | GATGGCCATCTAGGCCTGCTCTCGGCGATTGCTG |
| oSL530 | CATAAGCTTATGACACAGCTTCAGGTGC |
| oSL531 | CATGGCCTGAGTGGCCGTTACTTCGATTCCCTCTC |
| oRL33 | CCGCGGCGCAGAATTCCTCGAGCAT |
| oRL34 | GTATCTCTGGTGTAGCCCAT |
| oMF503 | TTCACACAGGAAACAGCTATGACC |
| oRL50 | GTCGACAAGAGCTCAACTCTTTCTTGG |

## Legends to Supplementary Movies

### Movie S1

Rrm4C and Pab1G (upper and lower part, respectively) co-localize on endosomes in hyphae of AB33rrm4C/pab1G (Baumann et al, 2012). Real-time movies were recorded simultaneously using dual-color detection and correspond to Fig. S1B (timescale in seconds, 150 ms exposure time, 60 frames, 6 frames/s display rate; QuickTime format, 774 kB).

### Movie S2

RNA live imaging of $\lambda N^{*}G^{3}$-labeled *cdc3B*$^{16}$ mRNA. *cdc3B*$^{16}$ mRNA accumulates in processively moving mRNPs that shuttle bidirectionally through the hypha. Movie

corresponds to Fig. 1D (timescale in seconds, 150 ms exposure time, 154 frames, 6 frames/s display rate; QuickTime format, 1633 kB).

**Movie S3**

RNA live imaging of *cdc3* mRNA in a bipolar *rrm4Δ* hypha. Processive movement of *cdc3* mRNA is lost. Only stochastic movement is detectable. Movie corresponds to Fig. 1H (timescale in seconds, 150 ms exposure time, 103 frames, 6 frames/s display rate; QuickTime format, 3268 kB).

**Movie S4**

Cdc3G is recruited to young retraction septa. The localization is transient as Cdc3G disappears from the hyphal septum after ~15 minutes (timescale in minutes, maximum projection of z-stacks, exposure time 500 ms per plane, 30 frames, 3 frames/s display rate; QuickTime format, 127 kB).

**Movie S5**

Cdc3G localizes to hyphal septum, ring structures and septin filaments. The localization in septin filaments is strongest at the hyphal apex. In addition, Cdc3G moves bidirectionally through the fungal hypha (best seen in tip region) reminiscent of Rrm4 (150 ms exposure time, 125 frames, 6 frames/s display rate; QuickTime format, 1375 kB).

**Movie S6**

Bipolar hypha of AB33cdc3G/rrm4Δ. Cdc3G localizes to septin filaments and small circles. However, strong tip accumulation and bidirectional movement is abolished (150 ms exposure time, 70 frames, 6 frames/s display rate; QuickTime format, 1386 kB).

**Movie S7**

Rrm4C and CdcG (upper and lower part, respectively) co-localize in shuttling units in filaments of AB33rrm4C/cdc3G. Real-time movies were recorded with msALEX and correspond to Figure 2G (timescale in seconds, 120 ms exposure time [60 ms per color], 100 frames, 6 frames/s display rate; QuickTime format, 339 kB).

**Movie S8**

Rps19G localizes to processively moving units that resemble Rrm4 movement. Since Rps19G shows strong cytoplasmic localization, the hyphal apex was photobleached to visualize moving units (150 ms exposure time, 201 frames, 6 frames/s display rate; QuickTime format, 1970 kB).

**Movie S9**

Fluorescence recovery after photobleaching of CdcG in a wild type hypha. CdcG that localizes in septin filaments at the hyphal apex was photobleached by a 405 nm laser pulse. Bleached Cdc3G in the apical region is being replaced by fluorescent Cdc3G (timescale in minutes, maximum projection of z-stacks, exposure time 500 ms per plane, 35 frames, 3 frames/s display rate; QuickTime format, 250 kB).

**Acknowledgements**

We acknowledge Dr. K. Zarnack and lab members for discussion and reading of the manuscript. We are grateful to P. Happel, U. Gengenbacher, and S. Esch for technical assistance and to Drs. H. Tschochner and M. Leibundgut for insights on the tagging of ribosomal proteins. Thanks to Dr. R. Kahmann from the Max Planck Institute for Terrestrial Microbiology for support. The work was funded by grants from the Deutsche Forschungsgemeinschaft to MF (FE 448/3-2).

*Author Contributions:* M.F., S.B., and J.Kö. designed this study and analysed data. J.Kö., J.Ko., and S.B. performed wet bench experiments. S.B. established the λN*-based RNA live imaging system, performed microscopic analysis, quantification, and data evaluation. M.F. and S.B. wrote the manuscript with input from all co-authors. M.F. directed the project.

**Conflict of interest**

The authors declare that they have no conflict of interest.

**Supplementary information** is available at The EMBO Journal Online

# 3 Research Perspectives

In three consecutive studies we used a combination of different *in vivo* methods that enabled us to draw a detailed map of MT-based mRNA transport in *Ustilago maydis* (Fig. 3-1). CLIP identified the target mRNAs *ubi1*, *rho3* and *cdc3*. These mRNAs were investigated via λN-based RNA live imaging which was subsequently improved to analyse *cdc3* mRNA at endogenous expression levels. All target mRNAs move processively within fungal hyphae without accumulating subcellulary, which resembles dendritic mRNA transport (Doyle & Kiebler, 2011). This process appears to be increased through a 3'UTR sequence containing a CA-rich element and depends on functional RRMs of Rrm4. Removing RRMs revealed that Rrm4 is an integral part of the transport machinery since it still associates with transport units and travels like wild-type Rrm4. Additionally Rrm4 was found to be the major player in mRNA trafficking because deletion causes complete loss of mRNA transport, as visualised by Pab1.

This result was the foundation to use Pab1 as a molecular mRNA marker in order to investigate MT-dependent motors carrying out mRNA trafficking. Rrm4-dependent mRNA transport is mediated by a balance of Kin3 and dynein which also transport endosomes in *U. maydis* (Schuster et al, 2011c, this study). This led to the discovery of co-transport of mRNAs and endosomes. Rrm4 co-localises with Rab5a-positive endosomes even in the absence of functional motors, but mRNA trafficking relies on intact moving Rab5a-positive endosomes. Thus, we hypothesise Rrm4 to be hitchhiking on endosomes. Interestingly, mRNA is bound by Rrm4 in the absence of functional motors indicating that Rrm4 is a barge that can load cargo without docks.

Importantly, the protein encoded by the target mRNA *cdc3* localises asymmetrically in fungal hyphae. The strong accumulation at growth cones depends on Rrm4. Furthermore, we discovered the Rrm4-dependent co-transport of *cdc3* mRNA and its encoded protein on shuttling endosomes. Since co-localisation of mRNA and protein is indicative for local protein synthesis, we tested whether septin mRNA is directly translated on endosomes. Consistently, the accumulation of septin protein on endosomes is tightly linked to the recruitment of septin mRNA. Furthermore, ribosomal proteins co-localise with shuttling endosomes, but only in the presence of mRNA. FRAP experiments revealed that endosomal trafficking is essential for an efficient assembly of septin protein into septin filaments at growth cones, a process apparently necessary to establish unipolar growth. Thus, we hypothesise that local mRNA translation loads

endosomes with septin protein for correct endosomal delivery to septin filaments. This provides a new explanation for the mystery of extensive shuttling mRNAs that do not accumulate subcellularly.

*Rrm4-dependent zipcode*

By analysing the localisation of the poly(A)-binding protein we found that Rrm4 is the key factor mediating mRNA transport since upon deletion of *rrm4* shuttling of Pab1 is completely abolished. This makes *U. maydis* an ideal model organism to study mRNA transport, because no rescue effects of other factors are expected if one interferes with Rrm4 function. However, one cannot exclude that additional factors aid Rrm4 in recruiting or binding mRNAs (see below). This might be the reason why no common motif could be identified in the more than 50 different transcripts identified by CLIP. A CA-rich motif was found in a subset of sequences which might contribute to a binding site. This is supported by the fact, that the 3'UTR of *ubi1* confers increased processivity to a control mRNA which is otherwise non processive. In other species non-canonical RNA-binding proteins were identified to bind either mRNA secondary or tertiary structures (Müller et al, 2011; Böhl et al, 2000; Long et al, 2000; Bullock et al, 2010). The application of advanced techniques like iCLIP will help to gain more specific information about potential binding sites. iCLIP is able to detect mRNA binding sites with single nucleotide resolution. Combined with high-throughput sequencing, generation of saturating amount of data will be provided (König et al, 2011).

*Rationale for mRNA transport*

The reason for transport of the Rrm4 cargo mRNAs *ubi1* and *rho3* is still elusive. Small GTPases act very early in processes linked to polarity, as has been described for Cdc42 during cytokinesis in *S. cerevisiae* and Rac1 that is required for hyphal extension in *U. maydis* (Bi & Park, 2012; Mahlert et al, 2006). Since Rho3 localises predominantly to the hyphal septum it might have a function in e.g. regulating actin dynamics that drive septum formation. Unfortunately deletion of *rho3* does not result in polarity defects which might be due to redundant Rho GTPases. Therefore it might be worth to study double or triple deletion mutants. It is also conceivable that other Rho GTPase encoding mRNAs are targets of Rrm4. We hypothesise that Rrm4-mediated mRNA transport is important for the subcellular localisation of Rho3. But deletion of Rrm4 does not abolish Rho3 association with septa, arguing for a potential

second route for protein delivery or simply diffusion. It might be possible that mRNA transport supports the fast and efficient delivery of proteins to target sites as demonstrated for Cdc3 (see section 2.3).

In case of *ubi1* it is even more difficult to identify the molecular function. Since deletion is most likely lethal one needs to generate conditional mutants. Also it would be necessary to dissect the genetic information of ubiquitin and Rpl40 in order to analyse both proteins individually. Unfortunately there are indications that the ubiquitin fusion is necessary for efficient assembly with ribosomes as shown for Rps31, that is another natural fusion of a ribosomal protein with ubiquitin (Lacombe et al, 2009). This complicates the separate analysis of both proteins. The traditional view is that after translation, ribosomal proteins enter the nucleus/nucleolus for ribosome assembly (Panse & Johnson, 2010). Recently different populations of ribosomes were discussed, that have alternative protein compositions and carry out specialised function (Gilbert, 2011). Supporting this idea Rpl38 and importantly Rpl40 were found to be involved in translation of only a subset of mRNAs in vertebrate tissue and *S. cerevisiae*, respectively (Kondrashov et al, 2011; Lee et al, 2013). The current hypothesis regarding mRNA transport in *U. maydis* is that a subset of mRNAs is translated on endosomes (see section 2.3). Therefore one could think of specialised ribosomes translating those moving mRNAs.

Considering the transport of ubiquitin mRNA one could hypothesise a role in local endocytosis at hyphal tips. Supportive for enhanced endocytosis at hyphal tips is the predominant localisation of the Epsin-like protein Ent1 in an actin patch-like pattern at growth cones (J. König and M. Feldbrügge, unpublished). Internalisation of protein cargo has been shown to depend on monoubiquitination. Epsins and the ESCRT-0 component Hrs/Vps27 bind to monoubiquitin and sort cargo into the endocytic pathway (Rusten et al, 2012; Shih et al, 2002). Since endocytosis is crucial for polar growth in fungal hyphae (Penalva, 2010) *ubi1* is well suited candidate for future research on mRNA transport and polar growth.

*Interplay of molecular motors*

In different model systems the contribution of dynein and kinesins in MT-dependent mRNA transport were reported. Bi-directional transport as reported for *Drosophila* and neurons can be explained by the action of a single motor along antiparallel or weakly polarized MTs or by two or more motors with opposite polarity

along parallel and highly polarized MTs (Doyle & Kiebler, 2011; Singer, 2008). In *Xenopus* oocytes the localization of RNAs to the vegetal cortex underlies a combination of kinesin-1 and kinesin-2 that is supposed to happen along a subpopulation of MTs with plus ends facing to the vegetal cortex. This subpopulation is surrounded by MTs with mixed polarity (Messitt et al, 2008). In *Drosophila* oocytes *oskar* mRNA moves kinesin-dependent bidirectionally along a weakly polarised MT-cytoskeleton with a slight bias, so that *oskar* accumulates at the posterior. Dynein mutants have no effect on *oskar* movement (Zimyanin et al, 2008). A similar biased movement has been proposed for *Drosophila* embryos. Here the localization of specific transcripts to MT minus-ends is mediated by dynein and opposed by a yet unknown motor (Bullock et al, 2006).

So far *U. maydis* is the only model organism that explains bidirectional mRNA transport with both, a minus and a plus-end directed motor. Kinesin-3 is present on almost all Rrm4-positive endosomes and *vice versa* regardless of which direction, suggesting an exclusive role in Rrm4-positive endosome trafficking. Furthermore Kin-3 appears to be directly recycled without falling off endosomes. On the contrary, dynein shows a different localization. It forms a reservoir at MT plus ends and the absence from anterogradely moving Rrm4-positive endosome suggests a different recycling route. Indeed, in *Caenorhabditis elegans* conventianl kinesin interacts via the adaptor protein UNC-16 with dynein and transports dynein to MT plus ends (Arimoto et al, 2011).

That dynein mediates retrograde transport in *U. maydis* is based on three observations. (i) Rrm4 is present predominantly on retrogradely moving dynein (ii) Without dynein function Rrm4 and Pab1 accumulate at the poles of bipolarly growing hyphae where MT plus-ends are located. (iii) Additionally if we raise temperature in *dyn2$^{ts}$/rrm4G* while observing cells microscopically we can detect anterograde movement but no reversal to retrograde movement. In a recently proposed model, dynein only mediates initial retrograde movement of Rab5a-positive endosomes in pole regions that contain polarised MTs and in subapical regions with antiparallel MTs, Kin-3 takes over similar to a relay race to mediate long range retrograde transport (Schuster et al, 2011c). The authors claim that in *dyn2$^{ts}$* retrograde movement still occurs at restrictive temperature, although dynein is inactive. This is explained by the action of Kin-3, but it needs to be shown, that dynein function is indeed completely abolished under these conditions, e.g. with a temperature sensitive *dyn2* allele fused to *gfp*. Moreover, they show that at the pole where MTs are polarised no movement of endosomes is detectable under restrictive conditions in *dyn2$^{ts}$*. However, it has to be

taken into account, that MTs are shortened under these conditions (Steinberg, 2012). Therefore some questions remain open and the exact involvement of dynein in retrograde transport of Rrm4/Rab5a-postitve endosomes needs to be readdressed.

*Co-transport of mRNPs and endosomes*

The most interesting finding of this study is the co-transport of mRNA with endosomes. This was unexpected, because these endosomes were thought to be involved in endocytosis (Steinberg, 2007b). Co-transport with membraneous structure appears to emerge as a common theme in mRNA transport. For example in *S. cerevisiae* the co-transport of mRNAs and the ER was observed (Schmid et al, 2006). And in *Drosophila* oocytes the ESCRT-II complex and Rab11 are involved in mRNA trafficking (Irion & St Johnston, 2007; Cohen, 2005). On the other hand in the *Drosophila* syncytial blastoderm embryo mRNA transport appears to be independent of vesicular structures, since the RNA-binding protein Egl binds directly to the C-terminal domain of BicD which links Egl and mRNA to to dynein (Dienstbier et al, 2009). Interestingly, the C-terminal domain of BicD interacts also with Rab6 and is implicated in endosomal trafficking in the *Drosophila* nervous system (Li et al, 2010). Likewise in mouse brain, kinesin heavy chain (KIF5) seems to interact with RNA-binding proteins and associated mRNAs independently of vesicles (Kanai et al, 2004) and kinesin light chain interacts directly with the RNA-binding protein FMRP (Dictenberg et al, 2008). Since in hippocampal neurons it was shown that different species of mRNAs are co-transported in the the same mRNPs (Doyle & Kiebler, 2011), it would be of great value to identify the stoichiometry of mRNAs, RNA-binding proteins and associated motors. In order to transport a whole set of mRNAs, hitchhiking on endosomes would constitute an elegant mechanism to increase the surface of mRNA transport units in order to transport several mRNAs simultaneously.

*Additional factors involved in mRNA transport*

The most interesting questions for the future to be adressed are, (i) how is Rrm4 coupled to endosomes? (ii) Which additional factors are associated with Rrm4 and its target mRNAs that might act as specificity factors for recruitment of mRNAs or function in translational regulation? The prime candidate protein Pam1 could be involved in either process. The subcellular localisation of Pam1 seems to be 100% identical with Rrm4 and also both deletion phenotypes are congruent with each other (S. Baumann &

M. Feldbrügge, unpublished). Deletion of Pam1 does not alter Rrm4 localisation drastically, but abolishes completely Pab1 shuttling indicating that mRNA-binding by Rrm4 is lost. Conversely, interfering with Rrm4 shuttling also affects Pam1 shuttling. If the MLLE domain of Rrm4 is mutated, Rrm4 shuttling is stopped and it accumulates in few static cytoplasmic particles in which also Pam1 is found, suggesting both proteins still interact directly or indirectly. Indeed if RNA-binding of Rrm4 is inhibited by deletion of the RNA recognition motifs, co-localisation of Rrm4 and Pam1 is lost, pointing towards an indirect interaction through mRNA. The mutated Rrm4 still shuttles along MTs but Pam1 does not, rather it shows Brownian motion in the cytoplasm (S. Baumann & M. Feldbrügge, unpublished). Importantly deletion of Pam1 also abolishes endosomal localisation of Cdc3, strongly supporting the model of local translation at endosomes (S. Baumann & M. Feldbrügge, unpublished). These results make Pam1 the next exciting candidate protein for studying mRNA transport and local translation in *U. maydis*.

*Shuttling of cdc3 mRNA and encoded protein*

Why do mRNAs shuttle in hyphae of *U. maydis* rather than being deposited somewhere in the cell? A potential explanation for shuttling mRNAs in neurons was recently published (Doyle & Kiebler, 2011). The authors propose a model in which mRNAs move in a circuit like sushi on a sushi-belt. "Hungry" synapses that demand a certain mRNA can take those at any time. In *U. maydis* we found that the encoded protein shuttles together with its cognate mRNA (Fig. 3-1), therefore the sushi-belt model could be extended in this respect. Not the mRNA is delivered, but the encoded protein instead. This seemingly complicated mode of transport might have several advantages. (i) mRNAs that are just deposited at hyphal tips would spread to fast within the cytoplasm because of rapid diffusion. The diffusion constant of freely diffusing cytoplasmic proteins (Gfp 27 kDa) was estimated to be 20 $\mu m^2$ / s. Since diffusion only weakly depends on the molecular mass (Sprague & McNally, 2005) *cdc3* mRNA (ca. 440 kDa) would take only few seconds to distribute in the whole cytoplasm of *U. maydis*. (ii) Therefore diffusion of mRNAs would have to be restricted via anchoring. This mechanism might be unsuitable for *U. maydis* especially for septin mRNAs, because of a fast and constant remodelling of the complete hypha. (iii) In fact, this fast and constant remodelling could require the transport of protein rather than the transcript. Via fission and fusion of endosomes, just a few transported mRNAs could supply a

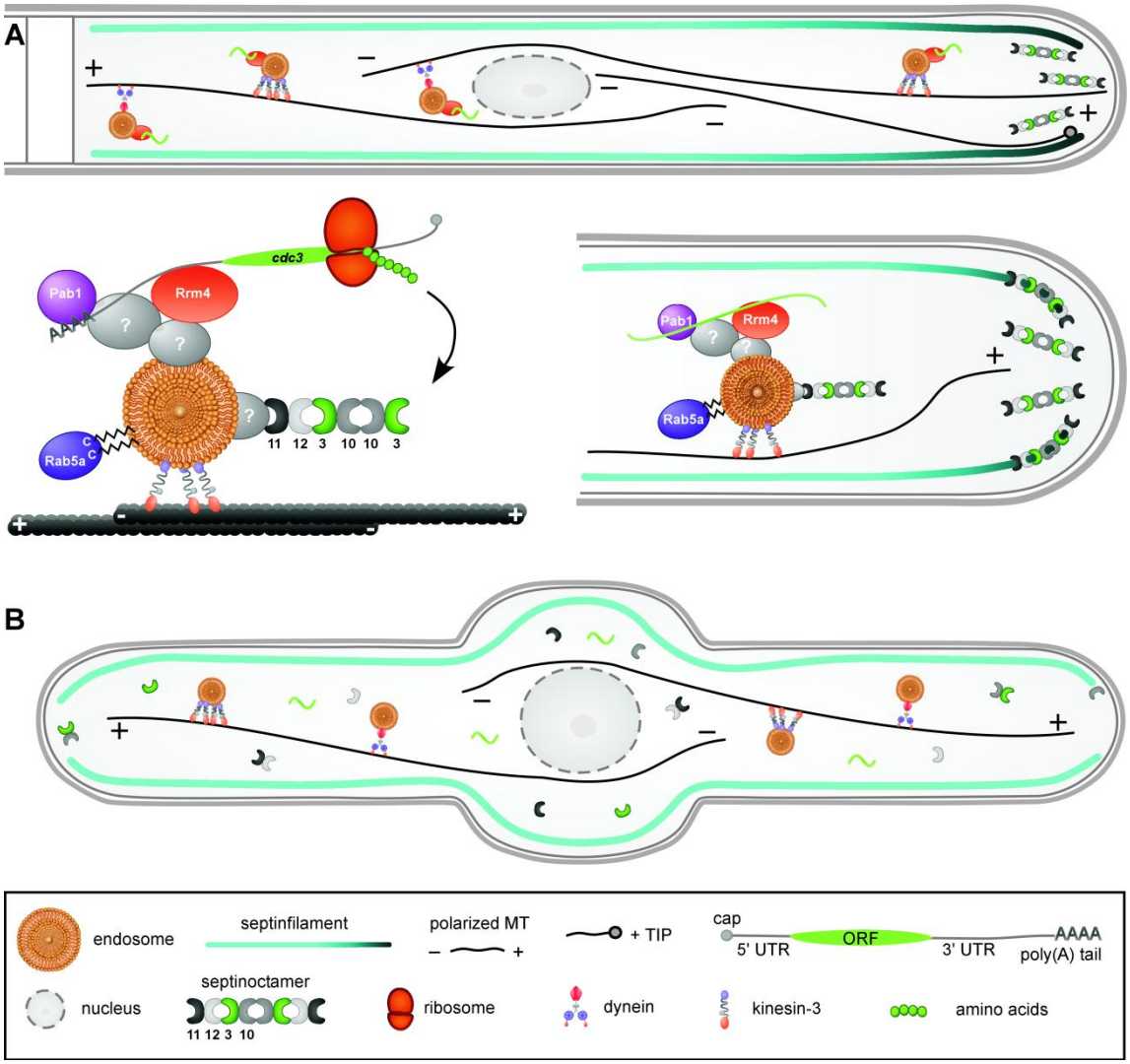


**Fig. 3-1** Endosome-coupled translation mediates preassembly of septin octamers. **(A)** Local translation of septin mRNAs on endosomes is crucial for efficient assembly of septin octamers into septinfilaments at hyphal growth cones of *wt* strains. Rrm4 transports mRNAs via hitchhiking on endosomes (top). During transport septin mRNAs are translated to co-translationally preassemble septinoctamers (bottom left). Loaded endosomes deliver septin octamers to growth cones of *wt* hyphae and ensure proper assembly at tips of septinfilaments (bottom right). Septinfilaments guide MT plus ends at the apex and promote MT polymerization (top). **(B)** In *rrm4* deletion strains endosomes cannot be loaded with septin mRNA and protein. Thus, septinoctamers are not preassembled leading to a dispersed localization of septin-monomers and dimers which hinders septinfilament assembly.

large number of endosomes with protein. Since hyphae undergo remodelling over their total length it suggests, that not only the septin filaments at the growth cone are in need of septin subunits but also subapical parts of the cell, although probably to a lesser extent. Therefore shuttling of the protein might serve all parts of hyphae depending on the growth phase. Supporting this idea is the observation of hyphae expressing a fusionprotein of Cdc3 and Gfp over several hours. Hyphae do not grow continuously but stop tip expansion while inserting a septum. Delay in tip growth correlates with the presence of Cdc3 at septa and transient disappearance of strong Cdc3 tip localization (S.

Baumann & M. Feldbrügge, unpublished) (iv) Given that a single septin mRNA is transported and locally translated at endosomes it is tempting to speculate that the other three septin mRNAs share the same fate. Since septin higher-order structures are composed of septin octamers, the co-translation of all four septins at endosomes would be an elegant way to bring the septins in a physically restricted environment. This might aid the efficient preassembly of protofilaments (octamers) that are subsequently delivered to and assembled with growing septin filaments (Fig. 3-1), rather than having all subunits mixed in the cytoplasm. First indications for such a mechanism derive from deletion studies of individual septin genes. If the genes for septins Cdc10, 11 or 12 are deleted, the localisation of Cdc3 at endosomes is drastically reduced or completely abolished. Likewise the formation of septin filaments is disturbed. Only short or no filaments are detectable (S. Baumann & M. Feldbrügge, unpublished). Future studies should aim to investigate a potential co-transport of all septin mRNAs and proteins via endosomes. At least on the protein level we were able to confirm a localisation for Cdc10 and Cdc12 on endosomes (S. Baumann & M. Feldbrügge, unpublished). Co-localisation studies should reveal a potential co-transport of different septin proteins. The detection of co-transported mRNAs under endogenous conditions makes the establishment of a second RNA live imaging system like the MS2 system mandatory (Beach et al, 1999; Bertrand et al, 1998; Lange et al, 2008). In yeast there is evidence for co-transport of *ASH1* and *IST2* mRNAs and in hippocampal neurons three different injected RNAs *αCaMKII*, *NG* and *ARC*, all containing the response element for hnRNP A2, are co-delivered into dendrites (Gao et al, 2008). In contrast to these results two studies show that in dendrites of hippocampal neurons, that *αCaMKII*, *MAP2*, *β-actin* and *Septin7* RNAs are differentially sorted into distinct particles (Mikl et al, 2011; Tubing et al, 2010). The co-transport of septin mRNAs would be the first example of the coordination of mRNAs whose encoded proteins are members of the same super-structure. This is in agreement with a previous hypothesis which proposes a so called mRNA regulon in which functionally related mRNAs are coordinately regulated including the posttranscritptional processing and cytoplasmic transport as well as preassembly of the encoded proteins (Keene, 2007).

*Septin filaments as diffusion barriers and scaffold*

One function of septin filaments might be the generation of certain membrane domains at the hyphal tip as earlier proposed. Septins could act together with sphingolipids and membrane rigidifying ergosterol to form diffusion barriers that restrict certain polarity factors to the growth cone (Lichius et al, 2011). Supporting this assumption is the observation that in *U. maydis* filipin stainable SRDs localize to hyphal tips (Canovas & Perez-Martin, 2009). Importantly, the polarisome scaffold protein Spa2 localise to hyphal tips, too (Carbo & Perez-Martin, 2008). It would be exciting to investigate further components of the polarisome as for example the homologue of the formin Bni1 and further the interdepence of tip localization of septins, SRDs and polarisome components. Alternatively or additionally septin filaments could directly interact with polarity factors serving as a scaffold (Estey et al, 2011). Since septins have a role in secretion in polarized neuronal cells, it is hypothesized that septins additionally could guide and direct exocytic vesicles to rapidly growing tips (Gladtfelter, 2006).

*Interaction of septinfilaments with actin/MT cytoskeleton*

In mammalian epithelial cells septins were found to inhibit MT depolymerisation and to constitute a railroad network for MT plus ends to grow along. This suggests that septins promote growth and control directionality of MTs (Bowen et al, 2011). Therefore it was speculated that molecular motors might interact with MT plus ends and mediate septin–MT interations (Bowen et al., 2011). Interestingly, in *U. maydis* the MTs at hyphal growth cones proceed cortically where septin filaments are located, indicating a similar connection of septins and MTs (S. Baumann & M. Feldbrügge, unpublished). Recently it was shown, that actin integrity is a prerequisite for stability of septin filaments in *U. maydis* (Böhmer et al, 2009). Taken together this would probably establish a role for septins as a bridge between the actin and microtubule cytoskeleton. Actin is needed for septin filament integrity and septin filaments in turn for MT stabilization (Fig. 3-1A). It would also be possible that all three cytoskeleton components influence each others stability/integrity interdependently, but at least MTs seem not to be important for septin integrity since septins are still formed when hyphae are treated with benomyl. Additionally FRAP experiments on Cdc3Gn in *rrm4* deletion strains show no difference in recovery at hyphal tips with or without benomyl treatment,

indicating no influence of MTs on septin dynamics (S. Baumann & M. Feldbrügge, unpublished).

*Conclusion*

Generally it is accepted that active mRNA transport via molecular motors leads to the subcellular accumulation of mRNAs. During transport translation is repressed and upon arrival at destination sites repression is released (Meignin & Davis, 2010; Holt & Bullock, 2010). We discovered endosome-coupled translation of septin mRNA during transport, which loads endosomes with septin protein for efficient delivery to hyphal growth cones. This novel mechanism might also apply to other septin mRNAs. Therefore endosomes could act as a platform to join septin monomers co-translationally and provides the required space for preassembly of building blocks. This highly coordinated mechanism targets the cargo to the correct subcellular site, supporting rapid and efficient polymerization of septin filaments at growth cones.

# 4 Supplemental Material

## 4.1 Movie CD

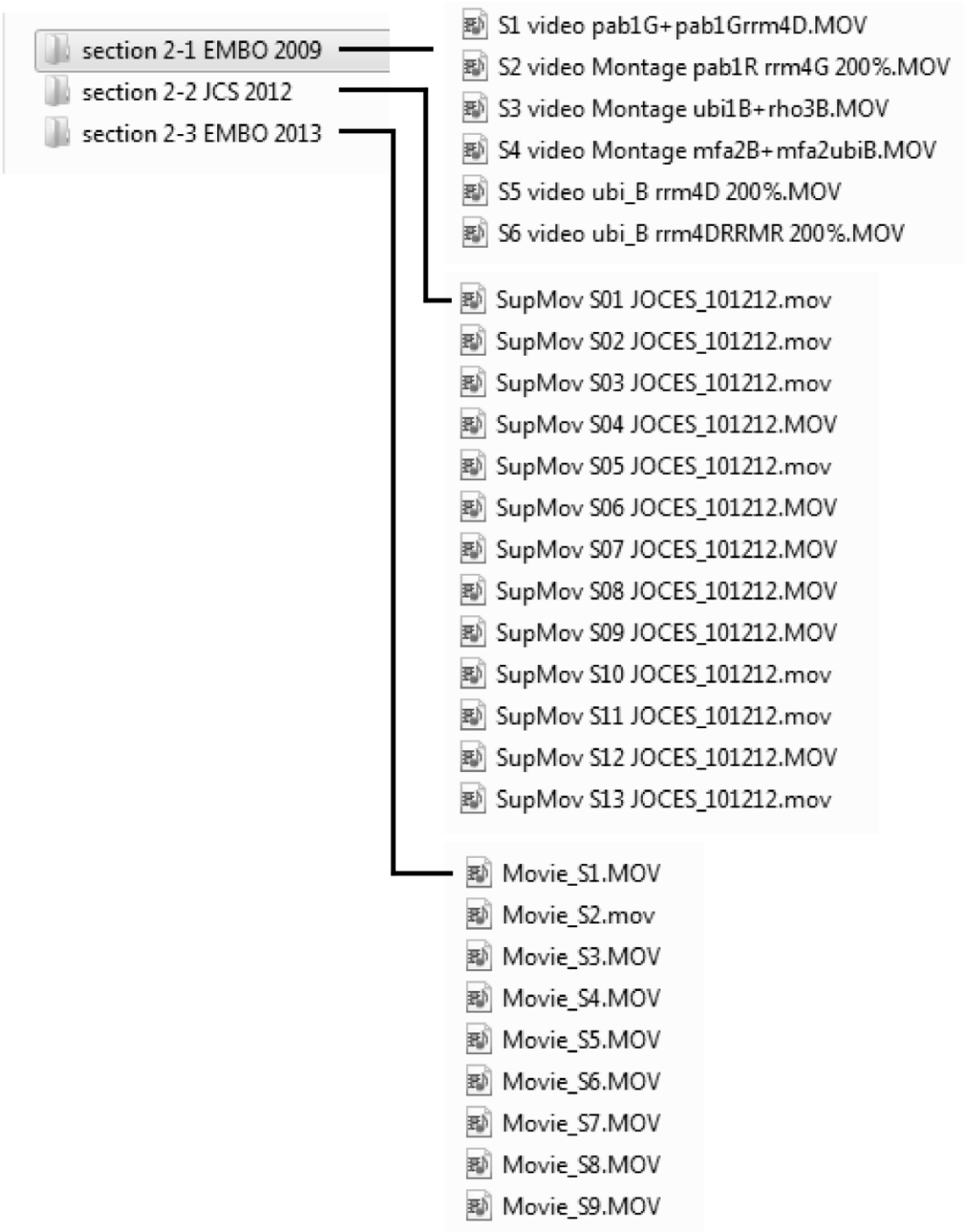

# 5 References

Alvarez-Tabares I, Perez-Martin J (2010) Septins from the phytopathogenic fungus *Ustilago maydis* are required for proper morphogenesis but dispensable for virulence. *PloS one* **5:** e12933

Amrute-Nayak M, Bullock SL (2012) Single-molecule assays reveal that RNA localization signals regulate dynein-dynactin copy number on individual transcript cargoes. *Nat Cell Biol* **14:** 416-423

Andken BB, Lim I, Benson G, Vincent JJ, Ferenc MT, Heinrich B, Jarzylo LA, Man HY, Deshler JO (2007) 3'-UTR SIRF: a database for identifying clusters of short interspersed repeats in 3' untranslated regions. *BMC Bioinform* **8:** 274-287

Arimoto M, Koushika SP, Choudhary BC, Li C, Matsumoto K, Hisamoto N (2011) The Caenorhabditis elegans JIP3 protein UNC-16 functions as an adaptor to link kinesin-1 with cytoplasmic dynein. *The Journal of neuroscience : the official journal of the Society for Neuroscience* **31:** 2216-2224

Aronov S, Gelin-Licht R, Zipor G, Haim L, Safran E, Gerst JE (2007) mRNAs encoding polarity and exocytosis factors are co-transported with cortical ER to the incipient bud in yeast. *Mol Cell Biol* **27:** 3441-3455

Austin RJ, Xia T, Ren J, Takahashi TT, Roberts RW (2002) Designed arginine-rich RNA-binding peptides with picomolar affinity. *J Am Chem Soc* **124:** 10966-10967

Bailey TL, Williams N, Misleh C, Li WW (2006) MEME: discovering and analyzing DNA and protein sequence motifs. *Nucleic Acids Res* **34:** W369-373

Banuett F, Herskowitz I (1989) Different *a* alleles of *Ustilago maydis* are necessary for maintenance of filamentous growth but not for meiosis. *Proc Natl Acad Sci USA* **86:** 5878-5882

Barral Y (2010) Cell biology. Septins at the nexus. *Science* **329:** 1289-1290

Barral Y, Kinoshita M (2008) Structural insights shed light onto septin assemblies and function. *Curr Opin Cell Biol* **20:** 12-18

Bastock R, St Johnston D (2008) Drosophila oogenesis. *Current biology : CB* **18:** R1082-1087

Basyuk E, Galli T, Mougel M, Blanchard JM, Sitbon M, Bertrand E (2003) Retroviral genomic RNAs are transported to the plasma membrane by endosomal vesicles. *Dev Cell* **5:** 161-174

Baumann S, Pohlmann T, Jungbluth M, Brachmann A, Feldbrügge M (2012) Kinesin-3 and dynein mediate microtubule-dependent co-transport of mRNPs and endosomes. *J Cell Sci* **125:** 2740-2752 E.A., Du bist das Beste was mir je passiert ist!

Beach DL, Salmon ED, Bloom K (1999) Localization and anchoring of mRNA in budding yeast. *Curr Biol* **9:** 569-578

Becht P, König J, Feldbrügge M (2006) The RNA-binding protein Rrm4 is essential for polarity in *Ustilago maydis* and shuttles along microtubules. *J Cell Sci* **119:** 4964-4973

Becht P, Vollmeister E, Feldbrügge M (2005) Role for RNA-binding proteins implicated in pathogenic development of *Ustilago maydis*. *Euk Cell* **4:** 121-133

Beites CL, Xie H, Bowser R, Trimble WS (1999) The septin CDCrel-1 binds syntaxin and inhibits exocytosis. *Nature neuroscience* **2:** 434-439

Bertin A, McMurray MA, Grob P, Park SS, Garcia G, 3rd, Patanwala I, Ng HL, Alber T, Thorner J, Nogales E (2008) Saccharomyces cerevisiae septins: supramolecular organization of heterooligomers and the mechanism of filament assembly. *Proceedings of the National Academy of Sciences of the United States of America* **105:** 8274-8279

Bertrand E, Chartrand P, Schaefer M, Shenoy SM, Singer RH, Long RM (1998) Localization of *ASH1* mRNA particles in living yeast. *Mol Cell* **2:** 437-445

Bi E, Park HO (2012) Cell polarization and cytokinesis in budding yeast. *Genetics* **191:** 347-387

Böhl F, Kruse C, Frank A, Ferring D, Jansen RP (2000) She2p, a novel RNA-binding protein tethers *ASH1* mRNA to the Myo4p myosin motor via She3p. *EMBO J* **19:** 5514-5524

Böhmer C, Böhmer M, Bölker M, Sandrock B (2008) Cdc42 and the Ste20-like kinase Don3 act independently in triggering cytokinesis in *Ustilago maydis*. *J Cell Sci* **121:** 143-148

Böhmer C, Ripp C, Bölker M (2009) The germinal centre kinase Don3 triggers the dynamic rearrangement of higher-order septin structures during cytokinesis in *Ustilago maydis*. *Mol Microbiol* **74:** 1484-1496

Böhmer M, Colby T, Böhmer C, Brautigam A, Schmidt J, Bölker M (2007) Proteomic analysis of dimorphic transition in the phytopathogenic fungus *Ustilago maydis*. *Proteomics* **7:** 675-685

Bölker M, Urban M, Kahmann R (1992) The *a* mating type locus of *U. maydis* specifies cell signaling components. *Cell* **68:** 441-450

Bowen JR, Hwang D, Bai X, Roy D, Spiliotis ET (2011) Septin GTPases spatially guide microtubule organization and plus end dynamics in polarizing epithelia. *The Journal of cell biology* **194:** 187-197

Boyce KJ, Chang H, D'Souza CA, Kronstad JW (2005) An *Ustilago maydis* septin is required for filamentous growth in culture and for full symptom development on maize. *Eukaryot Cell* **4:** 2044-2056

Brachmann A, König J, Julius C, Feldbrügge M (2004) A reverse genetic approach for generating gene replacement mutants in *Ustilago maydis*. *Mol Gen Genom* **272:** 216-226

Brachmann A, Weinzierl G, Kämper J, Kahmann R (2001) Identification of genes in the bW/bE regulatory cascade in *Ustilago maydis*. *Mol Microbiol* **42:** 1047-1063

Brand A, Gow NA (2009) Mechanisms of hypha orientation of fungi. *Current opinion in microbiology* **12:** 350-357

Brefort T, Doehlemann G, Mendoza-Mendoza A, Reissmann S, Djamei A, Kahmann R (2009) *Ustilago maydis* as a Pathogen. *Annu Rev Phytopathol* **47:** 423-445

Bullock SL (2007) Translocation of mRNAs by molecular motors: Think complex? *Semin Cell Dev Biol* **18:** 194-201

Bullock SL (2011) Messengers, motors and mysteries: sorting of eukaryotic mRNAs by cytoskeletal transport. *Biochem Soc Trans* **39:** 1161-1165

Bullock SL, Nicol A, Gross SP, Zicha D (2006) Guidance of bidirectional motor complexes by mRNA cargoes through control of dynein number and activity. *Curr Biol* **16:** 1447-1452

Bullock SL, Ringel I, Ish-Horowicz D, Lukavsky PJ (2010) A'-form RNA helices are required for cytoplasmic mRNA transport in *Drosophila*. *Nat Struct Mol Biol* **17:** 703-709

Bullock SL, Zicha D, Ish-Horowicz D (2003) The *Drosophila hairy* RNA localization signal modulates the kinetics of cytoplasmic mRNA transport. *EMBO J* **22:** 2484-2494

Campbell RE, Tour O, Palmer AE, Steinbach PA, Baird GS, Zacharias DA, Tsien RY (2002) A monomeric red fluorescent protein. *Proc Natl Acad Sci U S A* **99:** 7877-7882

Canovas D, Perez-Martin J (2009) Sphingolipid biosynthesis is required for polar growth in the dimorphic phytopathogen *Ustilago maydis*. *Fungal Genet Biol* **46:** 190-200

Carbo N, Perez-Martin J (2008) Spa2 is required for morphogenesis but it is dispensable for pathogenicity in the phytopathogenic fungus *Ustilago maydis*. *Fungal Genet Biol* **45:** 1315-1327

Caviston JP, Longtine M, Pringle JR, Bi E (2003) The role of Cdc42p GTPase-activating proteins in assembly of the septin ring in yeast. *Mol Biol Cell* **14:** 4051-4066

Clague MJ, Liu H, Urbe S (2012) Governance of endocytic trafficking and signaling by reversible ubiquitylation. *Developmental cell* **23:** 457-467

Cohen RS (2005) The role of membranes and membrane trafficking in RNA localization. *Biol Cell* **97:** 5-18

Collinge AJ, Trinci AP (1974) Hyphal tips of wild-type and spreading colonial mutants of Neurospora crassa. *Archives of microbiology* **99:** 353-368

Crampin H, Finley K, Gerami-Nejad M, Court H, Gale C, Berman J, Sudbery P (2005) Candida albicans hyphae have a Spitzenkorper that is distinct from the polarisome found in yeast and pseudohyphae. *Journal of cell science* **118:** 2935-2947

Crooks GE, Hon G, Chandonia JM, Brenner SE (2004) WebLogo: a sequence logo generator. *Genome Res* **14:** 1188-1190

Czaplinski K, Singer RH (2006) Pathways for mRNA localization in the cytoplasm. *Trends Biochem Sci* **31:** 687-693

Daigle N, Ellenberg J (2007) LambdaN-GFP: an RNA reporter system for live-cell imaging. *Nat Methods* **4:** 633-636

Delanoue R, Davis I (2005) Dynein anchors its mRNA cargo after apical transport in the *Drosophila* blastoderm embryo. *Cell* **122:** 97-106

Delanoue R, Herpers B, Soetaert J, Davis I, Rabouille C (2007) *Drosophila* Squid/hnRNP helps Dynein switch from a *gurken* mRNA transport motor to an ultrastructural static anchor in sponge bodies. *Dev Cell* **13:** 523-538

DeMay BS, Bai X, Howard L, Occhipinti P, Meseroll RA, Spiliotis ET, Oldenbourg R, Gladfelter AS (2011) Septin filaments exhibit a dynamic, paired organization that is conserved from yeast to mammals. *J Cell Biol* **193:** 1065-1081

Deng Y, Singer RH, Gu W (2008) Translation of ASH1 mRNA is repressed by Puf6p-Fun12p/eIF5B interaction and released by CK2 phosphorylation. *Genes & development* **22:** 1037-1050

Dictenberg JB, Swanger SA, Antar LN, Singer RH, Bassell GJ (2008) A direct role for FMRP in activity-dependent dendritic mRNA transport links filopodial-spine morphogenesis to fragile X syndrome. *Dev Cell* **14:** 926-939

Dienstbier M, Boehl F, Li X, Bullock SL (2009) Egalitarian is a selective RNA-binding protein linking mRNA localization signals to the dynein motor. *Genes Dev* **23:** 1546-1558

Dienstbier M, Li X (2009) Bicaudal-D and its role in cargo sorting by microtubule-based motors. *Biochem Soc Trans* **37:** 1066-1071

Dobbelaere J, Gentry MS, Hallberg RL, Barral Y (2003) Phosphorylation-dependent regulation of septin dynamics during the cell cycle. *Dev Cell* **4:** 345-357

Dollar G, Struckhoff E, Michaud J, Cohen RS (2002) Rab11 polarization of the *Drosophila* oocyte: a novel link between membrane trafficking, microtubule organization, and oskar mRNA localization and translation. *Development* **129:** 517-526

Dong Y, Pruyne D, Bretscher A (2003) Formin-dependent actin assembly is regulated by distinct modes of Rho signaling in yeast. *J Cell Biol* **161:** 1081-1092

Doyle M, Kiebler MA (2011) Mechanisms of dendritic mRNA transport and its role in synaptic tagging. *EMBO J* **30:** 3540-3552

Egan MJ, McClintock MA, Reck-Peterson SL (2012) Microtubule-based transport in filamentous fungi. *Current opinion in microbiology* **15:** 637-645

Estey MP, Kim MS, Trimble WS (2011) Septins. *Current biology : CB* **21:** R384-387

Evan GI, Lewis GK, Ramsay G, Bishop JM (1985) Isolation of monoclonal antibodies specific for human c-myc proto-oncogene product. *Mol Cell Biol* **5:** 3610-3616

Evangelista M, Zigmond S, Boone C (2003) Formins: signaling effectors for assembly and polarization of actin filaments. *Journal of cell science* **116:** 2603-2611

Farkasovsky M, Herter P, Voss B, Wittinghofer A (2005) Nucleotide binding and filament assembly of recombinant yeast septin complexes. *Biological chemistry* **386:** 643-656

Feldbrügge M, Bölker M, Steinberg G, Kämper J, Kahmann R (2006) Regulatory and structural netwoks orchestrating mating, dimorphism, cell shape, and pathogenesis in *Ustilago maydis*. In *The Mycota I*, Kües U, Fischer R (eds), pp 375-391. Berlin Heidelberg: Springer-Verlag

Feldbrügge M, Zarnack K, Vollmeister E, Baumann S, Koepke J, König J, Münsterkötter M, Mannhaupt G (2008) The posttranscriptional machinery of *Ustilago maydis*. *Fungal Genet Biol* **45:** S40-S46

Field CM, al-Awar O, Rosenblatt J, Wong ML, Alberts B, Mitchison TJ (1996) A purified Drosophila septin complex forms filaments and exhibits GTPase activity. *The Journal of cell biology* **133:** 605-616

Fink G, Steinberg G (2006) Dynein-dependent motility of microtubules and nucleation sites supports polarization of the tubulin array in the fungus *Ustilago maydis*. *Mol Biol Cell* **17:** 3242-3253

Fischer R (2007) The cytoskeleton and polarized growth of filamentous fungi. In *The Mycota VIII*, Howard RJ, Gow NAR (eds), pp 121-135. Berlin Heidelberg: Springer-Verlag

Fischer R, Zekert N, Takeshita N (2008) Polarized growth in fungi - interplay between the cytoskeleton, positional markers and membrane domains. *Mol Microbiol* **68:** 813-826

Frazier JA, Wong ML, Longtine MS, Pringle JR, Mann M, Mitchison TJ, Field C (1998) Polymerization of purified yeast septins: evidence that organized filament arrays may not be required for septin function. *The Journal of cell biology* **143:** 737-749

Fuchs U, Hause G, Schuchardt I, Steinberg G (2006) Endocytosis is essential for pathogenic development in the corn smut fungus *Ustilago maydis*. *Plant Cell* **18:** 2066-2081

Fuchs U, Manns I, Steinberg G (2005) Microtubules are dispensable for the initial pathogenic development but required for long-distance hyphal growth in the corn smut fungus *Ustilago maydis*. *Mol Biol Cell* **16:** 2746-2758

Fundakowski J, Hermesh O, Jansen RP (2012) Localization of a Subset of Yeast mRNAs Depends on Inheritance of Endoplasmic Reticulum. *Traffic* **13:** 1642-1652

Fusco D, Accornero N, Lavoie B, Shenoy SM, Blanchard JM, Singer RH, Bertrand E (2003) Single mRNA molecules demonstrate probabilistic movement in living mammalian cells. *Curr Biol* **13:** 161-167

Gao Y, Tatavarty V, Korza G, Levin MK, Carson JH (2008) Multiplexed dendritic targeting of alpha calcium calmodulin-dependent protein kinase II, neurogranin, and activity-regulated cytoskeleton-associated protein RNAs by the A2 pathway. *Molecular biology of the cell* **19:** 2311-2327

Gennerich A, Vale RD (2009) Walking the walk: how kinesin and dynein coordinate their steps. *Curr Opin Cell Biol* **21:** 59-67

Gerst JE (2008) Message on the web: mRNA and ER co-trafficking. *Trends Cell Biol* **18:** 68-76

Gilbert WV (2011) Functional specialization of ribosomes? *Trends in biochemical sciences* **36:** 127-132

Gladfelter AS (2006) Control of filamentous fungal cell shape by septins and formins. *Nat Rev Microbiol* **4:** 223-229

Gladfelter AS (2010) Guides to the final frontier of the cytoskeleton: septins in filamentous fungi. *Curr Opin Microbiol* **13:** 720-726

Göhre V, Vollmeister E, Bölker M, Feldbrügge M (2012) Microtubule-dependent membrane dynamics of *Ustilago maydis*: trafficking and function of Rab5a-positive endosomes. *Comm Integra Biol* **5:** 482-487

Gould GW, Lippincott-Schwartz J (2009) New roles for endosomes: from vesicular carriers to multi-purpose platforms. *Nat Rev Mol Cell Biol* **10:** 287-292

Guil S, Cáceres JF (2007) The multifunctional RNA-binding protein hnRNP A1 is required for processing of miR-18a. *Nat Struct Mol Biol* **14:** 591-596

Guo W, Tamanoi F, Novick P (2001) Spatial regulation of the exocyst complex by Rho1 GTPase. *Nat Cell Biol* **3:** 353-360

Haim L, Zipor G, Aronov S, Gerst JE (2007) A genomic integration method to visualize localization of endogenous mRNAs in living yeast. *Nat Methods* **4:** 409-412

Hamada S, Ishiyama K, Choi SB, Wang C, Singh S, Kawai N, Franceschi VR, Okita TW (2003) The transport of prolamine RNAs to prolamine protein bodies in living rice endosperm cells. *Plant Cell* **15:** 2253-2264

Harris SD (2006) Cell polarity in filamentous fungi: shaping the mold. *Int Rev Cytol* **251:** 41-77

Harris SD, Read ND, Roberson RW, Shaw B, Seiler S, Plamann M, Momany M (2005) Polarisome meets spitzenkörper: microscopy, genetics, and genomics converge. *Euk Cell* **4:** 225-229

Heimel K, Scherer M, Vranes M, Wahl R, Pothiratana C, Schuler D, Vincon V, Finkernagel F, Flor-Parra I, Kämper J (2010) The transcription factor Rbf1 is the master regulator for b-mating type controlled pathogenic development in *Ustilago maydis*. *PLoS Pathog* **6:** e1001035

Hernandez-Rodriguez Y, Hastings S, Momany M (2012) The septin AspB in *Aspergillus nidulans* forms bars and filaments and plays roles in growth emergence and conidiation. *Eukaryotic cell* **11:** 311-323

Heym RG, Niessing D (2011) Principles of mRNA transport in yeast. *Cell Mol Life Sci*

Hogan DJ, Riordan DP, Gerber AP, Herschlag D, Brown PO (2008) Diverse RNA-binding proteins interact with functionally related sets of RNAs, suggesting an extensive regulatory system. *PLoS Biol* **6:** e255

Holt CE, Bullock SL (2009) Subcellular mRNA localization in animal cells and why it matters. *Science* **326:** 1212-1216

Hui J, Hung LH, Heiner M, Schreiner S, Neumüller N, Reither G, Haas SA, Bindereif A (2005) Intronic CA-repeat and CA-rich elements: a new class of regulators of mammalian alternative splicing. *EMBO J* **24:** 1988-1998

Huotari J, Helenius A (2011) Endosome maturation. *EMBO J* **30:** 3481-3500

Iden S, Collard JG (2008) Crosstalk between small GTPases and polarity proteins in cell polarization. *Nature reviews Molecular cell biology* **9:** 846-859

Irion U, St Johnston D (2007) *bicoid* RNA localization requires specific binding of an endosomal sorting complex. *Nature* **445:** 554-558

Jambhekar A, Derisi JL (2007) Cis-acting determinants of asymmetric, cytoplasmic RNA transport. *RNA* **13:** 625-642

Jansen RP (2001) mRNA localization: message on the move. *Nat Rev Mol Cell Biol* **2:** 247-256

Jansen RP, Niessing D (2012) Assembly of mRNA-protein complexes for directional mRNA transport in eukaryotes--an overview. *Current protein & peptide science* **13:** 284-293

Januschke J, Gervais L, Dass S, Kaltschmidt JA, Lopez-Schier H, St Johnston D, Brand AH, Roth S, Guichet A (2002) Polar transport in the *Drosophila* oocyte requires Dynein and Kinesin I cooperation. *Curr Biol* **12:** 1971-1981

Jenny A, Hachet O, Zavorszky P, Cyrklaff A, Weston MD, Johnston DS, Erdelyi M, Ephrussi A (2006) A translation-independent role of oskar RNA in early *Drosophila* oogenesis. *Development* **133:** 2827-2833

Jung H, Yoon BC, Holt CE (2012) Axonal mRNA localization and local protein synthesis in nervous system assembly, maintenance and repair. *Nature reviews Neuroscience* **13:** 308-324

Kämper J (2004) A PCR-based system for highly efficient generation of gene replacement mutants in *Ustilago maydis*. *Mol Gen Genom* **271:** 103-110

Kämper J, Kahmann R, Bölker M, Ma LJ, Brefort T, Saville BJ, Banuett F, Kronstad JW, Gold SE, Müller O, Perlin MH, Wösten HA, de Vries R, Ruiz-Herrera J, Reynaga-Pena CG, Snetselaar K, McCann M, Pérez-Martín J, Feldbrügge M, Basse CW, Steinberg G, Ibeas JI, Holloman W, Guzman P, Farman M, Stajich JE, Sentandreu R, González-Prieto JM, Kennell JC, Molina L, Schirawski J, Mendoza-Mendoza A, Greilinger D, Münch K, Rössel N, Scherer M, Vranes M, Ladendorf O, Vincon V, Fuchs U, Sandrock B, Meng S, Ho EC, Cahill MJ, Boyce KJ, Klose J, Klosterman SJ, Deelstra HJ, Ortiz-Castellanos L, Li W, Sanchez-Alonso P, Schreier PH, Häuser-Hahn I, Vaupel M, Koopmann E, Friedrich G, Voss H, Schlüter T, Margolis J, Platt D, Swimmer C, Gnirke A, Chen F, Vysotskaia V, Mannhaupt G, Güldener U, Münsterkötter M, Haase D, Oesterheld M, Mewes HW, Mauceli EW, DeCaprio D, Wade CM, Butler J, Young S, Jaffe DB, Calvo S, Nusbaum C, Galagan J, Birren BW (2006) Insights from the genome of the biotrophic fungal plant pathogen *Ustilago maydis*. *Nature* **444:** 97-101

Kämper J, Reichmann M, Romeis T, Bölker M, Kahmann R (1995) Multiallelic recognition: nonself-dependent dimerization of the bE and bW homeodomain proteins in *Ustilago maydis*. *Cell* **81:** 73-83

Kanai Y, Dohmae N, Hirokawa N (2004) Kinesin transports RNA: isolation and characterization of an RNA-transporting granule. *Neuron* **43:** 513-525

Keene JD (2007) RNA regulons: coordination of post-transcriptional events. *Nat Rev Genet* **8:** 533-543

King ML, Messitt TJ, Mowry KL (2005) Putting RNAs in the right place at the right time: RNA localization in the frog oocyte. *Biol Cell* **97:** 19-33

Klinge S, Voigts-Hoffmann F, Leibundgut M, Ban N (2012) Atomic structures of the eukaryotic ribosome. *Trends Biochem Sci* **37:** 189-198

Klopfenstein DR, Tomishige M, Stuurman N, Vale RD (2002) Role of phosphatidylinositol(4,5)bisphosphate organization in membrane transport by the Unc104 kinesin motor. *Cell* **109:** 347-358

Klopfenstein DR, Vale RD (2004) The lipid binding pleckstrin homology domain in UNC-104 kinesin is necessary for synaptic vesicle transport in *Caenorhabditis elegans*. *Mol Biol Cell* **15:** 3729-3739

Koepke J, Kaffarnik F, Haag C, Zarnack K, Luscombe NM, König J, Ule J, Kellner R, Begerow D, Feldbrügge M (2011) The RNA-binding protein Rrm4 is essential for efficient secretion of endochitinase Cts1. *Mol Cell Proteom* **10:** M111.011213 011211-011215

Kondrashov N, Pusic A, Stumpf CR, Shimizu K, Hsieh AC, Xue S, Ishijima J, Shiroishi T, Barna M (2011) Ribosome-mediated specificity in Hox mRNA translation and vertebrate tissue patterning. *Cell* **145:** 383-397

König J, Baumann S, Koepke J, Pohlmann T, Zarnack K, Feldbrügge M (2009) The fungal RNA-binding protein Rrm4 mediates long-distance transport of *ubi1* and *rho3* mRNAs. *EMBO J* **28:** 1855-1866

König J, Julius C, Baumann S, Homann M, Göringer HU, Feldbrügge M (2007) Combining SELEX and yeast three-hybrid system for *in vivo* selection and classification of RNA aptamers. *RNA* **13:** 614-622

Kozlov G, Menade M, Rosenauer A, Nguyen L, Gehring K (2010) Molecular determinants of PAM2 recognition by the MLLE domain of poly(A)-binding protein. *J Mol Biol* **397:** 397-407

Kozlov G, Trempe JF, Khaleghpour K, Kahvejian A, Ekiel I, Gehring K (2001) Structure and function of the C-terminal PABC domain of human poly(A)-binding protein. *Proc Natl Acad Sci U S A* **98:** 4409-4413

Kraut-Cohen J, Gerst JE (2010) Addressing mRNAs to the ER: cis sequences act up! *Trends Biochem Sci* **35:** 459-469

Kumar J, Choudhary BC, Metpally R, Zheng Q, Nonet ML, Ramanathan S, Klopfenstein DR, Koushika SP (2010) The *Caenorhabditis elegans* Kinesin-3 motor UNC-104/KIF1A is degraded upon loss of specific binding to cargo. *PLoS Genet* **6:** e1001200

Kutateladze TG (2006) Phosphatidylinositol 3-phosphate recognition and membrane docking by the FYVE domain. *Biochimica et biophysica acta* **1761:** 868-877

Kutateladze TG (2007) Mechanistic similarities in docking of the FYVE and PX domains to phosphatidylinositol 3-phosphate containing membranes. *Progress in lipid research* **46:** 315-327

Lacombe T, Garcia-Gomez JJ, de la Cruz J, Roser D, Hurt E, Linder P, Kressler D (2009) Linear ubiquitin fusion to Rps31 and its subsequent cleavage are required for the efficient production and functional integrity of 40S ribosomal subunits. *Mol Microbiol* **72:** 69-84

Lange S, Katayama Y, Schmid M, Burkacky O, Brauchle C, Lamb DC, Jansen RP (2008) Simultaneous transport of different localized mRNA species revealed by live-cell imaging. *Traffic* **9:** 1256-1267

Lécuyer E, Yoshida H, Parthasarathy N, Alm C, Babak T, Cerovina T, Hughes TR, Tomancak P, Krause HM (2007) Global analysis of mRNA localization reveals a prominent role in organizing cellular architecture and function. *Cell* **131:** 174-187

Lee AS, Burdeinick-Kerr R, Whelan SP (2013) A ribosome-specialized translation initiation pathway is required for cap-dependent translation of vesicular stomatitis virus mRNAs. *Proceedings of the National Academy of Sciences of the United States of America* **110:** 324-329

Lee NK, Kapanidis AN, Wang Y, Michalet X, Mukhopadhyay J, Ebright RH, Weiss S (2005) Accurate FRET measurements within single diffusing biomolecules using alternating-laser excitation. *Biophys J* **88:** 2939-2953

Lehmler C, Steinberg G, Snetselaar KM, Schliwa M, Kahmann R, Bölker M (1997) Identification of a motor protein required for filamentous growth in *Ustilago maydis*. *EMBO J* **16:** 3464-3473

Lenz JH, Schuchardt I, Straube A, Steinberg G (2006) A dynein loading zone for retrograde endosome motility at microtubule plus-ends. *EMBO J* **25:** 2275-2286

Letunic I, Doerks T, Bork P (2009) SMART 6: recent updates and new developments. *Nucleic Acids Res* **37:** D229-232

Leung KM, van Horck FP, Lin AC, Allison R, Standart N, Holt CE (2006) Asymmetrical beta-actin mRNA translation in growth cones mediates attractive turning to netrin-1. *Nat Neurosci* **9:** 1247-1256

Li CR, Yong JY, Wang YM, Wang Y (2012) CDK regulates septin organization through cell-cycle-dependent phosphorylation of the Nim1-related kinase Gin4. *J Cell Sci* **125:** 2533-2543

Li R, Gundersen GG (2008) Beyond polymer polarity: how the cytoskeleton builds a polarized cell. *Nat Rev Mol Cell Biol* **9:** 860-873

Li X, Kuromi H, Briggs L, Green DB, Rocha JJ, Sweeney ST, Bullock SL (2010) Bicaudal-D binds clathrin heavy chain to promote its transport and augments synaptic vesicle recycling. *EMBO J* **29:** 992-1006

Licatalosi DD, Mele A, Fak JJ, Ule J, Kayikci M, Chi SW, Clark TA, Schweitzer AC, Blume JE, Wang X, Darnell JC, Darnell RB (2008) HITS-CLIP yields genome-wide insights into brain alternative RNA processing. *Nature* **456:** 464-469

Lichius A, Berepiki A, Read ND (2011) Form follows function -- the versatile fungal cytoskeleton. *Fungal biology* **115:** 518-540

Lionnet T, Czaplinski K, Darzacq X, Shav-Tal Y, Wells AL, Chao JA, Park HY, de Turris V, Lopez-Jones M, Singer RH (2011) A transgenic mouse for *in vivo* detection of endogenous labeled mRNA. *Nat Methods* **8:** 165-170

Long RM, Elliott DJ, Stutz F, Rosbash M, Singer RH (1995) Spatial consequences of defective processing of specific yeast mRNAs revealed by fluorescent *in situ* hybridization. *RNA* **1:** 1071-1078

Long RM, Gu W, Lorimer E, Singer RH, Chartrand P (2000) She2p is a novel RNA-binding protein that recruits the Myo4p-She3p complex to *ASH1* mRNA. *EMBO J* **19:** 6592-6601

Loubradou G, Brachmann A, Feldbrügge M, Kahmann R (2001) A homologue of the transcriptional repressor Ssn6p antagonizes cAMP signalling in *Ustilago maydis. Mol Microbiol* **40:** 719-730

Mahlert M, Leveleki L, Hlubek A, Sandrock B, Bölker M (2006) Rac1 and Cdc42 regulate hyphal growth and cytokinesis in the dimorphic fungus *Ustilago maydis*. *Mol Microbiol* **59:** 567-578

Mallardo M, Deitinghoff A, Müller J, Goetze B, Macchi P, Peters C, Kiebler MA (2003) Isolation and characterization of Staufen-containing ribonucleoprotein particles from rat brain. *Proc Natl Acad Sci U S A* **100:** 2100-2105

Maris C, Dominguez C, Allain FH (2005) The RNA recognition motif, a plastic RNA-binding platform to regulate post-transcriptional gene expression. *FEBS J* **272:** 2118-2131

Martin KC, Ephrussi A (2009) mRNA localization: gene expression in the spatial dimension. *Cell* **136:** 719-730

Martin SW, Konopka JB (2004) Lipid raft polarization contributes to hyphal growth in Candida albicans. *Eukaryotic cell* **3:** 675-684

Mazumder B, Seshadri V, Fox PL (2003) Translational control by the 3'-UTR: the ends specify the means. *Trends Biochem Sci* **28:** 91-98

McMurray MA, Bertin A, Garcia G, 3rd, Lam L, Nogales E, Thorner J (2011) Septin filament formation is essential in budding yeast. *Dev Cell* **20:** 540-549

McMurray MA, Thorner J (2009) Reuse, replace, recycle. Specificity in subunit inheritance and assembly of higher-order septin structures during mitotic and meiotic division in budding yeast. *Cell Cycle* **8:** 195-203

Meignin C, Davis I (2010) Transmitting the message: intracellular mRNA localization. *Curr Opin Cell Biol* **22:** 112-119

Messitt TJ, Gagnon JA, Kreiling JA, Pratt CA, Yoon YJ, Mowry KL (2008) Multiple kinesin motors coordinate cytoplasmic RNA transport on a subpopulation of microtubules in *Xenopus* oocytes. *Dev Cell* **15:** 426-436

Mikl M, Vendra G, Kiebler MA (2011) Independent localization of MAP2, CaMKIIalpha and beta-actin RNAs in low copy numbers. *EMBO reports* **12:** 1077-1084

Milkereit P, Strauss D, Bassler J, Gadal O, Kuhn H, Schutz S, Gas N, Lechner J, Hurt E, Tschochner H (2003) A Noc complex specifically involved in the formation and nuclear export of ribosomal 40 S subunits. *J Biol Chem* **278:** 4072-4081

Misra S, Miller GJ, Hurley JH (2001) Recognizing phosphatidylinositol 3-phosphate. *Cell* **107:** 559-562

Molle D, Segura-Morales C, Camus G, Berlioz-Torrent C, Kjems J, Basyuk E, Bertrand E (2009) Endosomal trafficking of HIV-1 gag and genomic RNAs regulates viral egress. *J Biol Chem* **284:** 19727-19743

Morrissey JP, Deardorff JA, Hebron C, Sachs AB (1999) Decapping of stabilized, polyadenylated mRNA in yeast *pab1* mutants. *Yeast* **15:** 687-702

Müller M, Heuck A, Niessing D (2007) Directional mRNA transport in eukaryotes: lessons from yeast. *Cell Mol Life Sci* **64:** 171-180

Muller M, Heym RG, Mayer A, Kramer K, Schmid M, Cramer P, Urlaub H, Jansen RP, Niessing D (2011) A cytoplasmic complex mediates specific mRNA recognition and localization in yeast. *PLoS biology* **9:** e1000611

Munn AL, Heese-Peck A, Stevenson BJ, Pichler H, Riezman H (1999) Specific sterols required for the internalization step of endocytosis in yeast. *Molecular biology of the cell* **10:** 3943-3957

Nashchekin D, St Johnston D (2009) Egalitarian recruitment of localized mRNAs. *Genes & development* **23:** 1475-1480

Nelson WJ (2003) Adaptation of core mechanisms to generate cell polarity. *Nature* **422:** 766-774

Neukirchen D, Bradke F (2011) Neuronal polarization and the cytoskeleton. *Seminars in cell & developmental biology* **22:** 825-833

Nickel W (2010) Pathways of unconventional protein secretion. *Curr Opin Biotechnol* **21:** 621-626

Niman HL, Houghten RA, Walker LE, Reisfeld RA, Wilson IA, Hogle JM, Lerner RA (1983) Generation of protein-reactive antibodies by short peptides is an event of high frequency: implications for the structural basis of immune recognition. *Proc Natl Acad Sci U S A* **80:** 4949-4953

Oh Y, Bi E (2011) Septin structure and function in yeast and beyond. *Trends Cell Biol* **21:** 141-148

Palacios IM (2007) How does an mRNA find its way? Intracellular localisation of transcripts. *Semin Cell Dev Biol* **18:** 163-170

Panse VG, Johnson AW (2010) Maturation of eukaryotic ribosomes: acquisition of functionality. *Trends in biochemical sciences* **35:** 260-266

Paquin N, Chartrand P (2008) Local regulation of mRNA translation: new insights from the bud. *Trends Cell Biol* **18:** 105-111

Patterson GH, Lippincott-Schwartz J (2002) A photoactivatable GFP for selective photolabeling of proteins and cells. *Science* **297:** 1873-1877

Penalva MA (2010) Endocytosis in filamentous fungi: Cinderella gets her reward. *Curr Opin Microbiol* **13:** 684-692

Rattei T, Arnold R, Tischler P, Lindner D, Stumpflen V, Mewes HW (2006) SIMAP: the similarity matrix of proteins. *Nucleic Acids Res* **34:** D252-256

Ray PS, Arif A, Fox PL (2007) Macromolecular complexes as depots for releasable regulatory proteins. *Trends Biochem Sci* **32:** 158-164

Requena N, Alberti-Segui C, Winzenburg E, Horn C, Schliwa M, Philippsen P, Liese R, Fischer R (2001) Genetic evidence for a microtubule-destabilizing effect of conventional kinesin and analysis of its consequences for the control of nuclear distribution in *Aspergillus nidulans*. *Mol Microbiol* **42:** 121-132

Rodriguez AJ, Czaplinski K, Condeelis JS, Singer RH (2008) Mechanisms and cellular roles of local protein synthesis in mammalian cells. *Curr Opin Cell Biol* **20:** 144-149

Ruepp A, Zollner A, Maier D, Albermann K, Hani J, Mokrejs M, Tetko I, Guldener U, Mannhaupt G, Münsterkötter M, Mewes HW (2004) The FunCat, a functional annotation scheme for systematic classification of proteins from whole genomes. *Nucleic Acids Res* **32:** 5539-5545

Rusten TE, Vaccari T, Stenmark H (2012) Shaping development with ESCRTs. *Nat Cell Biol* **14:** 38-45

Saarikangas J, Barral Y (2011) The emerging functions of septins in metazoans. *EMBO Rep* **12:** 1118-1126

Scherer M, Heimel K, Starke V, Kämper J (2006) The Clp1 protein is required for clamp formation and pathogenic development of *Ustilago maydis*. *Plant Cell* **18:** 2388-2401

Schink KO, Bölker M (2009) Coordination of cytokinesis and cell separation by endosomal targeting of a Cdc42-specific guanine nucleotide exchange factor in *Ustilago maydis*. *Mol Biol Cell* **20:** 1081-1088

Schmid M, Jaedicke A, Du TG, Jansen RP (2006) Coordination of endoplasmic reticulum and mRNA localization to the yeast bud. *Curr Biol* **16:** 1538-1543

Schuchardt I, Assmann D, Thines E, Schuberth C, Steinberg G (2005) Myosin-V, Kinesin-1, and Kinesin-3 cooperate in hyphal growth of the fungus *Ustilago maydis*. *Mol Biol Cell* **16:** 5191-5201

Schuster M, Kilaru S, Ashwin P, Lin C, Severs NJ, Steinberg G (2011a) Controlled and stochastic retention concentrates dynein at microtubule ends to keep endosomes on track. *EMBO J* **30:** 652-664

Schuster M, Lipowsky R, Assmann MA, Lenz P, Steinberg G (2011b) Transient binding of dynein controls bidirectional long-range motility of early endosomes. *Proc Natl Acad Sci U S A* **109:** 3618-3623

Schuster M, Sreedhar K, Fink G, Collemare J, Roger Y, Steinberg G (2011c) Kinesin-3 and dynein cooperate in long-range retrograde endosome motility along a non-uniform microtubule array. *Mol Biol Cell* **22:** 3645-3657

Seiler S, Nargang FE, Steinberg G, Schliwa M (1997) Kinesin is essential for cell morphogenesis and polarized secretion in *Neurospora crassa*. *EMBO J* **16:** 3025-3034

Sellin ME, Sandblad L, Stenmark S, Gullberg M (2011) Deciphering the rules governing assembly order of mammalian septin complexes. *Molecular biology of the cell* **22:** 3152-3164

Shaner NC, Campbell RE, Steinbach PA, Giepmans BN, Palmer AE, Tsien RY (2004) Improved monomeric red, orange and yellow fluorescent proteins derived from *Discosoma* sp. red fluorescent protein. *Nat Biotechnol* **22:** 1567-1572

Shih SC, Katzmann DJ, Schnell JD, Sutanto M, Emr SD, Hicke L (2002) Epsins and Vps27p/Hrs contain ubiquitin-binding domains that function in receptor endocytosis. *Nature cell biology* **4:** 389-393

Simonsen A, Wurmser AE, Emr SD, Stenmark H (2001) The role of phosphoinositides in membrane transport. *Current opinion in cell biology* **13:** 485-492

Singer RH (2008) Highways for mRNA transport. *Cell* **134:** 722-723

Sirajuddin M, Farkasovsky M, Hauer F, Kuhlmann D, Macara IG, Weyand M, Stark H, Wittinghofer A (2007) Structural insight into filament formation by mammalian septins. *Nature* **449:** 311-315

Spiliotis ET, Gladfelter AS (2012) Spatial guidance of cell asymmetry: septin GTPases show the way. *Traffic* **13:** 195-203

Sprague BL, McNally JG (2005) FRAP analysis of binding: proper and fitting. *Trends Cell Biol* **15:** 84-91

St Johnston D (2005) Moving messages: the intracellular localization of mRNAs. *Nat Rev Mol Cell Biol* **6:** 363-375

Steinberg G (2007a) Hyphal growth: a tale of motors, lipids, and the Spitzenkörper. *Euk Cell* **6:** 351-360

Steinberg G (2007b) On the move: endosomes in fungal growth and pathogenicity. *Nat Rev Microbiol* **5:** 309-316

Steinberg G (2007c) Tracks for traffic: microtubules in the plant pathogen *Ustilago maydis*. *New Phytol* **174:** 721-733

Steinberg G (2012) The transport machinery for motility of fungal endosomes. *Fungal Genet Biol* **49:** 675-676

Steinberg G, Perez-Martin J (2008) *Ustilago maydis*, a new fungal model system for cell biology. *Trends Cell Biol* **18:** 61-67

Steinberg G, Schliwa M, Lehmler C, Bölker M, Kahmann R, McIntosh JR (1998) Kinesin from the plant pathogenic fungus *Ustilago maydis* is involved in vacuole formation and cytoplasmic migration. *J Cell Sci* **111:** 2235-2246

Steinberg G, Schuster M, Theisen U, Kilaru S, Forge A, Martin-Urdiroz M (2012) Motor-driven motility of fungal nuclear pores organizes chromosomes and fosters nucleocytoplasmic transport. *The Journal of cell biology* **198:** 343-355

Straube A, Brill M, Oakley BR, Horio T, Steinberg G (2003) Microtubule organization requires cell cycle-dependent nucleation at dispersed cytoplasmic sites: polar and perinuclear microtubule organizing centers in the plant pathogen *Ustilago maydis*. *Mol Biol Cell* **14:** 642-657

Straube A, Enard W, Berner A, Wedlich-Söldner R, Kahmann R, Steinberg G (2001) A split motor domain in a cytoplasmic dynein. *EMBO J* **20:** 5091-5100

Thanbichler M (2009) Spatial regulation in Caulobacter crescentus. *Current opinion in microbiology* **12:** 715-721

Trautwein M, Dengjel J, Schirle M, Spang A (2004) Arf1p provides an unexpected link between COPI vesicles and mRNA in *Saccharomyces cerevisiae*. *Mol Biol Cell* **15:** 5021-5037

Tubing F, Vendra G, Mikl M, Macchi P, Thomas S, Kiebler MA (2010) Dendritically localized transcripts are sorted into distinct ribonucleoprotein particles that display fast directional motility along dendrites of hippocampal neurons. *The Journal of neuroscience : the official journal of the Society for Neuroscience* **30:** 4160-4170

Ule J, Jensen K, Mele A, Darnell RB (2005) CLIP: a method for identifying protein-RNA interaction sites in living cells. *Methods* **37:** 376-386

Ule J, Jensen KB, Ruggiu M, Mele A, Ule A, Darnell RB (2003) CLIP identifies Nova-regulated RNA networks in the brain. *Science* **302:** 1212-1215

Versele M, Gullbrand B, Shulewitz MJ, Cid VJ, Bahmanyar S, Chen RE, Barth P, Alber T, Thorner J (2004) Protein-protein interactions governing septin heteropentamer assembly and septin filament organization in Saccharomyces cerevisiae. *Molecular biology of the cell* **15:** 4568-4583

Vida TA, Emr SD (1995) A new vital stain for visualizing vacuolar membrane dynamics and endocytosis in yeast. *J Cell Biol* **128:** 779-792

Vollmeister E, Feldbrügge M (2010) Posttranscriptional control of growth and development in *Ustilago maydis*. *Curr Op Microbio* **13:** 693-699

Vollmeister E, Schipper K, Baumann S, Haag C, Pohlmann T, Stock J, Feldbrügge M (2012) Fungal development of the plant pathogen *Ustilago maydis*. *FEMS Microbiol Rev* **36:** 59-77

Wang Z, Tollervey J, Briese M, Turner D, Ule J (2009) CLIP: Construction of cDNA libraries for high-throughput sequencing from RNAs cross-linked to proteins *in vivo*. *Methods***:** doi:10.1016/j.ymeth.2009.1002.1021

Wedlich-Söldner R, Altschuler S, Wu L, Li R (2003) Spontaneous cell polarization through actomyosin-based delivery of the Cdc42 GTPase. *Science* **299:** 1231-1235

Wedlich-Söldner R, Bölker M, Kahmann R, Steinberg G (2000) A putative endosomal t-SNARE links exo- and endocytosis in the phytopathogenic fungus *Ustilago maydis*. *EMBO J* **19:** 1974-1986

Wedlich-Soldner R, Li R (2003) Spontaneous cell polarization: undermining determinism. *Nature cell biology* **5:** 267-270

Wedlich-Söldner R, Straube A, Friedrich MW, Steinberg G (2002) A balance of KIF1A-like kinesin and dynein organizes early endosomes in the fungus *Ustilago maydis*. *EMBO J* **21:** 2946-2957

Weil TT, Forrest KM, Gavis ER (2006) Localization of *bicoid* mRNA in late oocytes is maintained by continual active transport. *Dev Cell* **11:** 251-262

Weinzierl G, Leveleki L, Hassel A, Kost G, Wanner G, Bölker M (2002) Regulation of cell separation in the dimorphic fungus *Ustilago maydis*. *Mol Microbiol* **45:** 219-231

Weirich CS, Erzberger JP, Barral Y (2008) The septin family of GTPases: architecture and dynamics. *Nat Rev Mol Cell Biol* **9:** 478-489

White J, Stelzer E (1999) Photobleaching GFP reveals protein dynamics inside live cells. *Trends Cell Biol* **9:** 61-65

Wu KY, Hengst U, Cox LJ, Macosko EZ, Jeromin A, Urquhart ER, Jaffrey SR (2005) Local translation of RhoA regulates growth cone collapse. *Nature* **436:** 1020-1024

Xie Y, Vessey JP, Konecna A, Dahm R, Macchi P, Kiebler MA (2007) The GTP-binding protein Septin 7 is critical for dendrite branching and dendritic-spine morphology. *Curr Biol* **17:** 1746-1751

Yap CC, Winckler B (2012) Harnessing the power of the endosome to regulate neural development. *Neuron* **74:** 440-451

Yeo GW, Coufal NG, Liang TY, Peng GE, Fu XD, Gage FH (2009) An RNA code for the FOX2 splicing regulator revealed by mapping RNA-protein interactions in stem cells. *Nat Struct Mol Biol* **16:** 130-137

Zarnack K, Eichhorn H, Kahmann R, Feldbrügge M (2008) Pheromone-regulated target genes respond differentially to MAPK phosphorylation of transcription factor Prf1. *Mol Microbiol* **69:** 1041-1053

Zarnack K, Feldbrügge M (2007) mRNA trafficking in fungi. *Mol Gen Genom* **278:** 347-359

Zarnack K, Feldbrügge M (2010) Microtubule-dependent mRNA transport in fungi. *Euk Cell* **9:** 982-990

Zarnack K, Maurer S, Kaffarnik F, Ladendorf O, Brachmann A, Kämper J, Feldbrügge M (2006) Tetracycline-regulated gene expression in the pathogen *Ustilago maydis*. *Fungal Genet Biol* **43:** 727-738

Zhang J, Li S, Fischer R, Xiang X (2003) Accumulation of cytoplasmic dynein and dynactin at microtubule plus ends in *Aspergillus nidulans* is kinesin dependent. *Mol Biol Cell* **14:** 1479-1488

Zimyanin VL, Belaya K, Pecreaux J, Gilchrist MJ, Clark A, Davis I, St Johnston D (2008) *In vivo* imaging of *oskar* mRNA transport reveals the mechanism of posterior localization. *Cell* **134:** 843-853

# 6 Author contributions

The research on which this dissertation is based, is published (Section 2.1and 2.2) or submitted for publication in a peer-reviewed journal (Section 2.3). This declaration is intended to clarify the contribution of Sebastian Baumann to all three sections.

**Section 2.1** - The fungal RNA-binding protein Rrm4 mediates long-distance transport of *ubi1* and *rho3* mRNAs – published in the EMBO Journal (2009)
This study was carried out by Julian König, Sebastian Baumann, Janine Koepke, Thomas Pohlmann, Kathi Zarnack and Michael Feldbrügge. The first two authors contributed equally. M.F., S.B., and J.Kö. designed this study and analysed data unless otherwise stated. S.B., J.Kö., J.Koe. and T.P. performed wet bench experiments including generation of plasmids and strains. J.Kö performed CLIP experiments. T.P. carried out the TAP-tag purification and contributed to its evaluation. K.Za. wrote the PIA script and contributed to FISH analysis. J.Koe performed the yeast complementation assay for Pab1 and performed microscopy on AB33pab1G and AB33pab1G/rrm4Δ strains and evaluated the results. S.B. performed microscopy of all other AB33 derivatives, carried out FISH experiments and qRT-PCR as well as RNA live imaging microscopy and quantification. M.F., J.Kö, K.Za. and S.B. wrote the manuscript with input from all co-authors. M.F. directed the project. S.B. established the RNA-live imaging system already during his diploma thesis.

**Section 2.2** - Kinesin-3 and dynein mediate microtubule-dependent co-transport of mRNPs and endosomes – published in Journal of Cell Science (2012)
This study was carried out by Sebastian Baumann, Thomas Pohlmann, Marc Jungbluth, Andreas Brachmann and Michael Feldbrügge. M.F., S.B. designed this study. M.F., S.B., and T.P. analysed data. S.B., T.P., M.J. and A.B. performed wet bench experiments including generation of plasmids and strains. T.P. performed experiments resulting in figure 3, including microscopy and Wersten Blot. Additionally T.P analysed kinesin-3 mutants in figure 4. S.B. performed experiments resulting in all ther main and supplementary figures. M.F. and S.B. and T.P. wrote the manuscript with input from all co-authors. M.F. directed the project.

**Section 2.3** - Endosomal transport of septin mRNA and encoded protein mediates correct septin filamentation - The manuscript is submitted to the EMBO Journal and currently under first revision

This study was carried out by Sebastian Baumann, Julian König, Janine Koepke and Michael Feldbrügge. M.F., S.B., and J.Kö. designed this study and analysed data. J.Kö., J.Koe., and S.B. performed wet bench experiments including generation of plasmids and strains. S.B. established the λN*-based RNA live imaging system, performed microscopic analysis, quantification, and data evaluation. M.F. and S.B. wrote the manuscript with input from all co-authors. M.F. directed the project.

**Danksagung**

Diese Arbeit ist meinem Vater und meiner Mutter gewidmet.

An erster Stelle gebührt mein tiefster Dank meiner Familie, die an mich glaubt und mich immer unterstützt. Ich liebe Euch alle.

Bei Michael möchte ich mich sehr herzlich für die außerordentliche Unterstützung und die Freiheiten, die ich mir nehmen konnte, bedanken. Die Gespräche mit Dir haben mich wirklich weitergebracht.

Vielen lieben Dank an das „alte“ STaR lab! Ihr wart echt Klasse☺
Herzlichsten Dank an die besten TAs der Welt, Petra Happel und Ute Gengenbacher.

Ich möchte mich noch sehr bei denjenigen bedanke, die mir in den letzten Wochen während des Schreibens zur Seite gestanden haben. Vielen vielen Dank!

# 7 Curriculum Vitae

## Daten

| | |
|---|---|
| Name | Sebastian Baumann |
| Geburtsdatum | 29.01.1980 |
| Geburtsort | Gelsenkirchen |
| Nationalität | deutsch |

## Allgemein

| | | |
|---|---|---|
| Studium | 12/2009 – 04/2013 | Fortsetzung Dissertation an der Heinrich-Heine-Universität Düsseldorf |
| | 10/2007 – 11/2009 | Dissertation am Max-Planck-Institut für terrestrische Mikrobiologie in Marburg |
| | 12/2006 – 08/2007 | Diplomarbeit am Max-Planck-Institut für terrestrische Mikrobiologie in Marburg; Thema: *In vivo*-Nachweis des Rrm4 vermittelten, Mikrotubuli abhängigen mRNA-Transports in *Ustilago maydis* |
| | 10/2002 – 08/2007 | Biologie-Studium an der Philipps-Universität Marburg<br>Schwerpunkte: Genetik, Biochemie, Mikrobiologie<br>Abschluss: Diplom |
| Zivildienst | 07/2001 – 04/2002 | Christlicher Verein Junger Menschen, Essen |
| Schulausbildung | 08/1997 – 06/2001 | Gesamtschule Horst, Gelsenkirchen<br>Abschluss: Allgemeine Hochschulreife |
| | 08/1990 – 06/1997 | Schalker Gymnasium, Gelsenkirchen |
| | 07/1986 – 06/1990 | Grundschule an der Schonnebecker Strasse, Gelsenkirchen |